



HAL
open science

Développement d'un nouveau concept de refroidisseurs à absorption compact et à bas coût : application au cas du rafraîchissement solaire pour des climats chauds

Amín Altamirano Cundapi

► To cite this version:

Amín Altamirano Cundapi. Développement d'un nouveau concept de refroidisseurs à absorption compact et à bas coût : application au cas du rafraîchissement solaire pour des climats chauds. Thermics [physics.class-ph]. Université Savoie Mont Blanc, 2021. English. NNT : 2021CHAMA002 . tel-03600792

HAL Id: tel-03600792

<https://theses.hal.science/tel-03600792>

Submitted on 7 Mar 2022

HAL is a multi-disciplinary open access archive for the deposit and dissemination of scientific research documents, whether they are published or not. The documents may come from teaching and research institutions in France or abroad, or from public or private research centers.

L'archive ouverte pluridisciplinaire **HAL**, est destinée au dépôt et à la diffusion de documents scientifiques de niveau recherche, publiés ou non, émanant des établissements d'enseignement et de recherche français ou étrangers, des laboratoires publics ou privés.

THÈSE

Pour obtenir le grade de

DOCTEUR DE L'UNIVERSITÉ SAVOIE MONT BLANC

Spécialité : **Énergétique et Génie des Procédés**

Arrêté ministériel : 25 Mai 2016

Présentée par

Amín ALTAMIRANO CUNDAPI

Thèse dirigée par **Benoît STUTZ** et **Nolwenn LE PIERRÈS**

préparée au sein du **Laboratoire LOCIE UMR CNRS 5271**
dans l'**École Doctorale SISEO**

Development of a new concept of compact and low-cost absorption chillers: application in solar cooling for hot climates

Développement d'un nouveau concept de refroidisseurs à absorption compact et à bas coût : application au cas du rafraîchissement solaire pour des climats chauds

Thèse soutenue publiquement le **14 janvier 2021**,
devant le jury composé de :

M. Alberto CORONAS SALCEDO

Professeur, Universitat Rovira i Virgili, Président

M. Frédéric LEFEVRE

Professeur, Institut National des Sciences Appliquées Lyon, Rapporteur

M. Wilfrido RIVERA GÓMEZ FRANCO

Professeur, Universidad Nacional Autónoma de México, Rapporteur

Mme. Florine GIRAUD

Maître de Conférences, Institut Français du Froid Industriel et de génie climatique, Examinatrice

M. Benoît STUTZ

Professeur, Université Savoie Mont Blanc, Directeur de thèse

Mme. Nolwenn LE PIERRÈS

Professeure, Université Savoie Mont Blanc, Directrice de thèse

Dedication

*Dedicado a mi familia (en México y el mundo)
y a todos aquellos que nos dejaron físicamente
en este contexto sanitario complicado;
entre ellos mis abuelitos Adelfa y Chusi.*

*Dedicated to my family (in Mexico and around the world)
and to all those who have passed away
in this difficult sanitary context;
among them my grandpas Adelfa and Chusi.*

This page intentionally left blank

Table of contents

Abstract.....	V
French abstract	VII
Acknowledgements	IX
Scientific dissemination	XI
Articles in scientific journals	XI
Patents.....	XI
Communications in congresses, conferences, seminars, and workshops.....	XI
Participation in projects and IEA Tasks.....	XII
Internships and training.....	XII
List of figures.....	XIII
List of tables	XVII
Nomenclature	XIX
French detailed summary.....	1
Introduction Générale	3
Chapitre I. État de l'art sur les refroidisseurs à absorption à simple étage.....	6
Chapitre II. Les efficacités thermique et massique comme outil pour la caractérisation des refroidisseurs à absorption et comparaison de modèles.....	9
Chapitre III. Climatisation à absorption solaire dans le contexte mexicain.....	10
Chapitre IV. Nouvelle génération d'échangeur de masse adiabatique à film tombant.....	13
Perspectives	14
Références.....	16
General introduction	21
Residential air conditioning global energy challenge	23
The Mexican context.....	24
Solar absorption chillers	25
Research objectives.....	27
Thesis organization	27
References.....	29
Chapter I. State of the art on single-stage absorption chillers	31
1.1. Introduction.....	33
1.2. Review of theoretical, experimental, and commercial cycles.....	34
1.2.1. Comparative criteria.....	34
1.2.2. Ammonia-based working fluids.....	36
1.2.2.1. Conventional ammonia-based working pair: NH ₃ -H ₂ O.....	36

Table of contents

1.2.2.2. NH ₃ -LiNO ₃ and NaSCN	40
1.2.2.3. NH ₃ -Ionic Liquids: Theoretical studies.....	43
1.2.2.4. Comparisons of NH ₃ -based absorption systems	44
1.2.3. Water-based working fluids.....	46
1.2.3.1. Conventional water-based working pair: H ₂ O-LiBr	46
1.2.3.2. H ₂ O-LiI and LiCl	51
1.2.3.3. H ₂ O-Ionic Liquids: Theoretical studies and experimental prototypes	51
1.2.3.4. Comparisons of the water-based working fluids.....	52
1.2.4. Working fluids with other refrigerant bases	53
1.2.4.1. Alcohol-based working fluids.....	53
1.2.4.2. HFCs and HCFCs-based working fluids.....	54
1.2.4.3. Other refrigerant bases	55
1.2.5. General comparisons between working pairs	56
1.2.5.1. Theoretical general comparisons in the literature	56
1.2.5.2. Discussion of the developed prototypes and commercial systems	58
1.3. Review of compact exchanger technologies.....	61
1.3.1. Heat and mass transfer comparative criteria	62
1.3.2. Non-adiabatic exchangers	65
1.3.2.1. Falling film.....	65
1.3.2.2. Two-phase flow exchangers.....	74
1.3.2.3. Membrane-based exchanger	80
1.3.3. Adiabatic exchangers	81
1.3.3.1. Falling film.....	82
1.3.3.2. Two-phase flow	84
1.3.3.3. Membrane-based exchangers.....	85
1.3.4. General discussion	86
1.3.4.1. Technologies used in experimental prototypes	86
1.3.4.2. Comparison of the technologies studied	90
1.4. Conclusion	92
References.....	95
Chapter II. Thermal and mass effectivenesses as a tool for the characterization of absorption chillers and models comparison.....	109
2.1. Introduction.....	111
2.2. Characterization of the sorption exchangers.....	111
2.2.1. Thermal and mass effectivenesses definition.....	111
2.2.2. Exchanger's geometries and experimental conditions.....	113
2.2.3. Results.....	114
2.3. Characterization methods applied to a NH ₃ -LiNO ₃ single stage prototype	116

2.3.1. System description	117
2.3.2. Characterization of the system.....	119
2.3.2.1. Characteristic equation method.....	119
2.3.2.2. Adapted characteristic equation method and Carnot function model	121
2.3.2.3. Effectiveness model	121
2.3.3. Results and validation of the models	122
2.3.3.1. Characteristic equation method.....	122
2.3.3.2. Adapted characteristic equation method and Carnot function model	124
2.3.3.3. Effectiveness model	125
2.3.4. Discussion of the internal operating conditions through the effectiveness model	128
2.3.4.1. Solution concentration conditions.....	129
2.3.4.2. Equilibrium factor.....	129
2.3.4.3. Solution flow conditions	130
2.3.4.4. Equilibrium deviation temperatures.....	131
2.3.4.5. Thermal and mass effectivenesses of the sorption exchangers	132
2.4. Conclusions.....	133
References.....	134
Chapter III. Solar absorption air conditioner in the Mexican context	137
3.1. Introduction.....	139
3.2. Selection of high-performance working fluid for a solar-geothermal absorption cooling system and techno-economic study in the northern Mexican conditions	140
3.2.1. Climatic conditions and ground temperature profiles.....	140
3.2.2. Thermodynamic comparison of the working fluids	142
3.2.2.1. Description of the system.....	142
3.2.2.2. Assumptions for the thermodynamic analysis	142
3.2.2.3. Thermodynamic analysis	143
3.2.2.4. Results and discussion	143
3.2.3. Integrated solar-geothermal system and economic feasibility study	145
3.2.3.1. Solar-geothermal absorption cooling system and dimensioning.....	145
3.2.3.2. Economic assessment.....	147
3.3. Solar absorption air conditioner with an innovative bi-adiabatic configuration: dynamic model, nominal conditions and typical day operation	148
3.3.1. System description	148
3.3.2. Dynamic model.....	149
3.3.2. Results and discussion	151
3.3.2.1. System's optimum operating conditions.....	151
3.3.2.2. Typical day operation	152
3.4. Conclusions.....	158

References.....	159
Chapter IV. New-generation adiabatic falling film mass exchanger for absorption chillers .	163
4.1. Introduction.....	165
4.2. Experimental set-up	166
4.2.1. Experimental facility.....	166
4.2.2. Adiabatic sorption exchanger.....	167
4.3. Data reduction and operating conditions	169
4.3.1. Temperature equilibrium deviations	169
4.3.2. Desorbed mass and mass effectiveness.....	169
4.3.3. Design of experiments and uncertainties	170
4.4. Results and discussion	172
4.4.1. Mass effectiveness regression.....	172
4.4.2. Model interpretation.....	174
4.5. Comparison with other technologies.....	178
4.5.1. Membrane desorbers effectiveness	178
4.5.2. Performance comparison.....	179
4.5.3. Pressure drop comparison	183
4.6. Conclusions.....	186
References.....	187
Conclusions and future work.....	191
Conclusions.....	193
Future work.....	194

Abstract

Energy consumption worldwide is increasing at alarming rates, especially in developing countries. In the building sector alone (most energy demanding sector), the energy consumption for space cooling has more than tripled in 26 years (from 1990 to 2016), and it is expected to triple again by 2050, with around 70% of this increase coming from the residential sector. Nowadays, the need for cooling is almost totally covered by conventional vapor compression systems. This dependence on electricity is already generating problems of electricity distribution grid saturation in hot-climate countries, reaching over 70% of peak residential electrical demand during hot days in some regions of the world. In this context, the Mexican case is especially delicate since it is the second country in the world with the highest share of electricity used for space cooling (14%). Moreover, Mexico depends energetically and economically on fossil fuels.

Absorption chillers represent an alternative to vapor compression systems since they operate with natural refrigerants and can run on clean heat sources such as solar energy and waste heat. However, these systems are, until now, expensive and bulky. In spite of the efforts to address different aspects to reduce the manufacturing costs, size, and improve the efficiency of absorption chillers, they cover until now a very small niche market (1% of the total cooling needs in the building sector). The present PhD thesis shows the development of a new generation of absorption chillers based on a new adiabatic sorption technology. Specifically, the proposed technology was studied for small capacity residential applications with a solar thermal source in countries with high solar irradiation, such as Mexico.

[Chapter I](#) provides a deep state of the art on the investigated working fluids and exchanger technologies for absorption chillers in small-capacity applications. Since no standard characterization parameter for the sorption exchangers was found in the literature, [Chapter II](#) presents the concepts of thermal and mass effectivenesses generalized for non-adiabatic sorption exchangers (the mass effectiveness of adiabatic sorption exchangers being intrinsically included in this definition). The implementation of these effectivenesses to characterize the sorption exchangers of absorption chillers is shown through examples at the component and at the system scales with the $\text{NH}_3\text{-LiNO}_3$ working fluid. Furthermore, given the importance of the characterization of absorption chillers, other absorption chiller modelling methods with different insight levels are also presented and discussed.

The study of a solar-geothermal absorption air conditioning system in the Monterrey (Mexico) context was addressed in [Chapter III](#). In the first part, the comparison of the two conventional working fluids ($\text{NH}_3\text{-H}_2\text{O}$ and $\text{H}_2\text{O-LiBr}$) and an innovative working fluid ($\text{NH}_3\text{-LiNO}_3$) was performed through a steady-state model. Moreover, the dimensioning of the components of the system and a short economic viability study are proposed. In the second part, a single-stage absorption chiller with an innovative bi-adiabatic configuration is presented and studied by means of a dynamic model. The model was first used to define the nominal operating conditions of the absorption chiller and the minimum performance requirements of the components. After this, its use to cool down a house on a typical sunny day in the Monterrey climate conditions is analyzed and discussed. Finally, the last chapter presents a new generation of adiabatic falling film sorption exchanger for absorption chillers. The characterization of this exchanger in desorption mode was performed for a wide range of operating conditions. The experimental results show very high performances and validate the potential of the proposed adiabatic sorption technology. Therefore, based on these results, the construction of an absorption chiller based on this technology seems very promising.

Keywords: absorption chiller, solar air conditioning, working fluid, exchanger technology, falling film, adiabatic exchanger.

This page intentionally left blank

French abstract

La consommation énergétique mondiale augmente à vitesse alarmante. Dans le secteur du bâtiment, la consommation énergétique pour la climatisation a plus que triplé depuis 1990 et elle devrait encore tripler d'ici 2050, environ 70 % de cette augmentation provenant du secteur résidentiel. Aujourd'hui, ces besoins sont presque entièrement couverts par les systèmes à compression de vapeur. Cette dépendance à l'égard de l'électricité engendre déjà des problèmes de saturation des réseaux de distribution. Dans ce contexte, le cas du Mexique est particulièrement délicat car il est le deuxième pays au monde avec la plus grande proportion d'électricité utilisée pour le refroidissement des locaux (14%) et il dépend énergétiquement et économiquement des combustibles fossiles.

Les refroidisseurs à absorption sont une alternative car ils utilisent des réfrigérants naturels et peuvent fonctionner avec des sources de chaleur non polluantes telles que l'énergie solaire et la chaleur résiduelle. Cependant, ces systèmes restent, jusqu'à présent, coûteux et encombrants. De ce fait, ils représentent un très petit marché de niche (1% des besoins totaux de refroidissement dans le secteur du bâtiment). Cette thèse décrit le développement d'une nouvelle génération de refroidisseurs à absorption basés sur une nouvelle technologie de sorption adiabatique. La technologie proposée a été étudiée pour des applications résidentielles avec une source solaire thermique dans des pays à forte irradiation solaire, comme le Mexique.

Le Chapitre I fournit un état de l'art sur les fluides de travail étudiés et les technologies d'échangeurs pour les refroidisseurs à absorption. Puisqu'aucun paramètre normalisé pour la caractérisation des échangeurs à sorption n'a été trouvé dans la littérature, le Chapitre II présente les concepts d'efficacité thermique et massique généralisés pour les échangeurs à sorption non-adiabatiques (l'efficacité massique des échangeurs à sorption adiabatiques étant intrinsèquement incluse dans cette définition). La mise en œuvre de ces efficacités pour caractériser les échangeurs de sorption des refroidisseurs à absorption est montrée au travers d'applications avec le fluide de travail $\text{NH}_3\text{-LiNO}_3$. En outre, étant donné l'importance de la caractérisation des refroidisseurs à absorption, d'autres méthodes de modélisation de refroidisseurs à absorption avec différents niveaux de compréhension sont également présentées et discutées.

L'étude d'un système de climatisation à absorption solaire-géothermique pour la ville de Monterrey (Mexique) a été abordée au Chapitre III. Dans une première partie, la comparaison des deux fluides de travail classiques ($\text{NH}_3\text{-H}_2\text{O}$ et $\text{H}_2\text{O-LiBr}$) et d'un fluide de travail innovant ($\text{NH}_3\text{-LiNO}_3$) a été réalisée à l'aide d'un modèle en régime stationnaire. En outre, le dimensionnement des composants du système et une brève étude de viabilité économique sont proposés. Dans la deuxième partie, un refroidisseur à absorption à simple étage avec une configuration bi-adiabatique innovante est présenté et étudié par le biais d'un modèle dynamique. Le modèle a d'abord été utilisé pour définir les conditions de fonctionnement nominales du refroidisseur à absorption et les performances minimales requises des composants. Par la suite, son utilisation pour refroidir une maison lors d'une journée ensoleillée typique dans les conditions climatiques de Monterrey est étudiée et analysée. Finalement, le dernier chapitre présente une nouvelle génération d'échangeur de sorption adiabatique à film ruisselant pour les refroidisseurs à absorption. La caractérisation de cet échangeur en désorption a été réalisée dans une large gamme de conditions de fonctionnement. Les résultats expérimentaux montrent des performances très élevées et valident le potentiel de la technologie de sorption adiabatique proposée. Par conséquent, sur la base de ces résultats, la construction d'un refroidisseur à absorption basé sur cette technologie semble très prometteuse.

Mots-clés : rafraîchisseur à absorption, climatisation solaire, fluide de travail, technologie d'échangeur, film ruisselant, échangeur adiabatique.

This page intentionally left blank

Acknowledgements

After three years of hard work, but also numerous adventures, it is time for me to close a chapter in my life, and this manuscript is a very good way to do so. During these three years, I have learned so much about science (it works!), about life, and about this magnificent world around us. I am very fortunate to have visited so many places and met so many wonderful people in this beautiful journey. A couple of lines would never be enough to express my gratitude to all of the people that contributed to this success, but at least it leaves a symbolic mark of what it means to me.

First of all, I would like to thank from the bottom of my heart, my two supervisors: Nolwenn Le Pierrès and Benoît Stutz: merci infiniment ! Without knowing it, we started this journey in the summer of 2015, when I decided to come to the lab to perform my end of studies master's project. You know it already, but allow me to leave a written mention here of how much I admire you both and how much it means to me that you have believed in me since the beginning. You never hesitated when I contacted you to tell you I wanted to do a PhD, and you took the time to construct with me from scratch the work that is being presented in this manuscript. You have always been there for me and I have always tried so hard to get as much knowledge from you as my capacity allows me, but there's so much that I am so happy that I still get some time to continue to do so, at least for one more year.

Together with my supervisors, back in 2015, I got to know for the first time the LOCIE Laboratory, and I'm very thankful to this lab since it has given me great colleagues that are so good at what they do, friends on which I can rely, and even a life companion with whom I am creating a future. Many thanks to the directors that I have seen pass and that have always performed their functions with a great sense of responsibility: when I first arrived, my own supervisor, Benoît Stutz, and then Monika Wolozyn. In 2021, a new director assumed the position: Christophe Ménézo. I wish him plenty of success with this adventure, and I am sure that he will do a great job with the support of the wonderful team he has. Of course, many thanks to the technical support team: Jonathan and David, but also to those who were there during my master's project, and that left very good memories: Cédric and Thierry. The same goes for the administrative team: Odile and Pierre (thanks Pierre, for being so committed to unblock the numerous administrative procedures that are part of our everyday life), but also to Elisabeth, Martine, and Isabelle. Merci à tous !

I sincerely thank the members of the jury: Frédéric Lefevre, Wilfrido Rivera, Alberto Coronas, and Florine Giraud, for giving me the honor of reviewing this work. Your very enriching comments have helped me analyze my work from a broader view. I am especially grateful to Wilfrido Rivera, since he placed his confidence in me and in this project since the beginning when I contacted him for the first time back in 2017 to ask him for a letter of support. His support, coming from a great Mexican institution (UNAM), was fundamental to get the financing through which I have been able to do my PhD. For the same reason, I would like to express my gratitude to Alejandro García, Antonio Favela, Armando Céspedes, Vicente Parra, and Julio Noriega, from my Mexican alma mater: Tecnológico de Monterrey. Muchas gracias !

I would like to thank the Mexican Sectorial Fund "CONACYT – SENER – ENERGY SUSTAINABILITY" and the PACs-CAD project for their financial support. And thanks to the SATT Linksum Grenoble Alpes for their support on what comes next. Also, special thanks to the InnoEnergy PhD School Programme of the European Institute of Technology (EIT). Thanks to this program, I learned so much about research, innovation, and entrepreneurship in the energy sector in different top universities around Europe. Moreover, the financed international mobility helped me broaden my vision and strengthen my knowledge in the field. But what is best, the program has allowed me to meet amazing people (some of them I call friends now) contributing to a more sustainable future. Thanks to the team that made this possible, among others, those who were in special contact: Fabien Gauthier, Christine

Durand, and of course Isabelle Schuster, but also the most recent marvelous acquaintances: Madis, Ivan, and Scarlett.

A very special thanks to Alberto Coronas for the opportunity to work with him in the framework of a mobility at the CREVER Research Group of the Rovira I Virgili University, in Spain. It was a great privilege to work surrounded by a group of very competent people, among them I could mention Manel, Dereke, Mahmoud, and Joan Carles (who also was a marvelous office partner), but also Juan, Daniel, and Arturo, with whom I also shared great moments during leisure time. And last but not least, thanks to the group of PhD/Master researchers and friends that I had the chance to meet in Tarragona, we lived so many memorable moments that I will happily remember for the rest of my life.

Now it is time to thank the people that were not directly involved in the technical part of this work, but who were yet a fundamental part to make this happen. Many thanks to my friends in LOCIE. Especially before the sanitary crisis, we were able to enjoy many moments together. It was and continues to be a privilege to exchange with many of the permanent professors: you have no idea of how much I have learned from your experiences (in and outside the lab). Also, many thanks to the post-docs, PhD students, and Master students in the lab for the many moments we shared. Among them, special thanks to the popos multicultural group, or as I call it: the bad hombres group, that was formed as time passed. You made this journey plenty of fun! Finally, I would like to thank the friends and non-blood family that have accompanied me physically far but close to the hearth. During my life I have had the chance to get to know so many wonderful people from all around the world, I wish I could express my gratitude in all your languages, but this goes to all of you: thank you!

This thesis belongs to my family. Muchas gracias a mis papás (Lupita y Amín) por siempre esforzarse para que no nos falte nada ni a mí, ni a mis hermanos: les debemos todo. Muchas gracias a mis hermanos, primos, tíos, y mis abuelitos (en la tierra y en el cielo), por siempre estar ahí y mantenernos unidos a pesar de las circunstancias. Como siempre lo he dicho: la familia es primero! Estou também muito agradecido com a minha família brasileira, que tem me acolhido com muito carinho: muito obrigado por tudo! Y gracias, Lorena, por haberme apoyado desde el inicio de esta aventura y por siempre dar lo mejor de ti con tu amor incondicional: no imagino cómo hubiera sido todo sin ti, y lo mismo con el futuro.

Finally, I would like to thank God for bringing me to Chambéry for the first time in 2012. You indeed work in mysterious ways, and I am at your disposal to see where you will take my life next.

Scientific dissemination

Articles in scientific journals

- Altamirano, A., Le Pierrès, N., Stutz, B., 2019a. Review of small-capacity single-stage continuous absorption systems operating on binary working fluids for cooling: Theoretical, experimental and commercial cycles. *Int. J. Refrig.* 106, 350–373. <https://doi.org/10.1016/j.ijrefrig.2019.06.033>
- Altamirano, A., Stutz, B., Le Pierrès, N., 2020a. Review of small-capacity single-stage continuous absorption systems operating on binary working fluids for cooling: Compact exchanger technologies. *Int. J. Refrig.* 114, 118–147. <https://doi.org/10.1016/j.ijrefrig.2020.02.033>
- Altamirano, A., Le Pierrès, N., Stutz, B., Coronas, A., 2020b. Performance characterization methods for absorption chillers applied to an $\text{NH}_3\text{-LiNO}_3$ single-stage prototype. *Appl. Therm. Eng.* 185, 116435. <https://doi.org/10.1016/j.applthermaleng.2020.116435>.
- Altamirano, A., Stutz, B., Le Pierrès, N., 2020c. Adiabatic desorber for absorption chillers. Submitted to *Heat Transfer Engineering*.

Patents

- Altamirano Cundapí, A., Stutz, B., Le Pierrès, N., 2020. Sorption exchanger (in French). Patent FR 2009477.

Communications in congresses, conferences, seminars, and workshops

- Altamirano, A., Stutz, B., Le Pierrès, N., 2019b. Energetic and exergetic analysis of a solar absorption air conditioning system (in French), Congrès JNES, June 17-19. Annecy le Vieux, France.
- Altamirano, A., Stutz, B., Le Pierrès, N., 2018. Selection of High-Performance Working Fluid for a Solar-Geothermal Absorption Cooling System and Techno-Economic Study in the Northern Mexican Conditions, 12th International Conference on Solar Energy for Buildings and Industry, September 10-13. Rapperswil, Switzerland. <https://doi.org/10.18086/eurosun2018.04.15>
- Altamirano, A., Stutz, B., Le Pierrès, N., Coronas, A., 2020d. Experimental characterization by thermal and mass effectivenesses of plate heat exchangers in $\text{NH}_3\text{-LiNO}_3$ absorption chillers, ISHPC 2021 – Online Pre-Conference. Berlin, Germany, pp. 56–60. <https://doi.org/10.14279/depositonce-10430.2>
- Altamirano, A., Stutz, B., Le Pierrès, N., Coronas, A., 2019c. Modelling of a small-capacity $\text{NH}_3\text{-LiNO}_3$ absorption chiller using thermal and mass effectivenesses of the exchangers, 9th International Seminar on Thermodynamic Engineering of Fluids, July 25-26. Tarragona, Spain.
- Altamirano, A., Stutz, B., Le Pierrès, N., Domain, F., 2019d. $\text{H}_2\text{O-LiBr}$ Single-Stage Solar Absorption Air Conditioner with an Innovative Bi-Adiabatic Configuration: Dynamic Model, Nominal Conditions and Typical Day Operation, Solar World Congress, November 4-7. <https://doi.org/10.18086/swc.2019.55.01>

Participation in projects and IEA Tasks

2017-2020: Mexican sectorial fund “CONACYT-SENER-SUSTENTABILIDAD ENERGÉTICA”, supported by the Mexican Secretary of Energy.

2017-2020: PACs-CAD project (Absorption Heat Pumps Application in District Heating Networks, in French), supported by Interreg France-Switzerland.

2020-2021: Startup project CONFOTHER, supported by the SATT (Technology Transfer Accelerator Office) Linksium.

2020-2024: “Task 65: Solar Cooling for the Sunbelt Regions” of the International Energy Agency.

Internships and training

Internship at the CREVER group from the Rovira I Virgili University (Spain). Host supervisor: Prof. Alberto Coronas. Period: June 3 – October 4, 2019. Subject: Characterization of a small-capacity $\text{NH}_3\text{-LiNO}_3$ absorption chiller through the thermal and mass effectivenesses of its components. Financed by: Innoenergy.

International Summer School on Renewable Energies 2018: “Renewable energies, profitable energies?”, July 8-17, Chamonix (France).

- Award to the best innovative project with the startup SOLITEC. Proposition: food preservation in off-grid regions of sub-Saharan Africa through solar absorption chillers.

Innoenergy PhD School program by the European Institute of Innovation & Technology (EIT).

- “Energy economics” at Grenoble École de Management (GEM), Grenoble (France).
- “Energy solutions design for Eco-Districts” at Grenoble Institute of Technology (INP Grenoble), Grenoble (France).
- “Managing Innovation & Entrepreneurship (MIE)” at ESADE Business School, Barcelona (Spain).
- “Intellectual Property Strategy/Academic Innovator Law” at Uppsala University, Uppsala (Sweden).
- “Data Science Essentials: the case of the wind energy” at Technical University of Denmark (DTU), Roskilde (Denmark).
- Online PhD School Annual Conference. November 25-27, 2020.

List of figures

Figure 1: World primary energy demand by fuel and related CO₂ emissions by scenario (IEA, 2019)...23

Figure 2: World energy use for space cooling by subsector (IEA, 2018a).24

Figure 3: Market development of small to large-scale solar cooling systems worldwide (Weiss et al., 2017).26

Figure 4: Specific costs for ab-/adsorption machines and water- and air-cooled vapor compression chillers (Mugnier et al., 2017).26

Figure I.1: Schematic of a single-effect solar absorption chiller (adapted from (Aliane et al., 2016)). ...33

Figure I.2: Proposed innovations in the vapor purification process of NH₃-H₂O systems. (a) Bubble vapor purifier (Ahachad et al., 1992) and (b) refining spray directly integrated in the desorber (Mendes et al., 2007).38

Figure I.3: NH₃-NaSCN single-stage system's (a) simulated COP against generator temperature ($t_a=t_c=15^\circ\text{C}$, $t_e=-20^\circ\text{C}$) and (b) COP experimental vs. simulated ($t_a=t_c=23^\circ\text{C}$, $t_g=100^\circ\text{C}$) (Zhu et al., 2008).43

Figure I.4: Comparison of COP against generator temperature (a) for the NH₃-H₂O, NH₃-LiNO₃, and NH₃-NaSCN working pairs (Sun, 1998) and (b) for the NH₃-LiNO₃ and NH₃-NaSCN working pairs at different evaporator temperatures ($T_a=T_c=40^\circ\text{C}$) (Cai et al., 2014a).45

Figure I.5: Experimental and simulated COP comparison for the (a) NH₃-LiNO₃ system and the (b) NH₃-NaSCN system (Cai et al., 2016).45

Figure I.6: COP against generator equilibrium temperature ($T_g=T_8$) for a (a) water-cooled ($T_e=5^\circ\text{C}$) and (b) air-cooled single-effect absorption chiller (Marcos et al., 2011).47

Figure I.7: Römich and colleagues' COP against driving temperature for the H₂O-[dema][CH₃SO₃] working fluid, simulated and experimental results ($T_c=T_a=24^\circ\text{C}$, $T_e=11^\circ\text{C}$) (Römich et al., 2011).52

Figure I.8: COP comparison against generator temperature for different binary [(1) H₂O-NaOH, (2) H₂O-LiI, (3) H₂O-LiCl, (4) H₂O-LiBr] and other multi-component working fluids (5 to 16) (Saravanan and Maiya, 1998).53

Figure I.9: Experimental results for different H₂O-ILs and H₂O-LiBr working pairs (Kühn, 2013).53

Figure I.10: Results for COP vs. T_g for the H₂O-LiBr and NH₃-H₂O working fluids at $T_e=2^\circ\text{C}$ (Karakas et al., 1990).56

Figure I.11: Comparison of different working fluids in terms of COP against T_g at $T_a=T_c$ of (a) 30°C and (b) 44°C (Cerezo et al., 2018b).57

Figure I.12: COP vs. T_g for different refrigerant-IL systems (Moreno et al., 2018).58

Figure I.13 Single-stage absorption chillers. (a) Percentage of available brands by working fluid and (b) percentage of the experimental prototypes developed during the past 35 years.58

Figure I.14: Graphical representation of the laboratory-developed prototypes and commercial systems in separate colors by working pair.59

Figure I.15: Graphical representation of the systems grouped by working pair. (a) COP_{exp} vs. COP_{carnot} of laboratory-developed prototypes and (b) COP_{cat}/COP_{exp} vs. COP_{carnot} for the commercial systems and the experimentations performed on them.60

Figure I.16: Control volume of the (a) falling film and (b) two-phase exchangers.63

Figure I.17: Falling film exchanger geometries. (a) Horizontal tubes and (b) vertical surface (either vertical tubes or plates).66

Figure I.18: Different tube surfaces. (a) Smooth tube and (b) integral-fin tube (Fernández-Seara et al., 2009), (c) turbo helix tube (Fernández-Seara and Uhía, 2012), (d) knurled tube, (e) floral tube, and (f) twisted floral tube (Yoon et al., 1999a).69

Figure I.19: Special horizontal tube configurations. (a) Film inverter system (Islam et al., 2003), (b) two-step evaporator/absorber system (for water-based systems) (Dixit, 2018), and (c) helical coil falling film configuration (Kwon and Jeong, 2004).....70

Figure I.20: (a) Microtube absorber (Meacham and Garimella, 2002) and (b) screen mesh as an enhancement method (Goel and Goswami, 2007).71

Figure I.21: Solution distribution device for a microtube generator. (a) Top view and (b) bottom view (Determan and Garimella, 2011).71

Figure I.22: Macrostructuration on PHEs. (a) Comparison of wetting rate for a flat plate and a patterned surface (Mortazavi et al., 2015) and (b) front view and back view of grooved plate absorbers (Michel et al., 2017).73

Figure I.23: (a) Generator/condenser unit diagram, (b) front view and side view of the generator vacuum channel plates, and (b) cross-sectional view of the directly connected spillway solution distributor (Hu et al., 2017).73

Figure I.24: Gonda et al.'s (a) corrugated plate with the distributor, (b) cross-view of the distributor, and (c) falling film image from high-speed camera (Gonda et al., 2014).74

Figure I.25: Two-phase exchanger geometries. (a) Horizontal tubes and (b) vertical surface (either vertical tubes or plates).74

Figure I.26: Bubble absorber distributors. (a) Diagram (Cerezo et al., 2009) and (b) experimental implementation on an Alfa-Laval PHE (Chan-González et al., 2017).75

Figure I.27: Microscale monolithic absorption chiller. (a) Exploded view and (b) individual components on shim A (Determan and Garimella, 2010, 2012).....79

Figure I.28: (a) Diagram and (b) photograph of a membrane-based absorber (Nasr Isfahani and Moghaddam, 2013). (c) Microstructured membrane-based absorber (Nasr Isfahani et al., 2015).81

Figure I.29: Test section of adiabatic absorbers with solution distribution by gravity in the form of droplets and jets (left), and inclined falling film (right) (Arzoz et al., 2005).82

Figure I.30: Functioning diagram of the adiabatic evaporator/absorber configuration, adapted from (Obame Mve, 2014).....84

Figure I.31: Typical two-phase solution distribution methods in an adiabatic exchanger. (a) Falling drops, (b) flat fan sheets (Gutiérrez-Urueta, 2009), and (c) fog jet atomization (Ventas et al., 2012).84

Figure I.32: Diagram of the hydrophobic hollow fiber membrane-based generator (adapted from (Hong et al., 2018)).86

Figure I.33: Exchanger technologies used in the prototypes of single-stage absorption chillers based on the NH₃-H₂O working pair for (a) the absorber and (b) the generator.87

Figure I.34: Exchanger technologies used in the prototypes of single-stage absorption chillers based on the NH₃-LiNO₃ working pair for the (a) absorber and (b) generator.88

Figure I.35: Exchanger technologies used in the prototypes of single-stage absorption chillers based on the NH₃ refrigerant for the (a) evaporator and (b) condenser components.88

Figure I.36: Exchanger technologies used in the prototypes of single-stage absorption chillers based on the H₂O-LiBr working pair for the (a) absorber and (b) generator.89

Figure I.37: Exchanger technologies used in the prototypes of single-stage absorption chillers based on the H₂O refrigerant for the (a) evaporator and (b) condenser components.90

Figure I.38: (a) Mass transfer and (b) heat transfer performance criteria for the absorbers operating with the NH₃-H₂O working fluid.91

Figure I.39: (a) Mass transfer and (b) heat transfer evaluation parameters for absorbers operating with the H₂O-LiBr working fluid.....91

Figure I.40: Absorption ratio (Ra) for the different H₂O-based adiabatic absorbers by (a) continuity of the phases and (b) distribution methods.92

Figure II.1: Control volume of the bubble absorber.113

Figure II.2: Evolution of R with (a) Re_{sol} (Test 1) and (b) Re_{htf} (Test 2), and evolution of (c) ε_m and (d) ε_{th} vs Re_{sol} for both Test 1 and Test 2 in the absorber.....115

Figure II.3: Evolution of (a) R , (b) ϵ_m and (c) ϵ_{th} vs Re_{sol} for the different tested conditions in the desorber.	116
Figure II.4: Simplified diagram of the 10-kW NH_3 - $LiNO_3$ water-cooled absorption chiller developed by Zamora (Zamora, 2012).	118
Figure II.5: Results of the characteristic equation method vs. experimental results represented in the (a) $\Delta\Delta t$ domain and in the (b) COP_{carnot} domain.	124
Figure II.6: Results of the adapted characteristic equation method vs. experimental results in the COP_{carnot} domain.	125
Figure II.7: Evaporator thermal effectiveness against COP_{carnot}	126
Figure II.8: Thermal and mass effectiveness correlations of the exchanger components and correlation factor of the sorption exchangers (solid dots for the nominal experimental effectivenesses values).	127
Figure II.9: Results of the effectiveness method vs. experimental results in the COP_{carnot} domain.	128
Figure II.10: Simulated machine internal solution concentrations and concentration differences at part-load operation.	129
Figure II.11: Equilibrium factor for the sorption components (absorber and generator) in the different tested conditions.	130
Figure II.12: Inlet solution conditions in the absorber and generator. (a) Dynamic viscosity and (b) Reynolds number.	131
Figure II.13: Temperature deviation from the internal solution equilibrium conditions of the (a) heat transfer fluid and the (b) solution.	132
Figure III.1: Diagram of the proposed solar-geothermal absorption cooling system.	140
Figure III.2: Monterrey city maximum solar irradiance in 2017 (SIMA, 2018) and temperature profiles from 1981 to 2010 (SMN, 2018).	141
Figure III.3: Underground temperature profile of Monterrey city for different seasons.	141
Figure III.4: Studied geometry of NH_3 - H_2O single stage absorption cooling system (for the NH_3 - $LiNO_3$ and H_2O - $LiBr$ working fluids, the rectifier is eliminated and points 11 and 12 disappear).	142
Figure III.5: Effect of T_{int} on COP at $T_e=10^\circ C$ and two different generator temperatures ($T_g=75^\circ C$ and $T_g=85^\circ C$).	144
Figure III.6: Effect of T_{int} on Circulation Ratio at $T_e=10^\circ C$ and two different generator temperatures ($T_g=75^\circ C$ and $T_g=85^\circ C$).	144
Figure III.7: Effect of T_g on COP at $T_e=10^\circ C$ and $T_{int}=40^\circ C$	145
Figure III.8: Effect of T_g on COP at $T_e=10^\circ C$ and $T_{int}=40^\circ C$	145
Figure III.9: H_2O - $LiBr$ single effect bi-adiabatic absorption chiller.	149
Figure III.10: Thermal COP and R vs \dot{m}_{p1} for a (a) $\epsilon_m = 0.4$ and (b) $\epsilon_m = 0.6$ in the mass exchangers (● nominal conditions).	151
Figure III.11: (a) Diagram of the integrated solar-geothermal absorption cooling system (adapted from (Altamirano et al., 2018) and (b) Monterrey city climate conditions of the 23 July 2018 (SIMA, 2019).	153
Figure III.12: Studied single-family house. (a) Ground floor and (b) first floor plans, and (c) 1R1C thermal model considering the cooling power and irradiance on the south face.	154
Figure III.13: Evolution of the absorption chiller's external temperatures, the ambient temperature, and home temperature with and without the cooling power.	155
Figure III.14: Evolution of the heat exchanged in the different components of the absorption system for the studied period.	155
Figure III.15: Evolution of the (a) mass contained in the solution and refrigerant storage tanks and the (b) inlet-outlet solution concentrations at the absorber and desorber.	156
Figure III.16: Condensed (\dot{m}_{15}) and evaporated (\dot{m}_{21}) mass flow rates for the studied period.	156
Figure III.17: Operating pressures in the system for the studied period.	157
Figure III.18: Exergy destruction in the main components and total exergy destruction.	157
Figure IV.1: Experimental test facility for the characterization of adiabatic absorbers and desorber for small capacity absorption chillers: (a) 3D design and (b) experimental facility.	166

Figure IV.2: Schematic diagram of the experimental test facility for the characterization of adiabatic generators.167

Figure IV.3: 3D design of the adiabatic sorption exchanger. (a) Isometric view, (b) section side view, and (c) section view A-A.168

Figure IV.4: Experimental and second-order model effectiveness comparison.174

Figure IV.5: Experimental results of the desorber mass effectiveness as function of the inlet solution mass flow rate, for three different $x_{s,i}/Pd$ levels, and with iso- ΔT_s , ieq lines.176

Figure IV.6: Mass effectiveness as function of the inlet solution mass flow rates a three different ΔT_s , ieq and with iso- $x_{s,i}$ lines ($P=4.75$ kPa).177

Figure IV.7: Mass effectivenesses of different investigated desorbers in representative operating conditions. (a) HFM₁ module by Wang et al. (2009) at $x_{s,i}=0.5$, (b) HFM₂ module by Hong et al. (2018) at $T_{s,i}= 80^\circ\text{C}$ and $P=4.7$ kPa, (c) FM₁ module by Ibarra-Bahena et al. (2017) at $x_{s,i}=0.5$ amd 2.56 kPa $<P_v<3.1$ kPa and (d) FM₂ module by Ibarra-Bahena et al. (2020) at $m_{s,i}=90$ kg h⁻¹, $x_{s,i}=0.4978$, and 2.32 kPa $>P_v<3.38$ kPa.179

Figure IV.8: Maximum values of performance evaluation parameters for different adiabatic desorbers. (a) desorbed flow rate per unit volume, (b) desorption mass flux, (c) desorption ratio, and (d) mass effectiveness.181

Figure IV.9: Pressure drop of different desorbers geometries with (a) 220 and (b) 440 mm of length; and hydraulic power requirements for the different desorbers with (c) 220 and (d) 440 mm of length.185

List of tables

Table I.1: In-lab developed prototypes of small-capacity $\text{NH}_3\text{-H}_2\text{O}$ absorption cooling systems and operating conditions. -----	39
Table I.2: $\text{NH}_3\text{-H}_2\text{O}$ small-capacity commercial absorption chillers and their catalog data. -----	39
Table I.3: Experimental studies on small-capacity commercial $\text{NH}_3\text{-H}_2\text{O}$ absorption chillers reporting the operating conditions. -----	40
Table I.4: In-lab developed prototypes of small-capacity $\text{NH}_3\text{-LiNO}_3$ absorption cooling systems and operating conditions. -----	41
Table I.5: In-lab developed prototypes of small-capacity $\text{NH}_3\text{-NaSCN}$ absorption cooling systems and operating conditions. -----	42
Table I.6: In-lab developed prototypes of small-capacity $\text{H}_2\text{O-LiBr}$ absorption cooling systems and operating conditions. -----	48
Table I.7: $\text{H}_2\text{O-LiBr}$ small-capacity commercial absorption chillers and their catalog data.-----	49
Table I.8: Experimental studies on small-capacity commercial $\text{H}_2\text{O-LiBr}$ absorption chillers reporting the operating conditions. -----	51
Table I.9: In-lab developed prototypes of small-capacity $\text{H}_2\text{O-IL}$ absorption cooling systems and operating conditions. -----	52
Table I.10: In-lab developed prototypes of small-capacity absorption cooling systems with refrigerant bases other than H_2O and NH_3 and operating conditions. -----	56
Table I.11: Falling film exchangers for absorption chillers: experimental results (~: approximated data).-----	67
Table I.12: Two-phase and membrane-plate-based exchangers in absorption chillers: experimental results (~: approximated data). -----	76
Table I.13: Adiabatic exchangers in absorption chillers: experimental results (~: approximated data). -	83
Table I.14: In-Lab-developed prototypes of small-capacity NH_3 -based absorption cooling systems and the exchanger technologies used in their main components. -----	87
Table I.15 In-Lab-developed prototypes of small-capacity $\text{H}_2\text{O-LiBr}$ absorption cooling systems and the exchanger technologies used in their main components. -----	89
Table I.16: Comparison of the main binary working fluids studied for single-stage absorption cooling.	93
Table I.17: General comparison for the different technologies of exchangers used in small-capacity single-stage absorption chillers operating with binary working fluids. -----	94
Table II.1: Geometrical characteristics of the studied absorber (Amaris Castilla, 2013) and desorber (Zacaría Santiago, 2009).-----	114
Table II.2: Experimental operating conditions of the tested absorber (Amaris Castilla, 2013) and desorber (Zacaría Santiago, 2009).-----	114
Table II.3: Operating conditions of the characterized $\text{NH}_3\text{-LiNO}_3$ absorption chiller prototype (Zamora, 2012).-----	118
Table II.4: Experimental results of the characterization test campaign of the $\text{NH}_3\text{-LiNO}_3$ absorption chiller prototype (Zamora, 2012).-----	119
Table II.5: Coefficients of the characteristic equation (Eqs. (II.18)-(II.20)) (Ochoa and Coronas, 2016).-----	123
Table II.6: Coefficients of the adapted characteristic equation (Eqs. (II.25)-(II.27)). -----	125
Table II.7: Coefficients of the Carnot function model for the cooling capacity and COP (Eq. (II.28)).	125
Table II.8: Evaporator internal and external operating temperatures.-----	126
Table II.9: Condenser internal and external temperature operating conditions. -----	126
Table II.10: Thermal and mass effectiveness correlations of the system components for the range of $\text{COP}_{\text{carnot}} \in [1.2; 3.4]$.-----	128

Table III.1: Requirements and dimensioning for the studied conditions and the three studied working fluids. ----- 146

Table III.2: Economic data for the initial investment of the solar-geothermal absorption cooling system.----- 147

Table III.3: Considered costs for the initial investment of the solar-geothermal absorption cooling system and economic analysis considering two scenarios. ----- 148

Table IV.1: Operating conditions and uncertainties. ----- 170

Table IV.2: Four-variables Doehlert design for the desorber characterization. The coded variable values are represented in parenthesis. ----- 171

Table IV.3: Experimental results of the four-variables Doehlert design for the desorber characterization. ----- 173

Table IV.4: Fitted coefficients of the mass effectiveness function (Eq. (IV.9)) with the experimental results of tests 1-28 (Table IV.3). ----- 174

Table IV.5: Adiabatic desorbers for absorption chillers: experimental results (~: approximated data).182

Table IV.6: Non-adiabatic desorbers for absorption chillers: experimental results (~: approximated data). ----- 182

Table IV.7: Geometrical characteristics of the desorbers used for the comparison of the pressure drop.----- 184

Nomenclature

<i>A</i>	enthalpy coefficient (-) or area (m ²)
<i>a</i>	thermal diffusivity (m ² s ⁻¹)
<i>a</i> ₁	linear coefficient of a solar thermal collector (K m ² kW ⁻¹)
<i>a</i> ₂	quadratic coefficient of a solar thermal collector (K m ² kW ⁻¹)
<i>a</i>	characteristic parameter (-)
<i>B</i>	isostere slope in a Dühring chart (-)
<i>B</i> _{solar}	solar gain factor (-)
<i>b</i>	characteristic parameter (-)
<i>C</i>	enthalpy coefficient (-)
<i>c</i>	characteristic parameter (-)
<i>CE</i>	characteristic equation
<i>CFM</i>	Carnot function model
<i>COP</i>	coefficient of performance (-)
<i>C_D</i>	coefficient of Darcy friction factor
<i>C_p</i>	heat capacity (kJ kg ⁻¹ K ⁻¹)
<i>CR</i>	circulation ratio
<i>C_{th}</i>	thermal capacitance (Wh K ⁻¹)
<i>D</i>	diameter
<i>d</i>	observed day of the year (s)
<i>d_c</i>	coldest day (s)
<i>e</i>	characteristic parameter (-)
<i>EM</i>	effectiveness model
<i>F</i>	Carnot function model parameter (-)
<i>F_{ad}</i>	adiabatic equilibrium factor (-)
<i>f_D</i>	Darcy friction factor
<i>G</i>	enthalpy coefficient (-)
<i>G*</i>	global horizontal solar irradiance (W m ⁻²)
<i>H</i>	specific enthalpy (kJ kg ⁻¹)
<i>h</i>	heat transfer coefficient (W m ⁻² K ⁻¹)
<i>HT</i>	horizontal tube
<i>HTF</i>	heat transfer fluid
<i>K</i>	overall mass transfer coefficient (m s ⁻¹)
<i>k(θ)</i>	solar thermal collector tilt angle factor (-)
<i>M</i>	mass content (kg)
<i>ṁ</i>	mass flow rate (kg s ⁻¹)
<i>m̈"</i>	mass flux (kg m ⁻² s ⁻¹)
<i>n</i>	depth (m)
<i>P</i>	pressure (kPa)
<i>p</i>	wetted perimeter (m)
<i>PHE</i>	plate heat exchanger
<i>PR</i>	pumping ratio
<i>Q̇</i>	heat transfer rate (kW)
<i>Q̈"</i>	heat flux (W m ⁻²)
<i>q</i>	characteristic parameter (kW K ⁻¹)
<i>q'</i>	characteristic parameter (-)
<i>R</i>	equilibrium factor (-)
<i>r</i>	characteristic parameter (-)
<i>Ra</i>	absorption ratio (-)
<i>Re</i>	Reynolds number (-)
<i>Rd</i>	desorption ratio (-)
<i>RHX</i>	refrigerant heat exchanger
<i>R_{th}</i>	thermal resistance (K W ⁻¹)
<i>S</i>	solar thermal collector area (m ²)
<i>s</i>	specific entropy (kJ kg ⁻¹ K ⁻¹)
<i>SHX</i>	solution heat exchanger
<i>T</i>	internal absorption chiller temperature (K)

Subscripts and superscripts

<i>0</i>	Carnot function model y-intercept
<i>a</i>	absorber
<i>abs</i>	absorption
<i>ac</i>	absorber/condenser parallel flow
<i>ad</i>	adiabatic
<i>amb</i>	ambient
<i>avg</i>	average
<i>c</i>	condenser or characteristic equation variable
<i>c'</i>	adapted characteristic equation variable
<i>cat</i>	catalog
<i>cfm</i>	Carnot function model
<i>col</i>	collector
<i>cool</i>	cooling
<i>corr</i>	correlated
<i>cv</i>	coded variable
<i>d</i>	desorber
<i>dead</i>	dead state
<i>dist</i>	distributor
<i>e</i>	evaporator
<i>eff</i>	effective
<i>eq</i>	equilibrium
<i>exp</i>	experimental
<i>ff</i>	falling film
<i>g</i>	generator
<i>h</i>	high
<i>htf</i>	heat transfer fluid
<i>hyd</i>	hydraulic
<i>i</i>	inlet
<i>int</i>	intermediate
<i>iso</i>	isothermal
<i>l</i>	low
<i>loss</i>	solution heat exchanger loss
<i>m</i>	mass
<i>max</i>	maximum
<i>nom</i>	nominal
<i>o</i>	outlet
<i>p</i>	pump
<i>ref</i>	refrigerant
<i>sat</i>	saturation
<i>s</i>	solution
<i>sink</i>	heat sink
<i>sorp</i>	sorption
<i>st</i>	storage tank
<i>th</i>	thermal
<i>v</i>	vapor
<i>w</i>	wall

Accentuation

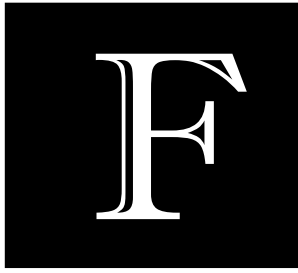
~	undisturbed by the exchanger
---	------------------------------

Nomenclature

T_{amp}	yearly amplitude of the ground-level temperature (K)
t	external absorption chiller temperature (K)
U	overall heat transfer coefficient ($\text{W m}^{-2} \text{K}^{-1}$)
UA	heat transmission (kW K^{-1})
V	volume (m^3)
v	velocity (m s^{-1})
VT	vertical tube
\dot{V}	volumetric flow rate ($\text{m}^3 \text{h}^{-1}$)
\dot{W}	work transfer (kW)
WF	working fluid
x	absorbent solution mass fraction (kg kg^{-1})
z	arithmetic temperature difference correction factor

Greek letters

α	characteristic parameter (-)
β	coefficient of the effectiveness' second degree polynomial
γ	kinematic viscosity ($\text{m}^2 \text{s}^{-1}$)
Δ	differential quantity
ΔT_{lm}	log-mean temperature difference (K)
$\Delta \Delta t$	characteristic temperature difference (K)
$\Delta \Delta t'$	adapted characteristic temperature difference (K)
$\Delta \Delta t_{min}$	minimum temperature difference (K)
ΔX_{lm}	log-mean mass concentration difference
δ	wall thickness (m)
ε	effectiveness
η_0	solar thermal collector optical efficiency
η_{col}	solar thermal collector efficiency
θ	inclination angle of the solar panel ($^\circ$)
λ	thermal conductivity ($\text{W m}^{-1} \text{K}^{-1}$)
ν	kinematic viscosity ($\text{mm}^2 \text{s}^{-1}$)
ρ	density (kg m^{-3})
τ	Carnot function model parameter (-)
ϕ	annual pulse (rad s^{-1})
ψ	specific exergy (kJ kg^{-1})
ω	Carnot function model parameter (-)



rench summary

The present section provides a detailed summary of the PhD work in French.

“

“L’intelligence ne vaut qu’au service de l’amour.”

“Intelligence has value only in the service of love.”

– Antoine de Saint-Exupéry

Introduction Générale

Contexte énergétique

En raison de la croissance démographique mondiale et du développement économique, en particulier dans les pays en voie de développement, la consommation énergétique augmente à un rythme alarmant. L'augmentation de la demande énergétique mondiale entre 2000 et 2040 devrait être d'environ 91% (de 10037 à 19177 Mtep, [Figure 1](#)). En outre, 78% de l'énergie totale consommée en 2040 proviendra des combustibles fossiles (dont la combustion génère de la pollution et contribue au réchauffement climatique). Cela ne représente pratiquement aucun changement par rapport à la part de 80 % qu'ils représentent aujourd'hui (IEA, 2019).

Le secteur du bâtiment est le secteur le plus consommateur d'énergie avec 35% de la consommation finale (IEA, 2019). Dans ce secteur, le besoin de refroidissement des locaux représente aujourd'hui 20 % de l'électricité totale consommée, et cette demande augmente plus vite que toute autre consommation finale dans les bâtiments, atteignant une part de 30 % d'ici 2050 (IEA, 2018a). En outre, la consommation d'énergie finale pour la climatisation dans le secteur du bâtiment a plus que triplé en 26 ans (de 1990 à 2016), et elle devrait encore tripler d'ici 2050 ([Figure 2](#)), environ 70% de cette augmentation provenant du secteur résidentiel, majoritairement des économies émergentes (IEA, 2018a).

La quasi-totalité de l'énergie consommée pour le rafraîchissement des locaux est sous forme d'électricité pour faire fonctionner des climatiseurs à compression de vapeur. Seulement 1% environ est sous forme de gaz naturel pour actionner des climatiseurs à absorption dans des bâtiments à usage industriel (IEA, 2018a). Cette dépendance à l'égard de l'électricité a engendré une série de problèmes et de défis pour l'environnement et le réseau de distribution d'électricité dans les pays à climat chaud (Casals, 2006). En effet, dans certaines régions du monde, cette demande de refroidissement atteint plus de 70% de la puissance électrique résidentielle de pointe pendant les journées chaudes (IEA, 2018a).

Le Mexique est un acteur important dans l'augmentation de la demande de refroidissement. Sa consommation d'énergie pour le refroidissement des bâtiments a été multipliée par plus de cinq entre 1990 et 2016 (de 7 à 37 TWh), représentant aujourd'hui 9,8% de l'énergie totale consommée dans les bâtiments, ce qui constitue la deuxième proportion la plus élevée dans un pays, juste après les États-Unis (IEA, 2018a). Par ailleurs, cette consommation d'énergie devrait encore être multipliée par 4 d'ici 2050 (IEA, 2018a).

Le Mexique est également le deuxième pays au monde ayant la plus grande part d'électricité utilisée pour le refroidissement des locaux, avec 14% déjà aujourd'hui. Même si les politiques et les objectifs déjà annoncés par le gouvernement sont mis en œuvre, cette part devrait passer à plus de 23 % d'ici 2050, ce qui signifie que le refroidissement représentera plus de 25 % de l'augmentation des émissions totales de CO₂ (la part la plus élevée au monde) (IEA, 2018a). En effet, le besoin de refroidissement du Mexique, mesuré en degrés-jours de refroidissement, devrait augmenter de 36,8 % de 2016 à 2050, ce qui représente la plus forte augmentation de tous les pays du monde (IEA, 2018a).

Sur le plan énergétique et économique, le Mexique est fortement dépendant des combustibles fossiles. En 2013, le secteur pétrolier a généré 13 % des recettes d'exportation du pays et 33 % des revenus de l'État (Alpizar-Castro and Rodríguez-Monroy, 2016). L'instabilité du prix du pétrole et sa baisse constante au cours des dernières années ont généré des difficultés et des inquiétudes économiques dans le pays. Jusqu'à présent, la demande croissante d'énergie est principalement couverte par les combustibles fossiles. En 2014, 93 % de la consommation totale d'énergie provenait du pétrole (45 %), du gaz naturel (40 %) et du charbon (8 %) (Pérez-Denicia et al., 2017).

Au Mexique, la réforme énergétique récemment approuvée a montré un manque d'expertise pour faire face aux défis énergétiques des prochaines années. Si aucun changement n'est apporté à la stratégie énergétique du pays, les chiffres alarmants concernant sa demande énergétique pour le refroidissement et sa dépendance aux combustibles fossiles laissent entrevoir une crise économique et énergétique dans les prochaines décennies.

Le Mexique doit opérer un changement dans sa politique énergétique. Entre autres possibilités, des efforts doivent être déployés pour la mise en place de systèmes utilisant des énergies renouvelables, comme l'énergie solaire, qui sont jusqu'à présent peu exploitées (Alpizar-Castro and Rodríguez-Monroy, 2016). Ce type d'actions serait non seulement utile pour équilibrer les flux énergétiques et les revenus économiques du pays, mais elles s'inscrivent également dans le cadre des différents efforts internationaux visant à protéger la couche d'ozone et à réduire l'impact du changement climatique, tels que le protocole de Montréal, le protocole de Kyoto et l'accord de Paris.

Les refroidisseurs solaires à absorption

La dépendance aux combustibles fossiles, le coût élevé de l'électricité et le réchauffement climatique figurent parmi les principaux obstacles pour couvrir les besoins énergétiques croissants dans le secteur du bâtiment. Dans ce contexte, l'énergie solaire est l'une des ressources énergétiques les plus intéressantes pour la climatisation car elle est largement répandue, abondante, inépuisable et propre (Bellos et al., 2016; Jafari and Poshtiri, 2017). Le Mexique possède l'avantage de se situer dans la ceinture solaire du monde (pays situés entre les latitudes de 20 et 40 degrés), qui correspond à des pays chauds avec des niveaux d'irradiation élevés permettant de faire fonctionner des refroidisseurs solaires thermiques.

Les refroidisseurs à absorption sont des systèmes consommant de la chaleur, remplaçant la compression mécanique des systèmes de réfrigération classiques par une compression thermochimique. Différentes configurations existent ; toutefois, la configuration à simple-étage est la plus avantageuse pour des applications de refroidissement solaire dans le secteur du bâtiment résidentiel en termes de coût, de faibles températures de source, de taille et de simplicité (Hassan and Mohamad, 2012). Même si d'autres technologies de refroidissement thermochimiques existent, telles que les systèmes à adsorption, à dessiccation ou à éjection, le principal avantage des systèmes à absorption est leur coefficient de performance (COP) plus élevé (Best and Rivera, 2015; Hassan and Mohamad, 2012). De plus, le couplage des machines à absorption avec l'énergie solaire thermique est une alternative très prometteuse, car le niveau d'irradiation est plus élevé lorsque le besoin de refroidissement est le plus important (Dube et al., 2017; Kim and Ferreira, 2008a). En outre, les panneaux solaires thermiques peuvent également être utilisés pour le chauffage des bâtiments ou pour la production d'eau chaude sanitaire en hiver (IEA, 2018a).

La pertinence des refroidisseurs à absorption dépend de plusieurs critères économiques, politiques, industrielles et géographiques (Herold et al., 2016). Malgré leurs différents avantages tels que l'utilisation d'énergies renouvelables, les faibles coûts d'exploitation et de maintenance, les bonnes performances thermiques et la faible nuisance sonore, ils constituent à ce jour une technologie de niche, comme décrit précédemment. En ce qui concerne le refroidissement solaire, ce marché de niche a connu une augmentation lente mais constante, passant de 40 unités installées en 2004 à 1 350 à la fin 2015 (Figure 3), dont 80 % en Europe (Mugnier and Jakob, 2015; Weiss et al., 2017).

Les principaux obstacles au déploiement à grande échelle des refroidisseurs à absorption sont leur coût d'achat élevé et leur faible compacité (Altamirano et al., 2019a). Cela est particulièrement vrai pour des applications de petite puissance (Figure 4), comme dans le secteur du refroidissement résidentiel. En effet, les systèmes à compression de vapeur classiques demandent une technologie de compresseur différente

pour des puissances supérieures à 250 kW afin de traiter un flux de vapeur de réfrigérant plus important, ce qui augmente leur coût et les rend encore légèrement plus chers que les refroidisseurs à absorption. Le marché des refroidisseurs à absorption devrait toutefois se développer à mesure que les coûts de production seront abaissés. Leurs coûts ont déjà été réduits de plus de la moitié depuis 2007, principalement grâce à la standardisation des équipements, ce qui fait que ces systèmes sont de plus en plus utilisés et semblent être une véritable alternative pour le refroidissement résidentiel, des petits commerces et des applications industrielles (Zhu and Gu, 2010). Néanmoins, à ce jour, leur coût n'est toujours pas compétitif par rapport aux refroidisseurs électriques (IEA, 2018a).

En raison de leur potentiel à satisfaire une grande partie de la demande énergétique croissante pour le rafraîchissement des locaux, la R&D en matière de systèmes de rafraîchissement solaire thermique fait partie des jalons technologiques pour parvenir à des bâtiments à haute efficacité énergétique selon le rapport Perspectives des Technologies de l'Energie de l'agence internationale de l'énergie (AIE) (IEA, 2012). De plus, ces systèmes sont inclus dans le Plan Stratégique de l'AIE pour le Chauffage et le Refroidissement Solaire - Technologies Clés (IEA, 2018b). Le rafraîchissement solaire a déjà fait l'objet de quatre Tâches SHC de l'AIE (n° 25, n° 38, n° 48 et n° 53), et une nouvelle Tâche (Tâche n° 65) a été lancée en 2020 pour adapter, vérifier et promouvoir le refroidissement solaire comme une solution abordable et fiable à la demande croissante de rafraîchissement dans les pays de la ceinture solaire tels que le Mexique (IEA, 2020).

Afin d'obtenir une plus grande part de marché dans le secteur du refroidissement résidentiel, d'un point de vue technologique, les refroidisseurs à absorption doivent encore réduire leur coût de production (par la simplification des procédés de fabrication), augmenter leur compacité et accroître leur efficacité (Altamirano et al., 2020b, 2019a; IEA, 2018a; Mugnier et al., 2017). D'autre part, d'un point de vue politique, la stimulation du marché est nécessaire par le biais de réglementations gouvernementales (Herold et al., 2016). En ce qui concerne la R&D, différentes solutions ont déjà été étudiées, telles que la recherche d'un couple de travail idéal (couple réfrigérant/absorbant), de nouvelles technologies d'échangeurs de chaleur et de masse, l'emploi de nouvelles méthodes de fabrication, une source de dissipation thermique mieux adaptée et des architectures de machines innovantes (Altamirano et al., 2020b, 2019a).

Objectifs de recherche et organisation de la thèse

L'objectif principal de cette thèse est le développement d'une nouvelle génération de refroidisseurs à absorption compacts et à faible coût pour des applications dans les pays de la ceinture solaire comme solution abordable et écologique aux besoins croissants de refroidissement dans le secteur résidentiel. Pour cela, les différents verrous technologiques et scientifiques mentionnés précédemment (le fluide de travail, la technologie des échangeurs, l'architecture de la machine, le dissipateur thermique et la méthode de fabrication) sont abordés. Le cas mexicain est plus spécifiquement étudié en raison des défis présentés précédemment. Pour atteindre ces objectifs, les questions suivantes restent à résoudre :

1. Quel est l'état de l'art des fluides de travail et des technologies des échangeurs utilisés dans les refroidisseurs à absorption ?
2. Existe-t-il des fluides de travail et des technologies d'échangeurs qui pourraient être viables sur le plan commercial et technologique pour un refroidisseur à absorption de petite puissance ?
3. Quels sont les critères les plus adaptés pour la caractérisation et l'évaluation des performances des composants de sorption dans les refroidisseurs à absorption ?
4. Quelles sont les méthodes de modélisation les plus adaptées pour les refroidisseurs à absorption ?

5. La climatisation à absorption solaire pour le secteur résidentiel est-elle techniquement et économiquement réalisable dans le contexte mexicain ?
6. Des modifications de l'architecture de la machine sont-elles une option pour réduire le coût des refroidisseurs à absorption ?
7. Comment les nouvelles méthodes de fabrication peuvent-elles être utilisées pour créer une nouvelle génération de refroidisseurs à absorption compacts et à faible coût ?

Afin de répondre aux objectifs de recherche, la thèse a été structurée en 3 chapitres qui se basent sur les résultats présentés dans des articles de revues et de conférences. Un résumé détaillé de ces chapitres est présenté ci-après.

Chapitre I. État de l'art sur les refroidisseurs à absorption à simple étage

Afin de développer une nouvelle génération de refroidisseurs à absorption compacts et peu coûteux basés sur une nouvelle technologie d'échangeur à sorption, de sélectionner le fluide de travail le plus adapté aux applications résidentielles dans les pays ensoleillés comme le Mexique et de proposer des innovations en matière d'architecture des machines, il est nécessaire de procéder à un bilan approfondi de l'état de l'art. Les systèmes à absorption peuvent être classés en fonction de différents critères. Par exemple, la source de chaleur, le type de dissipateur thermique, le nombre d'étages, le fluide de travail, l'application, la puissance ou le fonctionnement continu/discontinu. Compte tenu de leur cycle thermodynamique, les systèmes de réfrigération à absorption peuvent être divisés en trois catégories : les cycles à simple effet, à demi-effet et à multi-effet (par exemple à double ou triple effet) (Alefeld and Radermacher, 1993; Ziegler and Alefeld, 1987). Les cycles à simple effet et à demi-effet nécessitent des températures de source plus basses que les cycles à multi-effet (Aliane et al., 2016). Parmi toutes les configurations possibles, la configuration à simple effet est la plus avantageuse en termes de coût, de basses températures de source et de simplicité (Hassan and Mohamad, 2012). De plus, c'est la plus disponible sur le marché. Deux couples d'absorption sont couramment rencontrés : $\text{H}_2\text{O-LiBr}$ (eau-bromure de lithium) et $\text{NH}_3\text{-H}_2\text{O}$ (ammoniac-eau). Un système à absorption à simple étage classique comprend un évaporateur, un condenseur, un absorbeur, un générateur (parfois aussi appelé désorbeur), une pompe de solution, un échangeur de chaleur de solution (SHX) et deux vannes, comme le montre la [Figure I.1](#). La solution dans le générateur absorbe de la chaleur et désorbe de la vapeur de réfrigérant. Cette vapeur est condensée au niveau du condenseur avant de passer par une vanne de détente et d'être à nouveau vaporisée à une pression et une température plus faibles au niveau de l'évaporateur. La chaleur d'évaporation est prélevée à la source froide. La vapeur produite par l'évaporateur est absorbée par la solution pauvre (en réfrigérant) dans l'absorbeur. La solution riche qui en résulte est pompée de l'absorbeur vers le générateur, où le cycle recommence (Best and Rivera, 2015). Un échangeur de chaleur de solution (SHX) est ajouté entre l'absorbeur et le générateur pour augmenter l'efficacité de la machine par récupération de chaleur interne. Lorsqu'un sorbant volatil est utilisé, tel que pour le couple ammoniac/eau, un étage de purification de la vapeur doit être ajouté après le générateur pour améliorer la pureté du réfrigérant (Bogart, 1981; Ullah et al., 2013). Un échangeur de chaleur de réfrigérant (RHX) peut également être ajouté entre les débits d'entrée et de sortie de l'évaporateur comme méthode de récupération de chaleur interne, mais l'effet du SHX sur la performance globale du système est plus important (Herold et al., 2016; Shiran et al., 1982). De plus, un réservoir de stockage peut être mis en place dans le circuit de chauffe pour absorber les variations du flux de chaleur au niveau du générateur (Aliane et al., 2016).

Les systèmes à absorption existent depuis plus d'un siècle. Malgré leurs multiples avantages, leur faible compacité et leur coût élevé constituent deux des principaux inconvénients qui bloquent leur développement dans le secteur du rafraîchissement résidentiel. Actuellement, différentes équipes de recherche se concentrent sur l'amélioration de ces systèmes. Un exemple en est la recherche du réfrigérant

idéal, pour lequel, outre de bonnes propriétés thermiques, une préoccupation pour son impact environnemental s'est accrue ces dernières années (Calm, 2008). Le choix du réfrigérant est lié aux exigences spécifiques de l'application envisagée et a une grande influence sur la technologie et la configuration des échangeurs du système (Wu et al., 2014). Par ailleurs, contrairement aux systèmes de compression de vapeur classiques, l'étude de réfrigérants alternatifs dans les systèmes à absorption conduit à un autre domaine d'étude important qui est l'étude de la combinaison réfrigérant-absorbant (fluide de travail) la plus adaptée (Herold et al., 2016). Une autre voie de recherche est la quête de nouvelles technologies d'échangeurs compacts, qui pourraient réduire la taille du système et, si possible, son coût.

Analyse des cycles théoriques, expérimentaux et commerciaux

Ce premier chapitre fournit un aperçu global actualisé des systèmes à absorption continus à simple étage de petite puissance fonctionnant avec des couples de travail binaires pour le refroidissement, d'un point de vue théorique, expérimental et commercial. La limite supérieure du terme "petite puissance", en fonction de l'auteur, peut aller de 20 à 100 kW (Anies, 2011; Kühn, 2013; J. M. Labus et al., 2013; Zhai and Wang, 2009). Dans le cadre de ce travail, seuls les systèmes d'une puissance de 50 kW ou moins ont été abordés.

Afin de sélectionner un fluide de travail, différents aspects doivent être pris en compte en fonction de l'application souhaitée et des objectifs les plus importants à atteindre. Le choix du système doit être orienté non seulement vers les performances du cycle thermodynamique, mais aussi vers d'autres facteurs qui pourraient avoir un impact pour l'application réelle du système, qu'ils soient technologiques (propriétés connues, pressions et températures de fonctionnement, sécurité, prévention de la corrosion, rendement exergetique, moyen de dissipation thermique, type de source motrice et durée de vie du système), économiques (coût initial du système et des composants externes, coût du couple de travail, coûts de fonctionnement, gains économiques en fonction de l'évolution du prix de l'électricité et de l'inflation), ou même sociétaux (potentiel de réchauffement climatique et utilisation d'énergies renouvelables).

Dans le cas des couples de travail à base d'ammoniac comme réfrigérant, les nouveaux absorbants LiNO_3 et NaSCN semblent être de bons candidats pour remplacer l'eau. Toutefois, des études visant à obtenir des performances expérimentales satisfaisantes pour ces systèmes et des études économiques doivent être réalisées avant le lancement commercial d'une machine.

Dans le cas des systèmes avec l'eau comme réfrigérant, le couple $\text{H}_2\text{O-LiBr}$ reste le plus fiable et le plus adapté. Les autres candidats étudiés jusqu'à présent ne semblent pas présenter suffisamment d'avantages pour surmonter les inconvénients qui leur sont associés. Le couple $\text{H}_2\text{O-LiCl}$ a une performance théorique supérieure ; cependant, les risques de cristallisation sont plus élevés pour ce couple de travail que pour le couple $\text{H}_2\text{O-LiBr}$, pour lequel ce risque est déjà important. Par conséquent, un système commercial basé sur le couple de travail $\text{H}_2\text{O-LiCl}$ pour un cycle continu semble difficile. L'intérêt pour les liquides ioniques a connu une forte croissance ces dernières années en raison de leurs excellentes propriétés physiques et thermiques ; toutefois, des études plus approfondies sont nécessaires pour garantir leur performance et leur faible impact sur l'environnement à long terme. De nouveaux liquides ioniques respectueux de l'environnement et des solvants eutectiques provenant de sources naturelles telles que les acides organiques ou les acides aminés, ayant des propriétés similaires aux liquides ioniques et qui sont prétendument non toxiques et biodégradables, pourraient constituer la future orientation de ce domaine de recherche (Cvjetko Bubalo et al., 2014).

D'autre part, les hydrofluorocarbures (HFC) ne semblent pas être une option pour l'avenir puisque la plupart d'entre eux ont un potentiel de réchauffement climatique élevé et que, dans tous les cas, ils seront interdits en vertu de l'amendement de Kigali au protocole de Montréal (IEA, 2018a). Enfin, les alcools

semblent être mieux adaptés aux applications de chauffage et de pompes à chaleur. Aucun des couples étudiés (Figure I.13) n'a montré d'avantages particuliers en termes de performances par rapport aux couples de travail classiques H₂O-LiBr et NH₃-H₂O (Figure I.14 et Figure I.15). Le CO₂ a également été proposé ces dernières années comme réfrigérant pour les systèmes de refroidissement à absorption et pourrait être une option à l'avenir ; cependant, de nouveaux absorbants pour ce réfrigérant doivent être étudiés pour de meilleures performances et une attention particulière doit être accordée à ses pressions de fonctionnement élevées, qui posent de nouveaux défis en termes de conception.

Il est nécessaire d'obtenir davantage d'informations sur les interactions physiques et les propriétés de surface des nouveaux couples de travail (par exemple, le mouillage des surfaces ou la formation de gouttelettes) pour conduire à des systèmes plus efficaces. Des études doivent être menées dans la recherche de nouveaux additifs pour induire l'effet Marangoni, de meilleures propriétés de mouillabilité et une diminution de la corrosion (Seiler et al., 2013).

Analyse des technologies d'échangeurs compacts

Cette deuxième partie se concentre sur les études de technologies innovantes d'échangeurs à géométrie conventionnelle ou spécifique, avec ou sans traitements mécaniques, en portant une attention particulière aux études expérimentales. Le choix de la technologie des échangeurs est d'une grande importance et doit prendre en compte un grand nombre de critères en fonction de l'application spécifique. Outre le potentiel de transfert de chaleur et de masse, d'autres facteurs tels que le coût de fabrication, le fluide caloporteur et le type de source à utiliser, le fluide de travail, la compacité requise, le poids, la complexité technique, la puissance requise, la plage de températures de refroidissement, une application mobile ou fixe, entre autres, sont d'une importance fondamentale.

Les technologies à film tombant (Figure I.17) sont les géométries les plus couramment utilisées pour l'échange de chaleur et de masse car elles sont les plus polyvalentes et adaptables aux différents fluides de travail utilisés dans les technologies de refroidissement par absorption. Historiquement, les tubes horizontaux ont été la technologie prédominante dans les machines à absorption commerciales. Cependant, elles ne sont pas les plus efficaces en termes de poids et de compacité (Yoon et al., 2006). Dans la recherche d'autres options, les échangeurs de chaleur à plaques ont été étudiés expérimentalement comme composants des systèmes à absorption en raison de leur faible coût, de leur performance élevée et de leur compacité. De nouvelles technologies ont été étudiées pour améliorer les transferts de chaleur et de masse dans les composants des systèmes à absorption tels que les absorbeurs à bulles (Figure I.26), les échangeurs à microcanaux (Figure I.20), les absorbeurs ou désorbeurs à membrane (Figure I.28) et les absorbeurs adiabatiques (section 1.3.3). Les absorbeurs à film tombant à microtubes présentent une bonne performance parmi les technologies de tubes horizontaux pour les systèmes utilisant le NH₃ (Figure I.38). Cependant, il faut accorder une attention particulière aux pertes de charge du côté du fluide caloporteur, qui peuvent être contrôlées en modifiant la configuration de l'écoulement (Garimella, 1999). Les absorbeurs à membrane semblent être une technologie prometteuse pour surmonter les inconvénients des films tombants (Figure I.38, Figure I.39, et Figure I.40). Toutefois, la durabilité des membranes dans le temps reste à étudier. En effet, les pores pourraient avoir tendance à s'obstruer lors de l'utilisation d'absorbants salins (Riffat et al., 2004; Wang et al., 2009). D'autre part, le potentiel des absorbeurs adiabatiques doit encore être étudié de manière approfondie. De nouvelles méthodes de distribution ou géométries d'échangeurs auraient un impact significatif sur les performances de l'ensemble du système.

Enfin, l'analyse des technologies d'échangeurs a permis de constater qu'il n'existe pas de critères de caractérisation standard pour l'évaluation des performances des échangeurs à sorption dans les refroidisseurs à absorption. Les coefficients et les flux de transfert de chaleur couramment utilisés, adaptés des modèles d'échangeurs de chaleur classiques, négligent la chaleur de sorption. Quant à la définition

des coefficients de transfert de masse, elle varie selon les auteurs. Pour cette raison, le Chapitre II introduit le concept d'efficacités thermique et massique dans le contexte général des échangeurs à sorption. Ces efficacités sont mises en œuvre dans la simulation globale d'une machine.

Chapitre II. Les efficacités thermique et massique comme outil pour la caractérisation des refroidisseurs à absorption et comparaison de modèles

D'après l'état de l'art du Chapitre I, l'absorbeur et le désorbeur des refroidisseurs à absorption ont été identifiés comme le point faible des refroidisseurs à absorption (Goyal et al., 2017). Les coefficients ou les flux de transfert de chaleur/masse sont couramment utilisés comme critère pour les caractériser. Cependant, le coefficient global de transfert de chaleur utilisant la définition classique de la différence de température moyenne logarithmique n'est pas valable car il ne prend pas en compte la chaleur de sorption (Narayanan et al., 2009). En outre, ce coefficient néglige généralement la partie sensible de la chaleur impliquée dans les échangeurs à sorption (Herold et al., 2016). De plus, même si les transferts de chaleur et de masse sont couplés, ils représentent des processus physiques distincts et l'un ou l'autre peut contrôler le processus de transfert global (Herold et al., 2016).

Les refroidisseurs à absorption sont des machines plus complexes que les systèmes à compression de vapeur. Par conséquent, leur modélisation est d'une importance fondamentale pour l'évaluation et la caractérisation de leur performance, en particulier lorsqu'ils sont utilisés en dehors de leurs conditions nominales. À cet égard, la plupart des méthodes considèrent que le phénomène de sorption (à savoir l'absorption et la désorption) est contrôlé par le transfert de chaleur et que la solution atteint des conditions d'équilibre avec la phase vapeur à la sortie des composants (à savoir l'absorbeur et le générateur), ce qui n'est jamais le cas dans les conditions réelles de fonctionnement (Aiane et al., 2017b). Par ailleurs, le coefficient global de transfert thermique utilisé pour regrouper les phénomènes de transfert de chaleur et de masse est considéré comme constant pour toute la gamme des conditions de fonctionnement. Par conséquent, une approche plus précise pourrait être l'utilisation d'une efficacité thermique et d'une efficacité massique (ε_{th} et ε_m , respectivement) qui considèrent le transfert de chaleur et le transfert de masse comme indépendants.

Caractérisation des échangeurs à sorption

Une première partie du chapitre introduit la définition générale des efficacités thermique et massique appliquées aux échangeurs à sorption non adiabatiques (l'efficacité massique des échangeurs à sorption adiabatiques est intrinsèquement incluse dans cette définition). Tout d'abord, la caractérisation des échangeurs à plaque en tant qu'absorbeur et désorbeur à bulles d'un refroidisseur à absorption $\text{NH}_3\text{-LiNO}_3$ sur la base de leurs efficacités thermique et massique a été effectuée. L'impact des différentes conditions de fonctionnement de la machine sur les efficacités a été observé. L'absorbeur étudié présentait une efficacité massique comprise entre 0,31 et 0,76 et une efficacité thermique entre 0,33 et 0,77 (Figure II.2). D'autre part, le désorbeur étudié présentait une efficacité massique comprise entre 0,39 et 0,85 et une efficacité thermique entre 0,63 et 0,92 (Figure II.3). Comme le fluide limitant dans les échangeurs étudiés était toujours la solution, ε_{th} et ε_m étaient principalement influencés par son régime d'écoulement (Re_{sol}), ce qui a conduit à de meilleures performances à faible Re_{sol} et pour des viscosités dynamiques plus faibles (principalement en raison d'une amélioration du transfert de masse par les perturbations hydrodynamiques des bulles et un temps de résidence accru des bulles dans les canaux des plaques). Un Re_{htf} bas afin de maintenir un coefficient de partage supérieur à 1 est souhaitable dans les échangeurs à sorption pour avoir

une faible consommation d'énergie de pompage. Enfin, les propriétés thermophysiques de la solution et l'écart par rapport aux conditions d'équilibre de la solution en entrée de l'échangeur ont un impact plus important sur l'efficacité massique que sur l'efficacité thermique, en particulier pour des régimes de faible débit de solution.

Méthodes de caractérisation appliquées à un prototype à simple étage $\text{NH}_3\text{-LiNO}_3$

Après la caractérisation des composants, une caractérisation d'un refroidisseur à absorption de 10 kW (Figure II.4) a été réalisée au moyen de quatre méthodes différentes (avec des niveaux de compréhension physique différents) qui utilisent les températures des fluides caloporteurs pour représenter les conditions de fonctionnement de la machine, soit par une différence de température caractéristique (dans le cas des modèles basés sur la méthode de l'équation caractéristique), soit par le $\text{COP}_{\text{carnot}}$: la méthode de l'équation caractéristique (semi-empirique, Figure II.5), la méthode de l'équation caractéristique adaptée et le modèle de la fonction de Carnot (tous deux empiriques, Figure II.6), et un modèle thermodynamique (physique), appelé modèle des efficacités (Figure II.9), basé sur les efficacités thermique et massique. Le $\text{COP}_{\text{carnot}}$ a été utilisé comme paramètre commun pour représenter les différentes conditions de fonctionnement du refroidisseur et, par conséquent, pour représenter les résultats des différents modèles et les efficacités des composants. Lorsqu'aucune information sur les conditions internes du fluide de travail n'est requise et qu'une base de données étendue de résultats expérimentaux est disponible, les modèles empiriques offrent un outil simple pour calculer la puissance de refroidissement et le COP thermique du système. En revanche, si le nombre de résultats expérimentaux est limité mais que les données de conception des composants de la machine sont disponibles, la méthode de l'équation caractéristique est une option viable. Enfin, si des informations sur les efficacités thermiques et massiques des composants sont disponibles dans la gamme des conditions étudiées, le modèle des efficacités proposé peut être utilisé pour identifier les composants limitants du système et analyser à tout moment les conditions internes de non-équilibre de la solution avec la phase vapeur. De plus, cela a permis d'identifier des pistes d'amélioration du $\text{COP}_{\text{elect}}$ puisque les débits du fluide caloporteur dans tous les composants peuvent être réduits, en particulier pour des puissances de refroidissement faibles.

Les efficacités thermique et massique sont des paramètres qui, à la différence des coefficients/flux de transfert de chaleur/masse, dépendent de moins de paramètres et tiennent compte des conditions hors équilibre à l'entrée et à la sortie des composants. Par conséquent, ils peuvent être utilisés pour créer des modèles plus complets afin de caractériser le comportement à charge partielle des refroidisseurs à absorption (conditions thermodynamiques internes et externes) et identifier des possibilités d'optimisation pour chaque composant, ou être appliqués dans des modèles dynamiques pour l'étude de systèmes dans des conditions variables (par exemple, lorsque l'énergie solaire thermique ou l'air ambiant sont utilisés comme sources de chaleur). Par ailleurs, l'efficacité massique est à elle seule un paramètre fiable qui peut être utilisé pour la caractérisation des échangeurs de sorption adiabatiques, qui, comme indiqué au Chapitre I, constituent une technologie prometteuse pour les refroidisseurs à absorption. Ce sera l'objet de discussions dans les chapitres suivants.

Chapitre III. Climatisation à absorption solaire dans le contexte mexicain

Afin de développer une nouvelle génération de refroidisseurs solaires à absorption destinés aux pays ensoleillés, comme le Mexique, la simulation de la machine dans l'environnement local est nécessaire. Cela permet de mieux comprendre le comportement d'un tel système en conditions réelles et de définir

des exigences minimales en termes de coût et de performance. Le Chapitre III présente la simulation d'une machine à absorption dans le climat mexicain, en régime permanent et dynamique.

L'un des défis pour accroître la compétitivité des refroidisseurs à absorption par rapport aux systèmes conventionnels à compression de vapeur est une source de dissipation de chaleur adaptée. En effet, ces machines dégagent plus de chaleur que les systèmes à compression de vapeur. Habituellement, des tours de refroidissement sont utilisées à cette fin. Cependant, elles présentent certains inconvénients tels qu'une consommation d'eau élevée, des besoins de maintenance importants, leur consommation électrique, et des cas de prolifération des légionelles ont été signalés (Bailo et al., 2010; Monné et al., 2011). Pour ces raisons, certains groupes de recherche étudient d'autres possibilités de dissipation de chaleur. Les systèmes refroidis par air ont également fait l'objet d'études théoriques et expérimentales. Néanmoins, dans ce cas, les refroidisseurs à absorption exigent des températures de source chaude plus élevées et, lorsqu'ils fonctionnent avec le couple de travail H₂O-LiBr, il existe un risque de cristallisation de la solution. En outre, les performances des systèmes refroidis par air sont fortement influencées par les variations de la température ambiante (Chen et al., 2017). Les échangeurs de chaleur géothermiques ont récemment été proposés comme dissipateurs de chaleur pour les systèmes à absorption. Ils présentent certains avantages par rapport aux systèmes conventionnels en termes d'efficacité, de coût de fonctionnement et de maintenance (Noorollahi et al., 2018). Les différents types d'échangeurs de chaleur géothermiques courants présentent tous des inconvénients en termes de coût ou de surface requise (Moch et al., 2014). De plus, les échangeurs de chaleur géothermiques hélicoïdaux ont récemment été proposés car ils offrent un bon compromis en termes de surface requise et de coût. Cependant, il existe très peu d'études sur leur fonctionnement (Moch et al., 2015).

Les échangeurs de chaleur et de masse ont été pointés comme les composants limitants en termes de taille, de performance et de coût pour les machines à absorption, en particulier l'absorbeur (Beutler et al., 1996; Kays and London, 1984). Ainsi, les échangeurs adiabatiques ont attiré l'attention ces dernières années car ils pourraient conduire à des systèmes compacts, légers et peu coûteux, grâce à la séparation des transferts de chaleur et de masse en deux étapes (Gutiérrez-Urueta et al., 2012; Venegas et al., 2003; Ventas et al., 2010). Habituellement, un échangeur de chaleur à plaques fabriqué en série est utilisé pour le transfert de chaleur en raison de sa grande compacité (Wang et al., 2007) et de son faible coût. Le transfert de masse est effectué dans une chambre différente où la solution peut être distribuée ou dispersée sous différentes formes pour absorber ou désorber la vapeur de réfrigérant. Cela permet un très grand nombre de possibilités pour améliorer la surface d'échange et générer des instabilités dans l'écoulement, ce qui conduit à une meilleure performance et une grande compacité.

Sélection du fluide de travail et étude technico-économique

Un modèle en régime permanent d'un système à absorption de petite puissance pour des climats chauds couplé à un panneau solaire thermique et à un dissipateur de chaleur géothermique est présenté (Figure III.1). Le modèle est utilisé pour comparer 3 différents fluides de travail potentiels pour les conditions climatiques de la ville de Monterrey (dans le nord du Mexique). Monterrey, la 3^{ème} plus grande métropole du Mexique, a été choisie car c'est une ville représentative de cette région dans laquelle le besoin de climatisation et les niveaux d'irradiation sont tous les deux très élevés. Les deux fluides de travail classiques NH₃-H₂O et H₂O-LiBr et un troisième fluide de travail innovant (NH₃-LiNO₃) ont été comparés. Un dimensionnement rapide des principaux composants et une première étude technico-économique sont réalisés pour évaluer la faisabilité commerciale d'un tel système dans le contexte mexicain.

En termes de performances thermodynamiques, le H₂O-LiBr s'est avéré être le couple de travail le plus efficace dans les conditions nominales. Cependant, d'un point de vue économique et sur la base des

hypothèses envisagées pour la présente étude, le choix du fluide de travail semble avoir un impact relativement faible sur le coût d'investissement initial d'un système à absorption solaire-géothermique de petite capacité. D'autre part, le système proposé serait techniquement réalisable, mais, à moins que des incitations économiques telles que des subventions « écologiques » ne soient mises en œuvre, il ne semble pas économiquement viable dans le contexte mexicain. Le système géothermique a une forte incidence sur le coût d'investissement initial déjà élevé du système à absorption solaire. Une option pour augmenter la viabilité économique du système serait de prendre en compte l'utilisation du capteur solaire thermique et du réservoir de stockage d'eau chaude pour eau chaude sanitaire car, dans le nord du Mexique, le besoin de chauffage est également important pendant l'hiver. Dans le cadre de la réforme énergétique mexicaine récemment mise en œuvre, beaucoup de programmes de transition vers un marché de l'énergie plus durable sont attendus et mis en œuvre. Des nouvelles subventions « écologiques » pourraient être un facteur important pour stimuler cette transition et inciter les Mexicains à relever le défi.

Climatisation à absorption solaire avec une configuration bi-adiabatique innovante

Une fois le fluide de travail choisi, l'étude d'une nouvelle géométrie de système de refroidissement à absorption H₂O-LiBr à simple étage avec une configuration bi-adiabatique est proposée (Figure III.9). Cette nouvelle architecture permettrait non seulement d'obtenir une grande compacité, mais aussi d'éviter une production à la demande en ne sélectionnant que des échangeurs de chaleur standard produits en série. Un modèle dynamique 1^{er} et second principe de la machine, basé sur les efficacités thermiques et massiques de ses composants a été présenté. Le modèle a été utilisé pour identifier les conditions nominales du système et pour étudier son comportement sur une journée d'été typique en utilisant des données réelles de 2018 de la ville de Monterrey (Figure III.11). Le fonctionnement sur une journée typique a été simulé en couplant le système avec un capteur solaire thermique comme source haute température, un échangeur de chaleur géothermique hélicoïdal comme source de température intermédiaire et une maison individuelle. Cette configuration permettrait d'obtenir des températures intérieures confortables avec une différence de température pouvant atteindre 9°C par rapport à une maison non refroidie (Figure III.13). Dans la présente étude, le système a fourni jusqu'à 6,2 kW de refroidissement et un COP thermique moyen de 0,77. De plus, il n'y avait aucun risque de cristallisation dans les conditions étudiées. Le dimensionnement des réservoirs de stockage de la solution et du réfrigérant est d'une grande importance pour réduire le temps de réponse du système, mais en même temps, un compromis doit être trouvé pour donner une certaine inertie thermique au système afin de lisser les variations des conditions extérieures.

Finalement, l'étude exergétique a montré que les composants qui conduisent à la plus grande destruction d'exergie sont le désorbeur et l'absorbeur adiabatiques, respectivement (Figure III.18). Ceci est dû à la faible efficacité massique qui a été choisie pour ces composants et à l'impact de l'enthalpie de mélange. En effet, dans les conditions nominales de cette étude, une efficacité massique de 0,6 a été choisie ; cependant, des échangeurs à sorption ayant une efficacité massique supérieure à cette valeur permettraient d'améliorer considérablement les performances de la machine et de réduire sa destruction d'exergie. Pour cette raison, le Chapitre IV présente la conception et la caractérisation expérimentale d'une nouvelle génération d'échangeurs à sorption adiabatiques pour les refroidisseurs à absorption avec des efficacités élevées.

Chapitre IV. Nouvelle génération d'échangeur de masse adiabatique à film tombant

Les différents défis à surmonter pour rendre les refroidisseurs à absorption compétitifs par rapport aux systèmes de compression de vapeur conventionnels et les différentes solutions possibles ont fait l'objet de discussions dans les chapitres précédents. La nouvelle architecture de machine proposée au Chapitre III n'est utile que si des échangeurs à sorption adiabatiques efficaces, compacts et peu coûteux sont mis en œuvre.

Les échangeurs à sorption adiabatiques peuvent être divisés en trois principales catégories: les échangeurs gravitaires, les échangeurs à buses et les échangeurs à membrane. Les échangeurs à membrane et les échangeurs à buses ont prouvé qu'ils offrent des capacités d'absorption élevées. Cependant, ils nécessitent une quantité d'énergie supplémentaire pour surmonter les pertes de charge dans le composant. De plus, la durabilité des échangeurs à sorption membranaires reste à étudier et les échangeurs à buses, qui sont limités dans les débits de solution, nécessitent généralement un grand volume de chambre pour avoir une distribution optimale de la solution (Altamirano et al., 2020b). Les échangeurs adiabatiques gravitaires ne consomment pas d'électricité supplémentaire, car la solution s'écoule librement dans une chambre où la pression de vapeur reste constante, ce qui entraîne des pertes de charge négligeables. Ces échangeurs, qui ont montré des performances prometteuses en matière d'échange de masse, ont été principalement étudiés dans trois configurations différentes : gouttelettes tombantes (Arzoz et al., 2005; Gutiérrez-Urueta et al., 2011), jets instables (Arzoz et al., 2005), et film tombant (Arzoz et al., 2005; Boudard and Bruzzo, 2004; Michel et al., 2017; Obame Mve et al., 2015). Cependant, aucune méthode spéciale d'amélioration du transfert de masse (par exemple, une méthode de distribution spéciale ou une surface de film tombant améliorée) n'a été étudiée plus avant (Altamirano et al., 2020b). En effet, parmi les problèmes les plus bloquants dans ces échangeurs, on trouve la distribution non uniforme du film tombant sur la surface d'échange (Michel et al., 2017), la variation de température de l'interface du film due au phénomène de sorption, et le faible coefficient de diffusion massique de l'eau dans la solution (Islam et al., 2003).

La technologie de fabrication additive (impression 3D), qui consiste à imprimer des couches successives d'un matériau donné formées les unes sur les autres (Ngo et al., 2018), permet aujourd'hui de construire des pièces complexes autrement impossibles à fabriquer (Peng et al., 2018) et constitue une alternative viable pour la fabrication des produits finis (Peng et al., 2018; Plocher and Panesar, 2019). Sa mise en œuvre pourrait potentiellement réduire le temps et le coût de la fabrication de composants de petits volumes de production (Peng et al., 2018), ouvrant la voie à de nouveaux modèles commerciaux disruptifs (Savolainen and Collan, 2020).

Le Chapitre IV montre la caractérisation expérimentale d'une nouvelle génération d'échangeur adiabatique à sorption à film tombant breveté (Altamirano Cundapí et al., 2020) (Figure IV.3), fabriqué par fabrication additive, en utilisant la méthode du dépôt de fil fondu (DFF). La structure et le distributeur de solution sont conçus pour assurer une distribution uniforme de la solution sur la surface de l'échangeur. De plus, la conception de cet échangeur à sorption adiabatique permet de renforcer le phénomène de transfert de masse par le renouvellement des couches limites thermiques et massiques en raison des instabilités d'écoulement qui sont générées lorsque le film de solution s'écoule. Alors que la méthode d'impression 3D permet de s'attaquer au coût élevé et à l'absence de production en masse des systèmes d'absorption, la proposition de géométrie de l'échangeur propose de résoudre certains des problèmes majeurs liés à la performance des échangeurs à sorption. L'échangeur adiabatique a été testé en mode désorption, et sa performance a été caractérisée expérimentalement grâce à son efficacité massique (Altamirano et al., 2020c, 2020a, 2019b; Michel et al., 2017) en étudiant l'influence de cinq paramètres : la pression de fonctionnement, la surchauffe de la solution en entrée, le débit massique de la solution en entrée et la concentration de la solution en entrée. Un polynôme d'ordre 2 de l'efficacité massique en fonction de ces paramètres a été obtenu par un plan d'expériences.

Les résultats expérimentaux ont conduit à une efficacité massique comprise entre 88 et 100% (Figure IV.5 et Figure IV.6). De plus, la régression polynomiale de deuxième ordre résultant du plan d'expériences indique que le désorbeur peut fournir une capacité de refroidissement équivalente comprise entre 0,32 et 4,74 kW avec une efficacité comprise entre 69,5 et 100 % pour l'ensemble des conditions étudiées. Dans les conditions nominales de fonctionnement, le même modèle indique que le désorbeur fonctionnerait avec une efficacité massique proche de 1. Par conséquent, sur la base de ces résultats, la construction d'un refroidisseur à absorption basé sur cette technologie semble très prometteuse. En outre, le désorbeur conçu peut encore augmenter sa compacité par la réduction de son volume, au prix d'une efficacité massique légèrement inférieure.

La désorption se fait en deux étapes dans le désorbeur. D'abord dans le distributeur une ébullition spontanée se développe et s'intensifie avec la surchauffe de la solution à l'entrée. Ensuite, dans le film tombant, des phénomènes de diffusion ont lieu. L'augmentation du débit massique de la solution entraîne une diminution des performances due à l'augmentation de l'épaisseur du film de solution, qui augmente la résistance thermique entre la solution liquide et l'interface vapeur-liquide dans le film tombant. L'augmentation de la surchauffe de la solution à l'entrée entraîne une augmentation des performances en raison de l'intensification du phénomène d'ébullition dans le distributeur.

L'augmentation de la concentration de la solution conduit à une efficacité accrue par l'augmentation de la température d'équilibre, ce qui améliore les propriétés thermophysiques de la solution pour un meilleur phénomène de désorption. La même chose se produit avec l'augmentation de la pression de fonctionnement, mais à une échelle moindre, car la pression a un impact plus faible sur la température d'équilibre de la solution. Cela suggère que l'impact sur les propriétés thermophysiques dû aux variations de la température de la solution est dominant par rapport aux effets générés par les variations de la concentration de la solution. Enfin, à des concentrations ou des surchauffes importantes de la solution, l'impact de ses propriétés thermophysiques est réduit.

La régression proposée pour l'efficacité massique offre un outil pour caractériser de manière plus réaliste les échangeurs à sorption. Sa mise en œuvre pour simuler une machine entière permettrait de mieux décrire le comportement du refroidisseur et les conditions de non-équilibre de la solution dans la machine, en particulier en fonctionnement à charge partielle ou lorsqu'il est couplé à des sources qui sont en constante évolution (par exemple, une source solaire thermique ou la température ambiante).

Après une comparaison avec d'autres technologies testées en désorption (section 4.5), la technologie proposée semble être une alternative prometteuse puisqu'elle a montré des performances comparables à celles des désorbeurs à membrane adiabatique tout en ayant les avantages d'une perte de charge négligeable de la solution et d'une fabrication simple et peu coûteuse. Elle a même présenté des performances de transfert de masse similaires à celles d'un désorbeur non adiabatique.

Perspectives

Les résultats obtenus dans le cadre du présent travail sont très prometteurs. Par conséquent, la construction et la caractérisation expérimentale d'un prototype à échelle réelle basé sur la technologie proposée sont envisagées. Les prochaines étapes pour atteindre cet objectif sont les suivantes :

Caractérisation du désorbeur par des nombres adimensionnels

Même si le désorbeur a été caractérisé par différents paramètres tels que le débit massique de la solution, la pression, la température et la concentration, sa caractérisation par des nombres adimensionnels serait préférable pour étendre l'utilisation de la caractérisation à d'autres géométries similaires. Cela faciliterait

également la mise en œuvre de la caractérisation de l'échangeur dans des modèles de machines fonctionnant dans une large gamme de conditions. Pour ce faire, une analyse paramétrique visant à étudier la variation des différentes propriétés thermophysiques de la solution pour les différentes gammes de conditions étudiées pourrait être nécessaire pour comprendre les phénomènes physiques contrôlant les performances du désorbeur adiabatique.

Caractérisation de l'échangeur en mode absorption

Après avoir pleinement compris son comportement en désorption adiabatique, l'échangeur de masse sera testé en mode absorption. Les résultats obtenus permettront d'interpréter ce qui se passe dans le cas du phénomène d'absorption pour la géométrie proposée. Comme dans le cas du désorbeur, la caractérisation par des nombres adimensionnels et l'étude de l'influence des propriétés thermophysiques de la solution seront effectuées. Une fois la caractérisation des performances obtenue dans les deux modes de fonctionnement, la conception d'une machine entière sera possible.

Modifications de la conception

Certains aspects de la conception de l'échangeur proposé peuvent encore être améliorés. Une étude de conception améliorée peut être mise en œuvre pour lever les principaux points limitants en termes de coûts de fabrication et de temps de production. En effet, le processus d'impression 3D peut être lent en fonction de la complexité du composant à imprimer. Par conséquent, la réduction du nombre de pièces imprimées en 3D pourrait non seulement contribuer à réduire le temps de production, mais aussi à diminuer les coûts de fabrication de la machine finale.

Conception et caractérisation du prototype à l'échelle réelle

Enfin, la conception et la construction d'un prototype à l'échelle réelle seront réalisées. Des choix définitifs de conception seront faits en ce qui concerne la géométrie des échangeurs à changement de phase du réfrigérant. Il semble que des échangeurs de chaleur hélicoïdaux autour de la structure adiabatique permettraient une augmentation de la compacité de l'ensemble du système. Le prototype qui en résulterait ne serait alors composé que de composants peu coûteux fabriqués en série ou imprimés 3D, ce qui pourrait conduire à un système à la fois compact et efficace.

Un projet de maturation de start-up, intitulé CONFOTHER, a été approuvé et financé par la SATT (Société d'Accélération du Transfert de Technologies) grenobloise Linksium pour poursuivre le développement de la technologie présentée. L'objectif principal du projet est la construction et l'essai d'un prototype à l'échelle réelle et la recherche de partenaires industriels et commerciaux afin de mettre sur le marché un produit commercialement attractif.

Références

- Aiane, M., Ramousse, J., Stutz, B., Bouyaud, M., Boudard, E., 2017. Dynamic modeling of an automotive air-conditioning system by absorption, in: International Sorption Heat Pump Conference, August 7-10. Tokyo, Japan.
- Alefeld, G., Radermacher, R., 1993. Heat Conversion Systems, 1st ed. CRC Press, Boca Baton, Florida.
- Aliane, A., Abboudi, S., Seladji, C., Guendouz, B., 2016. An illustrated review on solar absorption cooling experimental studies. *Renew. Sustain. Energy Rev.* 65, 443–458. <https://doi.org/10.1016/j.rser.2016.07.012>
- Alpizar-Castro, I., Rodríguez-Monroy, C., 2016. Review of Mexico's energy reform in 2013: Background, analysis of the reform and reactions. *Renew. Sustain. Energy Rev.* 58, 725–736. <https://doi.org/10.1016/j.rser.2015.12.291>
- Altamirano, A., Le Pierrès, N., Stutz, B., 2019a. Review of small-capacity single-stage continuous absorption systems operating on binary working fluids for cooling: Theoretical, experimental and commercial cycles. *Int. J. Refrig.* 106, 350–373. <https://doi.org/10.1016/j.ijrefrig.2019.06.033>
- Altamirano, A., Le Pierrès, N., Stutz, B., Coronas, A., 2021. Performance characterization methods for absorption chillers applied to an NH₃-LiNO₃ single-stage prototype. *Appl. Therm. Eng.* 185, 116435. <https://doi.org/10.1016/j.applthermaleng.2020.116435>
- Altamirano, A., Stutz, B., Le Pierrès, N., 2020a. Review of small-capacity single-stage continuous absorption systems operating on binary working fluids for cooling: Compact exchanger technologies. *Int. J. Refrig.* 114, 118–147. <https://doi.org/10.1016/j.ijrefrig.2020.02.033>
- Altamirano, A., Stutz, B., Le Pierrès, N., Coronas, A., 2020b. Experimental characterization by thermal and mass effectivenesses of plate heat exchangers in NH₃-LiNO₃ absorption chillers, in: ISHPC 2021 – Online Pre-Conference. Berlin, Germany, pp. 56–60. <https://doi.org/10.14279/depositonce-10430.2>
- Altamirano, A., Stutz, B., Le Pierrès, N., Domain, F., 2019b. H₂O-LiBr Single-Stage Solar Absorption Air Conditioner with an Innovative Bi-Adiabatic Configuration: Dynamic Model, Nominal Conditions and Typical Day Operation, in: Solar World Congress. Santiago, Chili. <https://doi.org/10.18086/swc.2019.55.01>
- Altamirano Cundapí, A., Stutz, B., Le Pierrès, N., 2020. Sorption exchanger (in French). Patent FR 209477.
- Anies, G., 2011. Modélisation, simulation dynamique, validation expérimentale et optimisation énergétique d'une unité de rafraîchissement solaire par absorption (in French). PhD Université de Pau et des Pays de l'Adour.
- Arzoz, D., Rodriguez, P., Izquierdo, M., 2005. Experimental study on the adiabatic absorption of water vapor into LiBr-H₂O solutions. *Appl. Therm. Eng.* 25, 797–811. <https://doi.org/10.1016/j.applthermaleng.2004.08.003>
- Bailo, C.M., Garcés, S.A., Arizón, F.P., 2010. Analysis of a New Dissipation System for a Solar Cooling Installation. *J. Thermodyn.* 2010, 1–6. <https://doi.org/10.1155/2010/750675>
- Bellos, E., Tzivanidis, C., Antonopoulos, K.A., 2016. Exergetic and energetic comparison of LiCl-H₂O and LiBr-H₂O working pairs in a solar absorption cooling system. *Energy Convers. Manag.* 123, 453–461. <https://doi.org/10.1016/j.enconman.2016.06.068>
- Best, R., Rivera, W., 2015. A review of thermal cooling systems. *Appl. Therm. Eng.* 75, 1162–1175. <https://doi.org/10.1016/j.applthermaleng.2014.08.018>

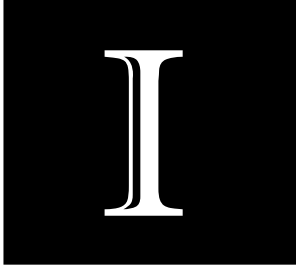
- Beutler, A., Hoffmann, L., Ziegler, F., Alefeld, G., Gommed, K., Grossman, G., Shavit, A., 1996. Experimental Investigation of Heat and Mass Transfer on Horizontal and Vertical Tubes, in: Proceedings of the International Absorption Heat Pump Conference, September 17-20. Montreal, Canada, pp. 409–419.
- Bogart, M.J.P., 1981. Ammonia Absorption Refrigeration in Industrial Processes. Gulf Publishing Company, Houston (US).
- Boudard, E., Bruzzo, V., 2004. Exchange Device and Heat Transfer Especially for Automotive Vehicle. Patent FR N°2,871,221.
- Calm, J.M., 2008. The next generation of refrigerants - Historical review, considerations, and outlook. *Int. J. Refrig.* 31, 1123–1133. <https://doi.org/10.1016/j.ijrefrig.2008.01.013>
- Chen, J.F., Dai, Y.J., Wang, R.Z., 2017. Experimental and analytical study on an air-cooled single effect LiBr-H₂O absorption chiller driven by evacuated glass tube solar collector for cooling application in residential buildings. *Sol. Energy* 151, 110–118. <https://doi.org/10.1016/j.solener.2017.05.029>
- Cvjetko Bubalo, M., Radošević, K., Radojčić Redovniković, I., Halambek, J., Gaurina Srček, V., 2014. A brief overview of the potential environmental hazards of ionic liquids. *Ecotoxicol. Environ. Saf.* 99, 1–12. <https://doi.org/10.1016/j.ecoenv.2013.10.019>
- Dube, E., Cha, A., Agboola, O.P., Orfi, J., Fakeeha, A.H., Al-fatesh, A.S., 2017. Energetic and exergetic analysis of solar-powered lithium bromide- water absorption cooling system. *J. Clean. Prod.* 151, 60–73. <https://doi.org/10.1016/j.jclepro.2017.03.060>
- García Casals, X., 2006. Solar absorption cooling in Spain: Perspectives and outcomes from the simulation of recent installations. *Renew. Energy* 31, 1371–1389. <https://doi.org/10.1016/j.renene.2005.07.002>
- Garimella, S., 1999. Miniaturized heat and mass transfer technology for absorption heat pumps, in: Proceedings of the International Sorption Heat Pump Conference. Munich, Germany, Germany, pp. 661–670.
- Goyal, A., Staedter, M.A., Hoysall, D.C., Ponkala, M.J., Garimella, S., 2017. Experimental evaluation of a small-capacity, waste-heat driven ammonia-water absorption chiller. *Int. J. Refrig.* 79, 89–100. <https://doi.org/10.1016/j.ijrefrig.2017.04.006>
- Gutiérrez-Urueta, G., Rodríguez, P., Venegas, M., Ziegler, F., Rodríguez-Hidalgo, M.C., 2011. Experimental performances of a LiBr-water absorption facility equipped with adiabatic absorber. *Int. J. Refrig.* 34, 1749–1759. <https://doi.org/10.1016/j.ijrefrig.2011.07.014>
- Gutiérrez-Urueta, G., Rodríguez, P., Ziegler, F., Lecuona, A., Rodríguez-Hidalgo, M.C., 2012. Extension of the characteristic equation to absorption chillers with adiabatic absorbers. *Int. J. Refrig.* 35, 709–718. <https://doi.org/10.1016/j.ijrefrig.2011.10.010>
- Hassan, H.Z., Mohamad, A.A., 2012. A review on solar cold production through absorption technology. *Renew. Sustain. Energy Rev.* 16, 5331–5348. <https://doi.org/10.1016/j.rser.2012.04.049>
- Herold, K., Rademacher, R., Klein, S., 2016. Absorbtion Chillers and Heat Pumps, 2nd ed. CRC Press, Taylor & Francis Group, Boca Raton, FL.
- IEA, 2020. TASK 65 - Solar Cooling for the Sunbelt Regions [WWW Document]. IEA SHC. URL <https://task65.iea-shc.org/> (accessed 9.20.20).
- IEA, 2019. World energy outlook. Paris, France.
- IEA, 2018a. The Future of Cooling. Paris, France.
- IEA, 2018b. IEA SHC TCP, Strategic Work Plan 2019 - 2024. SHC TCP Executive Committee.

- IEA, 2012. *Energy Technology Perspectives - Pathways to a Clean Energy System*. Paris, France.
- Islam, M.R., Wijesundera, N.E., Ho, J.C., 2003. Performance study of a falling-film absorber with a film-inverting configuration. *Int. J. Refrig.* 26, 909–917. [https://doi.org/10.1016/S0140-7007\(03\)00078-1](https://doi.org/10.1016/S0140-7007(03)00078-1)
- Jafari, A., Poshtiri, A.H., 2017. Passive solar cooling of single-storey buildings by an adsorption chiller system combined with a solar chimney. *J. Clean. Prod.* 141, 662–682. <https://doi.org/10.1016/j.jclepro.2016.09.099>
- Kays, W.M., London, A.L., 1984. *Compact heat exchanger*. New York: McGraw-Hill.
- Kim, D.S., Ferreira, C.A.I., 2008. Solar refrigeration options – a state-of-the-art review. *Int. J. Refrig.* 31, 3–15. <https://doi.org/10.1016/j.ijrefrig.2007.07.011>
- Kühn, A., 2013. *Thermally driven heat pumps for heating and cooling*. Deutsche Nationalbibliothek, Berlin.
- Labus, J.M., Bruno, J.C., Coronas, A., 2013. Review on absorption technology with emphasis on small capacity absorption machines. *Therm. Sci.* 17, 739–762. <https://doi.org/10.2298/TSCI120319016L>
- Michel, B., Le Pierrès, N., Stutz, B., 2017. Performances of grooved plates falling film absorber. *Energy* 138, 103–117. <https://doi.org/10.1016/j.energy.2017.07.026>
- Moch, X., Palomares, M., Claudon, F., Souyri, B., Stutz, B., 2015. Geothermal helical heat exchangers: Coupling with a reversible heat pump in Western Europe. *Appl. Therm. Eng.* 81, 368–375. <https://doi.org/10.1016/j.applthermaleng.2015.01.072>
- Moch, X., Palomares, M., Claudon, F., Souyri, B., Stutz, B., 2014. Geothermal helical heat exchangers: Comparison and use of two-dimensional axisymmetric models. *Appl. Therm. Eng.* 73, 689–696. <https://doi.org/10.1016/j.applthermaleng.2014.06.051>
- Monné, C., Alonso, S., Palacín, F., Serra, L., 2011. Monitoring and simulation of an existing solar powered absorption cooling system in Zaragoza (Spain). *Appl. Therm. Eng.* 31, 28–35. <https://doi.org/10.1016/j.applthermaleng.2010.08.002>
- Mugnier, D., Jakob, U., 2015. Status of solar cooling in the World: markets and available products. *Wiley Interdiscip. Rev. Energy Environ.* 4, 229–234. <https://doi.org/10.1002/wene.132>
- Mugnier, D., Neyer, D., White, S., 2017. *The Solar Cooling Design Guide: Case Studies of Successful Solar Air Conditioning Design*. Ernst & Sohn, Berlin, Germany.
- Narayanan, V., Kanury, A.M., Jenks, J., 2009. Heat Exchanger Analysis Modified to Account for a Heat Source, in: *ASME/JSME 2007 Thermal Engineering Heat Transfer Summer Conference Collocated with the ASME 2007 InterPACK Conference*. American Society of Mechanical Engineers Digital Collection, Vancouver, Canada, pp. 1063–1068.
- Ngo, T.D., Kashani, A., Imbalzano, G., Nguyen, K.T.Q., Hui, D., 2018. Additive manufacturing (3D printing): A review of materials, methods, applications and challenges. *Compos. Part B Eng.* 143, 172–196. <https://doi.org/10.1016/j.compositesb.2018.02.012>
- Noorollahi, Y., Saeidi, R., Mohammadi, M., Amiri, A., Hosseinzadeh, M., 2018. The effects of ground heat exchanger parameters changes on geothermal heat pump performance – A review. *Appl. Therm. Eng.* 129, 1645–1658. <https://doi.org/10.1016/j.applthermaleng.2017.10.111>
- Obame Mve, H., Rullière, R., Haberschill, P., 2015. Modeling and Parametric Study of the Heat Transfer Inside a Lithium Bromide Flow Confined by Wire Screen. *J. Energy Power Eng.* 9, 417–425. <https://doi.org/10.17265/1934-8975/2015.05.001>
- Peng, T., Kellens, K., Tang, R., Chen, C., Chen, G., 2018. Sustainability of additive manufacturing: An overview on its energy demand and environmental impact. *Addit. Manuf.* 21, 694–704.

<https://doi.org/10.1016/j.addma.2018.04.022>

- Pérez-Denicia, E., Fernández-Luqueño, F., Vilariño-Ayala, D., Manuel Montaña-Zetina, L., Alfonso Maldonado-López, L., 2017. Renewable energy sources for electricity generation in Mexico: A review. *Renew. Sustain. Energy Rev.* 78, 597–613. <https://doi.org/10.1016/j.rser.2017.05.009>
- Plocher, J., Panesar, A., 2019. Review on design and structural optimisation in additive manufacturing: Towards next-generation lightweight structures. *Mater. Des.* 183, 108–164. <https://doi.org/10.1016/j.matdes.2019.108164>
- Riffat, S.B., Wu, S., Bol, B., 2004. Pervaporation membrane process for vapour absorption system. *Int. J. Refrig.* 27, 604–611. <https://doi.org/10.1016/j.ijrefrig.2004.03.005>
- Savolainen, J., Collan, M., 2020. How Additive Manufacturing Technology Changes Business Models? – Review of Literature. *Addit. Manuf.* 32, 101070. <https://doi.org/10.1016/j.addma.2020.101070>
- Seiler, M., Kühn, A., Ziegler, F., Wang, X., 2013. Sustainable cooling strategies using new chemical system solutions. *Ind. Eng. Chem. Res.* 52, 16519–16546.
- Shiran, Y., Shitzer, A., Degani, D., 1982. Computerized Design and Economic Evaluation of an Aqua-Ammonia Solar Operated Absorption System. *Sol. Energy* 29, 43–54.
- Ullah, K.R.R., Saidur, R., Ping, H.W.W., Akikur, R.K.K., Shuvo, N.H.H., 2013. A review of solar thermal refrigeration and cooling methods. *Renew. Sustain. Energy Rev.* 24, 499–513. <https://doi.org/10.1016/j.rser.2013.03.024>
- Venegas, M., Arzo, D., Rodríguez, P., Izquierdo, M., 2003. Heat and mass transfer in LiNO₃-NH₃ spray absorption system. *Int. Commun. Heat Mass Transf.* 30, 805–815. [https://doi.org/10.1016/S0735-1933\(03\)00128-3](https://doi.org/10.1016/S0735-1933(03)00128-3)
- Ventas, R., Lecuona, A., Legrand, M., Rodríguez-Hidalgo, M.C., 2010. On the recirculation of ammonia-lithium nitrate in adiabatic absorbers for chillers. *Appl. Therm. Eng.* 30, 2770–2777. <https://doi.org/10.1016/j.applthermaleng.2010.08.001>
- Wang, L., Sundén, B., Manglik, R.M., 2007. Plate Heat Exchangers. Design, Applications and Performance. Wit Press. <https://doi.org/10.1081/E-EAFE>
- Wang, Z., Gu, Z., Feng, S., Li, Y., 2009. Application of vacuum membrane distillation to lithium bromide absorption refrigeration system. *Int. J. Refrig.* 32, 1587–1596. <https://doi.org/10.1016/j.ijrefrig.2009.07.002>
- Weiss, W., Spörk-Dür, M., Mauthner, F., 2017. Solar Heat Worldwide: Global Market Development Trends in 2016, Detailed Market Figures 2015. IEA Solar Heating and Cooling Programme.
- Wu, W., Wang, B., Shi, W., Li, X., 2014. An overview of ammonia-based absorption chillers and heat pumps. *Renew. Sustain. Energy Rev.* 31, 681–707. <https://doi.org/10.1016/j.rser.2013.12.021>
- Yoon, J.I., Kwon, O.K., Bansal, P.K., Moon, C.G., Lee, H.S., 2006. Heat and mass transfer characteristics of a small helical absorber. *Appl. Therm. Eng.* 26, 186–192. <https://doi.org/10.1016/j.applthermaleng.2005.05.009>
- Zhai, X.Q., Wang, R.Z., 2009. A review for absorption and adsorption solar cooling systems in China. *Renew. Sustain. Energy Rev.* 13, 1523–1531. <https://doi.org/10.1016/j.rser.2008.09.022>
- Zhu, L., Gu, J., 2010. Second law-based thermodynamic analysis of ammonia/sodium thiocyanate absorption system. *Renew. Energy* 35, 1940–1946. <https://doi.org/10.1016/j.renene.2010.01.022>
- Ziegler, F., Alefeld, G., 1987. Coefficient of performance of multistage absorption cycles. *Int. J. Refrig.* 10, 285–295.

This page intentionally left blank



General introduction

This section provides the general context and motivations that led to the presented work. First, a general context of the residential air conditioning energy challenge worldwide and the situation in the Mexican conditions is presented. Then, the potential of solar absorption chillers to diversify the Mexican energetic and economic sources is introduced. Furthermore, some data about the market development of absorption chillers during the last 15 years and the challenges for these systems to acquire a bigger share of the residential cooling market is provided. Finally, the research objectives of the present work and the global description of the structure of this manuscript are described.

“

“Cada suspiro es como un sorbo de vida del que uno se deshace.”

“Each sigh is like a sip of life that one gets rid of.”

– Juan Rulfo

Residential air conditioning global energy challenge

Due to the world population growth and the economic development, especially in developing countries, the energy consumption is increasing at alarming rates. Figure 1 shows the world primary energy demand categorized by fuel and the corresponding CO₂ emissions for three different scenarios established by the International Energy Agency: a Current Policies scenario, in which the policies applied until now remain unchanged; a Stated Policies scenario, in which the proposed policies by the different countries are implemented; and a Sustainable Development scenario, which is an ideal scenario in which the sustainable energy goals are met. According to this figure, the increase in the global energy demand between 2000 and 2040 is expected to be around 91% in the Current Policies scenario (from 10037 to 19177 Mtoe). Moreover, from the total energy consumed in 2040, 78% will be coming from fossil fuels (whose combustion generates pollution and causes global warming). This makes practically no change if compared with the share of 80% that it represents today (IEA, 2019).

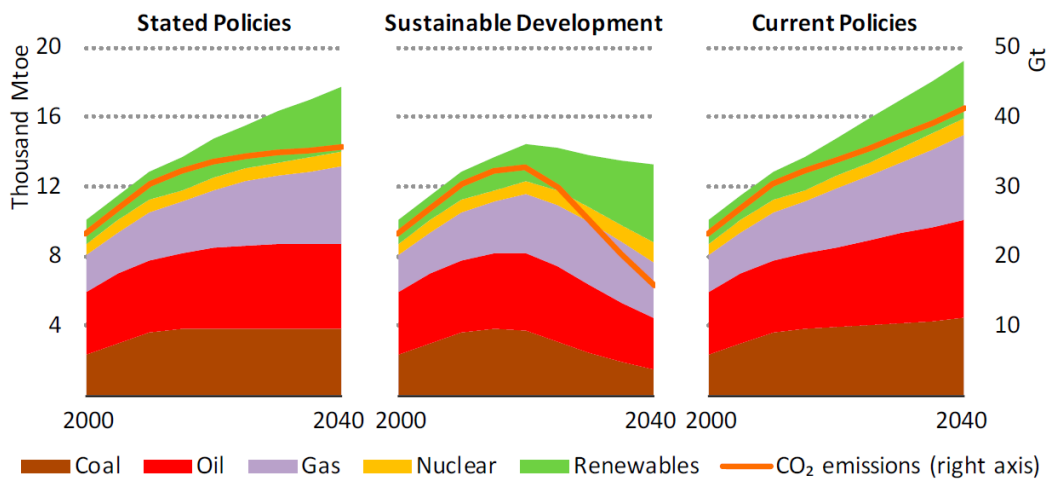


Figure 1: World primary energy demand by fuel and related CO₂ emissions by scenario (IEA, 2019).

The building sector is the most energy demanding sector with 35% of the final energy consumption (IEA, 2019). In this sector, the need for space cooling represents nowadays 20% of the total electricity used, and this demand is growing faster than any other end use in buildings, reaching a share of 30% by 2050 (IEA, 2018a). Figure 2 shows that the final energy consumption for space cooling in the building sector has more than tripled in 26 years (from 1990 to 2016), and it is expected to triple again by 2050, with around 70% of this increase coming from the residential sector, mostly in emerging economies (IEA, 2018a).

Nearly all the energy consumed for space cooling (Figure 2) is in the form of electricity to drive vapor compression chillers. Only around 1% is in the form of natural gas to drive thermally driven absorption chillers in commercial buildings (IEA, 2018a). This dependence on electricity has generated a series of problems and challenges for the environment and the electricity distribution grid in hot-climate countries (Casals, 2006). Indeed, in some regions of the world, this cooling demand reaches over 70% of the peak residential electrical demand during hot days (IEA, 2018a).

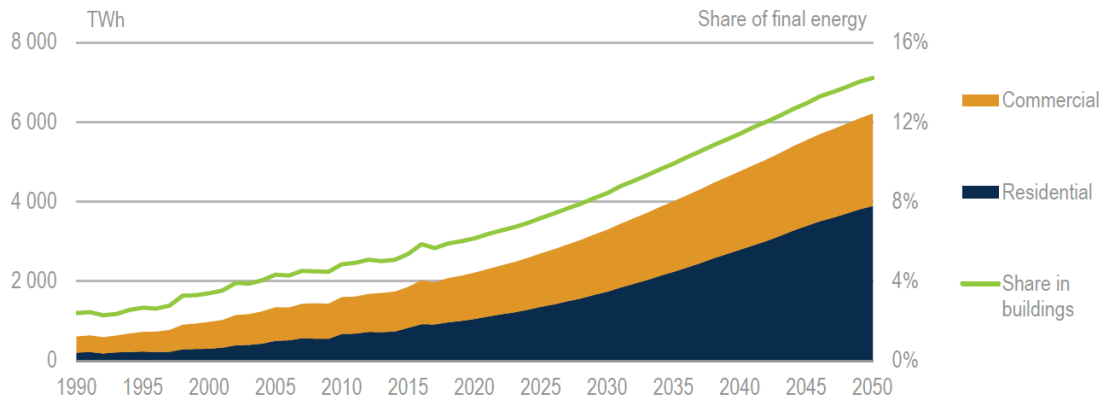


Figure 2: World energy use for space cooling by subsector (IEA, 2018a).

The Mexican context

Mexico is an important player in the increasing demand for cooling. Its energy consumption in buildings for cooling has increased by more than 5-fold times from 1990 to 2016 (from 7 to 37 TWh), representing nowadays 9.8% of the total energy consumed in buildings, which is the second highest share in a country, just after the United States (IEA, 2018a). Moreover, this energy consumption is expected to increase by 4-fold times again by 2050 (IEA, 2018a).

Mexico is also the second country in the world with the highest share of electricity used for space cooling with a 14% already today. Even if the policies and targets announced by the government until now are implemented, this share is expected to increase to more than 23% by 2050, which entails that cooling will account for more than 25% of the increase in total CO₂ emissions (the highest share of any country) (IEA, 2018a). Indeed, the need for cooling of Mexico, measured in cooling degree days (CDDs), is expected to increase of 36.8% from 2016 to 2050, which is the largest increase of any country in the world (IEA, 2018a).

Energetically and economically, Mexico is dependent on fossil fuels. In 2013, the oil sector generated 13% of the country's export earnings and 33% of the government's income (Alpizar-Castro and Rodríguez-Monroy, 2016). The instability in oil prices and its constant drop in recent years has generated economic problems and concern in the country. Until now, the increasing demand for energy is mainly covered by fossil fuels. In 2014, 93% of the total energy consumption came from oil (45%), natural gas (40%), and coal (8%) (Pérez-Denicia et al., 2017).

In Mexico, the recently approved energy reform has shown a lack of expertise to face the energetic challenges of the coming years. If no change in the Mexican energy policy is implemented, the dramatically increasing numbers regarding the energy demand for cooling and its dependence on fossil fuels forecast an economic and energy crisis in the coming decades.

Mexico has to operate a change in its energy policy. Among other options, efforts must be put on the implementation of systems that make use of renewable energy, such as solar energy, that are until now unexploited (Alpizar-Castro and Rodríguez-Monroy, 2016). Actions of this type would not only be useful to equilibrate the country energy flows and monetary incomes, but are also in line with the different international efforts to protect the ozone layer and reduce the impact of climate change such as the Montreal Protocol, the Kyoto Protocol, and the Paris Agreement.

Solar absorption chillers

The dependence on fossil fuels, the high cost of electricity, and global warming are some of the main obstacles to cover the increasing energy demands in the building sector. The use of clean and sustainable energy sources is the most promising alternative to generate clean energy without leaving CO₂ footprints (Bellos et al., 2016). In this context, solar energy is one of the most important energy resources that can be used for air conditioning since it is abundant, widespread, endless, and clean (Bellos et al., 2016; Jafari and Poshtiri, 2017). In this context, Mexico possesses the advantage of being part of the sunbelt countries (countries between the 20th and 40th degrees of latitude in the northern and southern hemisphere), which are hot countries with high irradiation levels that can be used to drive solar thermal chillers.

Absorption chillers are thermally driven systems that replace the mechanical compression of standard refrigeration systems by a thermochemical compression. Different categories of thermodynamic cycle arrangement exist for absorption chillers. However, the single-stage configuration is the most advantageous for solar thermal cooling applications in the residential building sector in terms of cost, low driving temperatures, size, and simple configuration (Hassan and Mohamad, 2012). Even though there exist other thermally driven chiller technologies such as adsorption, desiccant, or ejector systems, the main advantage of absorption cooling systems is their higher coefficient of performance (COP) (Best and Rivera, 2015; Hassan and Mohamad, 2012). Moreover, its coupling with solar thermal energy is a very promising alternative, as the irradiation level is higher when cooling is most needed (Dube et al., 2017; Kim and Ferreira, 2008a). In addition, the solar thermal panels can also be used for space heating or domestic hot water during winter (IEA, 2018a).

The suitability of absorption chillers relies on several economic, political, industrial, and geographical conditions (Herold et al., 2016). In spite of their different advantages such as the use of renewable energies, low operating/maintenance costs, good thermal performance, and reduced noise; they are to date a niche technology. From the total energy consumed for space cooling (Figure 2), 99% comes in the form of electricity. The remaining 1% is natural gas mainly used to drive H₂O-LiBr absorption chillers in the Far East (China, Japan, and South Korea), where regulatory incentives exist for gas-fired cooling (Herold et al., 2016). Regarding solar cooling, the niche market has experienced a slow but steady increase passing from 40 installed units in 2004 to 1,350 by the end of 2015 (Figure 3), of which 80% were in Europe (Mugnier and Jakob, 2015; Weiss et al., 2017).

The main obstacles for absorption chillers to be deployed on a much larger scale are their high initial investment cost and their lower compactness if compared with conventional vapor compression systems (Altamirano et al., 2019a). This is especially true for small-capacity application (Figure 4), such as in the residential cooling sector. Indeed, as observed in Figure 4, the conventional vapor compression systems require a different compressor technology at capacities higher than 250 kW to deal with the larger required refrigerant vapor flow, which increases their specific costs and make them even slightly more expensive than absorption chillers. The market of absorption chillers, however, is expected to grow as the fabrication costs are reduced. These costs have already been decreased by more than half since 2007, mainly thanks to the standardization of the equipment, making these systems to gain acceptance and seem like true alternative for cooling residential, light commercial, and industrial applications (Zhu and Gu, 2010). However, to date, they are still not cost-competitive with electrical chillers (IEA, 2018a).



Figure 3: Market development of small to large-scale solar cooling systems worldwide (Weiss et al., 2017).

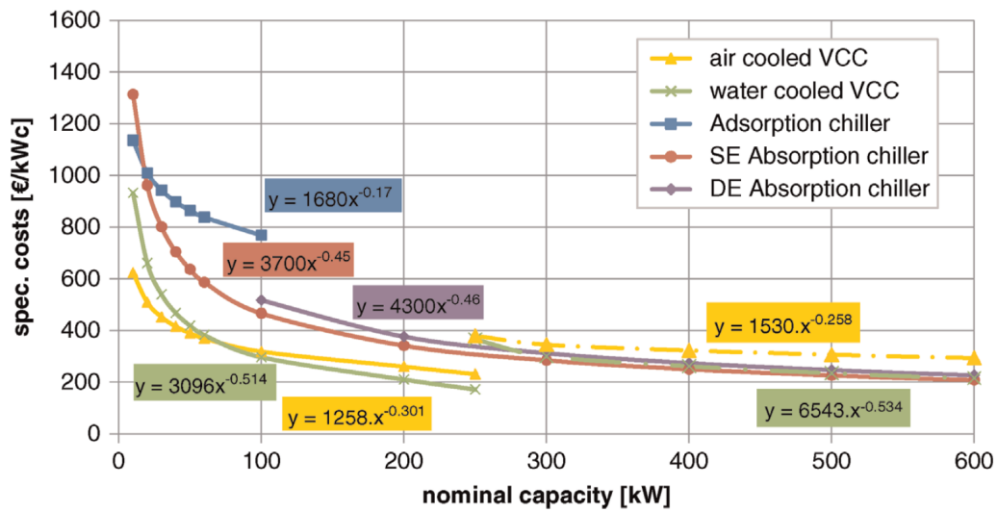


Figure 4: Specific costs for ab-/adsorption machines and water- and air-cooled vapor compression chillers (Mugnier et al., 2017).

Owing to their potential to cover a great part of the rising energy demand for space cooling, R&D in solar thermal cooling systems is part of the technology milestones to achieve energy efficient buildings in the IEA Energy Technology Perspectives report (IEA, 2012). Moreover, these systems are included in the IEA SHC Strategic Plan Key Technologies (IEA, 2018b). Solar cooling has already been the subject of four IEA SHC Taks (No. 25, No., 38, No. 48, and No. 53)., and a new Task (Task 65) has been created in 2020 to adapt, verify, and promote solar cooling as an affordable and reliable solution to the increasing cooling demand across the sunbelt countries such as Mexico (IEA, 2020).

In order to get a bigger market share in the residential cooling sector, from the technological point of view, absorption chillers still need to reduce their production costs (through the simplification of the manufacturing processes), increase their compactness, and increase their efficiency (Altamirano et al.,

2020b, 2019a; IEA, 2018a; Mugnier et al., 2017). On the other hand, from the political point of view, the stimulation of the market is required through governmental regulations (Herold et al., 2016). Regarding the R&D concern, different solution options have already been studied like the search of the perfect working pair (refrigerant/absorbent combination), new heat and mass transfer exchanger technologies, the cost reduction through the employment of new manufacturing methods, the appropriate heat sink source, and innovative machine architectures (Altamirano et al., 2020b, 2019a).

Research objectives

The main objective of the present thesis is the development of a new generation of compact and low-cost absorption chillers for applications in the sunbelt countries as an affordable and environmentally friendly solution to the increasing cooling needs in the residential sector. For this, the different technical aspects previously mentioned (the working fluid, the exchangers' technology, the machine architecture, the heat sink, and the manufacturing method) are addressed. The Mexican case is more specifically studied due to the challenges presented before. In order to achieve these goals, the following questions remained to be answered:

1. What is the state of the art of the working fluids and exchanger technologies employed in absorption chillers?
2. Are there recently investigated working pairs and exchanger technologies that might be commercially and technically viable for a small-capacity absorption chiller?
3. What are the most suitable parameters for the characterization and performance evaluation of the sorption elements in absorption chillers?
4. What modeling methods are the most adapted for absorption chillers and in which conditions?
5. Is a solar absorption air conditioner for the residential sector technically and economically feasible in the Mexican context?
6. Are machine architecture modifications an option to reduce the cost of absorption chillers?
7. How can the new manufacturing methods be employed to construct a new generation of compact and low-cost absorption chillers?

Thesis organization

In order to address the research objectives, the thesis was structured in the following chapters, which are based on results that were presented in per-reviewed journal and conference papers.

Chapter I aims to address questions 1 to 3 of the research objectives. It presents the state of the art regarding the investigation of working fluids and exchanger technologies for small-capacity (≤ 50 kW) single-stage continuous absorption chillers operating on binary working fluids. The first part performs a working fluids investigation. Even though some innovations of machine architecture are described (R&D in this area is scarcer), it has a special focus on the comparison of the cycle performance between the different families of refrigerants and working pairs. This comparison is performed for the theoretical, experimental and commercial machines. The second part studies innovative exchanger technologies with conventional or special geometries, with or without mechanical treatments, tested on the three most experimented working pairs ($\text{NH}_3\text{-H}_2\text{O}$, $\text{H}_2\text{O-LiBr}$, and $\text{NH}_3\text{-LiNO}_3$). Since there is no standard evaluation parameter for these exchangers, the comparison between the different technologies was performed on the basis of the most commonly used parameters.

Chapter II deals with the fourth question and is indirectly related to question three since it studies the characterization of absorption chillers from the component level to the system level. It shows the first-ever characterization of a pre-industrial $\text{NH}_3\text{-LiNO}_3$ absorption chiller prototype through a recently proposed parameter for the evaluation of the sorption exchangers of absorption chillers, called the mass effectiveness. In a first part, the characterization of plate heat exchangers used as sorption exchangers (i.e., the absorber and the desorber) for absorption chillers is presented. In a second section, the overall machine simulation is performed through a thermodynamic model that uses thermal and mass effectivenesses, called the effectiveness model. The proposed model is presented and compared with other empirical and semi-empirical models to analyze their advantages and disadvantages. Furthermore, the studied models use the $\text{COP}_{\text{carnot}}$ as a unique parameter to express the machine operating conditions.

Chapter III answers questions five and six. It studies a small-capacity geothermally cooled solar absorption system in the Monterrey city (Mexico) climate conditions. The geothermal heat sink source is investigated for its potential to replace cooling towers and air-cooled systems. In a first section, a steady-state model is used to compare the two more conventional working fluids ($\text{NH}_3\text{-H}_2\text{O}$ and $\text{H}_2\text{O-LiBr}$) and an innovative working fluid ($\text{NH}_3\text{-LiNO}_3$). In addition, the dimensioning of the components of the system and a short economic viability study of the proposed system is presented. After the selection of the most adapted working fluid, the second section deals with the study of an innovative absorption chiller architecture. It presents the dynamic simulation of a single-stage $\text{H}_2\text{O-LiBr}$ solar absorption system with a bi-adiabatic configuration, which allows for a wide range of possibilities to enhance the mass transfer, leading to efficient and compact systems. Moreover, apart from the adiabatic sorption exchangers, only mass-produced standard components would be required. The chiller is evaluated coupled to an evacuated tube collector and a simple model of a single-family house under a typical sunny day in the Monterrey climate conditions.

Chapter IV addresses the last question. It presents the design and experimental characterization of a new generation of adiabatic falling film mass exchanger for absorption chillers fabricated by additive manufacturing using the fused deposition modeling (FDM) method. In the proposed component, the mass transfer phenomenon is enhanced by the renewal of the thermal and mass boundary layers due to generated flow instabilities. The impact of four parameters were analyzed: the operating pressure, the solution mass flow rate, the solution concentration, and the solution equilibrium deviation temperature. The proposed exchanger would present a mass effectiveness close to 100% if installed in a 2-kW absorption chiller with the architecture proposed in **Chapter III**. Finally, a comparison with other technologies tested in desorption operation with the $\text{H}_2\text{O-LiBr}$ working fluid was performed.

References

- Alpizar-Castro, I., Rodríguez-Monroy, C., 2016. Review of Mexico's energy reform in 2013: Background, analysis of the reform and reactions. *Renew. Sustain. Energy Rev.* 58, 725–736. <https://doi.org/10.1016/j.rser.2015.12.291>
- Altamirano, A., Le Pierrès, N., Stutz, B., 2019. Review of small-capacity single-stage continuous absorption systems operating on binary working fluids for cooling: Theoretical, experimental and commercial cycles. *Int. J. Refrig.* 106, 350–373. <https://doi.org/10.1016/j.ijrefrig.2019.06.033>
- Altamirano, A., Stutz, B., Le Pierrès, N., 2020. Review of small-capacity single-stage continuous absorption systems operating on binary working fluids for cooling: Compact exchanger technologies. *Int. J. Refrig.* 114, 118–147. <https://doi.org/10.1016/j.ijrefrig.2020.02.033>
- Bellos, E., Tzivanidis, C., Antonopoulos, K.A., 2016. Exergetic and energetic comparison of LiCl-H₂O and LiBr-H₂O working pairs in a solar absorption cooling system. *Energy Convers. Manag.* 123, 453–461. <https://doi.org/10.1016/j.enconman.2016.06.068>
- Best, R., Rivera, W., 2015. A review of thermal cooling systems. *Appl. Therm. Eng.* 75, 1162–1175. <https://doi.org/10.1016/j.applthermaleng.2014.08.018>
- Casals, X.G., 2006. Solar absorption cooling in Spain: Perspectives and outcomes from the simulation of recent installations. *Renew. Energy* 31, 1371–1389. <https://doi.org/10.1016/j.renene.2005.07.002>
- Dube, E., Cha, A., Agboola, O.P., Or, J., Fakeeha, A.H., Al-fatesh, A.S., 2017. Energetic and exergetic analysis of solar-powered lithium bromide- water absorption cooling system. *J. Clean. Prod.* 151, 60–73. <https://doi.org/10.1016/j.jclepro.2017.03.060>
- Hassan, H.Z., Mohamad, A.A., 2012. A review on solar cold production through absorption technology. *Renew. Sustain. Energy Rev.* 16, 5331–5348. <https://doi.org/10.1016/j.rser.2012.04.049>
- Herold, K., Rademacher, R., Klein, S., 2016. *Absorbtion Chillers and Heat Pumps*, 2nd ed. CRC Press, Taylor & Francis Group, Boca Raton, FL.
- IEA, 2020. TASK 65 - Solar Cooling for the Sunbelt Regions [WWW Document]. IEA SHC. URL <https://task65.iea-shc.org/> (accessed 9.20.20).
- IEA, 2019. *World energy outlook*. Paris, France.
- IEA, 2018a. *The Future of Cooling*. Paris, France.
- IEA, 2018b. *IEA SHC TCP, Strategic Work Plan 2019 - 2024*. SHC TCP Executive Committee.
- IEA, 2012. *Energy Technology Perspectives - Pathways to a Clean Energy System*. Paris, France.
- Jafari, A., Poshtiri, A.H., 2017. Passive solar cooling of single-storey buildings by an adsorption chiller system combined with a solar chimney. *J. Clean. Prod.* 141, 662–682. <https://doi.org/10.1016/j.jclepro.2016.09.099>
- Kim, D.S., Ferreira, C.A.I., 2008. Solar refrigeration options – a state-of-the-art review. *Int. J. Refrig.* 31, 3–15. <https://doi.org/10.1016/j.ijrefrig.2007.07.011>
- Mugnier, D., Jakob, U., 2015. Status of solar cooling in the World: markets and available products. *Wiley Interdiscip. Rev. Energy Environ.* 4, 229–234. <https://doi.org/10.1002/wene.132>
- Mugnier, D., Neyer, D., White, S., 2017. *The Solar Cooling Design Guide: Case Studies of Successful Solar Air Conditioning Design*. Ernst & Sohn.
- Pérez-Denicia, E., Fernández-Luqueño, F., Vilariño-Ayala, D., Manuel Montaña-Zetina, L., Alfonso Maldonado-López, L., 2017. Renewable energy sources for electricity generation in Mexico: A review. *Renew. Sustain. Energy Rev.* 78, 597–613. <https://doi.org/10.1016/j.rser.2017.05.009>
- Weiss, W., Spörk-Dür, M., Mauthner, F., 2017. *Solar Heat Worldwide: Global Market Development Trends in 2016, Detailed Market Figures 2015*. IEA Solar Heating and Cooling Programme.

Zhu, L., Gu, J., 2010. Second law-based thermodynamic analysis of ammonia/sodium thiocyanate absorption system. *Renew. Energy* 35, 1940–1946. <https://doi.org/10.1016/j.renene.2010.01.022>

Chapter I.State of the art on single-stage absorption chillers

Based on:

Altamirano, A., Le Pierrès, N., Stutz, B.

Review of small-capacity single-stage continuous absorption systems operating on binary working fluids for cooling: Theoretical, experimental and commercial cycles

Int. J. Refrig. 106 (2019), 350–373

DOI: 10.1016/j.ijrefrig.2019.06.033

Altamirano, A., Stutz, B., Le Pierrès, N.

Review of small-capacity single-stage continuous absorption systems operating on binary working fluids for cooling: Compact exchanger technologies

Int. J. Refrig. 114 (2020) 118–147

DOI: 10.1016/j.ijrefrig.2020.02.033

The objective of the present chapter is to provide an overview of the exchanger technologies and working fluids investigated for small-capacity absorption chillers in order to understand their evolution over the past 40 years. In Section 1.1, the different investigated working fluids are presented and compared by means of their cycle performance from a theoretical, experimental, and commercial points of view. On the other hand, Section 1.2 presents the different exchanger technologies and compares their mass and thermal transfer performances through the most commonly used parameters.

“

وَ تحسب أنك جرمٌ صغيرٌ وفيك انطوى العالمُ الأكبرُ

*“A little celestial body thyself thou deem,
while the greatest world in thee dwells.”*

– Ali ibn Abi Talib

1.1. Introduction

In order to develop a new generation of compact and low-cost absorption chillers based on a new sorption exchanger technology, select the most adapted working fluid for the residential applications in sunny countries such as Mexico, and propose machine architecture innovations, a deep state-of-the-art review is necessary. Absorption systems can be categorized according to different variables. For example, the driving source, the heat sink type, the number of stages, the working fluid, the application, the capacity, or the continuous/discontinuous operation. Considering their thermodynamic cycle arrangement, absorption refrigeration systems can be divided into three categories: single-effect, half-effect, and multi-effect (e.g. double-effect or triple-effect) cycles (Alefeld and Radermacher, 1993; Ziegler and Alefeld, 1987). The single-effect and half-effect cycles require lower driving temperatures compared with the multi-effect cycles (Aliane et al., 2016). From all the possible configurations, the single-stage is the most advantageous in terms of cost, low driving temperatures, and simple configuration (Hassan and Mohamad, 2012). At the same time, it is the most commercially available. Two absorption pairs are commonly encountered: $\text{H}_2\text{O-LiBr}$ (water-lithium bromide) and $\text{NH}_3\text{-H}_2\text{O}$ (ammonia-water). A typical single-stage absorption system consists of an evaporator, a condenser, an absorber, a generator (sometimes also called a desorber), a solution pump, a solution heat exchanger (SHX), and two valves, as shown in Figure I.1. The solution at the generator absorbs heat and desorbs refrigerant vapor. This vapor is condensed at the condenser before passing through a throttle valve and being vaporized again at a lower pressure and a lower temperature at the evaporator. The evaporation heat is taken from the cold source. The vapor produced by the evaporator is absorbed by the weak solution (in refrigerant) in the absorber. The resulting rich solution is pumped from the absorber to the generator, where the cycle starts again (Best and Rivera, 2015). The solution heat exchanger (SHX) is added between the absorber and the generator to increase the efficiency of the machine by recovering internal heat. When a volatile solution is used, such as ammonia/water, a vapor purification process has to be added after the generator to improve the quality of the refrigerant (Bogart, 1981; Ullah et al., 2013). A refrigerant heat exchanger (RHX) can also be added between the inlet and outlet streams of the evaporator as an internal heat recovery method, but the effect of the SHX in the overall system performance is more important (Herold et al., 2016; Shiran et al., 1982). Moreover, a storage tank can be implemented in the heating circuit to absorb the heat rate variation at the generator (Aliane et al., 2016).

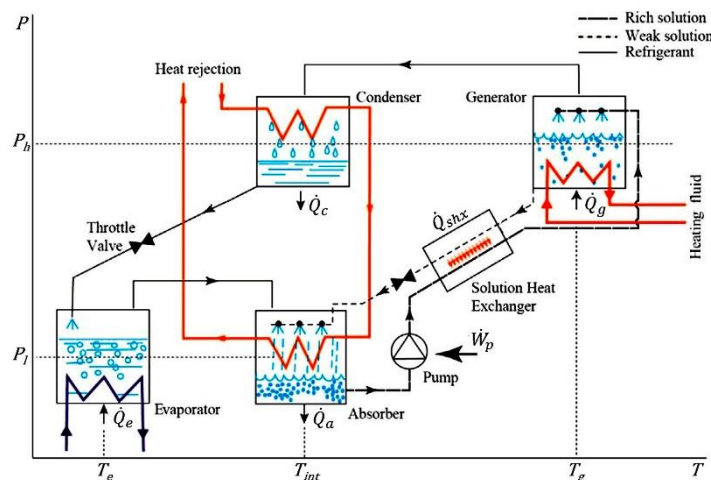


Figure I.1: Schematic of a single-effect solar absorption chiller (adapted from (Aliane et al., 2016)).

Absorption systems have been present for more than a century. Despite their multiple advantages, low compactness and elevated costs are two of the most important downsides which block their

expansion in the residential cooling sector. Currently, different research teams are focusing on improving these systems to reduce their manufacturing costs, complexity, volume, maintenance, and environmental concerns. One example of this is the search for the perfect refrigerant, for which, besides good thermal properties, the concern of its environmental impact has increased in recent years (Calm, 2008). The choice of refrigerant is related to the specific requirements of the envisaged application and has a strong impact on the system's exchangers technology and configuration (Wu et al., 2014). Moreover, different from conventional vapor compression systems, the study of alternative refrigerants in absorption systems leads to another important field of study which is the investigation of the best adapted refrigerant-absorbent combination (working pair) (Herold et al., 2016). Another research path is the search for new compact exchanger technologies, which might reduce the system's size and, if possible, its cost.

The first section of the present chapter aims to provide an up-to-date global overview of the small-capacity single-stage continuous absorption systems operating on binary working fluids for cooling from the theoretical, experimental, and commercial points of view. The very few machine architecture innovations present in the literature is also discussed. The second section focuses on the studies of innovative exchanger technologies with conventional or special geometries, with or without mechanical treatments, with particular attention paid to experimental studies. The upper limit for the term "small-capacity", depending on the author, can go from 20 to 100 kW (Anies, 2011; Kühn, 2013; J. M. Labus et al., 2013; Zhai and Wang, 2009). In the present work, only systems with a capacity of 50 kW or less were investigated.

1.2. Review of theoretical, experimental, and commercial cycles

The present section aims to provide an up-to-date global overview of the small-capacity single-stage continuous absorption systems operating on binary working fluids for cooling from the theoretical, experimental, and commercial points of view. Special focus is placed on comparing the cycle performance between the different families of refrigerants and working pairs as the choice of working fluid directly affects the performance of an absorption cycle (Hassan and Mohamad, 2012; Perez-Blanco, 1984). The main objective is to provide useful information about the cycles performance and the challenges faced by researchers in the development of such systems. It is not in the scope of this work to compare the brands or configurations. The main objective is to provide helpful information for a good understanding of the development of these systems over the past 40 years and of the main advantages and disadvantages of using different working pairs.

1.2.1. Comparative criteria

The performance of absorption systems depends on different factors and can be measured according to different criteria (Pons et al., 2012). These factors depend on internal parameters such as the working pair, the exchanger technology, or the monitoring procedure; and external parameters, such as the specific climate conditions or the type of source (liquid, solid or gas), which directly impact the operating temperatures and thermal transfers in the system. Compared with conventional compression systems, which possess two temperature sources (the heat rejection temperature and the cooling temperature), absorption cooling systems have three temperature sources. In addition to the heat rejection and the cooling temperature, there is an additional high-temperature driving source. All three temperature sources are of great importance for the system's performance. In the case of air-cooled systems, the ambient temperature is fundamental (since it cannot be modified). While the performance of conventional compression

AC is generally measured in terms of their electric coefficient of performance (COP_{elect} , defined as the cold production divided by the electricity consumption (Eq. (I.1))), the performance of absorption cooling systems is usually measured by a thermal coefficient of performance (COP) defined by Eq. (I.2). Some authors in the literature also use a combination of the two definitions, adding the electricity consumption (mainly consisting of the pumping power) to the energy consumption in the definition of the COP . Even though the pumping electricity consumption is considered negligible compared to the generator heat transfer rate, some studies have shown that it might be nonnegligible. Therefore, the COP_{elect} has earned a relevant importance in some studies (Zamora, 2012; Zamora et al., 2014).

$$COP_{elect} = \frac{\dot{Q}_e}{W_{elect}} \quad (I.1)$$

$$COP_{th} = \frac{\dot{Q}_e}{\dot{Q}_g} \quad (I.2)$$

Apart from the COP , which can be optimized by means of the first law (conservation of energy), the second law (quality of energy and material) can be used to maximize the exergetic efficiency and minimize the entropy generation within the system (Alefled and Radermacher, 1993). The exergetic efficiency represents the capacity of the system to avoid the destruction of available energy and is defined as the ratio between the recovered exergy at the evaporator and the provided exergy at the desorber (Kilic and Kaynakli, 2007). However, for the sake of the present review, special focus is given to the COP as the main parameter for comparing the different systems. Another important parameter is the Carnot COP (function of the system's operating temperatures), which represents the maximum possible coefficient of performance of the absorption cooling system. This is defined by Eq. (I.3).

$$COP_{carnot} = \left(\frac{t_g^i - t_a^i}{t_g^i} \right) \left(\frac{t_e^o}{t_c^i - t_e^o} \right) \quad (I.3)$$

The COP_{carnot} implies a reversible process with isothermal heat transfers at the three temperature levels, which ideally requires infinite energy sources. Therefore, for an ideal system, the temperatures from the external heat transfer fluids should be taken into account at the inlet of the generator (t_g^i), at the outlet of the evaporator (t_e^o), and at the inlet of the absorber and the condenser (t_a^i and t_c^i), or in the case of air-cooled systems, the ambient temperature (t_{amb}). In most experimental studies, the same source is used in parallel for the intermediate temperature, and in these cases, some authors use the term “intermediate temperature” or “heat sink temperature” ($t_a^i = t_c^i = t_{int}^i = t_{sink}^i$). The nominal external temperatures data of absorption chillers is provided by the manufacturers in their catalogs. However, theoretical studies generally use the temperatures of the internal working pair or refrigerant at the exit of the components. On the other hand, prototypes in the literature provide information depending on the research objectives and the specific configuration and instrumentation implemented in the machine (internal or external temperatures located in different sections), making it difficult to standardize the data. Therefore, this information was carefully extracted with the best possible accuracy if the values were not directly given and when the provided information allowed to, adding some degree of inaccuracy, to present the data contained in the tables and figures of the present review. Hence, these data may be interpreted with care and the reader must refer to the sources if more detailed information is required.

1.2.2. Ammonia-based working fluids

The general advantages of NH_3 over H_2O as the refrigerant are its low freezing point (-77°C) (Wang et al., 2011) and the higher working pressures, which allow for negative cooling temperatures and eliminate the need for special and expensive equipment for vacuum conditions (Wu et al., 2014). The present section covers the theoretical, experimental, and commercial systems operating on NH_3 -based systems.

1.2.2.1. Conventional ammonia-based working pair: NH_3 - H_2O

NH_3 - H_2O is, together with H_2O -LiBr, the most widely used working fluid in absorption systems (Herold et al., 2016; Taha Al-Zubaydi, 2011). It is commonly used for applications where negative refrigeration temperatures are required (Wu et al., 2014). Compared with H_2O -LiBr, it allows for a large range of operation with no risk of crystallization. However, a vapor purification process is needed at the output of the generator to remove the remaining water that evaporates together with the refrigerant (Medrano et al., 2001; Srihirin et al., 2001; Wu et al., 2014). This process is composed of a distillation column with partial or total condensation, a rectifier (externally cooled device to condense water vapor), or a combination of both (Bogart, 1981). The term “rectifier” is commonly used to refer to the vapor purification process in general. Indeed, a poor vapor purification would lead to a low system performance due to the presence of water in the evaporator (Bogart, 1982), reducing the COP by over 30% and requiring higher driving temperatures (Dardouch et al., 2018).

1.2.2.1.1. NH_3 - H_2O : Theoretical studies

Some theoretical studies have focused on identifying the parameters that most impact the performance of absorption systems. Very high t_g negatively impact the COP , in which case an increase in the t_c improves it (Kaushik and Bhardwaj, 1982). On the other hand, at low t_g , a decrease in the t_a and t_c improves the COP (Best et al., 1987; Bulgan, 1995), with t_a having the highest impact, and thus $t_a < t_c$ is more preferable (Kaushik and Bhardwaj, 1982).

Other studies have focused on analyzing the optimum operating conditions of these systems. In the case of negative refrigeration, Alvares and Trepp (1987) concluded that for a refrigeration temperature of -10°C , a single-stage system with a rectifier, SHX, and RHX could reach a maximum COP of 0.6021 at $t_g=120^\circ\text{C}$, $P_e=2.85$ bar, and a $t_{int}=25^\circ\text{C}$. Clerx and Trezek (1987) performed a computer-aided thermodynamic analysis and concluded that the evaporator pressure must be between 0.21 and 0.41 MPa to maintain negative evaporator temperatures, while the generator pressure must be between 1.38 MPa (to force a t_{int} of over 37.8°C and use air-cooled condensers) and 2.04 MPa (for a lower maintenance and safety requirements), the t_g between 82.2°C (to maintain an acceptable COP over 0.2) and 204°C (due to the maximum pressure determined before and also to avoid excessive water evaporation), and the preheater, SHX, and rectifier must have at least an effectiveness of 70% to maintain a COP of no less than 0.5 for ice production.

In the case of positive cooling, Shiran et al. (1982) developed a program that evaluates the cooling and heating demands of buildings depending on the location and design the absorption cycle along with the solar collectors and auxiliaries. Other studies centered on observing the behavior of the system in local geographic conditions (Kouremenos et al., 1987) or in a specific working range (Butz and Stephan, 1989; Hammad and Habali, 2000). Special configurations have also been theoretically analyzed. Uppal et al. (1986) proposed a system with no moving parts for vaccine storage in remote locations, and Ahachad et al. (1992) proposed to substitute the rectifier column

by a bubble exchanger fed with the strong solution coming out of the absorber (see [Figure I.2a](#)); the proposed system showed an improvement in the COP ranging from 15% to 35%.

Finally, optimization studies are also available in the literature. Bulgan (1995) observed that at fixed t_a and t_c , for each ammonia concentration level in the refrigerant and varying the t_g , there is a local COP_{max} . A theoretical maximum COP of 0.888 could be achieved. Le Lostec et al. (2010) presented an optimization study for a system under steady-state conditions. Three optimum COP values were identified: a COP of 0.56 with a minimum heat exchange surface, a COP of 0.62 with a minimum overall irreversibility, and a COP of 0.69 with a maximum exergetic efficiency. Finally, the destruction of exergy takes place mostly in the absorber and the desorber.

1.2.2.1.2. NH_3-H_2O : Experimental prototypes development and experimentation

A summary of the small-capacity prototypes of NH_3-H_2O absorption cooling systems developed in laboratories and their operating conditions is presented in [Table I.1](#). The prototypes described in the literature have often been built for the use of renewable energy sources. A prototype for the use of geothermal energy was constructed at the Cerro Prieto Geothermal Field (Mexico) to cool a small storage unit at negative temperatures. The system provided evaporating temperatures of $-10^\circ C$ at generator temperatures of $125^\circ C$ (Ayala Delgado, 1992). The use of solar energy for these systems is also of great interest. De Francisco et al. (2002) simulated and constructed a 2-kW air-cooled (by natural convection) solar system (with SHX and rectifier). The experimental $COPs$ were lower than 0.05, compared with 0.53 in the simulations. There were expected improvements in the solar collectors, new fans for forced convection, an ice storage tank, a new pump system, and a new automatic control process. Sözen et al. (2002) developed and tested a solar prototype in Ankara (Turkey) driven by a parabolic collector. The system reached cooling temperatures as low as $3^\circ C$, and the evaporator and absorber possessed the highest exergy losses. Mendes et al. (2007) designed and constructed a solar system with SHX and RHX in which the rectification column was substituted by a refining spray of rich solution directly integrated in the desorber (see [Figure I.2b](#)). The system showed an increase of 1% in ammonia content in the refrigerant after the refining process (before refining, the NH_3 content was in the range of 95.5–97.6%) at nominal conditions of 4 kW of cooling with a COP of 0.54. Said et al. (2015) designed and simulated a solar system (based on a design presented by the University of Stuttgart (Brendel et al., 2010; Zetsche et al., 2010)) that recovered waste heat from the rectifier and contained a refrigerant storage unit. A total increase of 18% in the COP was observed compared with a conventional generator/rectifier configuration and the system (installed in Saudi Arabia) delivered cooling capacities between 4 and 10 kW with COP values between 0.4 and 0.7 (Said et al., 2016). Another innovative proposal was made by Zotter and Rieberer (2015), who adapted a commercial PinkChiller PC19 with a thermally driven solution pump (instead of an electrically driven pump). Thermally driven pumps can be a suitable option owing to the lower production cost, fewer leakage problems, and no electricity consumption; however, the experimental system's COP was reduced by at least 0.1 (15%) compared with the system using an electrical pump. Boudéhenn et al. (2012) developed and constructed a compact and low-cost 5-kW system at INES (French National Institute for Solar Energy). The system, which uses compact plate heat exchangers (PHEs) available on the market, showed good potential. Nonetheless, further optimization opportunities exist for the SHX and the absorber.

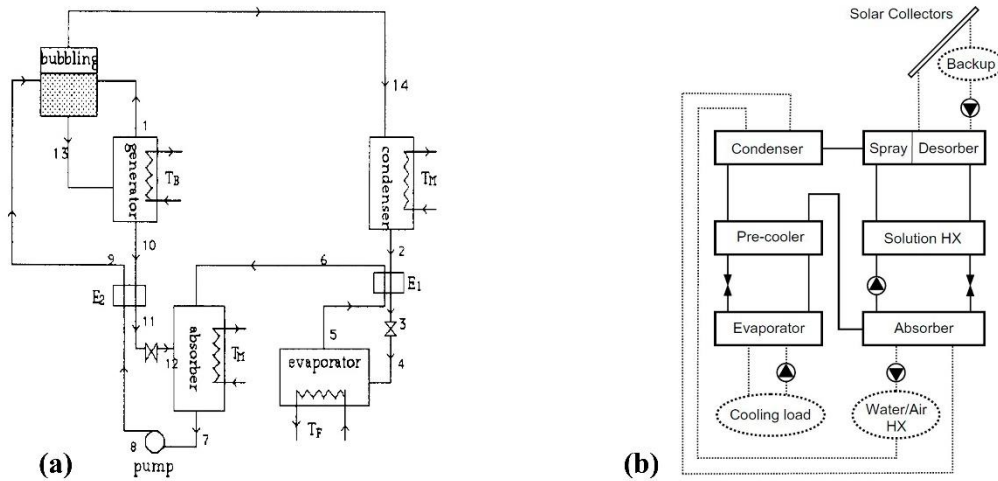


Figure I.2: Proposed innovations in the vapor purification process of $\text{NH}_3\text{-H}_2\text{O}$ systems. (a) Bubble vapor purifier (Ahachad et al., 1992) and (b) refining spray directly integrated in the desorber (Mendes et al., 2007).

Other uses of $\text{NH}_3\text{-H}_2\text{O}$ absorption chiller prototypes are miniaturized and mobile applications. Seeking to make use of the exhaust gases from trucks equipped with refrigeration systems for food transport, Koehler et al. (1997) simulated, constructed, and tested a system that delivered sufficient cooling capacities to be in compliance with the German Industrial Standard DIN 8959, but with low COP values due to the air-transfer medium in all the exchangers of the system. Determan and Garimella (2012) presented the design, fabrication and experimental demonstration of a microscale monolithic absorption heat pump with a nominal cooling capacity of 300 W. All the exchangers were fabricated in a single manufacturing process, reducing working fluid inventory and leakage. The system delivered cooling capacities of 136–300 W and COP s in the range of 0.25–0.43. However, the desorber and rectifier had to be improved to increase the system's COP . Garimella et al. (2016) later escalated the system to a 3.5-kW prototype that delivered 3.2 kW of cooling with a COP of 0.53, and Staedter and Garimella (2018) constructed a 7-kW system based on the same concept that delivered chilled water at 7.2°C with a COP of 0.51. Goyal et al. (2016, 2017) constructed a waste-heat-driven and air-cooled chiller designed for a thermal COP of 0.55. The machine provided between 1.91 and 2.54 kW of cooling at ambient temperatures between 29.7 and 44.2°C . The absorber and desorber were the limiting components while the rest of the components performed near design.

Table I.1: In-lab developed prototypes of small-capacity NH₃-H₂O absorption cooling systems and operating conditions.

$\dot{Q}_{e,nom}$ (kW)	Heat source	Heat sink	R E C T	S H X	R H X	t_g^i (°C)	t_c^i (°C)	t_c^e (°C)	t_e^o (°C)	$\dot{Q}_{e,exp}$ (kW)	COP_{exp}	COP_{carnot}	Comments	REF
10.5	Geothermal	Water	x	x		125	30	30	-10	-	0.4	1.57		(Ayala Delgado, 1992)
-	Exhaust gases	Air	x	x	x	180	30	30	0	7	0.255	3.01		(Koehler et al., 1997)
2	Solar	Air	x	x		109	40	40	20	-	0.05	2.65	Air-cooled by natural convection.	(De Francisco et al., 2002)
4	Solar	Air	x	x	x	110	32	32	11	-	0.54	2.75	Spray integrated in desorber for vapor purification	(Mendes et al., 2007)
10	Solar	Air	x	x	x	102	27	27	15	10.7	0.74	4.8	Focus on generator	(Brendel et al., 2010)
0.3	Electric heater	Water	x	x	x	115.4	30.2	30.2	7.1	0.24	0.34	2.66	Microscale monolithic AHP	(Zetzsche et al., 2010) (Determan and Garimella, 2012)
5	Electric heater	Water	x	x	x	80	27	27	18	-	0.65	4.86		(Boudéhen et al., 2012)
3.5	Combustion module	Water	x	x	x	180	38.5	38.5	9.5	3.2	0.53	3.04		(Garimella et al., 2016)
10	Solar	Air	x	x	x	114	23	23	-2	10.1	0.69	2.55		(Said et al., 2016)
2.71	Waste heat from diesel generator	Air	x	x	x	398.9	51.67	51.67	19.8	2.45	0.55	4.75	Nominal temperatures and COP values.	(Goyal et al., 2016) (Goyal et al., 2017)
7	Combustion module	Air	x	x	x	183	39.4	39.4	7.9	6.9	0.51	2.81		(Staedter and Garimella, 2018)

1.2.2.1.3. NH₃-H₂O Commercial systems: Presentation and experimentation

The absorption systems market has historically witnessed a slow but constant evolution at varying paces depending on the geographical region since the situation changes in terms of economics, needs, and governmental regulation (Herold et al., 2016). A summary of the companies producing small-scale NH₃-H₂O absorption cooling systems (to the best of our knowledge) is presented in Table I.2, and the experiments performed on these systems available in the literature are presented in Table I.3 (only the ones with enough data to be represented in the table are shown).

Table I.2: NH₃-H₂O small-capacity commercial absorption chillers and their catalog data.

Company	Model	$\dot{Q}_{e,cat}$ (kW)	Heat source	Heat sink	t_g^i (°C)	t_c^i (°C)	t_c^e (°C)	t_e^o (°C)	COP_{cat}	COP_{carnot}	Comments	REF
AGO (GER)	ago congelo	50	-	Water	95	20	20	0	0.6	2.78		(AGO AG Energie + Anlagen, 2019)
SolarNext (GER)	Chillii PSC10 / PSC12	10 / 12	-	Water	75	24	24	15	0.65	4.69	Cooling ceiling Fan coils	(SolarNext AG, 2008a) (SolarNext AG, 2008b)
Pink (AT)	PC19	12.3 18.6 19.5	- - -	Water Water Water	95 85 75	24 24 24	24 24 24	-3 6 15	0.47 0.62 0.72	1.93 2.64 4.69	Minus-cold Fan coils Cooling ceiling	(PINK, 2012)
ROBUR (IT)	GAHP-AR GAHP-GS GAHP-WS GA-ACF	16.9 7 / 12.1 / 16.4 10.6 / 16.6 / 18.7 13.3 17.1 / 17.7	Natural Gas or GPL	Air Geothermal Water Air Air	- - - - -	35 40 30 35 35	35 40 30 35 35	7 7 7 -5 7	0.67 0.67 0.72 0.52 0.7	- - - - -	Gas Utilization Efficiency (GUE) is used as COP_{cat} .	(ROBUR, 2017)
Tranter Solarice (GER)	XS30 / XS50	30 / 50	-	-	95	20	20	10	0.6	5.77		(Tranter Solarice, 2012a, 2012b)

The Robur brand was first investigated by Lazzarin et al. (1996), who simulated the performance of a 17.5-kW air-cooled machine with a rectifier and RHX by using a linear relationship between the inverse COP and a dimensionless temperature ratio (function of the inlet temperatures of the three temperature levels and the outlet temperature of the evaporator temperature) first proposed by Ng et al. (1994) (see Eqs. (I.4) and (I.5)). In Eq. (I.5), C_1 and C_2 are variables that depend on the operating temperatures and irreversible losses. The predicted results were close to the experimental ones, except for extreme temperature values (high t_{int} or low t_e). Horuz and

Callander modified a 10-kW Robur Servel ACD-3600 gas-fired system by replacing the air-cooled heat sink by a water-cooled one. The system performed slightly better (less than 10%) with the water-cooled heat exchanger (Horuz and Callander, 2004).

$$t^* = \frac{t_g^i - t_c^i}{t_e^i - t_e^o} \quad (I.4)$$

$$\frac{1}{COP} = C_1 + C_2 t^* \quad (I.5)$$

Another tested brand was SolarNext and their models Chilli PSC10 (10 kW) and Chilli PSC12 (12 kW), which have shown good experimental agreement in some studies (Labus et al., 2013; Le Lostec et al., 2013). Le Lostec et al. (2012) tested the PSC10 model and observed that when t_e decreases, the COP decreases significantly, perhaps due to an evaporator overfeed. Cooling capacity oscillations due to refrigerant expansion control were also observed. Finally, the chiller's performance is also impacted by the generator, condenser, and absorber temperatures as well as the solution flow.

Table I.3: Experimental studies on small-capacity commercial $\text{NH}_3\text{-H}_2\text{O}$ absorption chillers reporting the operating conditions.

<i>Model</i>	t_g^i (°C)	t_c^i (°C)	t_a^i (°C)	t_e^i (°C)	COP_{exp}	COP_{carnot}	$\dot{Q}_{e,exp}$ (kW)	<i>REF</i>
SolarNext Chilli PSC10	75	22	22	14	0.63	5.46	6.6	(Le Lostec et al., 2012)
	86.3	22.3	22.3	15.4	0.62	7.45	10.5	(Le Lostec et al., 2013)

1.2.2.2. $\text{NH}_3\text{-LiNO}_3$ and NaSCN

Some alternative absorbents to replace water have been proposed so as to avoid the need for a rectifier in ammonia-based systems and at the same time to improve other properties such as the solubility in ammonia, less corrosion of steel, and lower generator temperatures (Blytas and Daniels, 1962; Mansoori and Patel, 1979; Zhu and Gu, 2010). Ammonia/salt refrigeration systems seem to be the most plausible application in refrigeration units with small cooling capacity, thanks to their low driving temperature and good adaptability for high sink temperatures (t_a/t_c) (Cai et al., 2014a). The most popular salts are NaSCN and LiNO_3 (Blytas and Daniels, 1962; Srikihrin et al., 2001; Wu et al., 2012). According to Ferreira, the systems based on these working fluids both present $COPs$ about 10% (absolute) higher than the ones with $\text{NH}_3\text{-H}_2\text{O}$ (Infante Ferreira, 1984).

1.2.2.2.1. $\text{NH}_3\text{-LiNO}_3$: Theoretical studies and experimental prototypes

LiNO_3 has been more extensively studied than NaSCN (Kaushik and Kumar, 1985), probably because it was first discovered (Cai et al., 2016) or because it possesses a wider range of operating conditions (Davis et al., 1921). This salt was already mentioned as an absorbent for NH_3 in the GB358844 (A) patent filled by Electrolux Ltd in 1930 (Electrolux Ltd, 1930). LiNO_3 is slightly toxic, noncombustible, stable, and noncorrosive to stainless steel (Heard and Ayala, 2003). If appropriate security measurements are taken, the resulting system is considered safe (Cai et al., 2014b). $\text{NH}_3\text{-LiNO}_3$ has presented some disadvantages during experiments such as low heat and mass transfer (caused by elevated viscosity) in the absorber and desorber, which results in lower experimental performance than expected (Cera-Manjarres et al., 2018; Wu et al., 2014). Best et al. (1991) presented a simulation for systems using $\text{NH}_3\text{-LiNO}_3$ as the working fluid and provided the thermodynamic design data for this kind of system. They obtained thermal $COPs$ between 0.012 and 0.462.

A summary of the small-capacity prototypes of $\text{NH}_3\text{-LiNO}_3$ absorption cooling systems developed in laboratories and their operating conditions is given in Table I.4. To the best of our knowledge, the first experimental study on an $\text{NH}_3\text{-LiNO}_3$ system was reported in the PhD thesis of Infante Ferreira (1985), who constructed a single-stage chiller (with RHX and SHX) that provided between 0.8 and 3.69 kW of cooling capacity. One decade later, Ayala et al. (1994), adapted the 10.5-kW $\text{NH}_3\text{-H}_2\text{O}$ absorption chiller presented in (Ayala Delgado, 1992) to use $\text{NH}_3\text{-LiNO}_3$ instead. The system provided cooling temperatures between -10 and 0°C with $COPs$ between 0.3 and 0.6. Moreover, the cooling capacity was reduced by about half of the design value (with the $\text{NH}_3\text{-H}_2\text{O}$ working pair) (Heard et al., 1996). Some years later, other experimental prototypes were presented. For example, the HVAC manufacturer CIAT and the Rovira i Virgili University conducted a project to develop a 10-kW system operating with the $\text{NH}_3\text{-LiNO}_3$ working pair. Two pre-industrial prototypes were developed, a water-cooled (of 12.9 kW) and an air-cooled system (of 9.3 kW), both using brazed plate heat exchangers (BPHEs) in all the thermal components (Zamora et al., 2011). At $t_{amb} = 41^\circ\text{C}$, the air-cooled chiller could still provide 64% of its nominal capacity (at $t_{amb} = 35^\circ\text{C}$) (Zamora et al., 2014). Zamora et al. (2015) later determined the performance characteristics of the water-cooled prototype and concluded that at part-load operation, it is much more convenient to use an ON-OFF control than to change the hot water temperature; in this way, the behavior of the system was more agile and responsive. In a different context, Llamas-Guillén et al. (2014) changed the evaporator of an air-cooled 5-kW system (first presented in (Llamas et al., 2007)) to improve its performance and compactness (Best et al., 2011). The first prototype, which included an air-cooled evaporator, did not yield useful cooling temperatures. During experiments, the new prototype produced evaporator temperatures below 10°C with $COPs$ in the range of 0.3–0.4 and a maximum cooling capacity of 4.5 kW. Hernández-Magallanes et al. (2014) presented the development and experimental assessment of a 3-kW absorption solar cooling system. The system delivered up to 2.7 kW of cooling and a minimum evaporator temperature of 1°C . The experimental COP ranged between 0.45 and 0.7. Domínguez-Inzunza et al. (2016) reported on an experimental assessment of a system using a falling film shell-and-tube absorber and generator. The system achieved a cooling capacity of 4.5 kW at a generator temperature of 100°C . Evaporator temperatures as low as 4°C were obtained, and the COP ranged from 0.27 to 0.62. Finally, Jiménez-García and Rivera (2018) designed and constructed a system using only PHE in the thermal components. The system achieved a cooling power of 3.1 kW, cooling temperatures as low as 6°C , and a COP or around 0.62.

Table I.4: In-lab developed prototypes of small-capacity $\text{NH}_3\text{-LiNO}_3$ absorption cooling systems and operating conditions.

$\dot{Q}_{e,nom}$ (kW)	Heat source	Heat sink	S H X	R H X	t_g^i ($^\circ\text{C}$)	t_c^i ($^\circ\text{C}$)	t_a^i ($^\circ\text{C}$)	t_c^e ($^\circ\text{C}$)	$\dot{Q}_{e,exp}$ (kW)	COP_{exp}	COP_{carnot}	REF
-	Electric heater	Water	x	x	90	20	20	-10	1.6	0.54	1.69	(Infante Ferreira, 1985)
10.5	Geotherm al	Water	x		134.6	20	20	-7	5.24	0.4	2.77	(Ayala et al., 1994) (Heard et al., 1996)
7.82	Electric heater	Air	x		143	29	29	10	4.5	0.4	4.08	(Llamas-Guillén et al., 2014)
10	Electric heater	Air	x	x	90	35	35	15	9.3	0.6	2.18	(Zamora et al., 2014)
10	Electric heater	Water	x	x	90	37.5	37.5	15	10.16	0.67	1.85	(Zamora et al., 2014)
3	Electric heater	Water	x		95	18	18	6.6	2.63	0.68	5.13	(Hernández- Magallanes et al., 2014)
4.5	Electric heater	Water	x		100	20	20	8.6	4.5	0.42	5.3	(Domínguez-Inzunza et al., 2016)
-	Electric heater	Air	x		94	37.4	44.6	6	1.43	0.33	1.19	(Cai et al., 2016)
-	Electric heater	Water	x		95	20	20	8	3.1	0.62	4.77	(Jiménez-García and Rivera, 2018)

Cai et al. (2016) presented a system designed to operate with NH_3 -salt pairs. It was tested both with LiNO_3 and NaSCN . These results are presented in Section 1.2.2.4 as a comparison between the two working pairs.

1.2.2.2.2. NH_3 - NaSCN : Theoretical studies and experimental prototypes

NaSCN was first considered as a possible absorbent for the NH_3 refrigerant by Blytas and Daniels (1962). It is inexpensive, nonexplosive, chemically stable, and noncorrosive on iron, steel, and copper (Swartman, 1975; Tyagi, 1984). NH_3 - NaSCN seems to perform better than the NH_3 - LiNO_3 working pair, especially at high generator temperatures. Indeed, the $COPs$ of this working fluid are about 10% higher than the ones of the NH_3 - H_2O system working under the same conditions (Zhu and Gu, 2009). However, the system is limited to working at evaporator temperatures over -10°C to avoid crystallization (Abdulateef et al., 2007; Sun, 1998). NaSCN is considered a moderately toxic noncombustible material. Its use in absorption systems is considered safe if the appropriate security measures are taken (Cai et al., 2014b). The properties of this working pair have been studied and presented by different authors (Blytas and Daniels, 1962; Infante Ferreira, 1984; Sun, 1998). Best et al. (1993) presented thermodynamic design data for an absorption cooling system using NH_3 - NaSCN as a working fluid. They obtained a range of $COPs$ between 0.123 and 0.555 in the simulated conditions. A summary of the small-capacity prototypes of NH_3 - NaSCN absorption cooling systems developed in laboratories and their operating conditions is presented in Table I.5.

Table I.5: In-lab developed prototypes of small-capacity NH_3 - NaSCN absorption cooling systems and operating conditions.

$Q_{e,nom}$ (kW)	Heat source	Heat sink	S H X	R H X	t_g^i ($^\circ\text{C}$)	t_c^i ($^\circ\text{C}$)	t_a^i ($^\circ\text{C}$)	t_e^o ($^\circ\text{C}$)	$Q_{e,exp}$ (kW)	COP_{exp}	COP_{carnot}	REF
-	Electric heater	Water	x		100	23.5	23.5	5	0.82	0.481	3.08	(Zhu et al., 2008)
-	Electric heater	Air	x		104	33	43.8	-2.4	0.65	0.35	1.22	(Cai et al., 2016)

Zhu et al. (2008) presented a theoretical and experimental study on the characteristics and performance of an NH_3 - NaSCN system with SHX. This system can work with generator temperatures over 58°C (see Figure I.3a). Moreover, it can operate at high condenser and absorber temperatures (around 23°C) with low evaporator temperatures and reasonable $COPs$ (around 0.35, see Figure I.3b). Their simulated versus experimental COP comparison is shown in Figure I.3b; the discrepancies are mainly due to thermal losses and the mass transfer resistance of vapor ammonia in the absorber, not considered in the simulation. Zhu and Gu (2010) developed a second law-based thermodynamic analysis for the same system and concluded that the COP increases if t_g and t_e increase, while it decreases if t_a and t_c increase. On the other hand, when the COP increases, the second law efficiency may decrease mainly because of the exergy loss in some components. Cai et al. (2014a) later reported that the mean ionic activity coefficient of NaSCN in liquid ammonia had not been provided before and that the one used for the last analysis by Zhu and Gu (2010) seemed to be that of the LiBr in water, consequently, the entropy calculation results might be inaccurate (Cai et al., 2014b). Therefore, they presented the thermophysical properties of NH_3 - LiNO_3 and NH_3 - NaSCN based on a new regression of experimental data and studied their thermodynamic cycles (see Figure I.4b).

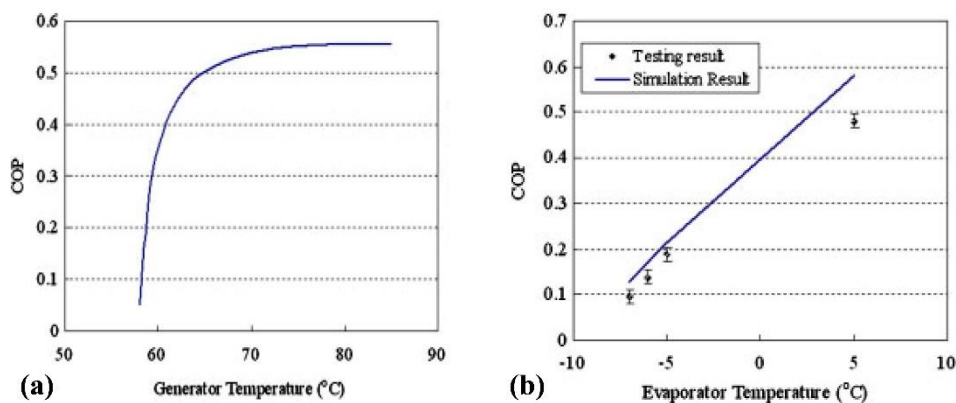


Figure I.3: $\text{NH}_3\text{-NaSCN}$ single-stage system's (a) simulated COP against generator temperature ($t_a=t_c=15^\circ\text{C}$, $t_e=-20^\circ\text{C}$) and (b) COP experimental vs. simulated ($t_a=t_c=23^\circ\text{C}$, $t_g=100^\circ\text{C}$) (Zhu et al., 2008).

1.2.2.3. NH_3 -Ionic Liquids: Theoretical studies

Ionic liquids (IL) are salts in liquid form at room temperature (with a melting point lower than 100°C) usually with organic cations and inorganic anions (Seddon, 2003). They have been proposed as new absorbents or additives to address the disadvantages presented by the conventional working pairs (Cera-Manjarres et al., 2018). Many of them present good physical and chemical properties such as chemical stability, thermal stability, high miscibility in most refrigerants, nonflammability, low corrosive character, nontoxicity, and a broad range of liquid temperatures (Khamooshi et al., 2013; Kim and Kohl, 2014; Ruiz et al., 2014). According to Liang et al. (2011), the most favorable working pairs with ILs are the ones with higher absorption properties, otherwise, they yield to high circulation ratios and low COP s. Scammells et al. (2005) warned that research on the potential problems of ILs lagged behind the explosion of interest in their application. In recent years, the scientific community warned about the risk of their application when considering the entire life cycle of the systems (Cvjetko Bubalo et al., 2014). Some issues discussed were the presence of impurities generated in their preparation, the degradation of their properties over time, their toxicity in some cases (which could lead to severe health threats), and the need for recycling due to poor biodegradability (Bubalo et al., 2017; Cvjetko Bubalo et al., 2014; Scammells et al., 2005).

Shiflett and Yokozeki (2006) patented the application of ILs as working fluid in absorption refrigeration. They later presented the solubilities of NH_3 in different ILs and a simple model for COP comparison. Results showed the highest ever observed solubilities in ILs, comparable to the $\text{NH}_3\text{-H}_2\text{O}$ case. However, lower COP s were obtained for the $\text{NH}_3\text{-ILs}$ working fluids (Yokozeki and Shiflett, 2007a, 2007b). Kotenko et al. (2011) compared various $\text{NH}_3\text{-ILs}$ using ASPEN Plus. $\text{NH}_3\text{-[bmim][PF}_6\text{]}$ led to the highest COP values, even higher than the $\text{NH}_3\text{-H}_2\text{O}$ system (around 8% better); however, the circulation rate (CR) was ten times higher. Moreover, $\text{NH}_3\text{-ILs}$ showed a greater COP decrease compared with the $\text{NH}_3\text{-H}_2\text{O}$ system when the difference between the heat rejection temperature and the evaporation temperature (temperature lift) increased. Bedia et al. (2012) screened ILs as NH_3 absorbents on the basis of thermodynamic and kinetic analysis and proposed [choline][NTf₂] as the most suitable solvent. Ruiz et al. (2014) studied the thermodynamic performance of $\text{NH}_3\text{-ILs}$ using COSMO-based process simulations with Aspen Plus/Aspen HYSYS and concluded that this method effectively predicts the properties of solutions and gives reasonably good estimations of the cycle performance. Metal ions were proposed to increase the solubility of NH_3 in common ILs (Sel et al., 2015). In this context, Chen and Bai (2016) proposed [emim] Cu_2Cl_5 as an NH_3 absorbent. They experimentally measured vapor pressures and simulated the system's thermal performance. The [emim] $\text{Cu}_2\text{Cl}_5\text{-NH}_3$ pair performed better than the $\text{NH}_3\text{-H}_2\text{O}$ working pair, and even if it had lower performance than the $\text{LiBr-H}_2\text{O}$ system, it had a wider scope of operating temperature conditions. Cera-Manjarres et al.

(2018) presented the measured vapor pressures of NH_3 with four different ILs, concluding that the most suitable absorbent is $[\text{EtOHmim}][\text{BF}_4]$, as it has a high affinity to NH_3 at $T < 60^\circ\text{C}$ in the absorber. However, this affinity decreases with the operating temperature in the generator ($80^\circ\text{C} < T < 100^\circ\text{C}$). More analyses need to be performed considering safety requirements, compatibility of materials, and all the range of possible operating conditions of the considered system. To the best of our knowledge, no experimental results on absorption chillers working on the NH_3 -ILs have been presented to date.

1.2.2.4. Comparisons of NH_3 -based absorption systems

As mentioned earlier, the NH_3 - H_2O working pair is the most conventional working pair for ammonia-based systems. However, its drawbacks have led scientists to look for other options to replace it. The theoretical thermodynamic cycle comparison is the first step in the study of the viability of new working pairs. The present section describes theoretical comparative studies that have been presented in the search for these innovative working pairs.

Kaushik and Kumar (1985) reported a comparative evaluation of a system using NH_3 - LiNO_3 and NH_3 - H_2O as working fluids. For a single-stage chiller, the *COP* of NH_3 - LiNO_3 is higher than the one of NH_3 - H_2O , especially for higher generator temperatures (due to the heat loss in the partial rectification process of the NH_3 - H_2O system). Considering that the need for a rectifier is also eliminated, this makes NH_3 - LiNO_3 a very suitable option for compact refrigeration units. Similar conclusions were obtained by Táboas et al. (2014), who compared the same working fluids for the use of waste heat provided by diesel engines of fishing ships.

Sun (1998) compared the performance of the NH_3 - LiNO_3 and NH_3 - NaSCN working pairs with the conventional NH_3 - H_2O pair (see Figure I.4a) and concluded that NH_3 - LiNO_3 and NH_3 - NaSCN lead to higher *COPs* and do not need a rectifier. The NH_3 - NaSCN working pair seems to be slightly better than NH_3 - LiNO_3 (especially at high t_g); however, it is limited to working at t_e over -10°C to avoid crystallization risks. Abdulateef et al. (2007, 2008) conducted a similar study and obtained similar results and conclusions. Farshi et al. (2014) confirmed this and also reported that the NH_3 - NaSCN is limited in the range of t_g (due to crystallization) and presents a higher *f*. Cai et al. (2014a) confirmed that the NH_3 - LiNO_3 working pair has a wider range of operating generator temperatures and that NH_3 - NaSCN has higher *COPs* at higher t_g (see Figure I.4b). In a separate paper, they presented an exergy analysis of the same system, which contains an air-cooled non-adiabatic type absorber, taking into account the variation in solution concentration for the ammonia/salt solution exergy calculation. The proposed configuration was proved theoretically viable as it showed relatively high performance for practical applications (Cai et al., 2014b). Rogdakis and Antonopoulos (1995) and Antonopoulos and Rogdakis (1996a) found that NH_3 - LiNO_3 is more suitable than NH_3 - NaSCN for heating purposes (winter), as it provides a superior heat-gain factor and useful thermal power; while for cooling (summer), however, the choice depends on the specific working conditions, as NH_3 - LiNO_3 offers a higher cooling power, while NH_3 - NaSCN provides a higher *COP*, especially for air-cooled systems.

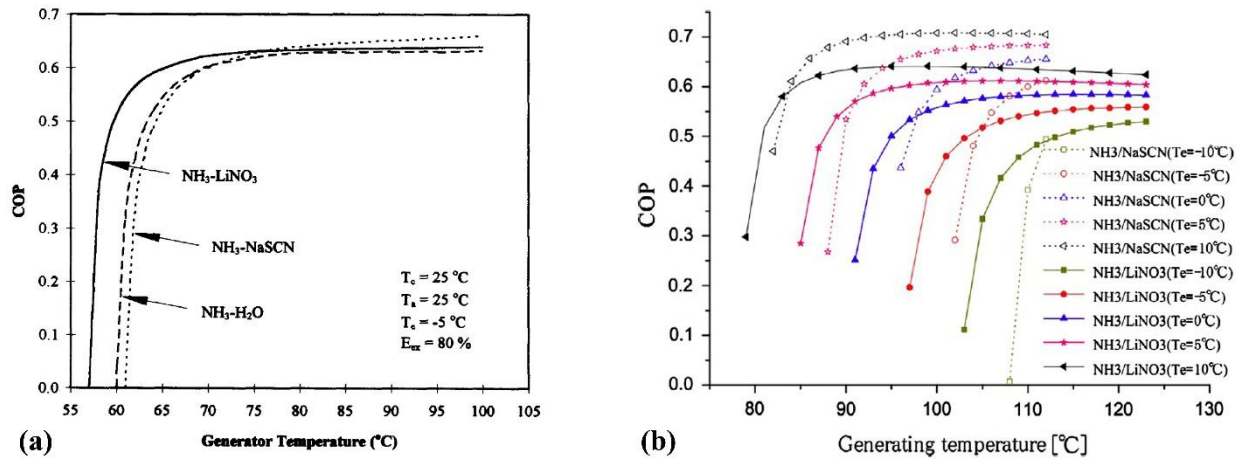


Figure I.4: Comparison of COP against generator temperature (a) for the $\text{NH}_3\text{-H}_2\text{O}$, $\text{NH}_3\text{-LiNO}_3$, and $\text{NH}_3\text{-NaSCN}$ working pairs (Sun, 1998) and (b) for the $\text{NH}_3\text{-LiNO}_3$ and $\text{NH}_3\text{-NaSCN}$ working pairs at different evaporator temperatures ($T_a = T_c = 40^\circ\text{C}$) (Cai et al., 2014a).

Regarding experimental comparisons, as mentioned in Section 1.2.2.2.1, Cai et al. (2016) presented a system designed to operate with NH_3 -salt working pairs. Two salt absorbents were tested, LiNO_3 and NaSCN , and two series of tests were run, one for ice production and another to test for variable working conditions. In the ice production test, the $\text{NH}_3\text{-LiNO}_3$ system reached the lowest evaporation temperature of -13.1°C at an average COP of 0.15. On the other hand, the $\text{NH}_3\text{-NaSCN}$ system reached -7.5°C at an average COP of 0.2. Concerning the variable working conditions test, the $\text{NH}_3\text{-NaSCN}$ system's COP ranged from 0.2 to 0.35, while for the $\text{NH}_3\text{-LiNO}_3$ system, the COP ranged from 0.15 to 0.29. The experimental COP of the $\text{NH}_3\text{-LiNO}_3$ system is on average 30–40% lower than that of the theoretical results, while for the $\text{NH}_3\text{-NaSCN}$ system the deviation is lower and even close to the theoretical results in some cases (see Figure I.5). The $\text{NH}_3\text{-NaSCN}$ system needs higher generator temperatures than the $\text{NH}_3\text{-LiNO}_3$ system for the same evaporator temperatures, and the $\text{NH}_3\text{-LiNO}_3$ can withstand higher values of generator temperatures with no risk of crystallization. Hence, the $\text{NH}_3\text{-LiNO}_3$ system is more suitable for practical applications where a lower temperature is needed.

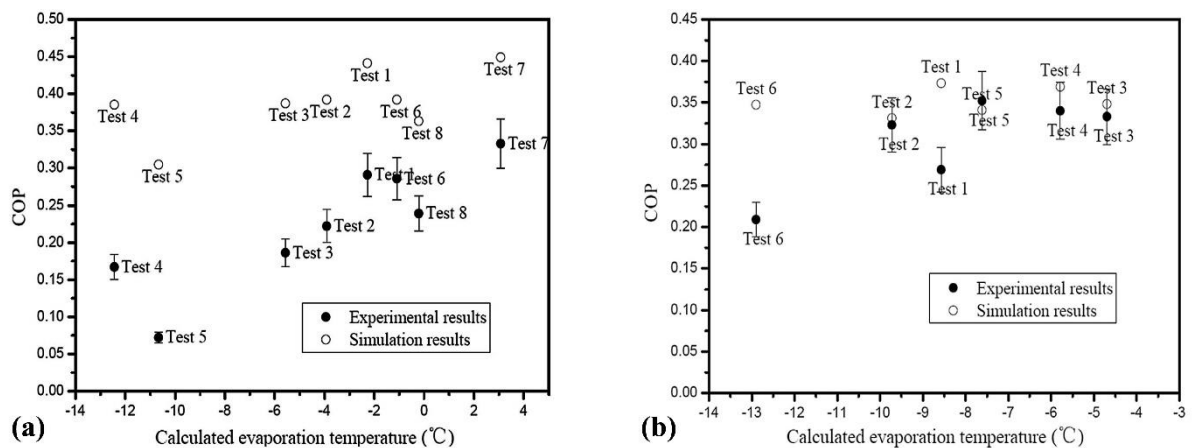


Figure I.5: Experimental and simulated COP comparison for the (a) $\text{NH}_3\text{-LiNO}_3$ system and the (b) $\text{NH}_3\text{-NaSCN}$ system (Cai et al., 2016).

Finally, Chen et al. (2014) compared the IL $[\text{bmim}]\text{Zn}_2\text{Cl}_5$ with NaSCN as ammonia absorbent through a thermodynamic analysis. The COP and exergetic efficiency of the $\text{NH}_3\text{-}[\text{bmim}]\text{Zn}_2\text{Cl}_5$ system were slightly higher than for the $\text{NH}_3\text{-NaSCN}$ system at high T_g (higher than 73°C for the exergetic efficiency and higher than 80°C for the COP at $T_{int} = 25^\circ\text{C}$ and $T_e = -10^\circ\text{C}$) and low T_c and T_a (lower than $28\text{-}30^\circ\text{C}$ at $T_g = 90^\circ\text{C}$ and $T_e = -10^\circ\text{C}$). In a separate paper, the same authors presented

the development of ILs as working pairs and concluded that the NH_3 -[bmim] Zn_2Cl_5 pair was the most ideal, similar to the H_2O -LiBr working pair, but with a wider range of operating conditions (Liang et al., 2013).

1.2.3. Water-based working fluids

Water is a natural refrigerant, abundant, low-cost, and harmless to the environment. Moreover, its good thermal properties such as high latent heat of evaporation make it a very good option as a refrigerant in absorption systems (Arshi Banu and Sudharsan, 2017). In general, the performance of water-based absorption systems is higher than that of ammonia-based systems. However, water has some disadvantages, such as its restriction to positive cooling temperatures and its subatmospheric evaporating pressure, which leads to leak problems and expensive components for vacuum operation (Karamangil et al., 2010; Muthu et al., 2008; Sun et al., 2012; Wu et al., 2014).

1.2.3.1. Conventional water-based working pair: H_2O -LiBr

H_2O -LiBr is preferred over NH_3 - H_2O because of its higher performance (de Vega et al., 2006; Horuz, 1998) and no need for a rectifier (Sun et al., 2012). However, besides the general drawbacks of water as refrigerant mentioned before, there is a risk of crystallization (especially for high t_a or low t_e , which cause problems for air-cooled absorption) (Izquierdo et al., 2004; Wang et al., 2011), a higher viscosity (which increases the pumping requirements and decreases the heat and mass transfer) (Sun et al., 2012), and corrosion problems (Brotzu et al., 2015) with the H_2O -LiBr solution.

1.2.3.1.1. H_2O -LiBr: Theoretical studies

Several studies in the literature focused on the impact of the different components or conditions on the performance of the system (Farnós et al., 2017). Eisa et al. (1986) simulated a system with no SHX and obtained a maximum COP of 0.857. De Vega et al. (2006) used correlations in the literature to simulate a system operating with PHEs and obtained COP values as high as 0.8 for low ambient temperatures (around 20°C). For specific cases of electronics cooling, Kim et al. (2008) presented a miniature system with a dual-channel evaporator, a micro-channel desorber, and a hydrophobic membrane condenser/absorber. Experimental validation is still needed. Other studies aimed to compare the heat sink or heat sources. Kühn et al. (2011) studied the constraints and demands of different heat sources and heat sinks (boreholes, groundwater, air) and concluded that every heat source and heat sink combination imposes different restrictions. More work has to be done regarding the seasonal performance and techno-economic studies for the different configurations (Kühn, 2013). Marcos et al. (2011) presented a new method for COP optimization in water- and air-cooled machines taking into account the effect of T_c , the solution concentration, and defining the crystallization limits (see [Figure I.6](#)). The problem with air cooling in H_2O -LiBr systems is that as the heat-rejection temperature is higher than for water-cooled systems and, consequently, the T_g needed to achieve the same T_e is higher and the cycle comes closer to the crystallization limit (Chen et al., 2017).

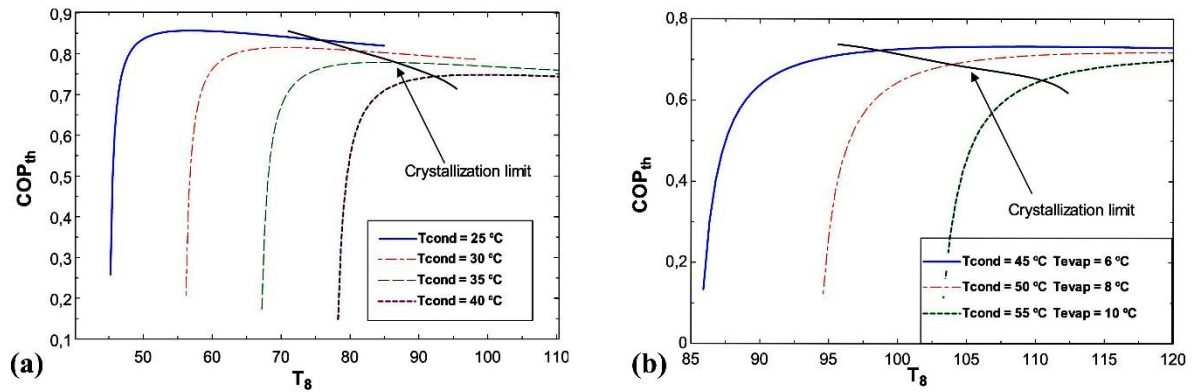


Figure I.6: COP against generator equilibrium temperature ($T_g=T_8$) for a (a) water-cooled ($T_c=5^\circ\text{C}$) and (b) air-cooled single-effect absorption chiller (Marcos et al., 2011).

1.2.3.1.2. $\text{H}_2\text{O-LiBr}$: Experimental prototypes development and experimentation

A summary of the small-capacity prototypes of $\text{H}_2\text{O-LiBr}$ absorption cooling systems developed in laboratories and their typical operating conditions is presented in Table I.6. Great attention has to be given to the design procedure of the system's components as the dimensioning of each one of them is of great importance (Florides et al., 2003; Kalogirou et al., 2001). The University of Jordan developed a low-cost solar cooling unit with $\text{H}_2\text{O-LiBr}$. The first-generation unit (FGU) consisted in a 1.75-kW unit manufactured locally with a 3.6-m^2 flat-plate solar collector in parallel with a 0.15-m^2 elliptical concentrating collector, without an SHX or RHX. This system presented a temporal COP_{max} of 0.55 (Hammad and Audi, 1992). An optimization study was developed to determine the minimum costs and maximum benefit/cost ratio, and Hammad and Abuzahra (1995) concluded that an optimum design only existed for systems with a capacity of at least 12 kW. After this study, Hammad and Zurigat (1998) presented a 5.27-kW system that replaced the workshop-fabricated components by commercially available ones. The system, coupled to a 14-m^2 flat-plate solar collector, presented a maximum experimental COP of 0.85. Air-cooled systems are an important challenge and subject of study in $\text{H}_2\text{O-LiBr}$ absorption chillers (Kim and Infante Ferreira, 2009). Some prototypes were developed and tested with success and far from the crystallization limits of the solution. Crystallization problems occurred owing to inadequate shutdowns of the machines (Castro et al., 2007; Castro et al., 2008; Ohuchi et al., 1994).

Drost and Friedrich (1997) studied miniature heat pumps that took advantage of the elevated heat and mass transfers attainable in microstructures (constrained micro-thin films and microchannels). A man-portable cooling device was designed to provide 0.68 W with a COP of 0.68 and a weight of around 4–5 kg, while a space conditioning device was designed to provide 350 W with a COP of 0.71. To our knowledge, no experimental results were presented. Another example of micro-technology in absorption chillers is the one of Hu and Chao (2008), who presented a micro-absorption cooling system with a target cooling capacity of 40 W. The experimental results were different from the design conditions owing to the presence of non-condensable gases, heat losses, and imperfect control of the flow rates.

After years of investigation and collaboration between Phönix SonnenWärme AG, TU Berlin, ZAE Bayern, and the Institute of Rehabilitation and Modernization of Buildings (IEMB), Kühn et al. (2005) presented a compact 10-kW chiller for low driving temperatures called *Suninverse*. At nominal conditions, the system produced chilled water at 15°C with a COP of around 0.76. This system was also tested in heating operation mode (Kühn et al., 2008) and was later commercialized under the brand SonnenKlima (Kohlenbach, 2006). Kohlenbach and Ziegler published two papers describing a dynamic simulation model for transient absorption chiller performance (Kohlenbach and Ziegler, 2008a), the numerical results, and sensitivity checks to prove the model's functionality (Kohlenbach and Ziegler, 2008b).

With the aim of developing a new generation of highly efficient absorption chillers, the TU Berlin, ZAE Bayern, and Vattenfall Europe developed a system with low heat losses, simple manufacturing, compact, and low weight. The 50-kW prototype, which can achieve $COPs$ of around 0.8, was operated in two field tests supplying 44 kW of office cooling driven by district heating and 35 kW of data center cooling driven by solar energy. The new machine was expected to decrease the manufacturing costs by around 50–70% compared with the current technologies (Kühn, 2013).

In recent years, there has been an increasing interest in adiabatic absorbers for absorption systems. Gutiérrez-Urueta et al. (2011) compared two adiabatic absorber configurations (droplets and liquid sheets). The liquid sheet configuration proved to be better in terms of performance and would lead to a significant reduction in the absorber's size (up to 50%). One year later, they presented an extended characteristic equation of the machine that showed good agreement with experimental results (Gutiérrez-Urueta et al., 2012). González-Gil et al. (2011) developed a solar direct air-cooled chiller that uses an adiabatic flat-fan sheets absorber and can switch to a double-effect mode. The prototype worked efficiently at COP values of around 0.6 with a cooling power of between 2 and 3.8 kW (about 85% of the nominal capacity). Lizarte et al. (2012) later tested the same system, obtaining an evaporator temperature of 14.3°C and a mean COP of 0.53. Chen et al. (2017) presented an experimental and analytical study of a 6-kW solar air-cooled chiller for residential buildings. The absorber was of an adiabatic type with a finned tube pre-cooler. Experimental results showed that the system's COP is significantly affected by the temperature conditions, with its average value being 0.61.

For heat transfer enhancement, Achuthan et al. (2011) added micro-nozzles to the evaporator and the absorber of a solar absorption system, obtaining an increase in the COP from 0.3 to 0.6. Finally, Yin et al. (2012) constructed and tested an 8-kW chiller coupled to 96 m² of solar collector arrays. The system delivered 4.5 kW of cooling to a 50-m² test room with an average COP of 0.32 (Zhai et al., 2015).

Table I.6: In-lab developed prototypes of small-capacity H₂O-LiBr absorption cooling systems and operating conditions.

$\dot{Q}_{e,nom}$ (kW)	Heat source	Heat sink	S H X	R H X	t_g^i (°C)	t_c^i (°C)	t_a^i (°C)	t_g^o (°C)	$\dot{Q}_{e,exp}$ (kW)	COP_{exp}	COP_{carnot}	Comments	REF
1.76	Solar	Water			90	27.5	27.5	15	-	0.55	3.97		(Hammad and Audi, 1992)
7	Hot water	Air	x		160	35	35	6	5	0.8	2.78		(Ohuchi et al., 1994)
5.28	Solar	Water	x		71	29.5	32.5	16.2	6.2	0.69	2.43		(Hammad and Zurigat, 1998)
10	Electric heater	Water	x		75	27	27	15	10.2	0.76	3.31		(Kühn et al., 2005)
2	Hot water	Air	x		95	35	35	12	2.6	0.62	2.02		(Kühn et al., 2008)
0.04	Electric heater	Water			100	45	30	15	-	0.47	1.80		(Castro et al., 2007)
-	Solar	Water			85	28	28	15.5	0.28	0.6	3.68	Micro nozzles in evaporator and absorber	(Achuthan et al., 2011)
3.5	Electric heater	Water	x		87	28	28	5	1.2	0.28	1.98	Adiabatic absorber	(Gutiérrez-Urueta et al., 2011)
4.5	Solar	Air			105	45	42.5	10	3.4	0.64	1.34	Adiabatic absorber	(González-Gil et al., 2011)
8	Solar	Water	x		88	30	30	11	4.5	0.27	2.40		(Yin et al., 2012)
-	Electric heater	Water	x		75	27	27	15	4	0.7	3.31		(Kühn, 2013)
-	Electric heater	Water	x		75	27	27	15	4.5	0.71	3.31	Condenser and generator improved from the last one	(Kühn, 2013)
50	Electric heater	Water			90	30	30	16	50	0.8	3.41		(Kühn, 2013)
6	Solar	Air	x		90	28	28	15	8.93	0.65	3.78	Adiabatic absorber	(Chen et al., 2017)

1.2.3.1.3. H_2O -LiBr commercial systems: Presentation and experimentation

A summary of the commercial small-scale H_2O -LiBr absorption cooling systems (to the best of our knowledge) presented in Table I.7, and the experiments performed on these systems are presented in Table I.8 (only experiments with enough data to be represented are shown). Yazaki is historically the most widely studied brand in the branch of commercial absorption systems. The commercial H_2O -LiBr chillers tested in the twentieth century were the discontinued Yazaki models WFC 400 (4.5 kW) and WFC 600 (7 kW). Yeung et al. (1992) reported the performance study of a solar-powered WFC 400S system installed in Hong Kong. The integrated system showed an annual overall system efficiency of 7.8%. In the case of the WFC 600 system, Nakahara et al. (1977) presented the results of the machine coupled to solar collectors and observed that the optimal operating generator temperature was about 78°C. Bong et al. (1987) also studied this system with solar collectors in Singapore. The system provided an average cooling capacity of 4 kW with a COP of 0.58. Ng et al. (1994) later presented a theoretical and experimental analysis of the same chiller. The theoretical model proposed a new linear correlation between the inverse COP and the non-dimensional temperature ratio (presented in Section 1.2.2.1.3). Experimental results in a wide range of operating conditions proved the theoretical model. The cooling capacities obtained from the test were lower than the ones in the catalog by 10–25%. Prasartkaew and Kumar (2010) studied the possibility of integrating solar/biomass sources to drive an absorption chiller. The experimental system used a renovated WFC 600 model (working fluid and control system) and operated at 75% of its nominal capacity reaching COP s of around 0.54 at steady state (Prasartkaew and Kumar, 2013). Moreover, the chiller needed to be operated at driving temperatures higher than 85°C to obtain high COP values (Prasartkaew, 2014).

Table I.7: H_2O -LiBr small-capacity commercial absorption chillers and their catalog data.

Company	Model	$\dot{Q}_{e,cat}$ (kW)	Heat sink	t_g^i (°C)	t_c^i (°C)	t_a^i (°C)	t_e^o (°C)	COP_{cat}	COP_{cannot}	REF
EAW GER)	Wegracal SE 15 / SE 30 / SE 50	15 / 30 / 50	Water	90	30	30	11	0.71	2.47	(EAW, 2010a)
	(Discontinued)							0.73	2.47	(EAW, 2010b, 2010c)
Jiangsu Huineng (CHIN)	Wegracal Maral 1 / Maral 2	15 / 30	Water	86	27	27	9	0.75	2.58	(EAW, 2018a, 2018b)
	RXZ-11	11	Water	90	30	30	10	0.65	2.34	(Jiangsu Huineng New Energy Technology Co., 2019)
	RXZ-23	23	Water	90	30	30	10	0.68	2.34	
Rotartica (SP)	RXZ-35	35	Water	90	30	30	10	0.7	2.34	
	045v (Discontinued)	4.5	Air	90	35	35	12	0.63	1.88	(ROTARTICA, n.d.)
Shandong Lucy New Energy Technology Co., Ltd (CHIN)	TX-11/TX-23/TX-35	11.5 / 23 / 35	Water	90	27	27	10	0.69	2.89	(Shandong Lucy New Energy Technology Co. LTD, 2014)
PURIX (DEN)	A25	2.5	Air	80	35	35	13	0.81	1.66	(PURIX ApS, 2018)
Sakura (JP)	SHL003/SHL005/SHL008/SHL010 / 35 (Discontinued)	10.5 / 17.5 / 28 / 35	Water	88	31	31	8	0.7	1.93	(Sakura Corporation, 2010)
SonnenKlima (GER)	suninverse 10 (Discontinued)	10	Water	75	27	27	15	0.76	3.31	(SONNENKLIMA, 2009)
Thermax (IN)	LT 0.5 / LT 1	17.5 / 35	Water	90	29	29	7	0.66	2.14	(THERMAX, 2010)
Yazaki (JAP)	WFC-400 / WFC-600	4.6 / 7	Water	75	29.5	29.5	9	0.6	1.80	(Yazaki Corporation, n.d.)
	(Discontinued)				5					
	WFC-SC5/WFC-SC10	17.6 / 35.2	Water	88	31	31	7	0.7	1.84	(Yazaki Energy Systems Inc., n.d.) (Yazaki Energy Systems Inc., n.d.)

Another model that has been extensively studied is the WFC-SC 5 (17.5 kW) from Yazaki. Asdrubali and Grignaffini (2005) simulated and tested an experimental system with this model. The machine operated with acceptable efficiency for driving temperatures in the range of 65–70°C, showing the highest COP values at 70°C. However, the experimental performance results were lower than in the catalog because of the refrigerant overflow and low flow rate in the heat sink. The same machine was modeled in TRNSYS and tested by Martínez et al. (2012) in Alicante (Spain) integrated with solar collectors, a cooling tower, hot-water storage tanks, and a cold-water storage tank. An average COP value of 0.691 was registered and a good accuracy was reported

with the theoretical model. For the cases in which the machine operates outside the designed temperature range, Martínez et al. (2016) developed a model in EES of a Yazaki WFC-SC5 chiller and later validated it. The simulated results show a deviation of 0.75 °C for the output generator temperature and of 0.35 °C for the output evaporator temperature. Rogríguez Carabias (2014) constructed a test bench to characterize small-capacity thermal refrigeration systems and heat pumps and tested a Yazaki WFC-SC 5. The experimental results showed good agreement with the catalog data.

Another model that has been extensively studied is the Yazaki WFC-SC 10 (35.2 kW) (Beausoleil-Morrison et al., 2015). Haywood et al. (2012) used a simulator provided by Yazaki to study the possibility of using data center waste heat as the driving source for this chiller. The heat produced by the data center under standard conditions is enough to run the system. The same model was studied for solar applications by Syed et al. (2005) in Madrid (Spain). It provided a maximum cooling capacity of 7.5 kW with a cut-off temperature of 65°C. At 81°C, the system provided 6.4 kW of cooling. The maximum measured *COP* was 0.6, and the maximum daily average *COP* was 0.42. The same installation was tested by Hidalgo et al. (2008). In this case, the system provided a mean cooling power of 3 kW for a period of 6.5 h of complete solar autonomy on an average day. Further improvements were to be made in terms of the machine size and control strategy. Pongtornkulpanich et al. (2008) presented their results with a solar-driven Yazaki WFC-SC 10 installed in Thailand. The solar collectors, which were designed for the nominal chiller's *COP* of 0.7, provided 81% of the total thermal energy required. Zambrano et al. (2008) installed this chiller integrated with a solar collector and developed its dynamic model, which showed good agreement with experimental results. Ali et al. (2008) tested a solar-powered Yazaki WFC-SC 10 chiller combined with free cooling (recuperation of low external ambient temperatures at times of the day when they are low to assist AC) installed in Germany. On sunny days, the chiller operated with *COPs* in the range of 0.37–0.81. Another big issue for absorption chillers is the overflow in the evaporator. Albers et al. (2010) presented a simulation model of the part load behavior of the WFC-SC 10 and its experimental validation. The model can predict the transition from partially dry to a refrigerant overflow in the evaporator.

The second most studied brand in the literature is Rotartica and its 045v model (4.5 kW). Izquierdo et al. (2008) studied the performance of this chiller installed in Spain in 2005. The driving temperature varied in the range of 80–107°C and the average *COP* for the total period was 0.49. The same model was installed in the UK coupled with solar collectors and tested in 2007. Results indicated that the average chiller's *COP* was 0.58, and chilled water temperatures as low as 7.4°C were achieved (Agyenim et al., 2010). Monné et al. (2011) developed a TRNSYS model and experimentally analyzed the performance of a solar-powered cooling installation in Zaragoza (Spain). In 2007, the average *COP* was 0.6 and the cooling power was between 4 and 5.6 kW. In 2008, the *COP* ranged from 0.46 to 0.56 and the cooling capacity from 3.6 to 5.3 kW. Both the simulated and experimental results showed a strong influence of the heat sink and driving temperature. For this reason, a geothermal heat sink was selected to integrate the system, and the first theoretical results showed a *COP* increase of up to 42%. Evola et al. (2013) presented a model for the dynamic simulation of a solar-assisted Rotartica 045v chiller considering the non-steady behavior due to thermal and mass storage in the components. The simulated and experimental results had a good agreement for both a daily and seasonal basis.

Some other machines were also tested in a few studies. Li et al. (2016) performed an experimental investigation of the performance of a solar cooling system with a TX-23 (23 kW) chiller model of the LUCY brand. The chiller presented *COP* values between 0.18 and 0.6, probably due to long pipelines (heat loss) and very low driving temperatures (48–73°C). Another studied brand is EAW and its model Wegracal SE 30 (30 kW) (Marc et al., 2015; Praene et al., 2011), which was

first tested by Marc et al. (2010) on a solar system operating with no backup installed in Reunion Island, achieving an indoor temperature 6°C below the outdoor ambient temperature.

Table I.8: Experimental studies on small-capacity commercial H₂O-LiBr absorption chillers reporting the operating conditions.

<i>Model</i>	t_g^i (°C)	t_c^i (°C)	t_a^i (°C)	t_e^i (°C)	COP_{exp}	COP_{carnot}	$\dot{Q}_{e,exp}$ (kW)	<i>REF</i>
EAW Wegracal SE 30	67.5	25	25	10	0.67	2.36	20	(Marc et al., 2015)
Rotartica 045v	100	33	33	15	0.52	2.87	4.6	(Izquierdo et al., 2008)
	77.1	24	24	10.1	0.66	3.09	2.82	(Agyenim et al., 2010)
	91	27.7	27.7	11.5	0.57	3.05	5.7	(Monné et al., 2011)
	92.5	31.2	31.2	11.5	0.51	2.42	4.4	
Yazaki WFC-600	90	33	33	13	0.74	2.25	5.6	(Evola et al., 2013)
	78	16	16	7.5	0.75	5.83	5.75	(Nakahara et al., 1977)
	81	28	28	12	0.58	2.67	4	(Bong et al., 1987)
	75	29.5	29.5	10.5	0.47	1.95	2.15	(Ng et al., 1994)
	86	32	32	14.5	0.54	2.47	5.25	(Prasartkaew and Kumar, 2013)
	80	32	32	15	0.51	2.30	4.2	(Prasartkaew, 2014)
Yazaki WFC-SC5	80.7	18	18	8.5	0.24	5.25	4.7	(Asdrubali and Grignaffini, 2005)
Yazaki WFC-SC10	90	28	28	16	0.66	4.11	29.5	(Zambrano et al., 2008)
	85	29.5	29.5	12	0.72	2.53	25	(Albers et al., 2010)
	93	29	29	9.5	0.75	2.53	40.5	(Beausoleil-Morrison et al., 2015)

1.2.3.2. H₂O-LiI and LiCl

As mentioned earlier, LiBr is the most common absorbent in water-based absorption chillers. However, other salts have been studied as possible alternatives. H₂O-LiI has been proposed as a viable working pair for absorption systems. Patil et al. (1991) presented the thermodynamic design data of this working fluid for cooling applications, achieving a similar performance to the H₂O-LiBr working pair. However, LiI has mostly been studied and used as one element in multi-component absorbents, and no other studies of this salt as single absorbent are available in the literature (Sun et al., 2012).

Another proposed working pair is H₂O-LiCl, which has various advantages over H₂O-LiBr such as triple-state point (for non-continuous systems), long-term stability, and lower cost. Several studies have also proved that compared with a H₂O-LiBr system, it presents higher *COPs* and exergy efficiency, mainly due to a lower circulation rate (Gogoi and Konwar, 2016; Grover et al., 1988; Patel et al., 2017). However, the higher risk of crystallization for the H₂O-LiCl system generates difficulties in its design and maintenance (Bellos et al., 2016; Patel et al., 2017). Moreover, it seems that depending on the studied operating conditions, the performance of the H₂O-LiCl pair might be lower than that of the conventional H₂O-LiBr working pair (de Vega et al., 2018; Parham et al., 2013). There are no experimental results with single-stage absorption systems for cooling using the H₂O-LiCl working pair, probably because of the high risks of crystallization (Bellos et al., 2016; Patel et al., 2017).

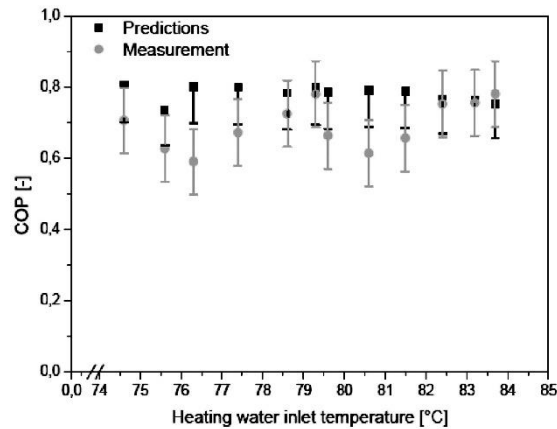
1.2.3.3. H₂O-Ionic Liquids: Theoretical studies and experimental prototypes

ILs have been proposed as H₂O absorbents. Shiflett and Yokozeki (2013) patented the use of water and at least one IL as the working fluid for absorption systems and presented a comparison for the H₂O-[emim][BF₄] and the conventional NH₃-H₂O and H₂O-LiBr working fluids, showing the proposed working pair a lower performance and much higher *f*. A summary of the small-capacity prototypes of H₂O-IL absorption cooling systems developed in laboratories and their operating conditions is presented in Table I.9.

Table I.9: In-lab developed prototypes of small-capacity H₂O-IL absorption cooling systems and operating conditions.

$\dot{Q}_{e,nom}$ (kW)	Heat source	Heat sink	S H X	R H X	t_g^i (°C)	t_c^i (°C)	t_a^i (°C)	t_e^i (°C)	$\dot{Q}_{e,exp}$ (kW)	COP_{exp}	COP_{carnot}	REF
10	Electric heater	Water	x	x	79	24	24	11	1.3	0.75	3.41	(Römich et al., 2011)
-	Electric heater	Water	x	x	75	27	27	15	2.7	0.73	3.31	(Kühn, 2013)

Römich et al. (2011) performed a simulated comparison between H₂O-[dema][CH₃SO₃] and H₂O-LiBr as working fluids. The H₂O-IL system yielded COP values around 6% close to but lower than the H₂O-LiBr system. However, during experiments (using the machine presented in (Kühn et al., 2005)) the COP of the H₂O-IL system was lower than simulated (see Figure I.7). Considering the experimental results of the H₂O-LiBr working fluid, both working fluids are comparable in terms of COP . In terms of experimental cooling capacity, the one with H₂O-IL was much lower than with H₂O-LiBr (1.3 kW vs. 10 kW) owing to the high viscosity and low wettability of the H₂O-IL solution in a system designed to work with the H₂O-LiBr working fluid (Seiler et al., 2013).


 Figure I.7: Römich and colleagues' COP against driving temperature for the H₂O-[dema][CH₃SO₃] working fluid, simulated and experimental results ($T_c=T_a=24^\circ\text{C}$, $T_e=11^\circ\text{C}$) (Römich et al., 2011).

Radspieler and Schweigler (2011) studied the H₂O-[emim][(CH₃)₂SO₄] working fluid with an experimental chiller Built at ZAE Bayern using an adiabatic desorber and absorber (spray chambers with external plate heat exchangers). COP values similar to the ones with the H₂O-LiBr working fluid were obtained but with a much lower cooling capacity (about one-third at $t_g^i=95^\circ\text{C}$, $t_c^i=t_a^i=27^\circ\text{C}$, and $t_e^i=17^\circ\text{C}$). Moreover, the tested working pair showed a lack of chemical stability (Kühn, 2013).

1.2.3.4. Comparisons of the water-based working fluids

Saravanan and Maiya (1998) performed a thermodynamic analysis of systems running on four binary working fluids (H₂O-LiBr, H₂O-NaOH, H₂O-LiI and H₂O-LiCl) and other multi-component working fluids (see Figure I.8). Among the binary working fluids, the H₂O-LiCl is the best option from the point of view of cut-off temperature and circulation ratio. Several studies have proved that the main advantages of H₂O-LiCl over H₂O-LiBr are a higher COP , higher exergy efficiency (and thus less solar collecting area), lower irreversibilities, and lower driving temperatures (Gogoi and Konwar, 2016; Patel et al., 2017; She et al., 2015). However, a higher crystallization risk exists compared with the H₂O-LiBr working pair (see Figure I.11) (Bellos et al., 2016), and this might be the main reason why there are no experimental prototypes running in continuous mode.

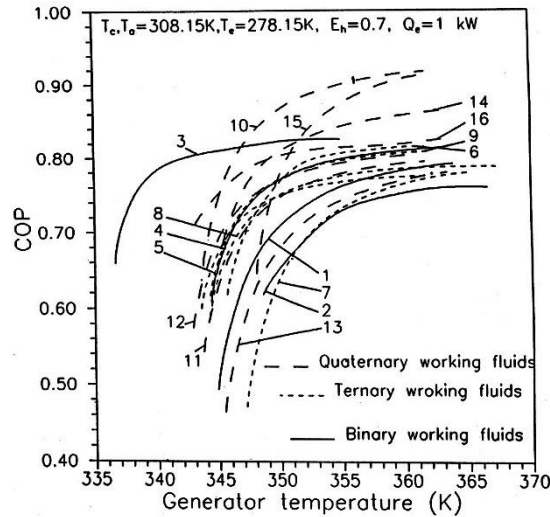


Figure I.8: COP comparison against generator temperature for different binary [(1) H₂O-NaOH, (2) H₂O-LiI, (3) H₂O-LiCl, (4) H₂O-LiBr] and other multi-component working fluids (5 to 16) (Saravanan and Maiya, 1998).

TU Berlin and Evonik Industries AG studied the potential of ILs in absorption chillers, and different ILs were tested in a glass shell prototype. Results are shown in Figure I.9 for the initial machine and the machine with an improved condenser and generator (new C/G) at $t_g^i = 75^\circ\text{C}$, $t_{int}^i = 27^\circ\text{C}$, $t_e^o = 18^\circ\text{C}$. H₂O-IL systems reach COP values close to the H₂O-LiBr system. However, their cooling capacity is always lower owing to a mass transfer inhibition probably due to a higher solution concentration (Kühn, 2013). According to Seiler et al. (2013), COP simulations using plain energy balances and phase equilibria are not enough to evaluate new working fluids, and thus in the future, more research has to be done to underline the heat and mass transfer phenomena.

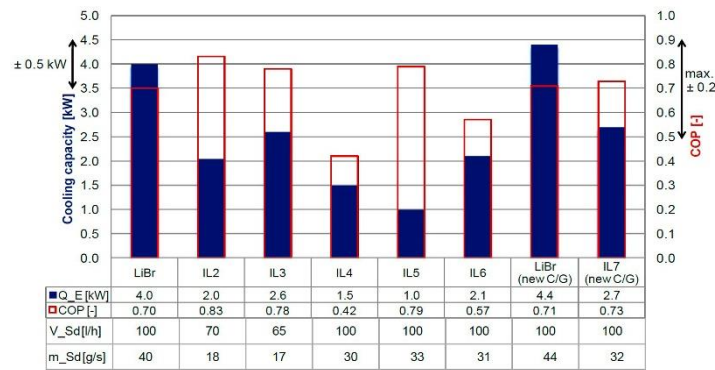


Figure I.9: Experimental results for different H₂O-ILs and H₂O-LiBr working pairs (Kühn, 2013).

1.2.4. Working fluids with other refrigerant bases

1.2.4.1. Alcohol-based working fluids

The properties of working pairs with alcohols as the refrigerant (thermal stability and high output temperature) make them more interesting for heating or heat transformer applications (Sun et al., 2012). However, there have been some theoretical studies for cooling applications, for which, just as with water as refrigerant, alcohols would usually operate in vacuum conditions (Chen et al., 2012). Wang and Zheng (2008) studied a system using TFE (2,2,2-trifluoroethanol) as the

refrigerant and three ILs as absorbents ([BMIM]Br, [BMIM]Br₄, and [EMIM]Br₄). The TFE-[BMIM]Br system presented the highest *COP* and lowest circulation ratio. Liang et al. (2010) presented a theoretical study of a system based on the [MMIM]DMP-CH₃OH working fluid, concluding that this new proposed working pair shows a higher *COP* with a lower T_g and T_c than the conventional ones (NH₃-H₂O and H₂O-LiBr). Moreover, it has a refrigerating capacity and circulation ratio that lie between them. Chen et al. (2012) studied a system using the [mmim]DMP-methanol working fluid and concluded that (1) f of the proposed working fluid is higher than that of the H₂O-LiBr working pair, but still acceptable and tolerable, (2) the *COP* of the new working fluid lies between the two conventional ones (NH₃-H₂O and H₂O-LiBr) under most operating conditions, and (3) the system working with the proposed working fluid operates with high *COPs* when the driving temperature is too high to drive the H₂O-LiBr system.

1.2.4.2. HFCs and HCFCs-based working fluids

Hydrochlorofluorocarbons (HCFCs) and chlorofluorocarbons (CFCs) are both banned under the 1987 Montreal Protocol owing to their ozone depleting potential. Hydrofluorocarbons (HFCs) raised as an alternative to those refrigerants as they are non-ozone depleting gases. These refrigerants have the advantages of immiscibility with water and aqueous streams for direct-contact heat transfer and a low-grade driving temperature; moreover, they operate at similar pressure levels as ammonia. However, these refrigerants have a considerable lower enthalpy of vaporization compared with NH₃ and H₂O, and most of them possess an important global warming potential (GWP) (Borde and Jelinek, 1987). For this reason, HFCs are also to be progressively phased down under the 2016 Kigali Amendment to the Montreal Protocol that will take effect between 2019 and 2028, depending on the country's level of development (IEA, 2018a).

The HCFC R22 together with the organic absorbent DMETEG have been extensively investigated as a working pair for absorption systems (Jelinek et al., 2007). Borde and Jelinek (1987) developed a model to test the R22 refrigerant with different organic absorbents such as the NMP, MCL, DMMP, DMETEG, and DMF. The most efficient working fluid in terms of *COP* and circulation ratio was the R22-DMF, and therefore, a prototype was constructed. Experimental results were close to the predicted performance. Borde et al. (1995) investigated the possibility of using the HFC R134a refrigerant coupled with three organic absorbents (DMETEG, MCL, and DMEU). At $T_g=100^\circ\text{C}$, R134a-DMETEG was the optimum working fluid with a similar *COP* to the others but a lower circulation ratio. Compared with R22 as refrigerant (Borde and Jelinek, 1987), R134a shows a reduction in *COP* and an increase in the circulation ratio (Borde et al., 1995). Borde et al. (1997) studied the possibility of using the HCFC R124 coupled with DMAC, NMP, MCL, DMEU, and DMETEG. In this case, the working fluid with the best performance was the R124-DMAC. Even if the NMP and DMEU options had a similar *COP* and circulation rate, they suffered from stability problems at high temperatures. Finally, when comparing the R124 (Borde et al., 1997) refrigerant with the R22 (Borde and Jelinek, 1987) and R134a (Borde et al., 1995), it was found that R124 had lower *COPs* than R22, but higher than R134a, and in terms of circulation ratio, R124 had lower values than both R22 and R134a (Borde et al., 1997). Levy et al. (2001) analyzed a system based on the HFCs R134a and R125 refrigerants and using DMETEG as absorbent. The maximum *COP* depended on the working pair, while the COP_{max} of R134a was slightly higher. However, the working fluid based on the R125 was preferred since the f and T_g were lower.

ILs have also been studied as suitable absorbents for HFCs. Kim et al. (2013) modeled an IL ([bmim][PF₆]) and five HFC refrigerants (R134a, R32, R125, R143a, R152a). R152a demonstrated the highest ratio of cooling capacity over pumping power, while R132 and R134a showed the highest and lowest *COP* values, respectively. After this, Kim (2014) presented a test bench for a system working with R134 or R134a as the refrigerant and [bmim][PF₆] as the

absorbent with no SHX. The R134a-[bmim][PF₆] system operated with a COP_{max} of 0.35 and a cooling capacity of 36 W. Experimental results were in fairly good agreement with the simulated ones (Kim et al., 2012). Kim and Kohl (2013) tested the R134a-[bmim][PF₆] working fluid and compared it with the results of the R134a-[bmim][PF₆] working fluid. The experimental performance was lower than the theoretical values because of heat losses. However, the R134a-[bmim][PF₆] working pair presented a cooling capacity 1.9-fold times higher than the R134a-[bmim][PF₆] working pair, which makes it more suitable for recycling low-grade waste heat. Finally, Kim and Kohl (2014) studied the performance of a system using R134a as the refrigerant and compared two ILs ([hmim][PF₆] and [hmim][Tf₂N]) as absorbents. The better properties of the R134a-[hmim][Tf₂N] working pair, such as the high overall solubility and its much lower viscosity, resulted in higher system performance.

1.2.4.3. Other refrigerant bases

A summary of the small-capacity prototypes of absorption cooling systems with refrigerant bases other than H₂O and NH₃ developed in laboratories and their operating conditions is presented in Table I.10. Pilatowsky et al. (2001) studied the monomethylamine-water working pair operating at low driving temperatures (60–80°C). This working fluid requires a rectifier. However, it possesses interesting properties at moderate heat sink temperatures (25–35°C) and a T_e between -10 and 10°C. Romero et al. (2005) compared the same system with the ammonia-water system, finding that the monomethylamine-water system possesses higher COP values in a short range of low T_g (between 63 and 80°C); however, the conventional working fluid keeps higher COP s in a wider range of temperatures for the rest of the T_g . Moreover, the proposed system operates at lower vapor pressures than the NH₃-H₂O cycle, which allows for smaller wall thickness in the system's components.

The acetone-zinc bromide (C₃H₆O-ZnBr₂) working pair was studied and modeled for an absorption chiller by Karno and Ajib (2008). The model was validated with an experimental plant that was operated at low T_g (higher than 50°C) achieving a COP of around 0.4. However, more work needs to be done to study the influence of the operating temperatures and the effectiveness of heat exchangers.

CO₂ is, together with ammonia and propane, an environmentally friendly substance studied for compression refrigeration. However, special attention should be paid to the operating pressures, since they are at higher levels than ammonia as the refrigerant, which creates new technological challenges. ILs have a high CO₂ absorption capacity, which indicates the possibility of both substances being used as the working fluid in absorption systems (Sen and Paolucci, 2006), and this is why this working pair has been studied during the past decade. Shelide (2006) proposed the CO₂-[bmim][PF₆] working fluid for absorption refrigeration systems. Shiflett and Yokozeki (2005) measured the solubilities and diffusivities of CO₂ in [bmim][PF₆] and [bmim][BF₄]. Cai et al. (2007) developed a dynamic modeling of a system using the CO₂-[bmim][PF₆] working pair and studied the transient response, design, and operating parameters affecting its performance. The COP of the system yielded much lower values compared with the NH₃-H₂O working fluid; however, the authors questioned the accuracy of the ideal-gas heat capacity coefficients for the working pair. (Martín and Bermejo, 2010) discussed the possibility of using CO₂ as the refrigerant with ILs as absorbents. The CO₂-IL working pair yielded lower COP values (around 0.21 for the CO₂-[bmpyrr][Tf₂N] working pair) compared with the conventional NH₃-H₂O working fluid (around 0.55) owing to the higher f required for the CO₂-IL system (2.4 times higher).

Table I.10: In-lab developed prototypes of small-capacity absorption cooling systems with refrigerant bases other than H₂O and NH₃ and operating conditions.

REF	ABS	$\dot{Q}_{e,nom}$ (kW)	Heat source	Heat sink	S H X	R H X	t_g^i (°C)	t_c^i (°C)	t_a^i (°C)	t_c^o (°C)	$\dot{Q}_{e,exp}$ (kW)	COP_{exp}	COP_{carnot}	REF
R134a	IL	0.1	Electric heater	Water			70	41	41	28	0.03	0.3	1.96	(Kim et al., 2012)
C ₃ H ₈ O	ZnBr ₂	10.6	Solar	Water	x	x	50.5	22	22	13	0.7	0.4	2.8	(Karno and Ajib, 2008)

1.2.5. General comparisons between working pairs

1.2.5.1. Theoretical general comparisons in the literature

Wilbur and Manchini (1976) compared the NH₃-H₂O and H₂O-LiBr working fluids for a solar AC in the conditions of Atlanta (USA). The comparison also included the type of collectors, the heat rejection alternative, and the thermal storage type. The H₂O-LiBr working fluid gave a significantly better performance, and the best configuration was a H₂O-LiBr air-cooled system with chilled water storage and a conventional flat-plate collector. For the same working fluids comparison, Alizadeh et al. (1979) confirmed the better performance and higher simplicity of the H₂O-LiBr system; moreover, they reported that the most important variable to take into account is T_g . Mansoori and Patel (1979) also confirmed the advantages of H₂O-LiBr, especially for hot climates, and mentioned that the NH₃-H₂O working pair is more versatile as it can work in a wider range of operating conditions, but with a lower COP . Finally, the NH₃-NaSCN working pair was considered to lie between the two options. The better efficiency of H₂O-LiBr over NH₃-H₂O was also verified by Karakas et al. (1990) and Sun (1997) (see Figure I.10); however, this working fluid also entails more design difficulties because of its working pressures at subatmospheric levels, and, moreover, crystallization and positive cooling temperatures must be taken into account (Horuz, 1998a).

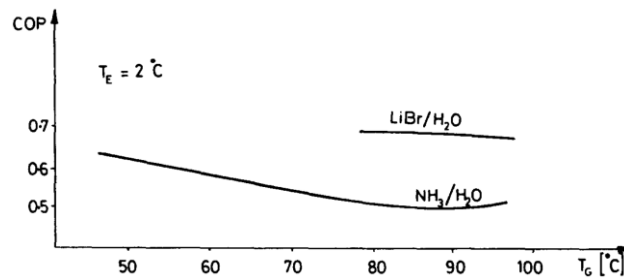


Figure I.10: Results for COP vs. T_g for the H₂O-LiBr and NH₃-H₂O working fluids at $T_c = 2^\circ\text{C}$ (Karakas et al., 1990).

Considering an application for storage rooms (frozen and chilled products that require storage temperatures between -35 and 6°C), Infante Ferreira (1985) compared 11 promising working pairs with 5 different refrigerants (H₂O, NH₃, CH₃OH, NH₂CH₃, and CHClF₂) and concluded that for the required cooling temperatures, the best adapted working pairs would be NH₃-LiNO₃ and NH₃-NaSCN, being the latter the most efficient but also the most restricted due to crystallization risks. Lecuona et al. (2015) determined the optimum driving temperature and compared a system working with H₂O-LiBr, another with NH₃-LiNO₃, and a third one with NH₃-LiNO₃ but with a low-pressure compressor booster. The NH₃-LiNO₃ working pair offers a lower refrigeration production at positive temperatures compared with the H₂O-LiBr system. However, the boosted cycle offers 15.6% more cold than the single-effect H₂O-LiBr cycle using a pressure ratio of 2. Absorption cooling systems working with the NH₃-LiNO₃ working fluid were found to be feasible and attractive. Flores Flores et al. (2014) studied six different working fluids (H₂O/LiBr, NH₃/H₂O, NH₃/NaSCN, NH₃/LiNO₃, H₂O/LiCl and H₂O/CaCl₂) using a mathematical model developed in the EES software. The NH₃-H₂O working fluid yielded the lowest COP values

(around 0.53) due to the absence of a rectifier. The H₂O-LiBr and H₂O-LiCl working pairs obtained the highest *COP* values (around 0.81). The NH₃-LiNO₃ and NH₃-NaSCN working pairs exhibited medium performance, the former having higher *COP* values than the latter. Cerezo et al. (2018b) developed a dynamic simulation of a system comparing the NH₃-H₂O, H₂O-LiBr, NH₃-NaSCN, NH₃-LiNO₃, and H₂O-LiCl working fluids using the EES and TRNSYS software tools. The H₂O-LiCl working pair demonstrated the best performance; however, its operating temperatures are restricted owing to crystallization (see Figure I.11). For the case of adiabatic microchannel membrane-based absorbers, De Vega et al. (2018) compared theoretically the H₂O-LiBr, H₂O-LiCl, and NH₃-LiNO₃ working pairs and observed that the NH₃-LiNO₃ working pair would provide the highest cooling capacities with the lowest absorber volume ratio, followed by H₂O-LiBr and H₂O-LiCl at last, while the driving temperatures required are the lowest for H₂O-LiCl, followed by NH₃-LiNO₃ and H₂O-LiBr at last. Moreover, the H₂O-LiBr working pair possesses the highest *COP*s. For the case of negative cooling, Crepinsek et al. (2009) compared the NH₃-H₂O, NH₃-LiNO₃, NH₃-NaSCN, CH₃NH₂-H₂O, R22-DMEU, R32-DMEU, R124-DMEU, R152a-DMEU, R125-DMEU, R134a-DMEU, TFE-TEGDME, CH₃OH-TEGDME, and R134a-DMAC working pairs in terms of *COP* and *f*, and concluded that R124-DMEU, R125-DMEU, NH₃-LiNO₃, and NH₃-NaSCN are possible alternatives.

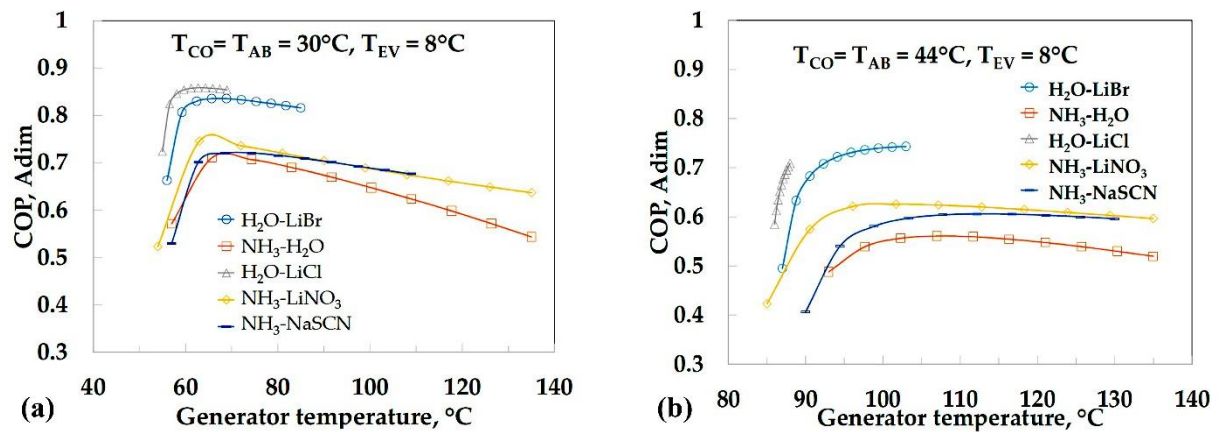


Figure I.11: Comparison of different working fluids in terms of *COP* against T_g at $T_a=T_c$ of (a) 30°C and (b) 44°C (Cerezo et al., 2018b).

Kim et al. (2011, 2012) compared seven ILs ([emim][Tf₂N], [emim][BF₄], [bmim][BF₄], [bmim][PF₆], [hmim][Tf₂N], [hmim][BF₄], and [hmim][PF₆]) as absorbents and HFCs (R125, R134a, R143a, R152a, R32), R114, R124, and H₂O as refrigerants. R32 presented the lowest *f* and relatively high *COP* combined with the ILs with [PF₆⁻] and [BF₄⁻] anions. R124 would not be considered owing to its negative environmental impact, and H₂O-[emim][BF₄] presented the highest *COP* (0.91). Kim and Gonzalez (2014) later presented an exergy analysis using different ILs and obtained an exergetic *COP* superior to the rest for the H₂O-[emim][BF₄] working pair. Zheng et al. (2014) presented a review of ILs in working pairs and observed that the *COP* of H₂O-ILs systems do not exceed the traditional H₂O-LiBr working fluid, but H₂O-[DMIM]DMP is close and overcomes crystallization and corrosion problems. Moreover, it broadens the operating range. For NH₃-ILs systems, *COP*s are lower than for NH₃-H₂O systems, but no rectifier is needed. Finally, the TFE-ILs system *COP* is commonly between that of the H₂O-LiBr and NH₃-H₂O systems (the TFE/[BMIM]Br system having the highest *COP*), but offers a wider operating range. Sujatha and Venkatarathnam (2018) studied the suitability of HFC and HFO as refrigerants for ILs and compared them using [hmim][TF₂N] as the absorbent. HFC refrigerants proved to be better (a *COP* of 0.5 can be achieved using the R32 refrigerant). Hence, IL-HFC working pairs are suitable for these systems. Moreno et al. (2018) presented a COSMO-based/Aspen HYSYS methodology to perform an extensive thermodynamic evaluation of ILs in absorption refrigeration cycles. In total, 7,200 systems were evaluated (900 ILs and eight refrigerants) and

adequate refrigerant-absorbent pairs competitive with conventional systems were selected (see Figure I.12). The optimum working fluid depends on the cooling temperature. Water showed excellent thermodynamic properties owing to its high enthalpy of vaporization and good affinity to ILs; however, because of its limitation to working at positive cooling temperatures, methanol and ammonia are good options for cooling temperatures between -5 and 5°C .

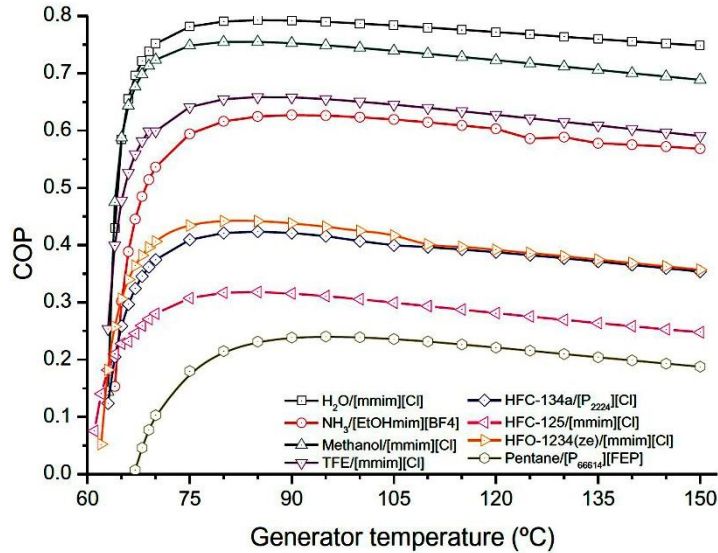


Figure I.12: COP vs. T_g for different refrigerant-IL systems (Moreno et al., 2018).

1.2.5.2. Discussion of the developed prototypes and commercial systems

Figure I.13 shows the percentage of existing brands and experimentally developed prototypes during the past 35 years of small-capacity single-stage continuous absorption chillers divided by working fluid. It is clear that the dominant working fluids are $\text{H}_2\text{O-LiBr}$ and $\text{NH}_3\text{-H}_2\text{O}$, the former being the most predominant. Indeed, the manufacturers of $\text{H}_2\text{O-LiBr}$ chillers seem to possess the largest market share (Labus et al., 2013). Moreover, Figure I.13b shows that the third most widely studied working pair is the $\text{NH}_3\text{-LiNO}_3$; most probably due to the advantages mentioned in the previous sections.

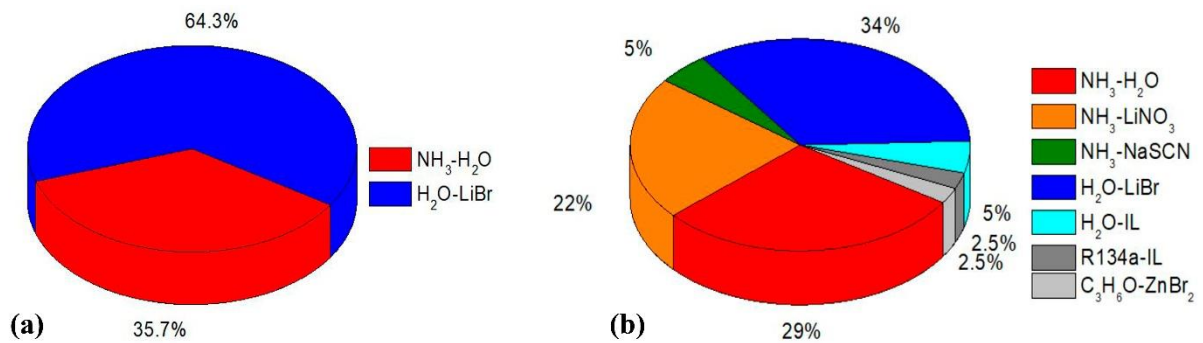


Figure I.13 Single-stage absorption chillers. (a) Percentage of available brands by working fluid and (b) percentage of the experimental prototypes developed during the past 35 years.

Most of the comparative studies between absorption systems and working fluids are theoretical (Alizadeh et al., 1979; Cerezo et al., 2018a; Crepinsek et al., 2009; Karakas et al., 1990; Kim et al., 2012; Mansoori and Patel, 1979; Wilbur and Manchini, 1976). At the same time, there is scarce information about the comparison of experimental systems owing to the different constraints in terms of technological design depending on the selected working fluid and the different experimental conditions (Pons et al., 2012). In order to make a representative

comparison between the different experimental systems found in the literature, their experimental $COPs$ were compared directly with their maximum theoretical performance (COP_{carnot}), since this is a reference for comparison in function of the source temperatures at the conditions of the represented COP_{exp} . An increase in the COP_{carnot} indicates an increase in the generator or evaporator temperatures or a decrease in the intermediate source temperature and vice versa. In real applications, the cooling temperature and intermediate temperature are regularly user-defined, which indicates that the main factor influencing a change in the COP and COP_{carnot} in a given machine is the generator temperature.

The data from the present comparisons were obtained from the different tables in the previous sections about experiments conducted on in-lab-developed prototypes and on commercial chillers. Figure I.14 shows the regrouping of the different working fluids (commercial systems and prototypes) and their experimental $COPs$ or catalog $COPs$. As mentioned earlier, only two working fluids are commercially available ($H_2O-LiBr$ and NH_3-H_2O). It is clear from this figure that there is a different value range of $COPs$ depending on the selected working fluid and that the three most experimentally studied working pairs in the literature are the $H_2O-LiBr$, NH_3-H_2O , and the NH_3-LiNO_3 working pairs. However, in the case of the experimental prototypes, a big dispersion can be observed mainly because of three reasons: the physical differences of the systems (heat exchanger technologies, piping, and insulation), the different operating temperatures, and the inconsistency added by the variability of the operating conditions presented in the literature regarding experimental machines (as discussed in Section 1.2.1). Similar value ranges are observed for the two commercially available working pairs compared with the experimental prototypes; however, as the commercial machines have already gone through an optimization process before the market launch, there is considerably less data dispersion (0.2–0.25 compared with 0.53–0.69 of the experimental prototypes).

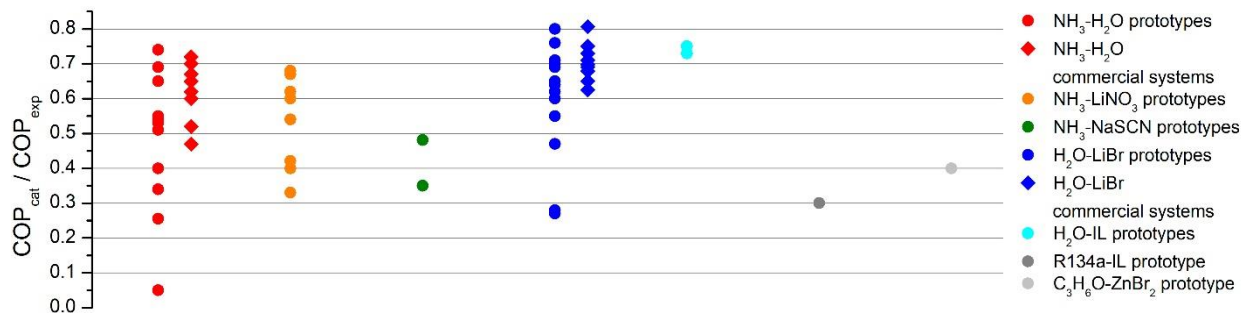


Figure I.14: Graphical representation of the laboratory-developed prototypes and commercial systems in separate colors by working pair.

For a better clarification of the dispersed data, a graphical representation of the prototypes and commercial systems comparing the system's experimental or catalog $COPs$ vs. their carnot $COPs$ is presented in Figure I.15. A linear trend line of the same color for each working pair was traced to reduce the effects of the differences between the systems. These trend lines show how the experimental $COPs$ of the different working pairs change as a function of the COP_{carnot} . One can see how the $H_2O-LiBr$ working fluid is restricted to working at low t_{sink} and t_g (low COP_{carnot}) to avoid crystallization, while the NH_3-H_2O and NH_3-LiNO_3 working pairs can operate at wider temperature ranges. Unfortunately, for the rest of the experimental working pairs, there are not enough experimental studies to allow for a comparison.

It can also be deduced from the trend lines in Figure I.15a and b that at the same source temperature conditions (COP_{carnot}), the $H_2O-LiBr$ working fluid has a higher performance than the NH_3-H_2O working pair, which is in good agreement with their differences in their theoretical performance. Finally, from Figure I.15a, a better performance can be observed at low COP_{carnot}

for the $\text{NH}_3\text{-LiNO}_3$ system compared with the conventional $\text{NH}_3\text{-H}_2\text{O}$ system, which proves the theoretical comparisons presented earlier. However, as the $\text{COP}_{\text{carnot}}$ increases, no substantial increase in the experimental performance can be observed, and at $\text{COP}_{\text{carnot}} > 3$, the $\text{NH}_3\text{-H}_2\text{O}$ working pair performs even better than the $\text{NH}_3\text{-LiNO}_3$ working pair, which might be due to the reported problems of the $\text{NH}_3\text{-LiNO}_3$ working pair regarding its elevated viscosity (Cera-Manjarres et al., 2018; Wu et al., 2014). For the rest of the experimental systems in Figure I.15a, the R134a-IL and the $\text{C}_3\text{H}_6\text{O-ZnBr}_2$ working pairs do not seem to have an especially advantageous performance, the performance of the $\text{NH}_3\text{-NaSCN}$ system seems to be comparable to those of the $\text{NH}_3\text{-H}_2\text{O}$ and $\text{NH}_3\text{-LiNO}_3$ systems, and the $\text{H}_2\text{O-IL}$ working pair performance seems to be similar to that of the $\text{H}_2\text{O-LiBr}$ working pair. However, more experimental data are needed to confirm these findings.

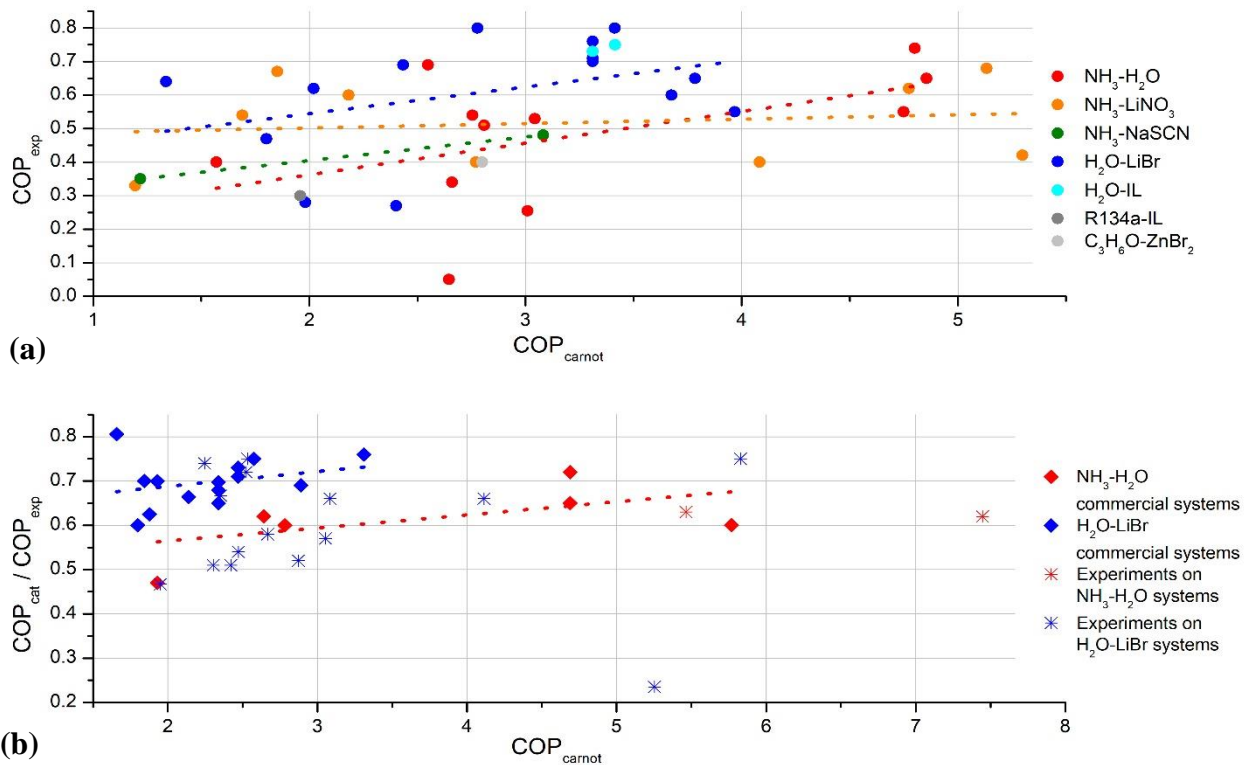


Figure I.15: Graphical representation of the systems grouped by working pair. (a) COP_{exp} vs. $\text{COP}_{\text{carnot}}$ of laboratory-developed prototypes and (b) $\text{COP}_{\text{cat}} / \text{COP}_{\text{exp}}$ vs. $\text{COP}_{\text{carnot}}$ for the commercial systems and the experimentations performed on them.

Finally, experimental studies on the commercial chillers are represented in the same Figure I.15b. Only the experimental studies with enough information to represent them graphically are shown. As expected, owing to the different and sometimes uncontrollable conditions in experimental installations, and also to the fact that for research purposes, the commercial machines are usually tested at conditions out of the optimal design values, the performance of the installed systems is generally lower than the one provided by the manufacturer. This is even more accentuated for driving temperatures higher than those of the nominal conditions (higher $\text{COP}_{\text{carnot}}$ than in the range of the trend lines). Indeed, as the generator temperature increases, the theoretical performance tends to increase; however, this generates exergy losses in the generator, condenser, and absorber as their average temperature increases, reducing the exergetic efficiency of the system. This and the dry zones generated at elevated t_g on the heat exchanger surface due to the elevated heating lead to an increase in the difference between the expected performance and the experimental performance of the systems, reducing the system's “ideality”.

Apart from the intrinsic properties of the different analyzed working fluids, the exchanger technology employed for the enhancement of the heat and mass transfer phenomena is of fundamental importance if a good global machine performance is desired. For this reason, the following section presents the state of the art on the exchanger technologies that have been developed and tested for absorption chillers.

1.3. Review of compact exchanger technologies

The particularity of absorption chillers is that they possess multifunctional exchangers, with coupled heat and mass transfers, where a sorption phenomenon takes place (i.e., the desorber or the absorber). These heat and mass transfer exchangers have been pointed out by some authors as the limiting components or the “bottleneck” in the system’s performance, especially the absorber (Goyal et al., 2017, 2016). In the 20th century, the design of these components was based on rules of thumb, which led to heavy, expensive, and bulky equipment (Miller and Keyhani, 2001). Nowadays, more research is needed to better understand the fundamental issues governing the sorption process and the enhancement methods needed to obtain more efficient designs (Giannetti et al., 2018; Matsuda et al., 1994).

Historically, tubular exchangers are the most commonly used exchangers in commercial machines (Hesselgreaves, 1990). Nevertheless, research groups have constantly been looking for new technologies which could provide more compact and low-cost systems (e.g., plate heat exchangers (PHEs) (Hesselgreaves et al., 2016; Kays and London, 1984)).

Chemical and mechanical treatments have been studied as mass and heat transfer enhancement methods for the exchangers in single-stage absorption systems (Kim et al., 2003). The chemical treatment consists in the addition of small quantities of surfactant, which generates interfacial turbulence (Marangoni convection), and increases the heat and mass transfer coefficients (Kim et al., 1996). On the other hand, the mechanical treatment consists in scratching or modifying the exchange surface (roughness treatment) or geometry (shape treatment) to increase its roughness or complexity, generate flow instabilities, and increase the wettability of the exchange area, leading to an increase in the heat and mass transfer rates (Amaris et al., 2014a).

Section 1.2 showed that $\text{NH}_3\text{-H}_2\text{O}$ and $\text{H}_2\text{O-LiBr}$ are the most common working pairs. In general, $\text{NH}_3\text{-H}_2\text{O}$ is used for negative refrigeration, while $\text{H}_2\text{O-LiBr}$ is used for applications where cooling temperatures higher than 0°C are required (e.g., air conditioning). As for their thermophysical properties, the lower viscosity of $\text{NH}_3\text{-H}_2\text{O}$ (allowing for smaller hydraulic diameters in confined exchangers) and the higher vapor-phase density of ammonia (allowing for smaller pipe diameters) lead to a more compact system. Moreover, the absence of crystallization and freezing concerns allows for a wider operation range and air-cooled systems (Staedter and Garimella, 2018). However, due to its volatile absorbent (Garimella et al., 2011), the low refrigerant purity requires the implementation of a vapor purification process, which implies additional costs, space, and weight (Fernández-Seara and Sieres, 2006; Sieres and Fernández-Seara, 2006). Moreover, in the case of air-cooled systems, the driving temperatures required in hot days are usually too high for flat plate solar collectors (Oronel et al., 2013) and would require the use of other solar thermal collector technologies. The $\text{H}_2\text{O-LiBr}$ working pair possesses a higher performance and a low mass transfer resistance in the vapor phase. On the other hand, the liquid phase presents significant mass transfer resistance (Garimella et al., 2011). $\text{H}_2\text{O-LiBr}$ requires lower driving temperatures compared to the $\text{NH}_3\text{-H}_2\text{O}$ working pair. However, it presents a number of drawbacks such as corrosion, vacuum operation, and crystallization. $\text{H}_2\text{O-LiBr}$ is a highly viscous and dense solution. Consequently, the falling film exchanger technology, for

which a solution distributor is required, is, in general, the best adapted. For the reasons mentioned before, the highest technological problems in H₂O-LiBr absorption systems are (1) non-condensable gases, (2) the solution distribution, and (3) the low thermal and molecular diffusions, which govern the sorption heat and mass transfers (Tsai and Horacio, 1998). Recently, the NH₃-LiNO₃ working pair was proposed as an option to overcome the disadvantages of the conventional working pairs (Oronel et al., 2013; Salgado et al., 2008) because it does not present crystallization in the typical range of operating conditions of single-stage absorption chillers (which allows for air cooling), does not operate in vacuum conditions, does not require a rectifier, and requires lower driving temperatures (Abdulateef et al., 2008; Antonopoulos and Rogdakis, 1996; Infante Ferreira, 1995; Sun, 1998). These advantages led this working pair to become the third most studied binary working fluid for absorption chillers (Altamirano et al., 2019a). However, experimental results with NH₃-LiNO₃ have sometimes yielded poor performance (Ayala et al., 1994; Heard et al., 1996; Infante Ferreira, 1995). This poor performance was attributed to the absorber and the high viscosity of the NH₃-LiNO₃ solution pair compared to NH₃-H₂O (Amaris et al., 2014b). Indeed, Rivera and Best (1999) confirmed that the average heat transfer coefficient (HTC) for the NH₃-H₂O was two to three times higher than the HTC of the NH₃-LiNO₃ mixture in a boiling process inside a stainless-steel vertical tube.

The main objective of this section is to introduce the different technologies of exchangers for small-capacity single-stage continuous absorption chillers operating on binary working fluids, regarding experimental studies and recent advances. The selection of such specific configuration reduces the range of possible concentrations, temperatures, and materials, allowing for an objective technology comparison. The review focuses on the studies of innovative exchanger technologies with conventional or special geometries, with or without mechanical treatments, with particular attention paid to experimental studies. The use of chemical treatments is not covered. Only the experiments operating on NH₃-H₂O, H₂O-LiBr, and NH₃-LiNO₃ and their refrigerants (water and ammonia) are reported, considering that these are the three most widely studied working pairs. This allows for a better comparison and the study of the advantages and drawbacks of the different exchanger technologies depending on the working fluid. The present review is divided into two large families: the first one includes exchangers that perform the heat and mass transfers together (non-adiabatic exchangers), while the second considers exchangers in which the heat transfers are externalized (adiabatic exchangers). These two exchanger families and their heat and mass transfer performance evaluation criteria will be further explained in Section 1.3.1.

1.3.1. Heat and mass transfer comparative criteria

As mentioned before, the multifunctional exchangers are the limiting components in absorption chillers given that the phenomena involved in these components are much more complex and less controllable (Goyal et al., 2016; Herold et al., 2016) than for the refrigerant phase-change exchangers. This is the reason why most recent studies have focused on multifunctional exchangers, which, classified by the continuity of the phases (solution-refrigerant), are divided into two types: falling film (both continuous phases) and two-phase flow exchangers. Both principles are presented in Figure I.16 for functioning either in absorption or desorption mode. The flow directions can be changed depending on the specific configuration and application. Figure I.16a represents the falling film mode, in which case a component is needed to distribute the solution falling by gravity over a vertical surface. As the falling film flows freely over the surface, the surrounding vapor pressure is constant and therefore there is no significant pressure drop. In the second case (Figure I.16b), the solution flow generates frictional shear forces with

the walls and therefore special attention has to be given to the pressure drop. The two-phase exchangers (Figure I.16b) only may require a solution distributor while performing an adiabatic sorption process (absorption or desorption). In nonadiabatic desorption mode, a separator of the refrigerant vapor and the solution is recommended, whereas in the nonadiabatic absorption mode, a refrigerant vapor distributor could be required.

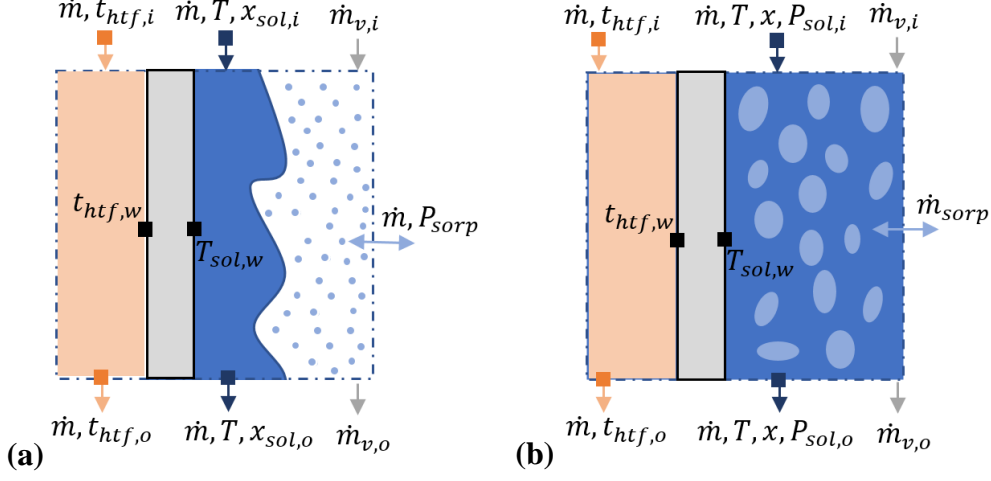


Figure I.16: Control volume of the (a) falling film and (b) two-phase exchangers.

In the present example, we consider a parallel flow (heat transfer fluid/solution and solution/refrigerant). For simplicity, thermal losses are ignored and the system is considered to operate at steady-state equilibrium. The heat of sorption is equal to the heat released by or transferred to the HTF and the energy balance, depending on the operation mode, is given by Eq. (I.6) for the desorber or Eq. (I.7) for the absorber.

$$\dot{Q}_{\text{des}} = \dot{m}_{\text{sol},o} H_{\text{sol},o} + \dot{m}_{\text{des}} H_{\text{v},o} - \dot{m}_{\text{sol},i} H_{\text{sol},i} \quad (\text{I.6})$$

$$\dot{Q}_{\text{abs}} = \dot{m}_{\text{sol},o} H_{\text{sol},o} - \dot{m}_{\text{sol},i} H_{\text{sol},i} - \dot{m}_{\text{abs}} H_{\text{v},i} \quad (\text{I.7})$$

To be consistent with most studies investigating sorption exchangers, the sorption heat can be expressed as a function of an overall heat transfer coefficient (U , see Eq. (I.8)) based on the analysis of traditional heat exchangers. However, this analysis ignores the effect of the generated heat by the sorption phenomenon (Narayanan et al., 2009). In Eq. (I.8), C is a correction factor that might be applied depending on the geometry of the heat exchanger, and ΔT_{lm} depends on the functioning mode and flow configuration. For the example presented, ΔT_{lm} is defined by Eq. (I.9) or (I.10), depending on the functioning mode.

$$\dot{Q}_{\text{sorp}} = UAC\Delta T_{lm} \quad (\text{I.8})$$

$$\Delta T_{lm,\text{des}} = \frac{(t_{\text{htf},i} - T_{\text{sol},i}) - (t_{\text{htf},o} - T_{\text{sol},o})}{\ln((t_{\text{htf},i} - T_{\text{sol},i})/(t_{\text{htf},o} - T_{\text{sol},o}))} \quad (\text{I.9})$$

$$\Delta T_{lm,\text{abs}} = \frac{(T_{\text{sol},i} - t_{\text{htf},i}) - (T_{\text{sol},o} - t_{\text{htf},o})}{\ln((T_{\text{sol},i} - t_{\text{htf},i})/(T_{\text{sol},o} - t_{\text{htf},o}))} \quad (\text{I.10})$$

The overall heat transfer coefficient (U) can also be expressed as a function of the sum of the HTF, wall, and solution thermal resistances, as defined by Eq. (I.11).

$$U = \frac{1}{1/h_{\text{htf}} + \delta/\lambda + 1/h_{\text{sol}}} \quad (\text{I.11})$$

In the literature, the heat transfer performance of sorption exchangers is characterized either by the overall heat transfer coefficient (U) or the solution side heat transfer coefficient (h_{sol}), derived from Eqs. (I.8) and (I.11). Finally, some authors use the heat flux as an indicator, defined by Eq. (I.12).

$$\dot{Q}''_{sorp} = \frac{\dot{Q}_{sorp}}{A} \quad (I.12)$$

Regarding mass transfer, a first indicator would be the sorption mass flow rate (\dot{m}_{sorp}). However, the sorption mass flux would be a more precise parameter as it takes into account the effective exchange area (Eq. (I.13)).

$$\dot{m}''_{sorp} = \frac{\dot{m}_{sorp}}{A} \quad (I.13)$$

Another important parameter that has been discussed is the sorption ratio (Eq. (I.14)), which indicates how much vapor is being absorbed or desorbed by each kg of solution circulated (Zacaría et al., 2011). Regarding the study of absorbers in single-stage systems, it is the inverse of the circulation ratio.

$$Ra = \frac{1}{CR} = \frac{\dot{m}_{sorp}}{\dot{m}_{sol,o}} \quad (I.14)$$

Assuming that the mass transfer resistance in the vapor phase is negligible compared to that in the liquid phase, the absorption rate can be expressed as a function of an overall mass transfer coefficient (K), whose definition might have slight variations, as explained in (Venegas et al., 2005). One example of these definitions is the one used by Zacaría et al. (2015) and presented in Eq. (I.15), where ΔX_{lm} is defined by Eq. (I.16).

$$\dot{m}_{abs} = K\rho_{sol,o}A\Delta X_{lm} \quad (I.15)$$

$$\Delta X_{lm} = \frac{(x_{sol,i}^{eq} - x_{sol,i}) - (x_{sol,o}^{eq} - x_{sol,o})}{\ln\left(\frac{(x_{sol,i}^{eq} - x_{sol,i})}{(x_{sol,o}^{eq} - x_{sol,o})}\right)} \quad (I.16)$$

In the case of adiabatic absorbers/desorbers, in which the heat transfer is externalized in a conventional single-phase heat exchanger to later perform the mass transfer in the absorber/desorber itself, special attention has to be given to the evaluation of the mass transfer performance and the parameters that affect it. In this case, there is no heat transfer in the control volume of Figure I.16 and $T_{s,i}$ is the temperature of the solution that has already been pre-cooled/pre-heated in a separate heat exchanger. Most of the studies in the literature focused on studying adiabatic absorption performance, in which case three parameters have been used: the inlet subcooling ($\Delta T_{sub}^i \geq 0$), the outlet subcooling ($\Delta T_{sub}^o \geq 0$) and the adiabatic equilibrium factor (F_{ad}). The first one, defined by Eq. (I.17), represents the temperature difference between the solution inlet at equilibrium conditions and the actual inlet temperature, while the second one, defined by Eq. (I.18), indicates how far from saturation the solution is at the outlet of the absorber. Finally, the third one (Eq. (I.19)) is an indicator of the saturation level that the solution has reached at the outlet of the absorber. The adiabatic equilibrium temperature ($T_{s,o}^{ad}$) and the adiabatic equilibrium concentration ($x_{s,o}^{ad}$) are defined at the equilibrium conditions of the solution at the outlet of the absorber with the sorption pressure and calculated with the procedure described by Zacaría et al. (2011). A similar procedure can be followed for the case of an adiabatic desorption. Arzoz et al. (2005) proposed a simplified approximation of the equilibrium factor using temperature measurements. However, Ventas et al. (2012) later experimentally proved that although this approximation is close to the real equilibrium factor, it is not accurate enough to predict the effect of slight variations in concentration. Adiabatic absorbers are generally evaluated

in terms of their F_{ad} and Ra . The \dot{m}''_{abs} and K might also be used. However, these parameters include a mass exchange area, which is one of the most important parameters impacting absorption performance (Osta-Omar and Micallef, 2017), difficult to measure experimentally and whose definition might vary depending on the distribution technology that is being used. Moreover, apart from being used in a reduced number of papers, F_{ad} not necessarily a good indicator, since it might show an elevated value, not for a good mass transfer performance, but instead for an evaporator malfunctioning (Gutiérrez-Urueta et al., 2011).

$$\Delta T_{sub}^i = T_{eq}(P_v, x_i) - T_{s,i} \quad (I.17)$$

$$\Delta T_{sub}^o = T_{s,o}^{ad} - T_{s,o} \quad (I.18)$$

$$F_{ad} = \frac{x_{s,o} - x_{s,i}}{x_{s,o}^{ad} - x_{s,i}} \quad (I.19)$$

For the reasons presented above, while comparing technologies in the following, particular attention was given to Ra as the comparative parameter for the adiabatic exchangers. On the other hand, for the nonadiabatic exchangers, besides Ra , \dot{m}''_{sorp} was also used for the mass transfer evaluation as the exchange area in these exchangers is more clearly defined. For the heat transfer evaluation, particular attention was also paid to the parameters that take into account the exchange area (h_{sol} and U).

1.3.2. Non-adiabatic exchangers

1.3.2.1. Falling film

Falling film exchangers are the most frequently used today in absorption systems. This technology consists in generating a stable film over a heat exchange surface, usually at low flow regimes to avoid heat and mass transfer resistance due to the increase in film thickness. The exchange surface can be a horizontal tube or a vertical surface (a vertical tube or a plate, [Figure I.17](#)). The horizontal tube baffle structures have been historically the predominant technology in commercial absorption machines thanks to their versatility and simplicity of functioning (Yoon et al., 2006). However, plate heat exchangers (PHEs) are now replacing them given their advantages in terms of compactness and low cost (Hesselgreaves et al., 2016). The selected falling film geometry directly affects the phenomena involved in the exchanger. With horizontal tube bundles, instabilities are generated automatically in the transition from one tube to another (Abed et al., 2015), while in vertical tubes and plates, instabilities are usually generated by capillary and inertial waves developed along the film (Kim and Kang, 1995; Kim et al., 1996; Stutz et al., 2016).

[Table I.11](#) summarizes the experimental results obtained on falling film exchangers. All the heat and mass transfer evaluation parameters mentioned in [Section 1.3.1](#) are included when available, and data that were not directly provided were calculated or approximated (if enough information was provided). Hence, calculated data from [Tables 1-3](#) (preceded by a ~ symbol) may be interpreted with care and the reader must refer to the source if more detailed information is required.

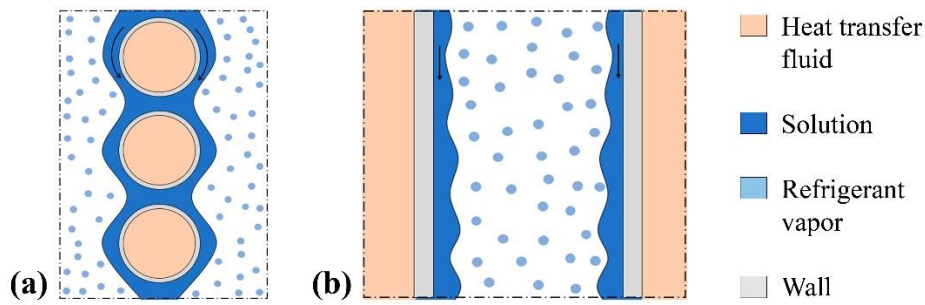


Figure I.17: Falling film exchanger geometries. (a) Horizontal tubes and (b) vertical surface (either vertical tubes or plates).

1.3.2.1.1. Horizontal tube falling film

With horizontal tube falling film exchangers, a solution distributor is located on top of the exchanger to let the solution flow down over the horizontal tubes (HTs), where the heat and mass transfer processes take place (Jeong and Garimella, 2002). The heat and mass transfer of falling films over tubes is a complex phenomenon influenced by the flow regime of the solution which can take different forms between the tubes such as drops, columns, or entire sheets, depending on the solution flow rate. The droplet formation and impact on tubes generate singular instabilities whose frequency depends on parameters such as the solution flow rate and its thermophysical properties (especially the density, viscosity, and surface tension), and the space between the tubes. These instabilities are beneficial to the transfer phenomena as they allow for an increase in the mass exchange area, enhance the convective transfer, and renew the solution exchange surface (Abed et al., 2015; Killion and Garimella, 2003). Experimental studies in this configuration have proven that the heat transfer, the heat transfer coefficients, and wettability are directly correlated with the flow regime (Re number) (Kim et al., 2003; Lee et al., 2012), while the mass transfers are mostly influenced by the inlet solution concentration and temperature and the HTF temperatures (Bredow et al., 2008; Deng and Ma, 1999). Moreover, the performance increases as the tube diameter decreases (Yoon et al., 2008).

Chapter I. State of the art

Table I.11: Falling film exchangers for absorption chillers: experimental results (~: approximated data).

Func	WF	Type	$\dot{m}_{sol,i}$ (kg h ⁻¹) (Re)	$x_{sol,i}$	$T_{sol,i}$ (°C)	P_{sorp} (kPa)	$\dot{m}_{hfg,i}$ (kg h ⁻¹) (Re)	$t_{hfg,i}$ (°C)	A (m ²)	\dot{m}''_{sorp} (g m ⁻² s ⁻¹)	Ra	K (mm s ⁻¹)	\dot{Q}_{sorp} (kW)	\dot{Q}''_{sorp} (kW m ⁻²)	U (W m ⁻² K ⁻¹)	h_{sol} (W m ⁻² K ⁻¹)	Comments	REF		
ABS	NH ₃ -H ₂ O	HT	68.4-122.4	5-40	-	150-500	-	-	0.21	-	-	0.006-0.03	3.26-10.75	~15.5-51.2	753-1853	923-2857	-	(Lee et al., 2012)		
			-	3-30	45-60	17-193	-	30	-0.31	-0.16-1.94	-	-	-	0.25-1.5	-0.81-4.84	-	-	Helical	(Kwon and Jeong, 2004)	
			38.2-130	-	-	-	-	-	1.5	-	-	-	-	4.9-16.2	~3.3-10.8	133-403	144.6-510.1	Microtubes	(Meacham and Garimella, 2002, 2003)	
			~57.6-95.4	-	-	-	-	~360-576	-	0.46	-	-	-	4.5-15.1	~9.9-33	545-940	638-1648	Microtubes	(Meacham and Garimella, 2004)	
			~97.2-165.6	-	-	-	-	~1152-1584	-	1.36	-	-	-	5.8-21	~4.3-15.5	540-1160	800-2900	Microtubes	(Garimella et al., 2011)	
		40-64	37	43.7	279.5	319	20-30	-0.23	-7.56	~0.12	-	-	3-4.3	~12.8-18.32	~1279-1577	-	Microtubes	(Goel and Goswami, 2007)		
		40-64	38.1	43.3	279.7	319	20-30	-0.23	-8.79	~0.14	-	-	3.5-5.3	~14.92-22.59	~1918-2643	-	Microtubes, screen mesh	(Goel and Goswami, 2007)		
		H ₂ O-LiBr	HT	-	19.9-21.94	35.29-48.97	94.16-139.1	2160-4680	26.5-30.9	1.76	-	-	-	0.6-1.31	~0.34-0.75	~356	-	-	Air-cooled	(Castro et al., 2009)
				Plate	14.4-36.54	5-15	17-37.2	-	355.79-436.5	-	-	-	-	0.01-0.55	-	-	-	500-2100	-	(Kang et al., 1999)
				~6-54	0-30	20	-	-	-	-	-	-	-	0.08-1.58	0.06-0.45	-	350-2750	-	-	(Lee et al., 2002a)
	60.12-81.36			46-49.4	38.85-43.95	601-609	1170-1173.6	25.95-27.05	0.82	~5.98-6.75	~0.22-0.33	-	-	7.61-8.39	~9.3-10.26	~1684-1757	-	-	(Triché et al., 2016)	
	(5-40)			59	39	0.667	601.2	30	-	-	-	-	0.003-0.07	-	-	-	1100-2100	Smooth tube	(Kiyota et al., 1996)	
	(5-40)	59	39	0.667	601.2	30	-	-	-	-	0.005-0.08	-	-	-	1100-4000	Knurled tube	(Kiyota et al., 1996)			
	(5-40)	59	39	0.667	601.2	30	-	-	-	-	0.002-0.07	-	-	-	1300-5000	Knurled tube	(Kiyota et al., 1996)			
	(10-100)	40-61	40-43	-	-	30	-	-	-	-	-	-	-	~133.33-1551	300-800	Smooth tubes	(Hoffmann et al., 1996)			
	(10-100)	40-61	40-43	-	-	30	-	-	-	-	-	-	-	~200-1900	450-980	knurled tubes	(Hoffmann et al., 1996)			
	102-498	58	40	1.1414	4800-18600	28	-	-	-	-	0.008-0.03	-	-	-	250-780	Bare tube	(Yoon et al., 1999b)			
	102-498	58	40	1.1414	4800-18600	28	-	-	-	-	0.017-0.036	-	-	-	400-770	Bumping tube	(Yoon et al., 1999b)			
	102-498	58	40	1.1414	4800-18600	28	-	-	-	-	0.019-0.064	-	-	-	550-1100	Floral tube	(Yoon et al., 1999b)			
	102-498	58	40	1.1414	4800-18600	28	-	-	-	-	0.039-0.069	-	-	-	660-1180	Twist floral tube	(Yoon et al., 1999b)			
(13-40)	60-64	52	-	-	30-32	~0.60	0.03-0.09	-	-	-	-	2.7-5.25	~4.48-8.7	1250-1900	1750-3300	-	(Deng and Ma, 1999)			
-	60	45	0.933	-	32	~0.96	-	-	-	-	-	-	-	650-1020	Smooth tube	(Yoon et al., 2002)				
-	60	45	0.933	-	32	~0.96	-	-	-	-	-	-	-	790-1050	Floral tube	(Yoon et al., 2002)				
-	60	45	0.933	-	32	~0.96	-	-	-	-	-	-	-	840-1100	Hydrophilic tube	(Yoon et al., 2002)				
-	36-162	57-60	-	-	0.45432	30	-	-	-	-	-	0.925-1.25	8.5-12	-	640-930	-	(Kyung and Herold, 2002)			

Chapter I. State of the art

			~51	60.4	39.8-49.7	2.1-2.95	226.8-410.4	26-35.5	-0.23	1.98-2.13	-0.032-0.034	-	-	-	-	-	(Islam et al., 2003)
			~51	60.4	39.8-49.7	2.1-2.95	226.8-410.4	26-35.5	-0.23	3.34-4.17	-0.054-0.067	-	-	-	-	-	Inverted falling film
			51.4512	60.4	39.8-50	1-3	227.448-319.536	26.5-35.2	-0.23	2.05-3	-0.033-0.049	-	-	-	-	-	(Islam, 2008)
			(12-25)	61	47	0.933	-	32	-0.20	2.1-2.5	-	0.02-0.032	-	-	700-880	570-800	(Yoon et al., 2008)
			(12-25)	61	47	0.933	-	32	-0.19	2.3-2.6	-	0.023-0.03	-	-	6650-720	610-830	(Yoon et al., 2008)
			(12-25)	61	47	0.933	-	32	-0.19	2.4-2.8	-	0.024-0.035	-	-	760-960	650-900	(Yoon et al., 2008)
			1800-3000	48-60	-	1-1.2	-	16-28	-34.38	-	-	-	-	-	1900-3000	-	(Bredow et al., 2008)
			50-210	60	45-50	0.93	300-900	28-34	-	1.45-2.25	-	0.014-0.017	-	4.2-7.6	400-660	420-620	Helical tubes
		VT	(70-250)	40-60	-	1.3-5.3	-	-	-0.03	0.26-2.7	-	-	-	-	-	-	(Matsuda et al., 1994)
			~61.26-486	62	~49-53	1.3	-	46	-0.09	~1.15-1.42	-0.001-0.08	-	0.32-0.52	~3.5-5.7	800	-	Smooth tube
			~61.26-486	62	~49-53	1.3	-	46	-0.09	~1.75-2.9	-0.001-0.02	-	0.52-0.8	~5.7-8.8	1584	-	Twisted tube
			~61.26-486	62	~49-53	1.3	-	46	-0.09	~2.19-3.07	-0.002-0.02	-	0.68-0.87	~7.5-9.5	1461	-	Grooved tube
			~61.26-486	62	~49-53	1.3	-	46	-0.09	~2.25-3.12	-0.002-0.02	-	0.63-0.93	~6.9-10.2	1303	-	Pin-fin tube
			6-36 (30-200)	58	40-46	0.93-1.22	60	30-36	-0.03	0.6-2.5	-0.002-0.049	-	-	2.2-3.8	-	-	(Kim and Kang, 1995)
			(60)	60	40	1.01	(10000)	30	-	-	-	0.005-0.04	-	-	800-1250	-	(Kim et al., 1996)
			50.4-93.6 (100-400)	60-64	-	1-1.5	(6000)	35-46	-0.09	~0.99-3.73	0-0.024	-	0.350-1.16	~3.8-12.7	-	-	(Miller and Keyhani, 2001)
			26-80 (100-290)	57.9-60	40	1-2.2	(6000)	30-40 (30)	-0.10	0.2-5.2	-0.001-0.075	-	0.4-1.35	~3.8-13	-	200-600	(Medrano et al., 2002)
			(5-200)	59	39	0.67-0.8	-	30	-0.02	~0.006-0.025	-	0.004-0.015	-	-	300-600	-	Air-cooled
			(5-200)	59	39	0.67-0.8	-	30	-0.08	~0.04-0.14	-	0.01-0.02	-	-	250-850	-	Air-cooled
			~14.4-20	49.1-49.2	27-27.5	1.06-1.08	~(1395)	9.71-9.73	-0.05	~2.29-5.04	-0.03-0.047	-	0.41-0.42	~8-8.2	~498-515	-	Smooth plate
			~11.4-20	48.9-49	26.2-26.7	1.013-1.074	~(1403)	9.87-10.33	-0.05	~1.55-4.68	-0.025-0.045	-	0.38-0.41	~7.4-8	~501-551	-	Wire screen over plate
			-	54-59	30-38	0.8-1.4	-	25-35	-0.01	2.3-5.8	-	-	-	-	-	-	Fin structure on plate
			20-150	57-60	20-40	1	30-80	10-30	-0.01	1-7.3	-0.001-0.03	-	-	-	-	-	Grooved plate
DES	H ₂ O-LiBr	Plate	93.6-100.8	50-53.82	53-71.8	3.55-6.72	648-972	58.2-83.8	0.24	~0.88-2.21	-0.008-0.02	-	0.82-2.01	~3.4-8.4	735-856	-	(Hu et al., 2017)
		HT	25.2-50.4	49.5-58	-	9.73	-	Elect. Res.	-0.05	-	-	-	~0.5-1.25	10-25	1130-1660	-	(Shi et al., 2010)

Corrugation and surface modification were studied as enhancement methods for ammonia condensation and evaporation, which would be especially high at low and medium Re numbers (lower than 700) (Kareem et al., 2015). Different tube surfaces are presented in Figure I.18. Fernández-Seara et al. (2009) and Fernández-Seara and Uhía (2012) studied titanium as a material for extreme applications (e.g., marine applications) and two surface enhancement methods (fins and spirally corrugated tubes, Figure I.18b and c). In the condenser operation mode, finned tubes resulted in a poor enhancement method as high condensate retention between the fins was observed because of the high surface tension of NH_3 . For this reason, they concluded that NH_3 should be considered as a high-surface-tension fluid (like H_2O) (Fernández-Seara et al., 2009). Moreover, the turbo helix tube showed no enhancement compared to a smooth tube (Fernández-Seara and Uhía, 2012).

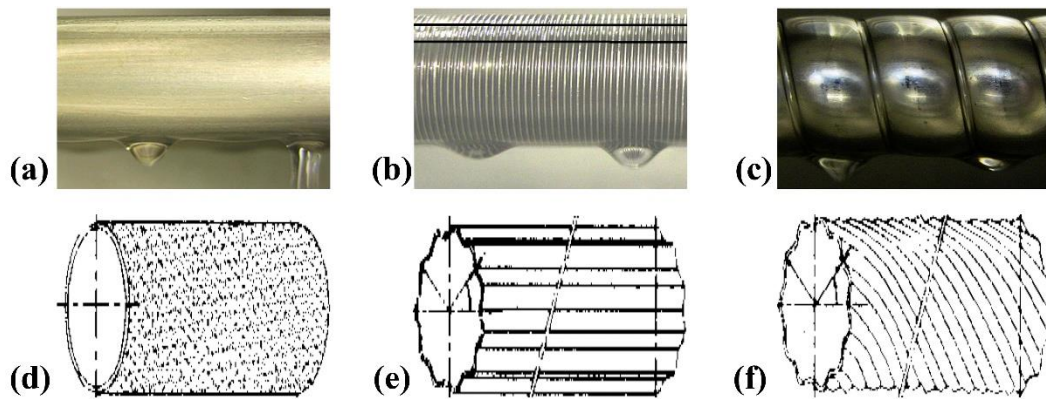


Figure I.18: Different tube surfaces. (a) Smooth tube and (b) integral-fin tube (Fernández-Seara et al., 2009), (c) turbo helix tube (Fernández-Seara and Uhía, 2012), (d) knurled tube, (e) floral tube, and (f) twisted floral tube (Yoon et al., 1999a).

For the multifunctional exchangers, several models of horizontal tube exchangers in absorption (Islam, 2008) and desorption (Herrera et al., 2010; Sánchez et al., 2017) modes with good experimental agreements were developed. One enhancement method is to generate a stable solution distribution over the tubes (Determan and Garimella, 2011, 2005; Meacham and Garimella, 2004). The spray distribution method could be an option for shell and tube exchangers in this regard (Abed et al., 2015). Another way to enhance the heat and mass transfers is to modify the surface geometry to generate flow instabilities. This was largely studied in the case of H_2O -LiBr absorbers. Furukawa et al. (1993), for example, studied fluted tubes as a mechanical enhancement method and found that floral tubes (Figure I.18e) have a higher performance compared to smooth tubes. Yoon et al. (1999b, 1999a) tested different configurations and confirmed the better performance of floral tubes and twisted floral tubes (Figure I.18f) over knurled (Figure I.18d) and smooth tubes. Hoffmann et al. (1996) compared the smooth tube and knurled tube geometries and obtained a 20–40% increase in the HTC for the knurled tubes. This better performance of the knurled tubes was confirmed by Kiyota et al. (1996), who reported that deeper knurls led to better performance. Kim et al. (2003) studied the effect of a micro-scale surface treatment on the tubes and found that the wettability was higher for a microhatched tube compared to a smooth tube. Yoon et al. (2002) studied a smooth tube, a floral tube, and a hydrophilic tube, and observed that the hydrophilic tube has the highest permeability and HTC, followed by the floral tube, and the smooth tube was the least effective. Islam et al. (2003) focused on the falling film flow characteristics and proposed a configuration in which the falling film is constantly inverted to cool down both of its surfaces (Figure I.19a). The design improved the absorption rate to about 100% compared to a conventional tubular absorber. Finally, another enhancement method specifically designed for systems that use water as refrigerant (owing to the low operating pressures) consists in a two-step evaporator/absorber (Figure I.19b), in which the evaporator and absorber are divided into two pressure levels (with a difference of pressure of

around 1.3 mbar) induced by holding refrigerant water in liquid distribution trays located between the two pressure levels. In this way, the absorption is enhanced by dividing it into two steps of different temperature, concentration, and pressure levels (Dixit, 2018).

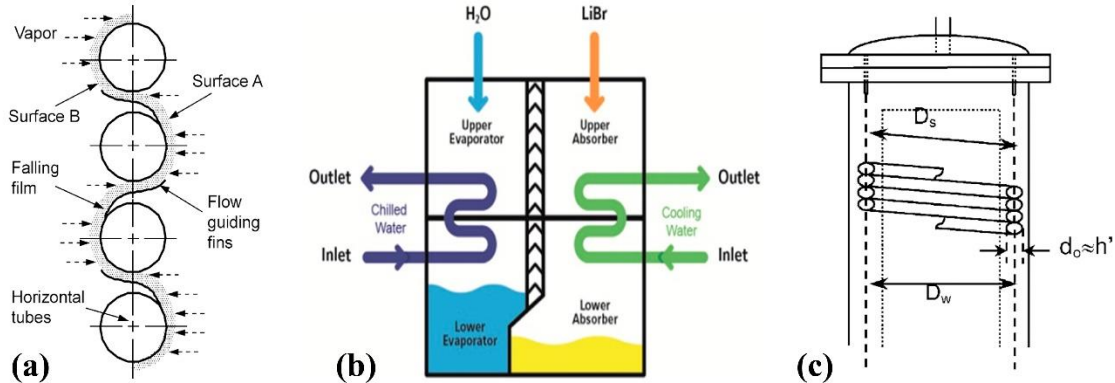


Figure I.19: Special horizontal tube configurations. (a) Film inverter system (Islam et al., 2003), (b) two-step evaporator/absorber system (for water-based systems) (Dixit, 2018), and (c) helical coil falling film configuration (Kwon and Jeong, 2004).

A special variant of horizontal tube heat exchangers are helical coil exchangers (Figure I.19c), which seem to have good potential compared to straight tubes due to the increased local HTC generated by turbulence and vorticity in the curves (Prabhanjan et al., 2002). However, some authors observed no experimental enhancement using a helical absorber compared to conventional horizontal tube absorbers (Yoon et al., 2006). Kwon and Jeong (2004) studied the effect of the vapor flow in this kind of absorber using the $\text{NH}_3\text{-H}_2\text{O}$ working pair and observed that in parallel flow, the HTC is highly influenced by the solution flow rate (SFR). On the other hand, for the countercurrent mode, it is mostly affected by the vapor flow. Demesa et al. (2017) developed and tested a 2-kW evaporator in low-pressure conditions (using water as refrigerant), which comprised three nested helical coils of different diameter connected in series. The proposed heat exchanger showed an overall HTC of $660 \text{ W m}^{-2} \text{ K}^{-1}$ and up to 83% efficiency. Regarding improvements in efficiency, Said et al. (2016) developed and successfully proved the concept of a solar-powered $\text{NH}_3\text{-H}_2\text{O}$ chiller (based on (Brendel et al., 2010; Zetsche et al., 2010)) with a special focus on the generator, which included an additional waste heat recovery from the rectifier. Finally, Rossi et al. (2005) studied the use of ultrasonic vibrations to reduce the surface tension of the $\text{H}_2\text{O-LiBr}$ solution and increase its kinetic and molecular diffusivity. However, no energy savings resulted from this method because the increase in the absorption performance is equivalent to the energy spent to activate the ultrasonic excitation.

Another enhancement method is the microchannel concept, for which the $\text{NH}_3\text{-H}_2\text{O}$ working pair is most suitable. Indeed, high-viscosity working pairs would create thicker films over the small-diameter tubes, resulting in low heat and mass transfers. The concept and a semi-empirical model were presented in (Garimella, 1999). It consists in the use of vertically stacked square arrays composed of tubes of tiny diameters, generating high HTCs on the coolant side at laminar regime. A first prototype was developed (Figure I.20a) and tested by Meacham and Garimella (2002). The experiments showed lower performance than predicted owing to a low wettability rate (20–30%) derived from a nonuniform solution distribution (Meacham and Garimella, 2003). A second prototype with an optical verification and an improved solution distributor similar to the one in Figure I.21, but without the vapor passage tubes (used in the generator mode), was presented by Meacham and Garimella (2004). This prototype achieved heat transfer duties within the same range as the first prototype with one-third the exchange area owing to a better flow distribution. A third-generation absorber was developed with bent tubes and a horizontal orientation to maximize the wetted ratio and reduce the number of tube sections. The absorber showed good

performance and a reduction in the flow rate per tube length, which reduces the film thickness, improving the heat and mass transfer performance (Garimella et al., 2011). Enhancement methods have also been tested for microtube absorbers. (Goel and Goswami, 2005a, 2005b) adapted wire mesh to the tubes to guide the $\text{NH}_3\text{-H}_2\text{O}$ solution and enhance the transfers (Figure I.20b). The authors predicted a size reduction of about 25%, and experimental results proved enhancement between 17 and 26% (Goel and Goswami, 2007).

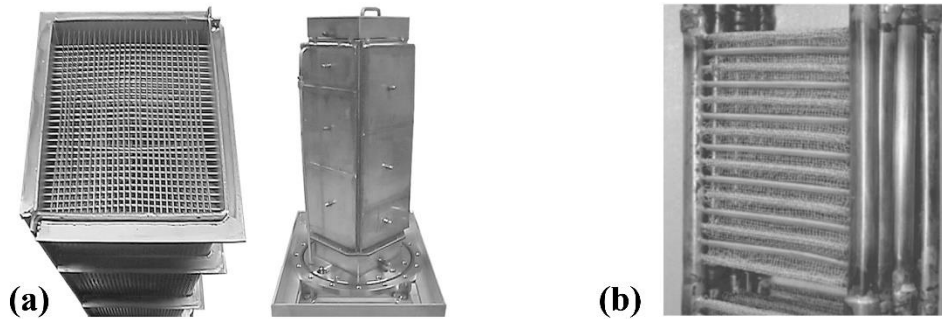


Figure I.20: (a) Microtube absorber (Meacham and Garimella, 2002) and (b) screen mesh as an enhancement method (Goel and Goswami, 2007).

The microtube concept was also tested in generator mode for the $\text{NH}_3\text{-H}_2\text{O}$ working pair. Determan et al. (2004) modified the prototype of Figure I.20a to operate as a desorber and adapted it with an improved solution distribution device (Figure I.21). A model was developed to predict the local heat and mass transfer rates in a microchannel desorber. Moreover, the concentrated solution flow rate (SFR) showed a great impact on the desorber's performance (the overall HTC increased linearly with the SFR). Determan and Garimella (2005) later modeled the desorber and determined that a 0.29–0.69 wetting ratio was obtained in the conditions studied. The vapor phase presented the highest mass transfer resistance; however, it was the wetted ratio that limited the generator's performance. Moreover, the vapor generated at the bottom conveniently heated the solution as it rose through the desorber (Determan and Garimella, 2011).

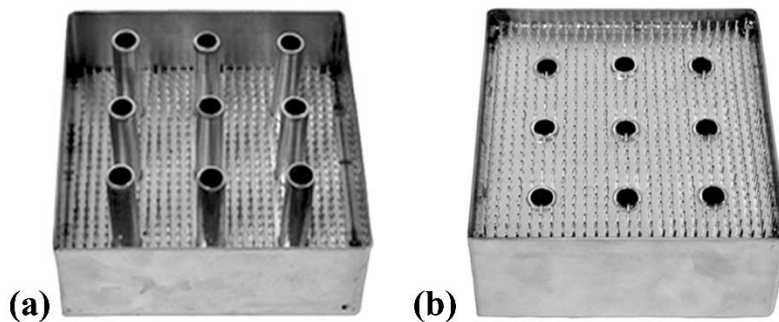


Figure I.21: Solution distribution device for a microtube generator. (a) Top view and (b) bottom view (Determan and Garimella, 2011).

1.3.2.1.2. Vertical tube falling film

The falling film on vertical tubes (VTs) can be inside or outside the tube; this choice does not seem to impact the exchanger performance. The choice relies only on the desired application (Medrano et al., 2002). Matsuda et al. (1994) studied the effect of the pressure and concentration (in absorbent) on a $\text{H}_2\text{O-LiBr}$ solution falling outside a VT and found that the mass exchange rate decreases while the pressure decreases and the solution concentration increases, and vice-versa. This impact of the LiBr concentration is the same on the heat transfer according to Shi et al. (2010), who studied a falling film inside a tube. Regarding the concentration gradient in the flow's direction, Miller and Keyhani (2001) stated that it is approximately constant.

Some studies also focused on heat and mass transfer enhancement in VT falling films. Amaris et al. (2014a) tested an internally microfinned tube as a $\text{NH}_3\text{-LiNO}_3$ absorber. The advanced surface presented absorption rates up to 1.7 times higher than for a smooth tube. Moreover, as the tube diameter decreases, the absorption mass flux increases. On the other hand, the absorption mass flux decreases if the tube length increases. Finally, Miller and Perez-Blanco (1994) tested different advanced surfaces (e.g., pin-fin, fluted tube, grooved tube, and twisted tube) to induce mixing in a $\text{H}_2\text{O-LiBr}$ solution film and compared them with a smooth tube. The pin-fin and grooved tubes yielded the best absorption enhancements (225% and 175%, respectively), which led to absorption levels close to those obtained in horizontal tube absorbers with chemical additives in commercial machines.

Vertical tubes are a good choice for air-cooled absorbers owing to the easy addition of fins on their external surface (Kiyota et al., 2003; Medrano et al., 2002). However, the required heat exchange area is from two to three times that of water-cooled heat exchangers for similar conditions (Kiyota et al., 2003; Medrano et al., 2002). Medrano et al. (2002) designed and tested an air-cooled absorber with vertical finned tubes, observing that short tubes reduce the subcooling and a high $\text{H}_2\text{O-LiBr}$ concentration increases the mass transfer driving force. Kiyota et al. (2003) proposed a similar air-cooled design for the $\text{H}_2\text{O-LiBr}$ solution and developed a mathematical model that showed good agreement for pipes with an inner diameter greater than 13 mm. The authors observed an optimum tube length after which the absorption rate remained unchanged.

1.3.2.1.3. Plate falling film

Commercial plate heat exchangers (PHEs) operate in falling film mode at low flow regimes. Their main advantages are their low cost, flexibility, easy maintenance, and high performance. Regarding their fabrication method, they can be gasketed or brazed. The heat exchange surface can be smooth or corrugated, in which case, the turbulent flows generated enhance the transfers and reduce the fouling effect thanks to its self-cleaning nature (Elmaaty et al., 2017). Special attention must be paid to the solution distribution method for good wettability; otherwise, the exchanger performance might be drastically reduced (Sterner and Sunden, 2006).

Different options were studied for heat and mass transfer enhancement in plate falling films. In the case of absorption operation using $\text{NH}_3\text{-H}_2\text{O}$, Kang et al. (1999) experimentally correlated the heat and mass transfers in a PHE with offset strip fins for surface enhancement and observed that transfers increased at a lower inlet solution temperature and a higher vapor temperature (the inlet subcooling has a higher impact on the heat transfer). Triché et al. (2017, 2016) tested a commercial gasketed plate-and-frame absorber and concluded that the falling film mass transfer resistance controls the mass transfer and that the liquid-side heat transfer resistance is negligible compared to the other heat transfer resistances.

Regarding the $\text{H}_2\text{O-LiBr}$ working pair, Kim and Ferreira (2008) studied the effects of wire screen and additives on a plate falling film heat exchanger at low Re numbers (40–110). The surface was never completely wetted and the wire screen did not seem to enhance the transfers. Mortazavi et al. (2015) installed a fin structure on a vertical flat plate to enhance the wetting rate, minimize the film thickness, and continuously interrupt the boundary layer (Figure I.22a). The design showed absorption rates up to twice as high compared to conventional falling film absorbers. Another interesting option are grooved plates since the grooves allow for a good and stable wettability rate, even at low flow regimes. However, the exchange area is reduced and the turbulence effects observed are lower compared to low solution flow regimes on smooth plates (Stutz et al., 2016). Michel et al. (2017) proposed a vertically grooved falling film absorber (Figure I.22b) whose performance was numerically and experimentally studied showing high absorption rates. The absorption rate showed a strong influence of the SFR and the cooling temperature.

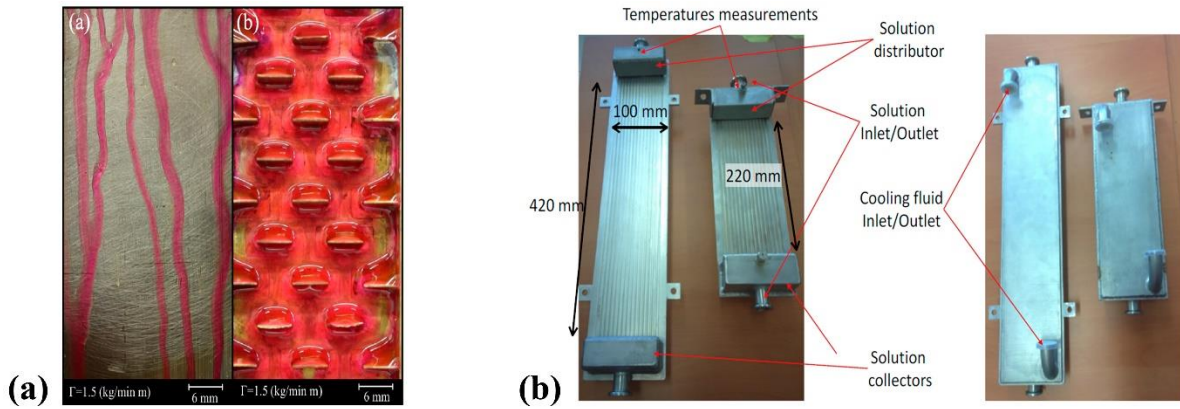


Figure I.22: Macrostructuration on PHEs. (a) Comparison of wetting rate for a flat plate and a patterned surface (Mortazavi et al., 2015) and (b) front view and back view of grooved plate absorbers (Michel et al., 2017).

Plate falling films can also be used as the generator in absorption chillers. Hu et al. (2017) designed a novel plate-type falling film generator/condenser unit (Figure I.23) for the H_2O -LiBr working pair. The generator comprises a three-channel heat exchanger with four stainless steel plates in a counter-flow configuration (solution/heat transfer fluid). Moreover, the internal plates contain horizontal circular columns to allow for vacuum operating conditions (Figure I.23b) and the spillway distributor is directly connected to the generator (Figure I.23c). During experiments, the dry areas observed disappeared while increasing the SFR or while heating the plates.

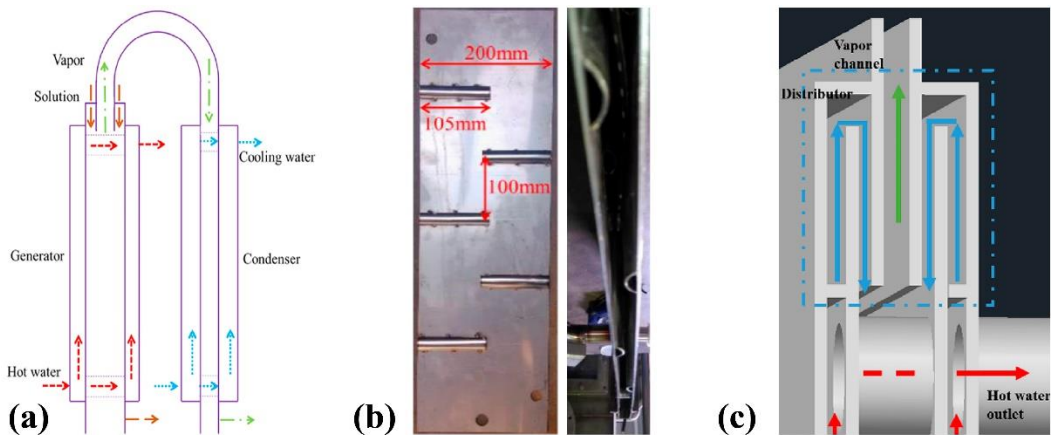


Figure I.23: (a) Generator/condenser unit diagram, (b) front view and side view of the generator vacuum channel plates, and (c) cross-sectional view of the directly connected spillway solution distributor (Hu et al., 2017).

The falling film configuration was also studied for the evaporation process in absorption systems. Djordjevic and Kabelac (2008) studied the NH_3 evaporation on a commercially available stainless-steel PHE with a chevron pattern (similar to the one illustrated in Figure I.26b). Experimental results showed that the parallel flow is more efficient than the counter-flow mode. Furthermore, low chevron angle corrugations yield a higher evaporation heat transfer. Gonda et al. (2014) studied the non-boiling falling water film evaporation on a corrugated plate and proposed a new correlation (Figure I.24a). The fluid distribution was divided into two parts to obtain an even distribution of a thin, continuous, and uniform liquid film (Figure I.24b). Interfacial turbulence was observed during tests (Figure I.24c) and the results showed a heat transfer enhancement. Moreover, hysteresis was observed in the wetting rate. Finally, a special configuration for NH_3 - H_2O proposed by Christensen et al. (1998) consists of an accordion fin assembly with perforations that allow the solution to flow downwards and the refrigerant vapor

to flow upwards. The assembly is located between heat transfer walls that cool the solution (Garrabrant and Christensen, 1997).

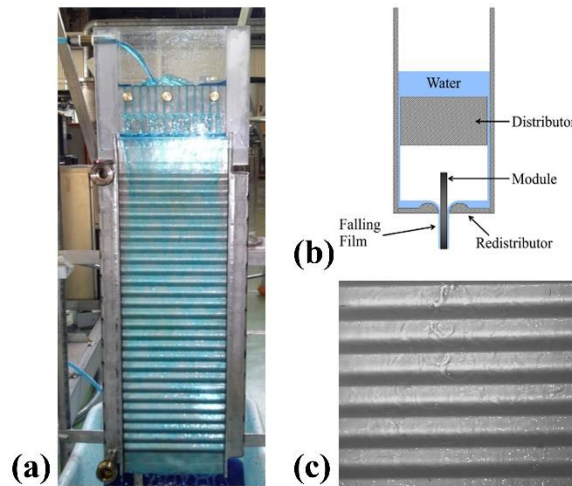


Figure I.24: Gonda et al.'s (a) corrugated plate with the distributor, (b) cross-view of the distributor, and (c) falling film image from high-speed camera (Gonda et al., 2014).

1.3.2.2. Two-phase flow exchangers

Since stable films that cover the entire exchange area are difficult to generate in falling film exchangers (Hartley and Murgatroyd, 1964), bubble exchangers were recommended for ammonia-based chillers (Figure I.25) (Ammari, 2012; Helbing et al., 2000; Herbine and Perez-Blanco, 1995; Kang et al., 1998; Van Rooyen, 2011), especially for low SFRs. Therefore, they are more suitable for small-capacity applications (Castro et al., 2009; Ibarra-bahena and Romero, 2014). The implementation of this technology is simple because it does not require a solution distributor. Nevertheless, a refrigerant vapor distributor might be required in absorption mode. Moreover, the heat transfer in this case is not as effective as in falling films (Kang et al., 2000). In addition, these exchangers are not recommended for working pairs using water as the refrigerant because of the vacuum operating pressure, which leads to a low vapor density (high pressure drops, risk of dry zones due to a higher bubble diameter, and smaller bubble departure frequency) and a considerable impact of the hydrostatic pressure, which generates a high variation of the saturation temperature of the liquid along its height, yielding low performance and difficult bubble generation (Giraud, 2015; Giraud et al., 2016). Furthermore, the most conventional water absorbent ($\text{H}_2\text{O-LiBr}$) is a highly viscous solution, which adds problems such as pressure drops and a lower vapor-phase velocity (Warnakulasuriya and Worek, 2008a). Table I.12 summarizes the experimental studies on the two-phase and membrane-based exchangers; the latter will be discussed in Section 1.3.2.3.

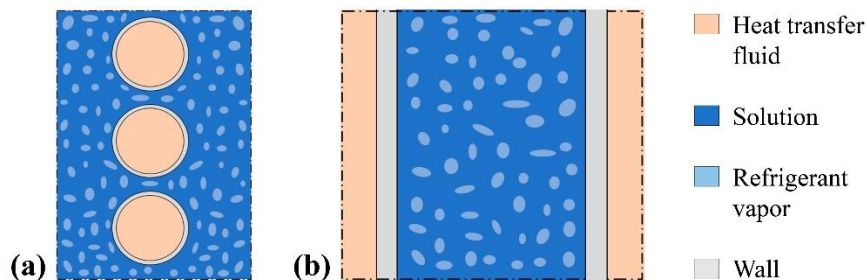


Figure I.25: Two-phase exchanger geometries. (a) Horizontal tubes and (b) vertical surface (either vertical tubes or plates).

1.3.2.2.1. Absorption

One application of bubble exchangers is absorption, for which a vapor distributor is required (Figure I.26) (Chan-González et al., 2017; Chan et al., 2018). While working with the $\text{NH}_3\text{-H}_2\text{O}$ working pair, Kang et al. (2002a, 2002b) separated the bubble absorption phenomenon into two processes: bubble growth and the disappearance process. Several studies with $\text{NH}_3\text{-H}_2\text{O}$ showed that lower inlet temperatures; higher operating pressures; lower solution inlet concentrations (in refrigerant); and higher solution, vapor, and HTF flow rates in counter-current mode result in higher absorption driving potential and smaller bubble diameters (Cerezo et al., 2010, 2009; Kang et al., 2002a, 2002b; Lee et al., 2003). However, Lee et al. (2002b) reported that the increase in the SFR has a stronger impact on the heat transfer than on the mass transfer, and, studying the $\text{NH}_3\text{-LiNO}_3$ working pair, Oronel et al. (2013) reported that the solution concentration has a strong impact on the absorption capacity.

Some researchers have tried to prove the advantages of bubble absorbers compared to the falling film absorbers. Castro et al. (2009) theoretically and experimentally compared the performance of $\text{NH}_3\text{-H}_2\text{O}$ falling film and bubble absorption inside vertical finned tubes for air-cooled small-capacity chillers. The results showed that bubble absorption is more efficient than falling films, especially at a low SFR, owing to the low wettability of the falling film at that regime. This confirmed the better suitability of bubble absorbers for small-capacity systems. However, the performance increase in comparison to a full-film wetted area was less than 1%. Kang et al. (2000) analytically compared the $\text{NH}_3\text{-H}_2\text{O}$ falling film and bubble type absorbers, finding a higher local absorption rate in the bubble mode that could lead to a 49% reduction in the exchanger size. This was later confirmed by Lee et al. (2002a) in an experimental study.

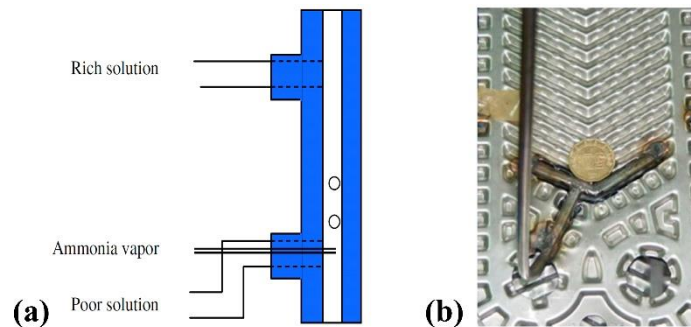


Figure I.26: Bubble absorber distributors. (a) Diagram (Cerezo et al., 2009) and (b) experimental implementation on an Alfa-Laval PHE (Chan-González et al., 2017).

Regarding enhancement methods, Cerezo et al. (2018) studied the effects of a helical static mixer inside the central tube of a double-pipe heat exchanger operating with $\text{NH}_3\text{-H}_2\text{O}$. The resulting heat flux was 32% higher compared to an exchanger with no mixer.

Chapter I. State of the art

Table I.12: Two-phase and membrane-plate-based exchangers in absorption chillers: experimental results (~: approximated data).

Func	WF	Type	$\dot{m}_{sol,i}$ (kg h ⁻¹) (<i>Re</i>)	$x_{sol,i}$	$T_{sol,i}$ (°C)	P_{sorp} (kPa)	$\dot{m}_{hfg,i}$ (kg h ⁻¹) (<i>Re</i>)	$t_{hfg,i}$ (°C)	A (m ²)	\dot{m}''_{sorp} (g m ⁻² s ⁻¹)	Ra	K (mm s ⁻¹)	\dot{Q}_{sorp} (kW)	\dot{Q}''_{sorp} (kW m ⁻²)	U (W m ⁻² K ⁻¹)	h_{sol} (W m ⁻² K ⁻¹)	Comments	REF		
ABS	NH ₃ - H ₂ O	Bubble PHE	18	0-30	20	-	-	-	~0.06	-	-	0.1-2.7	0.025- 0.45	~0.42- 0.76	300-2600	-	-	(Lee et al., 2002b)		
			~6-54	0-30	20	-	-	-	-	-	-	0.083- 2.75	0.09- 0.45	-	400-2550	-	-	(Lee et al., 2002a)		
			30-50	29- 33.4	35-55	160-200	140	30-38	0.1	2.5-6.3	~0.014 -0.07	-	1-2	0.5-1.3	~5-13	-	2700-5400	-	(Cerezo et al., 2009)	
			~30-50 (220- 480)	29-33	38-42	162-202	(270- 520)	30-35	0.1	2.5-5	~0.02- 0.06	-	-	0.5- 1.28	~5-12.8	-	510-1210	-	(Cerezo et al., 2010)	
			90- 118.8 (400- 470)	0-13	-	480	1116	20-26	0.05	65-80	~0.09- 0.16	-	54-109	-	-	-	2350-2500	-	(Chan-González et al., 2017)	
		Bubble tube	100.8	40.89	36.9	549	910.8	26.6	~0.32	~2.48	~0.03	-	-	1.026	3.18	~295	270	-	(Cerezo et al., 2018a)	
			100.8	40.76	37	577	918	26	~0.30	~3.31	~0.036	-	-	1.406	~4.65	~425	450	With a helical static mixer	(Cerezo et al., 2018a)	
			0.6-1.8 (15- 45)	0-15	22.5	250-400	16.14 (370)	10.6	0.002	~8.34-25	~0.03- 0.3	-	-	-	-	800-3300	-	Smooth wall	(Jenks and Narayanan, 2008)	
			0.6-1.8 (15- 45)	0-15	22.5	250-400	16.14 (370)	10.6	0.002	~8.34-25	~0.03- 0.3	-	-	-	-	2600-3900	-	Smooth wall	(Jenks and Narayanan, 2008)	
			0.6-1.8 (14- 43)	0-15	22.5	250-400	16.14 (370)	10.6	0.002	~8.34-25	~0.03- 0.3	-	-	-	-	1250-1800	-	Smooth wall	(Jenks and Narayanan, 2008)	
	NH ₃ - LiNO ₃	Bubble PHE	0.6-1.8 (15- 45)	0-15	22.5	250-400	16.14 (370)	10.6	0.002	~8.34-25	~0.03- 0.3	-	-	-	-	1050-2300	-	Cross-ribbed wall	(Jenks and Narayanan, 2008)	
			0.6-1.8 (14- 41)	0-15	22.5	250-400	16.14 (370)	10.6	0.002	~8.34-25	~0.03- 0.3	-	-	-	-	900-2900	-	Cross-ribbed wall	(Jenks and Narayanan, 2008)	
			0.6-1.8 (17- 50)	0-15	22.5	250-400	16.14 (370)	10.6	0.002	~8.34-25	~0.03- 0.3	-	-	-	-	1000-4300	-	Streamwise finned wall	(Jenks and Narayanan, 2008)	
			0.6-3.3 (27- 146)	10-55	75	620	12	30-58	~0.005	~3.7-11.1	~0.02- 0.3	-	-	0.06- 0.15	~13.3- 33.3	1080-2180	-	Smooth wall	(Cardenas and Narayanan, 2011)	
			0.6-3.3 (27- 146)	10-55	75	620	12	30-58	~0.005	~3.7-17.8	~0.02- 0.48	-	-	-	-	1020-1880	-	Stepped wall	(Cardenas and Narayanan, 2011)	
			15-60	45-48	45	510	130- 333	35-40	0.1	~2-60	~0.01- 0.14	-	0.15-0.39	-	-	-	1800-4900	-	(Oronel et al., 2013)	
			42- 127.7 (20- 450)	35-50	-	-	1116	-	0.05	15-24	~0.02- 0.1	-	8.2-15	-	-	-	900-3000	-	(Chan et al., 2018)	
			Bubble tube	10-72	45.2	45	510	80-435	35-40	0.025	3.2-5.6	0.004- 0.05	0.26-0.47	-	-	-	-	1100-1600	Smooth tube	(Amaris et al., 2014a)
				10-72	45.2	45	510	80-435	35-40	0.029	3.2-8	0.006- 0.1	0.38-0.72	-	-	-	-	1100-2600	-	(Amaris et al., 2014a)
				10-72	45.2	45	510	80-435	35-40	~0.034	3.4-60	~0.005 -0.06	0.28-0.39	0.34	~10	-	-	1000-1400	-	(Amaris et al., 2014a)
H ₂ O- LiBr	Membrane	0.6-2.1	60	25-35	0.8-1.8	-	25-35	0.008	1.7-62	~0.02- 0.3	-	-	-	-	-	160-μm microchannel	(Nasr Isfahani et al., 2013)			
		0.6-2.1	60	25-35	0.8-1.8	-	25-35	-	2.5-6.2	~0.03- 0.29	-	-	-	-	-	160-μm microchannel	(Nasr Isfahani and Moghaddam, 2013)			
		0.6-2.1	60	25-35	0.8-1.8	-	25-35	0.008	1.8-7.8	~0.02- 0.36	-	-	-	-	-	100-μm microchannel	(Nasr Isfahani and Moghaddam, 2013)			

Chapter I. State of the art

DES	NH ₃ -H ₂ O	Microchannel	0.6-2.1	60	25-35	0.8-1.8	-	25-35	~0.008	2.4-6.2	~0.03-0.3	-	-	-	-	160- μ m microchannel	(Bigham et al., 2014b)	
			2.5	60	31-43	0.8-1.6	-	25-35	0.007	2.5-60	~0.027-0.06	-	-	-	-	500- μ m microchannel, microstructure	(Nasr Isfahani et al., 2015)	
	NH ₃ -LiNO ₃	Vertical tube	64.8-126	-	-	-	396-684	-	1.5	4.53	-	-	5.4-17.5	~3.6-11.7	206-617	659-1795	-	(Determan et al., 2004) (Determan and Garimella, 2005) (Rivera and Best, 1999)
			-	39-48	-	960-1240	-	Elect. Res.	~0.12	-	-	-	~1.44-2.16	12-18	3300-5300	-	-	-
	NH ₃ -LiNO ₃	Vertical tube	-	33-62	-	700-1500	-	-	0.05	-	-	-	~1-3.5	20-70	-	5000-17500	-	(Táboas et al., 2010)
			-	40-48	-	870-1480	-	Elect. Res.	~0.12	-	-	-	~1.44-1.92	12-16	2200-2800	-	-	(Rivera and Best, 1999)
	NH ₃ -LiNO ₃	Tubes	20-55	45.5	-	992.3-1531.9	54-253	76.7-93.2	~0.028	-	-	-	~0.22-0.95	7.8-34.5	-	800-2100	-	(Jiang et al., 2017a)
			-	45	-	1030-1458	54-253	78-90	~0.021	-	-	-	~0.16-0.83	7.72-39.1	-	1320-2680	-	(Jiang et al., 2017b)
	NH ₃ -LiNO ₃	Tubes	-	45	-	1030-1458	54-253	78-90	~0.014	-	-	-	~0.11-0.54	7.72-39.1	-	1100-2350	-	(Jiang et al., 2017b)
			147.6-298.8	45.2-46.2	-	977.7-1606	-	72.8-90.1	~1.8	~0.28-13.9	~0.006-0.06	-	~2.16-8.32	1.2-4.62	-	660-1050	-	(Zacarias et al., 2010)
	NH ₃ -LiNO ₃	Plate	147.6-298.8	45.2-46.2	-	980-1610	-	78-97	1.8	~0.28-13.9	~0.006-0.06	-	~2.52-9	1.4-5	-	600-1000	-	(Venegas et al., 2012)
			-	49-54	-	1200-1500	-	-	-	-	-	-	-	5-20	-	2500-4800	-	(Taboas et al., 2016)
	H ₂ O-LiBr	Tubes	-	0-60	-	4-9.33	-	-	-	-	-	-	-	15-108	1600-4500	-	-	(Varma et al., 1994)
			-	0-50	-	7.38-101.3	-	-	-	-	-	-	-	-	20-40	-	800-1400	-
	H ₂ O-LiBr	Tubes	-	0-50	-	7.38-101.3	-	-	-	-	-	-	-	20-40	-	1000-1300	-	Corrugated tube (Sim and Kim, 2015a)
			-	0-50	-	7.38-101.3	-	-	-	-	-	-	-	20-40	-	1200-1800	-	Floral tube (Sim and Kim, 2015a)
	H ₂ O-LiBr	Tubes	-	0-50	-	7.38-101.3	-	-	-	-	-	-	-	20-40	-	1250-2000	-	Low fin tube (Sim and Kim, 2015a)
			-	0-50	-	7.38-101.3	-	-	-	-	-	-	-	20-40	-	1600-2600	-	Low fin tube (Kim, 2015)
H ₂ O-LiBr	Membrane	0.75-3.25	50	50-70	6-18	-	50-125	~0.008	1.5-9.5	~0.013-0.35	-	-	-	-	-	160- μ m microchannel	(Nasr Isfahani and Moghaddam, 2013)	
		0.75-3.25	48-51	70	6-18	-	50-125	~0.008	1.5-9.5	~0.013-0.35	-	-	-	-	-	200- μ m microchannel	(Nasr Isfahani et al., 2014)	

1.3.2.2.2. Boiling

The simplest pool boiling method in the desorber of absorption systems is by directly firing the solution container. However, when an external HTF loop is used, pool boiling has been conventionally implemented with horizontal tubes (Figure I.25a). For example, Sim and Kim (2015a, 2015b) experimentally tested different enhanced tube shapes H₂O-LiBr boiling (smooth, corrugated similar to Figure I.18c, floral, notched fin similar to Figure I.18d, and low fin similar to Figure I.18b). In both cases, the low-fin configuration led to the highest performance, followed by the floral and corrugated configurations. Moreover, a reduction in the tube diameter increased the heat transfer. Fernández-seara et al. (2016b) reported an average enhancement factor of 1.2 of a finned tube compared to a smooth tube for ammonia pool boiling; and the nucleation process showed strong hysteresis. Going further in the study of low-fin tubes for H₂O-LiBr pool boiling, Kim (2015) studied the impact of the fin's pitch and height in different configurations. The experimental studies led to an optimum fin geometry of 26 fins per inch (fpi) and a 0.18-mm fin height. Jiang et al. (2017a) presented a first study for NH₃-LiNO₃ boiling inside a smooth horizontal tube with an inner diameter (ID) of 8 mm, identifying that nucleate boiling was predominant during tests and that the heat fluxes have a considerable influence on the boiling HTC. In a separate paper, Jiang et al. (2017b) presented the results with the same working pair but for test sections of an inner diameter of 4 mm and 6 mm and developed a correlation that predicts the effects of the tube size, the heat flux, and the solution mass flux (solution mass flow rate divided by the exchange area, in kg m⁻² s⁻¹) on the HTCs with a deviation of less than 10%. Their experimental results show that for driving temperatures in the range of 78–90°C, there is no significant relationship between the boiling temperature and the boiling HTCs. Moreover, the solution mass flux positively impacts the boiling HTCs, especially for high heat fluxes. Finally, the boiling HTC in small-diameter tubes is lower than in large-diameter tubes at similar exit vapor qualities, but it is higher for the same mass flow rate.

Regarding the heat and mass transfer for the desorber operation, Varma et al. (1994) studied the pool boiling phenomenon of H₂O-LiBr over horizontal tubes in vacuum conditions and observed that the boiling phenomenon is significantly affected by the solution concentration, but not by the tube diameters. Moreover, the effect of the hydrostatic pressure on the saturation temperature along the height was observed as the local HTC was higher at the top of the desorber.

Another option that was recently proposed for pool boiling is the use of compact commercial PHE (Ayub, 2003; Thonon, 1995; Wang et al., 2007). Most experiments focused on the study of the desorption phenomenon in absorption chillers, which seems to result in more compact desorbers for the same capacity compared to the falling film desorbers (Roriz et al., 2004). Táboas (2006) and Táboas et al. (2012, 2010) experimentally studied a commercial BPHE Alfa Laval with Chevron-H type corrugation operating with NH₃-H₂O, and found that the boiling HTC is highly affected by the solution mass flux and almost not affected by the heat flux and pressure, especially at high vapor qualities. Moreover, the pressure drop increases while increasing the solution mass flux and vapor quality. For the NH₃-LiNO₃ working pair, Zacarías et al. (2010) presented an experimental evaluation of a commercial PHE and observed that nucleate boiling was dominant. Moreover, the mass and heat fluxes have an influence on the boiling HTC. This was later confirmed by Venegas et al. (2012) who tested subcooled and saturated boiling, proving that vapor could be present even before the arrival of the solution to the generator (subcooled boiling). Taboas et al. (2016) also observed subcooled boiling in an Alfa Laval PHE model NB51. On the other hand, while studying the frictional pressure drop, they observed that it seems to be highly affected by the vapor quality and the solution mass flux. Moreover, the correlations proposed in (Táboas et al., 2012) for NH₃-H₂O resulted in good agreement with the experimental results to predict the flow boiling HTC and frictional pressure drop of NH₃-LiNO₃. Finally, commercial PHEs are undoubtedly a good option for compactness and high performance. However, one must

be careful when working with the $\text{H}_2\text{O-LiBr}$ working fluid as the pressure drop in the desorber is a key factor. Indeed, changes in the saturation temperature as high as 30°C for a pressure drop as low as 20 kPa can exist. This is not the case for the $\text{NH}_3\text{-H}_2\text{O}$ working fluid, for which this effect is almost negligible thanks to its high operating pressures (García-Hernando et al., 2011).

1.3.2.2.3. Microchannel exchanger

A new exchanger concept similar to the one presented by Johnston and O’Sullivan (1981) was proposed by Nagavarapu and Garimella (2011a). This highly compact concept (around $500\text{ m}^2\text{ m}^{-3}$) consisted of an array of parallel, aligned alternating shims with integral microscale features (that allow the passage of the solution, vapor, and HTF) enclosed between cover plates. The microscale features can take different shapes and sizes depending on the requirements and can contain different components. Moreover, this geometry is more suitable for low-viscosity working pairs (such as $\text{NH}_3\text{-H}_2\text{O}$), since the small hydraulic diameters generate elevated pressure drops. Different prototypes were developed for $\text{NH}_3\text{-H}_2\text{O}$ with this technology; the first one being of a 300-W cooling capacity (Figure I.27) (Determan and Garimella, 2010, 2012). Other prototypes of 3.5 (Delahanty et al., 2015; Garimella et al., 2016; Keinath et al., 2015) and 7 kW (Staedter and Garimella, 2018) were also presented. The main challenges faced by this technology are the internal flow distribution and pressure drops (especially in the two-phase components) (Garimella et al., 2016), for which some solutions were proposed such as mixing sections (Hoysall et al., 2015), pin fins (Hoysall et al., 2017), and special headers (Mahvi and Garimella, 2017).

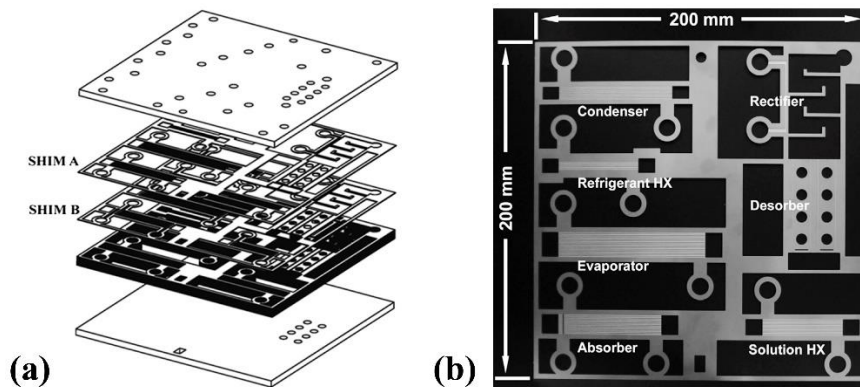


Figure I.27: Microscale monolithic absorption chiller. (a) Exploded view and (b) individual components on shim A (Determan and Garimella, 2010, 2012).

The generator in (Determan and Garimella, 2010, 2012) was in a co-flow configuration (vapor and liquid solution), which is more compact compared to the counter-flow configuration but with a refrigerant vapor of lower purity (Keinath et al., 2015). Therefore, for the second generation (Garimella et al., 2016; Keinath et al., 2015), Delahanty et al. (2015) developed a model for the design of a counter-flow microchannel desorber-rectifier and compared two design concepts in which the rectifier was included in the same envelope. Higher desorber heating rates than designed were required, probably because of a nonoptimal reflux to the absorber section. Moreover, at high temperatures (around 190°C), the performance decreased due to flooding and the increased sensible heating load of the solution (Keinath et al., 2015). Finally, a variation of microchannels consisting in fractal-like flow networks with elevated heat and mass transfer potential, low pressure drop, and low flow power penalties was proposed (Pence, 2010). Two $\text{NH}_3\text{-H}_2\text{O}$ generator prototypes (one with chemically etched disks (Mouchka et al., 2007) and another one with machined disks (Apreotesi et al., 2007)) proved the feasibility of the concept using two fractal disks separated by a thin layer of metal.

1.3.2.3. Membrane-based exchanger

Membrane-based exchangers are a very promising technology (Schaal et al., 2008; Thorud et al., 2006; Yu et al., 2012) because of their potential for portable applications, reliability, compactness, light weight, high performance, and simplicity (Robeson, 1999). However, while operating with salt-based solutions, some studies showed that their performance decreases gradually with constant use, probably due to salt accumulation in the pores, and therefore they might not be suitable for salt-based working fluids in the long-term (Riffat et al., 2004). The experimental studies on membrane-based exchangers were included in [Table I.12](#). In this case, the solution is constrained between a solid wall (used for heat transfer) and a vapor permeable wall (where the mass transfer takes place, [Figure I.28a](#)). Different from the commonly used plate falling film exchangers, here the solution film thickness and velocity can be controlled independently (Nasr Isfahani and Moghaddam, 2013) to enhance the mass transfer with forced convection. This leads to high compactness and low weight (Ali and Schwerdt, 2009). In general, the film in the exchanger is composed of a single phase; however, in the desorber mode, a two-phase flow can be observed at elevated heat fluxes (Nasr Isfahani et al., 2014). Ali and Schwerdt (2008, 2009, 2010) reported that the perfect membrane for aqueous solutions should be highly permeable to H₂O vapor, hydrophobic to the aqueous solution with high liquid entry pressure and should not allow capillary condensation of water vapor. Moreover, they reported desirable dimensions and porosity of the membrane. Venegas et al. (2016a, 2016b) later reported that the parameters that most impact the performance of these exchangers are the pore diameter, the porosity, the membrane thickness, the solution channels' depth, the solution concentration, the solution temperature, and the vapor pressure.

Jenks and Narayanan (2008), studied the effect of the channel geometry variations in a constrained microscale NH₃-H₂O single-film absorber. The authors found that there is an optimum film thickness for every required flow rate (capacity). This was later confirmed by Ali (2010) for the H₂O-LiBr working pair, who reported that the most important parameter is the aqueous solution channel thickness. Moreover, counter-current flow between the coolant fluid and the solution seems positive to the absorber compactness. Nasr Isfahani and Moghaddam (2013) observed that the reduction of the film thickness and the increase in the film velocity enhance the mass transfers up to 2.5 times compared to the existing H₂O-LiBr falling film absorbers ([Figure I.28a](#) and [b](#)). Moreover, while studying the efficiency of porous nanofibrous membranes in absorption and desorption operating modes, Nasr Isfahani et al. (2013) informed that absorption rates higher than those reported in previous studies were obtained and that this technology is more compact than the conventional shell-and-tube heat exchangers operating with H₂O-LiBr.

Other studies tried to look for transfer enhancement in membrane absorbers (Asfand et al., 2015). Cardenas and Narayanan (2011) compared smooth and stepped wall geometries with the NH₃-H₂O working pair, observing that the stepped one is more efficient at low HTF inlet temperatures (30–40°C) while the smooth-wall performs better at the highest HTF inlet temperature (58°C). Nasr Isfahani et al. (2015) used microstructuring to manipulate the thermohydraulic characteristics of the H₂O-LiBr solution flow ([Figure I.28c](#)) and change the laminar flow from diffusive to advective (Bigham et al., 2014b). Absorption rates comparable to those in membrane-based absorbers with much thinner solution films (a factor of five, from 500 μm to 100 μm) and at much lower pressure drops were achieved.

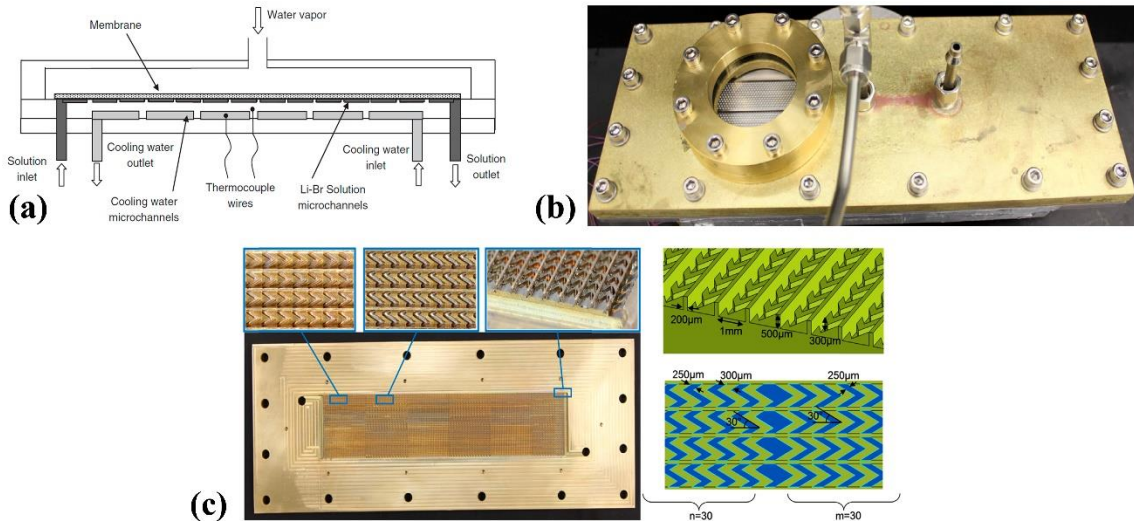


Figure I.28: (a) Diagram and (b) photograph of a membrane-based absorber (Nasr Isfahani and Moghaddam, 2013).
 (c) Microstructured membrane-based absorber (Nasr Isfahani et al., 2015).

Membrane-based absorbers were also tested in generation mode. Thorud et al. (2006) studied the performance of a H_2O -LiBr membrane-based desorber and observed that the desorption performance was increased for lower channel thickness, higher pressure differences, and lower inlet LiBr concentrations. Nasr Isfahani et al. (2014) built an experimental H_2O -LiBr chiller with a membrane-based generator of the same geometrical configuration as the absorber in Figure I.28a. The authors observed two desorption mechanisms: 1) direct diffusion of water molecules through the membrane and 2) bubble formation and their venting through the membrane. The first one was dominant at low wall temperatures and was highly influenced by the vapor pressure, solution concentration, and wall temperature. The second one appeared at high heat fluxes and was mostly influenced by the solution pressure and solution mass flow. At a critical solution mass flow, some bubbles never vent through the membrane.

1.3.3. Adiabatic exchangers

Adiabatic exchangers for absorption systems were first introduced at the end of the 1970s (Burdukov et al., 1989; Nakoryakov and Grigor'eva, 1977; Paniev, 1983) for their system size reduction potential because heat and mass transfers are greatly improved by doing them in separate components (Gutiérrez-Urueta et al., 2012; Venegas et al., 2003; Ventas et al., 2010). Here, the heat transfer is performed in a conventional single-phase heat exchanger (usually a PHE is used owing to its high compactness (Wang et al., 2007)), and the focus is given to the mass transfer (which limits the absorption rate as the liquid molecular diffusion controls the absorption process (Ibarra-bahena and Romero, 2014; Ventas et al., 2010; Zacarías et al., 2013)). The mass transfer is then performed in a separate chamber, where the solution can be distributed or dispersed in different forms (e.g., atomization, falling drops, or flat-fan sheets) to absorb or desorb refrigerant vapor. This opens a wide range of possibilities to enhance the exchange area and generate flow instabilities. The first studies based on adiabatic exchangers were focused on a solution distribution in the form of small droplets (typically less than 1 mm in diameter) produced with a nozzle, commonly called “spray absorption” (Morioka et al., 1992; Ryan, 1994; Summerer et al., 1996). Different options for solution distribution in the adiabatic chamber were then proposed and will be discussed hereafter. Table I.13 summarizes the experimental studies on adiabatic exchangers.

1.3.3.1. Falling film

Falling film is one way of distributing the solution for the mass transfer process in the adiabatic chamber. This method avoids the drawbacks of solution atomization (energy consumption and limited flow rates) (Arzoz et al., 2005) and is the most effective gravity driven distribution method. Arzoz et al. (2005) compared three gravity-driven H_2O -LiBr solution distribution methods in an adiabatic absorber (droplets, unstable jets, and inclined falling film on a sloping ramp, Figure I.29). The jets and falling film modes resulted in the most convenient methods, with falling films allowing the highest flow rates and the highest solution/refrigerant vapor contact area per unit length, and thus the solution saturated more quickly. However, gravity-driven distribution methods would require a large chamber volume.

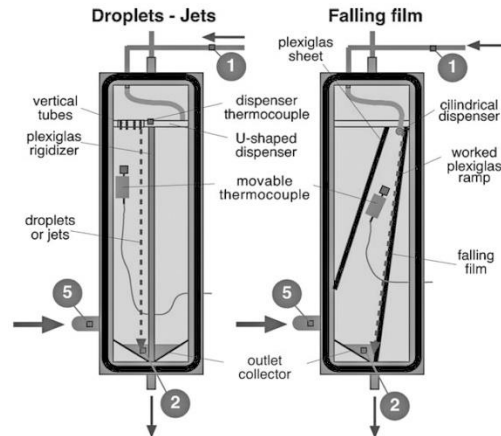


Figure I.29: Test section of adiabatic absorbers with solution distribution by gravity in the form of droplets and jets (left), and inclined falling film (right) (Arzoz et al., 2005).

For automobile applications (Horuz, 1998b; Salim, 2001), the PSA Group worked on the development of adiabatic exchangers (Aiane et al., 2017a). In their patented evaporator/absorber configuration (Boudard and Bruzzo, 2004), the saturated H_2O -LiBr solution flows down between finely meshed wire screens by capillary forces, the porosity of the meshes allowing the mass transfer (Figure I.30) (Obame Mve, 2014; Obame Mve et al., 2015, 2014). An adiabatic water evaporator was modeled simply and experimentally characterized, showing that its performance is significantly reduced at flow rates higher than 1.3 times the nominal SFR value (Thonon et al., 2018).

Chapter I. State of the art

Table I.13: Adiabatic exchangers in absorption chillers: experimental results (~: approximated data).

Func	WF	Falling film or two-phase	Type	$\dot{m}_{sol,i}$ (kg h ⁻¹) (Re)	$x_{sol,i}$	$T_{sol,i}$ (°C)	P_{sorp} (kPa)	ΔT_{sub}^i (°C)	\dot{m}_{sorp} (g s ⁻¹)	\dot{m}''_{sorp} (g m ⁻² s ⁻¹)	K (mm s ⁻¹)	F_{ad}	Ra	Area (m ²)	Comm	REF		
ABS	NH ₃ -LiNO ₃	Two-phase	Flat fan sheet	144-288	46	24.5-29.7	310-400	11.5-24	0.75-2.45	-	0.34-1.02	0.81-0.89	0.014-0.03	~0.263	-	(Zacarias et al., 2011)		
			Fog jet	195.12-208.08	41.9-58.6	26.67-30.66	429-945	5-55	0.47-4.1	-	-	0.83-1.11	0.008-0.07	-	-	(Ventas et al., 2012)		
			Fog jet	144-288 (880-1970)	46.08	25.9-30.2	355-411	15-21	0.8-2.1	~4-10	0.17-0.46	0.82-0.93	0.02-0.028	0.198	-	(Zacarias et al., 2013)		
			Full cone nozzle	144-288 (900-2280)	46	23.5-30.6	291-408	8.5-17.2	~0.5-2.1	-	0.08-0.33	0.64-0.87	0.012-0.026	-	-	(Zacarias et al., 2015)		
	H ₂ O-LiBr	Falling film	Plate	28.8-36	60	30	0.72	17-33.5	~0.09-0.2	~2.8-6.7	0.035-0.047	-	0.1-0.88	0.011-0.021	~0.032	-	(Arzoz et al., 2005)	
			Plate	11.27-24.88	0.488-0.491	11.8-12.3	2.48-2.79	~29.65-31.63	~0.06-0.13	~1.27-2.53	-	-	~0.019-0.021	~0.05	Smooth plate	(Kim and Ferreira, 2008b)		
			Plate	12-24.34	0.499-0.502	11-12.6	2.84-3	~33.69-36.63	~0.089-0.17	~1.7-3.25	-	-	~0.025-0.027	~0.05	Wire screen over plate	(Kim and Ferreira, 2008b)		
			Plate	20-150 (15-350)	57-60	20-40	1	~10-27.6	0.02-0.15	1-6.8	-	-	~0.0005-0.027	~0.0132	Grooved plate	(Michel et al., 2017)		
		Two-phase	Droplets	9.72-10.8	60	30	1.32-2.8	4-57	~0.005-0.008	-	0.012-0.058	-	0.03-0.67	0.002-0.028	-	-	(Arzoz et al., 2005)	
			Falling droplets	170-360	57.9-62.5	21.5-32	~0.9	~16.3-27.3	-	-	-	-	0.36-0.78	-	-	-	(Gutiérrez-Urueta et al., 2011)	
			Unstable jets	16.2-18	60	30	1.32-2.8	7.5-46	~0.016-0.11	-	0.023-0.078	0.09-0.68	0.004-0.022	-	-	(Arzoz et al., 2005)		
			Flat fan sheet	84-194	58-60	21-50	0.6-2.2	9-21	~0.08-0.86	~1.6-16.9	0.3-2.05	~0.42-0.92	~0.003-0.016	~0.051	-	(Palacios et al., 2009b)		
			Conical sheet	28-47	58-60	19-44	1-2.2	16-33	~0.06-0.18	~7.5-16.5	0.55-2	~0.71-0.92	~0.01-0.022	~0.009	-	(Palacios et al., 2009a)		
			Fan sheets	170-360	57.5-61.5	23.4-32.2	~0.9	~12.8-28.4	-	-	-	-	0.43-0.84	-	-	(Gutiérrez-Urueta et al., 2011)		
			Membrane	Plate	3-13.5	50.8-54.5	24-29	~1.94-3.16	~18-31.36	~0.004-0.006	0.92-1.36	-	-	~0.0003-0.0004	0.005	-	(Ali and Schwerdt, 2009)	
					0.54-1	58.6	27.3	-	~31-32	-	1-3.6	-	-	0.017-0.072	-	-	(García-Hernando et al., 2019a)	
				0.22-0.5	58.6	26-28	-	-	-	1.45-02.55	-	-	0.078-0.154	-	-	(García-Hernando et al., 2019b)		
				0.7-1	60	26-28	-	-	-	1.55-2.7	-	-	0.04-0.064	-	-	(García-Hernando et al., 2019b)		
		H ₂ O- lithium based solution	Two-phase	Whirl jet nozzle	64.8-90 (10-1500)	84	65-77	1.23	~15.2-27.2	~0.045-0.163	-	-	-	-	0.003-0.007	-	Absorbent: LZB™	(Warnakulasuriya and Worek, 2006)
				Whirl jet nozzle	97.2-122.4 (10-1500)	84	65-77	1.23	~15.2-27.2	~0.07-0.22	-	-	-	-	0.003-0.006	-	Absorbent: LZB™	(Warnakulasuriya and Worek, 2006)
Whirl jet nozzle	68.4-86.4 (10-1500)			84	65-77	1.23	~15.2-27.2	~0.04-0.1	-	-	-	-	0.002-0.004	-	Absorbent: LZB™	(Warnakulasuriya and Worek, 2006)		
Whirl jet nozzle	111.6-154.8 (10-1500)			84	71-77	1.23	~15.2-21.2	~0.08-0.19	-	-	-	-	0.003-0.004	-	Absorbent: LZB™	(Warnakulasuriya and Worek, 2006)		
Full jet nozzle	46.8-68.4 (10-1500)			84	65-77	1.23	~15.2-27.2	~0.03-0.1	-	-	-	-	0.002-0.005	-	Absorbent: LZB™	(Warnakulasuriya and Worek, 2006)		
Full jet nozzle	90-104.4 (10-1500)			84	69-77	1.23	~23.2-27.2	~0.05-0.13	-	-	-	-	0.002-0.005	-	Absorbent: LZB™	(Warnakulasuriya and Worek, 2006)		
DES	H ₂ O-LiBr			Membrane	Plate	55.44-88.2	45.7-58.7	74.4-95.9	101.325	-	-	0.083-2.69	-	-	-	-	-	(Ibarra-Bahena et al., 2017)
					Hollow fiber	~60-180	50-50.8	65-88	5-15	-	~0.025-0.17	~0.083-0.56	-	-	~0.0005-0.01	0.3	-	(Wang et al., 2009)
						-	51-58	65-83	2.6-5.5	-	-	0.056-1.3	-	-	-	-	-	(Hong et al., 2018)

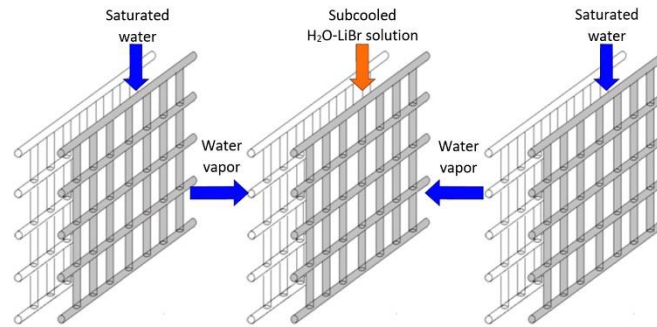


Figure I.30: Functioning diagram of the adiabatic evaporator/absorber configuration, adapted from (Obame Mve, 2014).

Michel et al. (2017) compared a grooved falling film H_2O -LiBr absorber in nonadiabatic and adiabatic conditions and at different SFRs, temperatures, and concentration conditions (Figure I.22b). The authors observed that the increase in the SFR was beneficial in the adiabatic mode because it induces a thickening of the film that increases the thermal inertia of the solution, increasing the absorption capacity. However, in the nonadiabatic case, the SFR film thickening increases the thermal resistance between the interface and the plate, reducing the cooling capacity.

1.3.3.2. Two-phase flow

Two-phase flow is the most common solution distribution method for adiabatic exchangers. This distribution can be done either by gravity (falling drops or unstable jets), in which case droplets measuring around 3 mm are generated (Figure I.31a), or be nozzle-driven, for which in general two types of flows are studied: sheet flows (e.g., conical or flat fan), in which a high-velocity flat sheet is generated and it eventually gets disintegrated into droplets (Figure I.31b), and small-diameter droplets (e.g., hollow cone, full cone, swirl cone, or fog jet) for which droplets typically less than 1 mm are dispersed in different patterns (Figure I.31c).

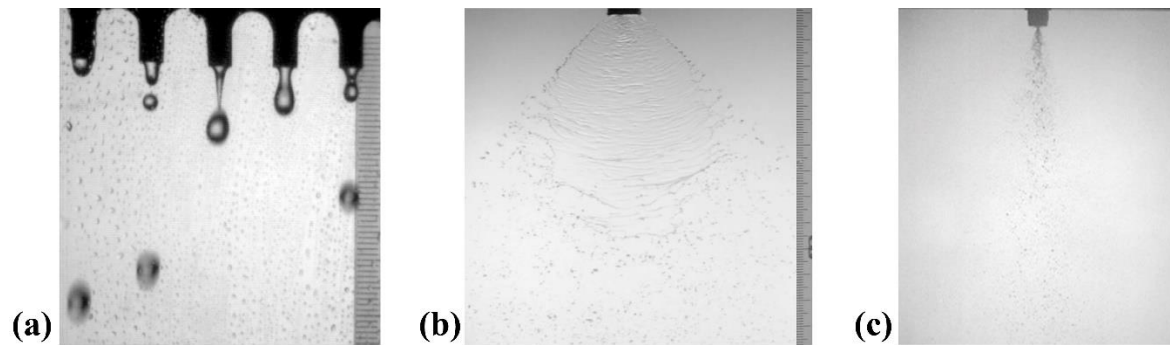


Figure I.31: Typical two-phase solution distribution methods in an adiabatic exchanger. (a) Falling drops, (b) flat fan sheets (Gutiérrez-Urueta, 2009), and (c) fog jet atomization (Ventás et al., 2012).

Gutiérrez-Urueta et al. (2011) compared the falling droplets and the flat fan nozzle distribution methods for water vapor absorption in H_2O -LiBr (Elperin et al., 2007). The authors determined that the droplet configuration presented lower performance and required twice the size of a fan sheet absorber. For small-diameter droplets, Venegas et al. (2003, 2004, 2005) proposed a NH_3 - LiNO_3 spray absorption system. According to their studies, the HTC and mass transfer coefficient (MTF) could be enhanced up to 50 (Venegas et al., 2003) and 37 (Venegas et al., 2005) times, respectively, which could greatly increase the compactness of absorbers. Moreover, the atomizers used in adiabatic exchangers can provide surface/volume ratios about ten times higher compared to conventional falling film exchangers (Ryan et al., 1995; Warnakulasuriya and Worek, 2006). However, they consume additional work and the flow rate in these kinds of injectors is limited (Arzoz et al., 2005). By means of a numerical model using the NH_3 - LiNO_3 working fluid, Ventás et al. (2010) concluded that the absorber heat exchange area could be down to six times smaller in the adiabatic arrangement compared to the diabatic one. Ventás et al. (2012) studied

the effects of the NH_3 concentration (from 0.419 to 0.586) and pressure (from 429 to 945 kPa) in a fog-jet spray NH_3 - LiNO_3 adiabatic absorber, and observed that the absorption rate increases with an increase in the pressure and inlet subcooling, while it decreases with an increase in the NH_3 concentration. Zacarías et al. (2013) later confirmed this with the same configuration but at a lower pressure range (355–411 kPa and a constant NH_3 concentration of 46.08%) for negative refrigeration temperatures. Regarding viscous solutions, Warnakulasuriya and Worek (2006, 2008b) presented an experimental study of an adiabatic spray absorber using a lithium-based solution with properties similar to H_2O - LiBr and tested two types of nozzles: a whirl jet and a full jet nozzle. During experiments, the drop size was 20% larger than expected due to the surface tension on drop formation. However, the absorption enhancement by H_2O atomization was clearly observed. Moreover, the swirl jet nozzle performed better than the full jet nozzle. Finally, Zacarías et al. (2015) proposed the use of a full cone nozzle for NH_3 - LiNO_3 adiabatic absorbers for its great compactness potential due to the high ratio of the mass exchange area to the occupied volume compared to other distribution methods. However, its performance was slightly lower than previously studied nozzles (flat fan and fog jet nozzles), probably due to the lower subcooling applied.

The last option studied are flat sheet nozzles (Acosta-Iborra et al., 2009), which consume less energy compared to liquid atomization (Palacios et al., 2009b). In this context, Palacios et al. (2009a) first studied the pressure drop and mass transfer in H_2O - LiBr conical sheets, finding that low SFRs are more convenient (around 30 kg h^{-1}) and that the absorber length should not exceed 100 mm for a good tradeoff between the absorption rate and the compactness. Moreover, the absorption takes place primarily in the liquid sheet prior to disintegration. This was later confirmed in a second study in which a flat-fan sheet adiabatic absorber was tested. The authors concluded that flat fan sheet absorption exhibits higher absorption performance than conventional falling film and spray absorbers, probably because of interface renewal, which according to the authors plays only a minor role in falling film and spray absorbers (Palacios et al., 2009b). Zacarías et al. (2011) used a flat fan nozzle to disperse a NH_3 - LiNO_3 solution in a chamber with NH_3 vapor (similar to the one in Figure I.31b). A linear correlation between the inlet subcooling and the absorption ratio was found. Moreover, the HTC's of the PHE used for the subcooling were twice as high as those of vertical tubular bubble absorbers, which indicates the integration potential of PHEs with adiabatic absorbers. According to González-Gil et al. (2011, 2012), flat-fan absorbers are the nozzle-driven H_2O - LiBr absorbers with the highest performance/compactness ratio and lowest mechanical energy demand. A patent was obtained based on this technology comprising a new absorber/evaporator assembly to operate in air-cooling conditions (Izquierdo et al., 2011). The proposed design proved to operate far from crystallization levels even at high ambient temperatures (around 40°C) (González-Gil, 2011; González-Gil et al., 2012, 2011).

1.3.3.3. Membrane-based exchangers

Membrane-based exchangers were also studied in the adiabatic configuration given that they could lead to a higher cooling power per unit volume of absorber and a higher manufacturing simplicity if compared to nonadiabatic membrane absorbers (Venegas et al., 2017). The first analytical and experimental adiabatic study of a membrane-based absorber was performed by Ali and Schwerdt (2008, 2009) using the H_2O - LiBr working pair, who aimed to identify the desired characteristics and properties of commercially available microporous hydrophobic membranes discussed in Section 1.3.2.3. Later, Venegas et al. (2017) compared a membrane-based H_2O - LiBr absorber in the adiabatic and nonadiabatic mode from a theoretical point of view, finding that both configurations offer a high capacity/volume ratio (higher than 1 MW m^{-3}). However, the adiabatic absorber was better for high inlet solution flow rates and solution inlet temperatures lower than 32°C . Moreover, the adiabatic mode is more sensitive to the solution inlet temperature and flow rate. Finally, seeking to increase the compactness of the absorber, García-Hernando et al. (2019a) experimentally tested the first adiabatic microchannel ($150 \mu\text{m}$ in depth) membrane-based H_2O - LiBr absorber. Absorption ratios higher than the previously studied adiabatic absorbers were obtained. However, the absorption rates were lower than in previous studies. In order to experimentally study the effect of the membrane characteristics and operating conditions on the

absorption rate and absorption ratio, García-Hernando et al., (2019b) characterized three different membranes using the same test bench as in (García-Hernando et al., 2019a), obtaining higher absorption ratios for the membrane with the highest pore diameter (owing to the decreased membrane mass transfer resistance). Finally, regarding the desorption operation mode with the H₂O-LiBr working fluid, Ibarra-Bahena et al. (2017) used the Air Gap Membrane Distillation as a desorber/condenser assembly to operate at atmospheric pressure. Results indicated that high solution temperatures and low concentrations lead to higher absorption rates. However, the dependence between the absorption rate and the solution temperature is not linear for similar solution concentration conditions.

A special case in membrane-based exchangers are the microporous hollow fiber membrane-based (HFM) exchangers (Chen et al., 2006; Hong et al., 2016; Schaal et al., 2015), which are composed of a bundle of HFMs enclosed in a housing (Figure I.32). The H₂O-LiBr solution flows inside the bundles and water vapor is desorbed through the membrane. Two experimental studies proved the feasibility of the technology in the generator mode, with good experimental agreement (Hong et al., 2018; Wang et al., 2009).

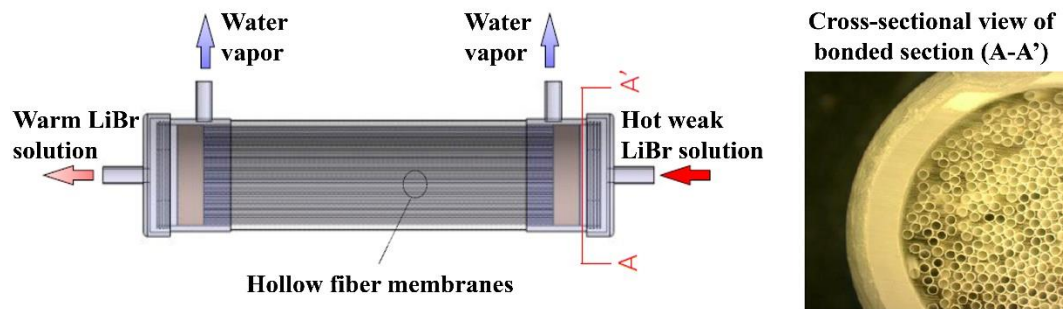


Figure I.32: Diagram of the hydrophobic hollow fiber membrane-based generator (adapted from (Hong et al., 2018)).

1.3.4. General discussion

1.3.4.1. Technologies used in experimental prototypes

1.3.4.1.1. NH₃-based prototypes

A summary of the exchanger technologies in small-capacity NH₃-based prototypes of absorption cooling systems developed in laboratories is presented in Table I.14. To the best of our knowledge, no prototype with adiabatic components has been presented for ammonia-based systems.

Table I.14: In-Lab-developed prototypes of small-capacity NH₃-based absorption cooling systems and the exchanger technologies used in their main components.

ABS	$\dot{Q}_{evaporator}$ (kW)	Heat source	Heat sink	Absorber	Generator	Condenser	Evaporator	Comments	REF
H₂O	10.5	Geothermal	Water	Shell-and-tube	Shell-and-tube	Shell-and-tube	Shell-and-tube		(Ayala Delgado, 1992)
	-	Exhaust gases	Air	Finned tubes	Tubes (pool boiling)	Finned tubes	Finned tubes		(Koehler et al., 1997)
	2	Solar	Air	Finned tubes	HT pool boiling	Finned tubes	Finned tubes	Air-cooled by natural convection.	(De Francisco et al., 2002)
	4	Solar	Air	Helical tubes (falling film)	Helical tubes (falling film)	Coaxial tubes	Coaxial tubes	Spray integrated in desorber for vapor purification	(Mendes et al., 2007)
	10	Solar	Air	PHE	Helical tubes (falling film)	PHE	PHE	Focus on the generator	(Brendel et al., 2010)
	0.3	Electric heater	Water	Microchannel	Microchannel	Microchannel	Microchannel	Microscale monolithic system	(Zetzsche et al., 2010)
	5	Electric heater	Water	PHE	PHE	PHE	PHE		(Determan and Garimella, 2012)
	3.5	Combustion module	Water	Microchannel	Microchannel	Microchannel	Microchannel		(Boudéhenn et al., 2012)
	10	Solar	Air	PHE	Helical tubes (falling film)	PHE	PHE	Focus on the generator	(Garimella et al., 2016)
	2.71	Waste heat	Air	Finned tubes	Shell-and-tube	Finned tubes	Microchannel		(Said et al., 2016)
LiNO₃	7	Combustion module	Air	Shell-and-tube	Microchannel	Microchannel	Microchannel		(Goyal et al., 2016)
	-	Electric heater	Water	Shell-and-tube	Helical tubes (falling film)	Double pipe	Double pipe (in serpentine)		(Goyal et al., 2017)
	10.5	Geothermal	Water	Shell-and-tube	Shell-and-tube	Shell-and-tube	Shell-and-tube	Same machine as in (Ayala Delgado, 1992)	(Goyal et al., 2018)
	7.82	Electric heater	Air	VT falling film	HT falling film	Finned tubes	PHE		(Ayala et al., 1994)
	10	Electric heater	Air	PHE	PHE	PHE	PHE		(Heard et al., 1996)
	10	Electric heater	Water	PHE	PHE	PHE	PHE		(Llamas-Guillén et al., 2014)
	3	Electric heater	Water	VT falling film	VT falling film	PHE	PHE		(Zamora et al., 2014)
	4.5	Electric heater	Water	HT falling film	HT falling film	PHE	PHE		(Hernández-Magallanes et al., 2014)
	-	Electric heater	Air	Atomizer nozzle & VT	Electric heater (pool boiling)	Finned tubes	Coiled tubes		(Domínguez-Inzunza et al., 2016)
	-	Electric heater	Water	PHE	PHE	PHE	PHE		(Cai et al., 2016)
									(Jiménez-García and Rivera, 2018)

Figures I-33 to I-35 are based on the data from Table I.14. Figure I.33 shows the exchanger technologies used in the absorber and the desorber of the prototypes operating with the NH₃-H₂O pair. The versatility of this working pair can be highlighted by the variability of the technologies that have been tested. Its high operating pressure, low viscosity, and low density allow it to operate in a single-phase or a two-phase flow (either with tubes, PHE, microchannel, or any other geometry) in both the absorber and desorber.

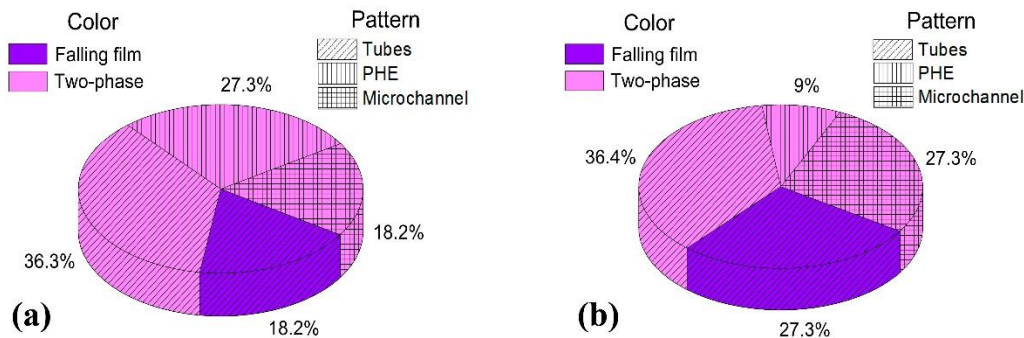


Figure I.33: Exchanger technologies used in the prototypes of single-stage absorption chillers based on the NH₃-H₂O working pair for (a) the absorber and (b) the generator.

The NH₃-LiNO₃ solution has properties that are between the two conventional working pairs (NH₃-H₂O and H₂O-LiBr) with the exception of its operating pressures, which are determined by the NH₃ refrigerant. This working pair has, as the NH₃-H₂O working pair, a wide range of operating conditions that allow it

to operate either in the falling film or two-phase flow. However, it can be observed from Figure I.34 that the microchannel technology has not been tested in a prototype with this working pair, probably owing to its higher viscosity compared to the $\text{NH}_3\text{-H}_2\text{O}$ pair, which would yield high pressure drops.

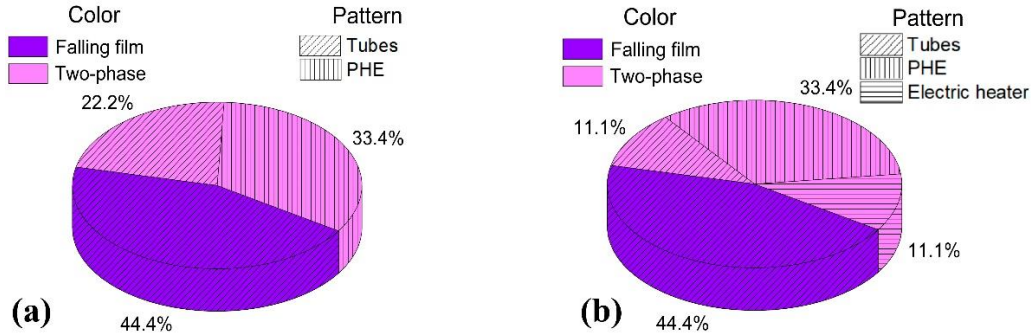


Figure I.34: Exchanger technologies used in the prototypes of single-stage absorption chillers based on the $\text{NH}_3\text{-LiNO}_3$ working pair for the (a) absorber and (b) generator.

Figure I.35 shows the technologies used in the condenser and the evaporator of the NH_3 -based prototypes. One can see that the NH_3 refrigerant has a wide range of adaptability to different technologies and geometries. Moreover, Figure I.35a shows a tendency to implement two-phase evaporators probably due to the ease of their implementation. The conventional condensers are the falling film type since it is the natural form of vapor condensation. However, in the case of microchannel condensers, a special phenomenon is involved in a very small hydraulic diameter and thus the fluid flow tends to be a two-phase flow.

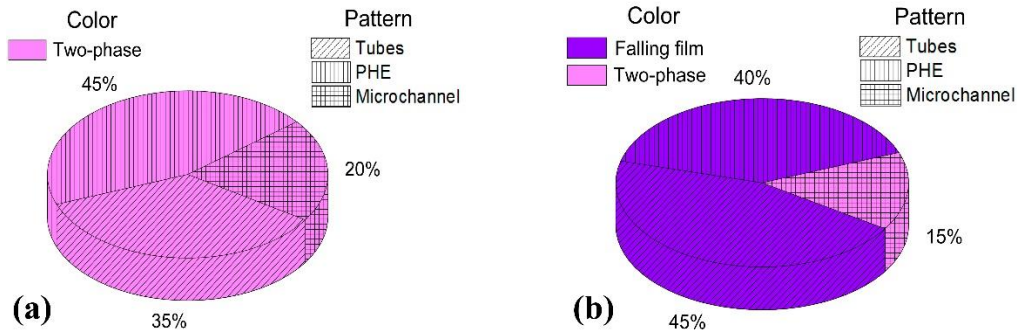


Figure I.35: Exchanger technologies used in the prototypes of single-stage absorption chillers based on the NH_3 refrigerant for the (a) evaporator and (b) condenser components.

1.3.4.1.2. $\text{H}_2\text{O-LiBr}$ prototypes

A summary of the main technologies of the small-capacity H_2O -based prototypes of absorption cooling systems developed in laboratories is presented in Table I.15.

Table I.15 In-Lab-developed prototypes of small-capacity H₂O-LiBr absorption cooling systems and the exchanger technologies used in their main components.

$Q_{ev,nom}$ (kW)	Heat source	Heat sink	Absorber	Generator	Condenser	Evaporator	Comments	REF
1.76	Solar	Water	Tubular	Tubular	Tubular	Tubular		(Hammad and Audi, 1992)
7	Hot water	Air	Finned VT	HT (pool boiling)	Finned VT	Flash evaporator		(Ohuchi et al., 1994)
5.28	Solar	Water	Shell-and-tube	Shell-and-tube	Shell-and-tube	Finned tubes		(Hammad and Zurigat, 1998)
10	Electric heater	Water	Tube bundle	Tube bundle	Tube bundle	Tube bundle		(Kühn et al., 2005)
2	Hot water	Air	Finned tubes	HT falling film	Finned tubes	HT falling film		(Kühn et al., 2008)
0.04	Electric heater	Water	Glass container	Electric heater (pool boiling)	Microchannel	Microchannel		(Castro et al., 2007)
-	Solar	Water	Horizontal tubes	Horizontal tubes	Horizontal tubes	Horizontal tubes	Micro-nozzles in the evaporator and the absorber	(Hu and Chao, 2008)
-	-	-	-	-	-	-	-	(Achuthan et al., 2011)
3.5	Electric heater	Water	Adiabatic flat-fan sheets absorber	PHE	PHE	Finned tubes	PHE pre-cooler for absorber	(Gutiérrez-Urueta et al., 2011)
4.5	Solar	Air	Adiabatic flat-fan sheets absorber	PHE	Finned tubes	Tube bundle	Finned tube pre-cooler for absorber	(González-Gil et al., 2011)
8	Solar	Water	Horizontal tubes	Horizontal tubes	Horizontal tubes	Horizontal tubes		(Yin et al., 2012)
-	Electric heater	Water	Horizontal tubes	Horizontal tubes	Horizontal tubes	Horizontal tubes		(Kühn, 2013)
-	Electric heater	Water	Horizontal tubes	Horizontal tubes	Horizontal tubes	Horizontal tubes	C and G improved from last one	(Kühn, 2013)
50	Electric heater	Water	U-shaped bent tubes	Cross-shaped parallel tubes	Cross-shaped parallel tubes	U-shaped bent tubes		(Kühn, 2013)
6	Solar	Air	Adiabatic absorber	Tubular	Finned tubes	Tubular	Finned tube pre-cooler for absorber	(Chen et al., 2017)

H₂O-LiBr is the most viscous and dense working fluid of those presented in this review, and this requires that special attention be paid to certain parameters. For example, high viscosity leads to elevated pressure drops in reduced hydraulic diameters. Therefore, the microchannel technology is not recommended for the H₂O-LiBr absorber or generator. Moreover, the elevated densities and vacuum operation lead to the hydrostatic pressure having a high impact on the saturation temperature gradient in thick H₂O-LiBr solution films. Hence, neither bubble absorbers nor pool boiling generators are recommended for H₂O-LiBr systems. This limited adaptability of the H₂O-LiBr working pair is confirmed in Figure I.36, which shows the technologies that have been used in the absorber and desorber of the H₂O-LiBr prototypes. Most of the prototypes use falling film absorbers, while a small percentage (23.1%) use adiabatic absorbers. Regarding the desorber, the falling film technology is also predominant. However, a small percentage of the prototypes use a two-phase flow with tubes and PHE, risking high pressure drops and low performance.

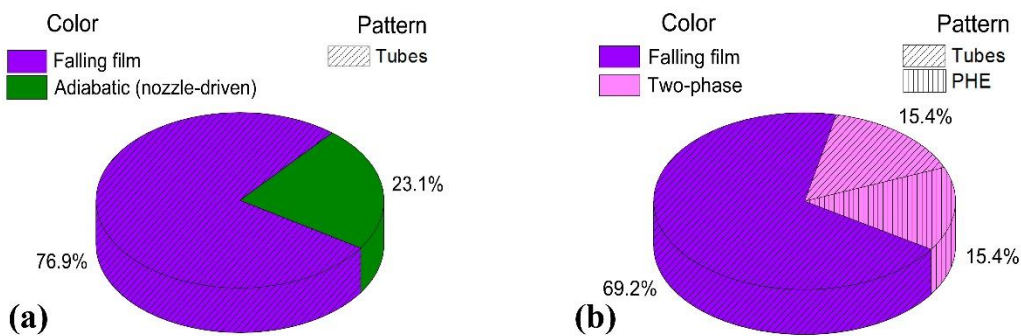


Figure I.36: Exchanger technologies used in the prototypes of single-stage absorption chillers based on the H₂O-LiBr working pair for the (a) absorber and (b) generator.

Regarding the heat exchanger technologies used in the evaporators and condensers of the prototypes, the falling film configuration is the dominant technology. Moreover, the tubular heat exchangers are predominant in both cases (Figure I.37).

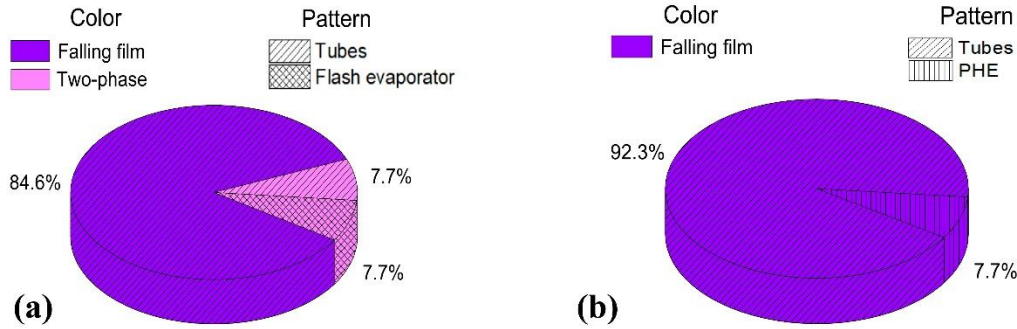


Figure I.37: Exchanger technologies used in the prototypes of single-stage absorption chillers based on the H₂O refrigerant for the (a) evaporator and (b) condenser components.

1.3.4.2. Comparison of the technologies studied

Data from Table I.11, Table I.12, and Table I.13 were used for a comparison of the different technologies studied. In the following figures, the NH₃-LiNO₃ working fluid and the generator operation mode were omitted because insufficient data were available. In the case of the generator mode, pool boiling has been recommended for high \dot{Q}''_{des} (≥ 20 kW m⁻²) and low \dot{m}_{sol} . For the rest of the operating conditions, the falling film technology has proven to possess an HTC up to 4.4 times higher than the immersed tube generators (Fernández-seara et al., 2016a; Shi et al., 2010). However, this difference decreases as the saturation temperature decreases (Zeng and Chyu, 1995).

The absorber is the component that has been more extensively studied. This is probably because it has been pointed out as the main “bottleneck” of the system (Beutler et al., 1996), and therefore its choice highly impacts the size of the system, its cost, its cycle performance, and the energy supply (Ibarra-bahena and Romero, 2014; Mittermaier and Ziegler, 2015; Nagavarapu and Garimella, 2011b). The following figures illustrate the conditions of the experimental results (minimum and maximum values) found in the literature, which might vary according to a large number of uncontrollable and controllable parameters whose effects are not represented. Therefore, the aim is to give a graphical overview of the heat and mass transfer performance of the different technologies that were developed for small-capacity absorption chillers.

As mentioned in Section 1.3.1, the main comparative parameters for the mass transfer performance in nonadiabatic absorbers are the absorption flux (\dot{m}''_{abs}), the absorption ratio (Ra), and the mass transfer coefficient (K). However, K was omitted to avoid confusion because its definition can vary depending on the author. Moreover, the absorption flux, which includes the exchange area, is simply a reference for the systems in which this definition of the exchange area is ambiguous or imprecise, such as in the case of the bubble and adiabatic absorbers (Zacarias et al., 2011).

Figure I.38 shows the heat and mass transfer performance criteria of the NH₃-H₂O absorbers. In Figure I.38a, the falling film technology seems to have a higher Ra and \dot{m}''_{abs} compared to the two-phase (bubble) absorbers. This suggests that even if bubble absorbers have proven to have better mass transfers than falling film exchangers at specific conditions of a low SFR, high heat flux, and small capacities (Castro et al., 2009; Ibarra-bahena and Romero, 2014; Kang et al., 2000; Lee et al., 2002a), if a good solution distributor and exchange surface geometry are implemented, the falling film technology has a similar (or even better) mass transfer performance for the rest of the operating conditions (Castro et al., 2009). Regarding the heat transfer performance, there is no major difference between these two technologies. However, the falling film technology in theory has a greater heat exchange area compared to the bubble absorbers owing to the dry areas generated by the bubbles, which should lead to a greater compactness. Finally, the potential of the membrane technology can be observed with similar or even higher performance than the other technologies. This might be due to the increase in the film velocity and a

reduction of the film thickness that membrane absorbers can provide. However, the integration of this technology into an entire machine is still missing (see Section 1.3.4.1).

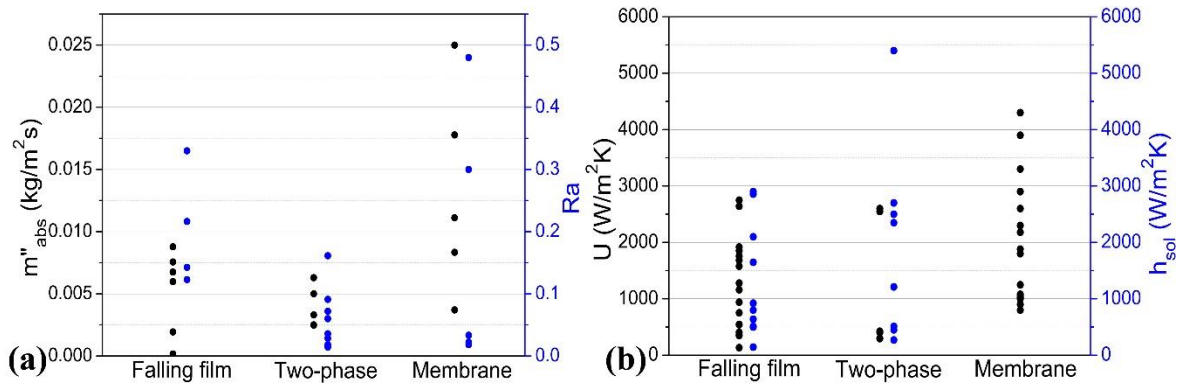


Figure I.38: (a) Mass transfer and (b) heat transfer performance criteria for the absorbers operating with the $\text{NH}_3\text{-H}_2\text{O}$ working fluid.

Figure I.39 shows the heat and mass transfer performance criteria of the $\text{H}_2\text{O-LiBr}$ absorbers. Figure I.39b suggests that the HTs are slightly more efficient than the VTs, and that the plate falling film absorbers may be the most efficient; however, there is not enough data to draw firm conclusions on this point. Figure I.39a shows that the membrane exchangers possess good potential. Moreover, adiabatic absorbers present a good m''_{abs} because they absorb very well with high-velocity films or drops. However, they require a high solution mass flow, which increases their circulation ratio, and therefore their Ra is low.

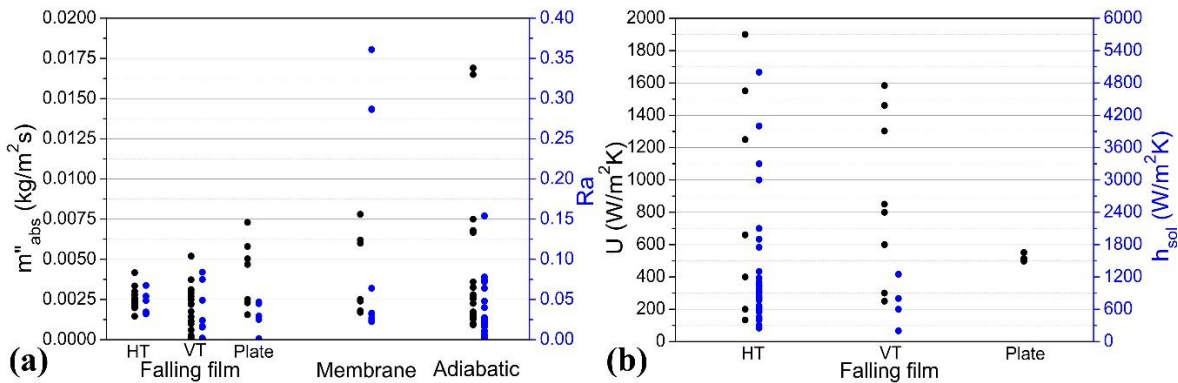


Figure I.39: (a) Mass transfer and (b) heat transfer evaluation parameters for absorbers operating with the $\text{H}_2\text{O-LiBr}$ working fluid.

The graphical comparisons presented in Figure I.40 for adiabatic absorbers are based on the Ra . It suggests that the two-phase flow in the adiabatic configuration was slightly better than for the falling film experiments. However, once divided by distribution method (gravity- or nozzle-driven), the potential for gravity-driven adiabatic absorbers is observed. The increase in the Ra might be due to the fact that the circulation of the solution, in this case, is slower, and the equilibrium factor attained can be as high as for the nozzle-driven absorbers (Arzoz et al., 2005). Finally, it can also be observed that the membrane technology has great potential for adiabatic absorbers, but their integration in an entire system remains to be studied, as for the NH_3 -based systems.

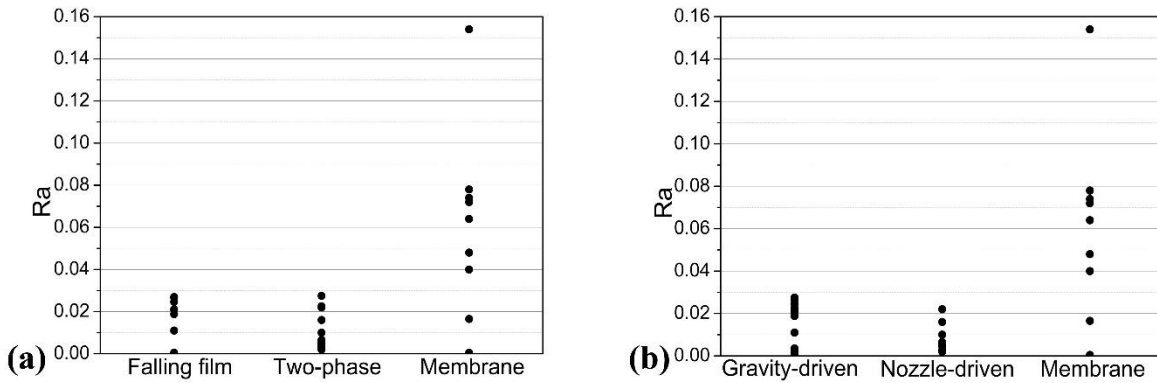


Figure I.40: Absorption ratio (Ra) for the different H₂O-based adiabatic absorbers by (a) continuity of the phases and (b) distribution methods.

1.4. Conclusion

Section 1.2 presented the state of the art of the different investigated working fluids for absorption chillers. In order to select a working fluid, different aspects have to be taken into account depending on the desired application and the most important objectives to be accomplished. Table I.16 summarizes the advantages and disadvantages of the different refrigerants and working pairs. As stated earlier, the choice of the system must not only be oriented toward the thermodynamic cycle performance but also toward other factors that might impact the real application of the system, either technological (available properties, operating pressures and temperatures, safety precautions, corrosion avoidance, exergetic efficiencies, heat sink medium, driving source type, and system lifetime), economic (initial cost of the system and external components, cost of the working pair, operating costs, economic gains depending on the electricity price changes and inflation), or even social (global warming potential and renewable energy use).

In the case of the ammonia-based working pairs, the new absorbents LiNO₃ and NaSCN seem to be good candidates to substitute H₂O. However, experimental studies to physically explain and avoid the lower-than-expected experimental performance on these systems and economic studies have to be performed before a commercial machine launch.

In the case of the water-based systems, H₂O-LiBr continues to be the most reliable and convenient working pair. The rest of the studied candidates up to date don't seem to present enough advantages to overcome their associated drawbacks. The H₂O-LiCl pair has a higher theoretical performance; however, crystallization risks are increased for this working pair compared with the H₂O-LiBr working pair, for which this problem is already important. Therefore, a commercial system based on the H₂O-LiCl working pair for continuous operation seems difficult. There was an explosion of interest in ILs in recent years because of their excellent physical and thermal properties; however, more in-depth studies are necessary to assure the long-term effects of their use. Novel environmentally friendly ILs and deep eutectic solvents from natural sources such as organic acids or aminoacids, with similar properties to ILs and which are claimed to be non-toxic and biodegradable, could be the future direction in this research area (Cvjetko Bubalo et al., 2014).

On the other hand, HFCs do not seem to be an option for the future since most of them have an elevated global warming potential and in any case, they will be banned under the Kigali Amendment to the Montreal Protocol (IEA, 2018a). Finally, alcohols seem to be better adapted for heating and heat pump applications. None of these mentioned refrigerants have shown special advantages in terms of performance compared with the conventional H₂O-LiBr and NH₃-H₂O working pairs. CO₂ has also been proposed in recent years as the refrigerant for absorption cooling systems and may be an option in the

future; however, new absorbents for this refrigerant have to be studied for better performance and special attention must be paid to its high operating pressures, which raise new challenges in terms of design.

More information is needed about the physical interactions and surface properties of the new working pairs (e.g., surface wetting or droplet formation) that lead to more efficient systems. Studies need to be conducted in the search for new additives to induce Marangoni convection, better wettability properties, and less corrosion (Seiler et al., 2013).

Table I.16: Comparison of the main binary working fluids studied for single-stage absorption cooling.

REFRIGERANT	ADVANTAGES AND DRAWBACKS OF REFRIGERANT	ABSORBENT	ADVANTAGES OF THE WORKING PAIR	DRAWBACKS OF THE WORKING PAIR
NH₃	<ul style="list-style-type: none"> + High enthalpy of evaporation. + Refrigeration under 0°C. + Moderate pressure ranges. - Toxicity of NH₃. - Explosion hazard potential for confined spaces. 	H ₂ O	<ul style="list-style-type: none"> + Well documented properties and materials compatibility. + No crystallization risks. 	<ul style="list-style-type: none"> - Rectifier needed. - Lower COP than H₂O-LiBr system. - Alkaline and corrosive solution.
		LiNO ₃	<ul style="list-style-type: none"> + Low driving temperature. + Higher COP than NH₃-H₂O. + No rectifier needed. + Low crystallization risk. + High solubility in NH₃. + No corrosion of steel. 	<ul style="list-style-type: none"> - Limited performance due to high viscosity.
		NaSCN	<ul style="list-style-type: none"> + Low driving temperature (higher than for LiNO₃). + Higher COP than NH₃-H₂O. + No rectifier needed. + High solubility in NH₃. + No corrosion of steel. 	<ul style="list-style-type: none"> - Risk of crystallization for evaporator temperatures below -10°C. - Limited performance due to high viscosity (but less than for LiNO₃).
		Ionic Liquids	<ul style="list-style-type: none"> + High solubility. + No rectification needed. + No crystallization risk. + Good performance. 	<ul style="list-style-type: none"> - Depending on the chemical structure, long-term thermal and toxicity problems. - High cost. - Absence of properties documentation.
H₂O	<ul style="list-style-type: none"> + High enthalpy of evaporation. + Abundantly available. + Low-cost. + Environmentally friendly. - Only positive refrigeration temperatures. - Vacuum operation. 	LiBr	<ul style="list-style-type: none"> + Well documented properties and materials compatibility. + High refrigerant vapor purity. + Higher COP compared to NH₃-H₂O systems. 	<ul style="list-style-type: none"> - High viscosity. - Corrosion risks. - Crystallization risks.
		LiCl	<ul style="list-style-type: none"> + Good stability. + Better cycle performance than H₂O-LiBr. 	<ul style="list-style-type: none"> - Crystallization risks (higher than for H₂O-LiBr).
		Ionic Liquids	<ul style="list-style-type: none"> + High solubility. + No crystallization risk. + Good performance. 	<ul style="list-style-type: none"> - Depending on the chemical structure, long-term thermal and toxicity problems. - High cost. - Absence of properties documentation.
HFC	<ul style="list-style-type: none"> + Moderate pressure ranges. - Low enthalpy of evaporation. - GWP. - Will be banned in the future. 	Organic absorbents	<ul style="list-style-type: none"> + Low driving temperature. + Non-toxicity of fluids. 	<ul style="list-style-type: none"> - Low performance. - Absence of techno-economic studies.
Alcohol	<ul style="list-style-type: none"> + High thermal stability. - Vacuum operation. 	Organic Solvents	<ul style="list-style-type: none"> + Only convenient for high driving temperature applications. 	<ul style="list-style-type: none"> - Low performance for cooling. - In most of the cases possess the same toxicity as NH₃. - Absence of techno-economic studies.

The state of the art of the exchanger technologies investigated for absorption chillers was presented in Section 1.3. The selection of the exchangers' technology is of great importance and must take into account a great number of variables depending on the specific application. A general comparison of the different technologies of heat exchangers studied for small-capacity absorption chillers operating with binary working fluids is presented in Table I.17. The choice of the technology has to take into account different aspects. Apart from the heat and mass transfer performance potential, other factors such as the manufacturing costs, the HTF and type of source to be used, the working fluid, the required compactness, the weight, the technical complexity, the required capacity, the range of cooling temperatures, static or mobile operation, among others, are of fundamental importance.

The falling film technologies are the most common geometries used for heat and mass exchange because they are the most versatile and adaptable technologies to the different solutions used in absorption cooling technologies. The horizontal tube baffle structures have been historically the predominant technology in commercial absorption machines. However, they are not the most effective in terms of weight and compactness (Yoon et al., 2006). In the search for other options, the plate heat exchangers have been

experimentally investigated as the main components in absorption systems owing to their low cost, high performance, and compactness (Section 1.3.4.1). New technologies have been studied to enhance the heat and mass transfers in the absorption systems' components such as the bubble absorbers, microchannel exchangers, membrane-based absorbers or generators, and adiabatic absorbers. Microtube falling film absorbers show good performance among the HT technologies for NH₃-based systems. However, particular attention has to be paid to the coolant side pressure drops, which can be regulated by modifying the flow configuration (Garimella, 1999). Membrane-based absorbers seem to be a promising technology to overcome the disadvantages of the conventional falling-film technology. However, the durability of the membranes over time remains to be studied. Indeed, the pores might tend to obstruct while operating with salt absorbents (Riffat et al., 2004; Wang et al., 2009). On the other hand, the potential of adiabatic absorbers has yet to be thoroughly explored. New or enhanced distribution methods and new configurations would significantly impact the performance of the entire system.

Table I.17: General comparison for the different technologies of exchangers used in small-capacity single-stage absorption chillers operating with binary working fluids.

Nonadiabatic	Falling film	<ul style="list-style-type: none"> + High heat transfer and mass transfer potential. + No pressure drop. - Wettability challenges. 	Tubes	<ul style="list-style-type: none"> + Easy manufacturing. + Good for air-cooled applications using VTs. - Low compactness.
			Plate	<ul style="list-style-type: none"> + Compactness. + Low cost.
			Microtubes	<ul style="list-style-type: none"> + High heat transfers for the HTF. - Pressure drop in the HTF. - Limited to low-viscosity solutions.
	Two-phase	<ul style="list-style-type: none"> + No wettability problems. + High mass transfer exchange area. + No need for a solution distributor. - Restricted to low-viscosity fluids. - Recommended for high-pressure operating conditions. - Lower heat transfer area compared to the mass transfer area. - Pressure drop. - Need for a refrigerant distributor in absorption mode. 	Tubular	<ul style="list-style-type: none"> + Good for air-cooled absorbers. - Small bubble diameter conservation in absorbers. - Low compactness.
Adiabatic	Membrane	<ul style="list-style-type: none"> + High compactness and low weight. - Fouling of the membrane with time. - System integration and related matters still to be studied (e.g., manufacturing costs, durability, and fouling). + A conventional single-phase heat exchanger can be used for the heat transfer. - Depending on the solution distribution method, the adiabatic chamber can have low compactness. 	Plate	<ul style="list-style-type: none"> + Elevated compactness. + Low cost.
			Microchannel	<ul style="list-style-type: none"> + Higher compactness. - Manufacturing complexity. - Particular attention must be paid to the pressure drop.
			Gravity-driven	<ul style="list-style-type: none"> + No extra energy consumption. + No solution flow rate limitations. + No pressure drops. + Good for compact applications. + Higher Ra than for nozzle-driven distribution. - Low velocity of solution. - Lower mass flux than for nozzle-driven distribution.
			Nozzle-driven	<ul style="list-style-type: none"> + Higher mass flux compared to gravity-driven distribution. + High surface/volume ratios. - Lower Ra compared to gravity-driven distribution.
			Membrane-based	<ul style="list-style-type: none"> + Simpler fabrication than the nonadiabatic membrane configuration. + Control over solution film thickness and velocity. + High compactness and low weight. - Fouling of the membrane with time. - System integration still to be studied.

Finally, Section 1.3 also served to observe that there is no standard characterization parameter for the performance evaluation of the sorption exchangers in absorption chillers. The commonly implemented heat transfers coefficient and fluxes, adapted from the models of conventional heat exchangers, neglect the heat of sorption. Whereas the definition of the mass transfer coefficients changes depending on the author. For this reason, Chapter II introduces the concept of thermal and mass effectivenesses for the general context of non-adiabatic sorption exchangers (the mass effectiveness of adiabatic sorption exchangers being intrinsically included in this definition). These effectivenesses are implemented in a global machine simulation.

References

- Abdulateef, J.M., Sopian, K., Alghoul, A., Sulaiman, M.Y., Zaharim, A., Ahmad, I., 2007. Solar absorption refrigeration system using new working fluid pairs. *Int. J. Energy* 1, 82–87.
- Abdulateef, J.M., Sopian, K., Alghoul, M.A., 2008. Optimum design for solar absorption refrigeration systems and comparison of the performances using ammonia-water, ammonia-lithium nitrate and ammonia-sodium thiocyanate solutions. *Int. J. Mech. Mater. Eng.* 3, 17–24.
- Abed, A.M., Alghoul, M.A., Yazdi, M.H., Al-shamani, A.N., Sopian, K., 2015. The role of enhancement techniques on heat and mass transfer characteristics of shell and tube spray evaporator: a detailed review. *Appl. Therm. Eng.* 75, 923–940. <https://doi.org/10.1016/j.applthermaleng.2014.10.020>
- Achuthan, M., Venkataraman, A., Rathnasamy, R., 2011. Experimental analysis on the performance and characteristics of compact solar refrigeration system. *Distrib. Gener. Altern. Energy J.* 26, 66–80. <https://doi.org/10.1080/21563306.2011.10462199>
- Acosta-Iborra, A., García, N., Santana, D., 2009. Modelling non-isothermal absorption of vapour into expanding liquid sheets. *Int. J. Heat Mass Transf.* 52, 3042–3054. <https://doi.org/10.1016/j.ijheatmasstransfer.2009.01.036>
- AGO AG Energie + Anlagen, 2019. ago congel@ product brochure.
- Agyenim, F., Knight, I., Rhodes, M., 2010. Design and experimental testing of the performance of an outdoor LiBr/H₂O solar thermal absorption cooling system with a cold store. *Sol. Energy* 84, 735–744. <https://doi.org/10.1016/j.solener.2010.01.013>
- Ahachad, M., Charia, M., Bernatchou, A., 1992. Study of an improved NH₃-H₂O solar absorption refrigerating machine in Rabat (Morocco). *Sol. Energy Mater. Sol. Cells* 28, 71–79. [https://doi.org/10.1016/0927-0248\(92\)90108-2](https://doi.org/10.1016/0927-0248(92)90108-2)
- Aiane, M., Ramousse, J., Bouyau, M., Boudard, E., Stutz, B., 2017. Modélisation dynamique d'un système de climatisation par absorption, in: *Congrès Société Française de Thermique*, 30 May - 2 Juin. Marseille, France.
- Albers, J., Nurzia, G., Ziegler, F., 2010. Simulation and Experimental Analysis of a Solar Driven Absorption Chiller With Partially Wetted Evaporator. *J. Sol. Energy Eng.* 132, 011016. <https://doi.org/10.1115/1.4000331>
- Alefeld, G., Radermacher, R., 1993. *Heat Conversion Systems*, 1st ed. CRC Press, Boca Baton, Florida.
- Ali, A.H.H., 2010. Design of a compact absorber with a hydrophobic membrane contactor at the liquid-vapor interface for lithium bromide-water absorption chillers. *Appl. Energy* 87, 1112–1121. <https://doi.org/10.1016/j.apenergy.2009.05.018>
- Ali, A.H.H., Noeres, P., Pollerberg, C., 2008. Performance assessment of an integrated free cooling and solar powered single-effect lithium bromide-water absorption chiller. *Sol. Energy* 82, 1021–1030. <https://doi.org/10.1016/j.solener.2008.04.011>
- Ali, A.H.H., Schwerdt, P., 2010. For designing a compact absorber with membrane contactor at liquid-vapor interface: influence of membrane properties on water vapour transfer. *ASHRAE Trans.* 116, 398–407.
- Ali, A.H.H., Schwerdt, P., 2009. Characteristics of the membrane utilized in a compact absorber for lithium bromide-water absorption chillers. *Int. J. Refrig.* 32, 1886–1896. <https://doi.org/10.1016/j.ijrefrig.2009.07.009>
- Ali, A.H.H., Schwerdt, P., 2008. Characteristics of the membrane utilized in a compact absorber for lithium bromide-water absorption chillers, in: *9th Int IEA Heat Pump Conference*. Switzerland.
- Aliane, A., Abboudi, S., Seladji, C., Guendouz, B., 2016. An illustrated review on solar absorption cooling experimental studies. *Renew. Sustain. Energy Rev.* 65, 443–458. <https://doi.org/10.1016/j.rser.2016.07.012>
- Alizadeh, S., Bahar, F., Geoola, F., 1979. Design and optimisation of an absorption refrigeration system operated by solar energy. *Sol. Energy* 22, 149–154. [https://doi.org/10.1016/0038-092X\(79\)90099-9](https://doi.org/10.1016/0038-092X(79)90099-9)
- Altamirano, A., Le Pierrès, N., Stutz, B., 2019. Review of small-capacity single-stage continuous absorption systems operating on binary working fluids for cooling: Theoretical, experimental and commercial cycles. *Int. J. Refrig.* 106, 350–373. <https://doi.org/10.1016/j.ijrefrig.2019.06.033>
- Alvares, S.G., Trepp, C., 1987. Simulation of a solar driven aqua-ammonia absorption refrigeration system Part 1: mathematical description and system optimization. *Int. J. Refrig.* 10, 40–48. [https://doi.org/10.1016/0140-7007\(87\)90095-8](https://doi.org/10.1016/0140-7007(87)90095-8)
- Amaris, C., Bourouis, M., Vallès, M., 2014a. Effect of advanced surfaces on the ammonia absorption process with NH₃/LiNO₃ in a tubular bubble absorber. *Int. J. Heat Mass Transf.* 72, 544–552. <https://doi.org/10.1016/j.ijheatmasstransfer.2014.01.031>
- Amaris, C., Bourouis, M., Vallès, M., Salavera, D., Coronas, A., 2014b. Thermophysical Properties and Heat and Mass Transfer of New Working Fluids in Plate Heat Exchangers for Absorption Refrigeration Systems. *Heat Transf. Eng.* <https://doi.org/10.1080/01457632.2014.923983>
- Ammari, A., 2012. Experimental investigation of two-phase flow in microchannels. KTH Royal Institute of Technology. <https://doi.org/10.1115/1.1797036>
- Anies, G., 2011. Modélisation, simulation dynamique, validation expérimentale et optimisation énergétique d'une unité de rafraîchissement solaire par absorption (in French). PhD Université de Pau et des Pays de l'Adour.
- Antonopoulos, K.A., Rogdakis, E.D., 1996a. Performance of solar-driven ammonia-lithium nitrate and ammonia-sodium thiocyanate absorption systems operating as coolers or heat pumps in Athens. *Appl. Therm. Eng.* 16, 127–147.
- Antonopoulos, K.A., Rogdakis, E.D., 1996b. Performance of solar-driven ammonia-lithium nitrate and ammonia-sodium thiocyanate absorption systems operating as coolers or heat pumps in Athens. *Appl. Therm. Eng.* 16, 127–147.
- Apreotesi, M., Mouchka, G., Davis, K., Tulchinsky, A., Pence, D., 2007. Effects of pressure and channel depth on desorption in microscale fractal-like branching heat exchangers, in: *Proceedings of IMECE2007*. ASME, Seattle, USA.
- Arshi Banu, P.S., Sudharsan, N.M., 2017. Review of water based vapour absorption cooling systems using thermodynamic analysis. *Renew. Sustain. Energy Rev.* 82, 3750–3761. <https://doi.org/10.1016/j.rser.2017.10.092>
- Arzoz, D., Rodriguez, P., Izquierdo, M., 2005. Experimental study on the adiabatic absorption of water vapor into LiBr-H₂O solutions. *Appl. Therm. Eng.* 25, 797–811. <https://doi.org/10.1016/j.applthermaleng.2004.08.003>

- Asdrubali, F., Grignaffini, S., 2005. Experimental evaluation of the performances of a H₂O-LiBr absorption refrigerator under different service conditions. *Int. J. Refrig.* 28, 489–497. <https://doi.org/10.1016/j.ijrefrig.2004.11.006>
- Asfand, F., Stiriba, Y., Bourouis, M., 2015. CFD simulation to investigate heat and mass transfer processes in a membrane-based absorber for water-LiBr absorption cooling systems. *Energy* 91, 517–530. <https://doi.org/10.1016/j.energy.2015.08.018>
- Ayala Delgado, R., 1992. An experimental study of heat driven absorption cooling systems. MSc University of Salford, England.
- Ayala, R., Frías, J.L., Lam, L., Heard, C.L., Holland, F.A., 1994. Experimental assessment of an ammonia/lithium nitrate absorption cooler operated on low temperature geothermal energy. *Heat Recover. Syst. CHP* 14, 437–446.
- Ayub, Z.H., 2003. Plate heat exchanger literature survey and new heat transfer and pressure drop correlations for refrigerant evaporators. *Heat Transf. Eng.* 24, 3–16. <https://doi.org/10.1080/01457630304056>
- Beausoleil-Morrison, I., Johnson, G., Kemery, B.P., 2015. The experimental characterization of a lithium bromide-water absorption chiller and the development of a calibrated model. *Sol. Energy* 122, 368–381. <https://doi.org/10.1016/j.solener.2015.09.009>
- Bedia, J., Palomar, J., Gonzalez-Miquel, M., Rodriguez, F., Rodriguez, J.J., 2012. Screening ionic liquids as suitable ammonia absorbents on the basis of thermodynamic and kinetic analysis. *Sep. Purif. Technol.* 95, 188–195. <https://doi.org/10.1016/j.seppur.2012.05.006>
- Bellos, E., Tzivanidis, C., Antonopoulos, K.A., 2016. Exergetic and energetic comparison of LiCl-H₂O and LiBr-H₂O working pairs in a solar absorption cooling system. *Energy Convers. Manag.* 123, 453–461. <https://doi.org/10.1016/j.enconman.2016.06.068>
- Best, R., Bujedo, L.A., Melograno, P., Velázquez, N., Pilatowsky, I., Gómez, V.H., García-Valladares, O., Fedrizzi, R., Corredera, A., Hernández, J.I., Sanz, S., Ortega, N., 2011. Two novel solar sorption refrigerators using salt-ammonia mixtures for air-conditioning and ice production. 30th ISES Bienn. Sol. World Congr. 2011, SWC 2011 4, 2983–2994.
- Best, R., Eisa, M., A.R., Holland, F.A., 1987. Thermodynamic design data for absorption heat pump systems operating on ammonia-water-Part I. Cooling. *Heat Recover. Syst. CHP* 7, 167–175. [https://doi.org/10.1016/0890-4332\(87\)90081-0](https://doi.org/10.1016/0890-4332(87)90081-0)
- Best, R., Porras, L., Holland, F.A., 1991. Thermodynamic design data for absorption heat pump systems operating on ammonia-lithium nitrate-Part One. Cooling. *Heat Recover. Syst. CHP* 11, 49–61. [https://doi.org/10.1016/0890-4332\(91\)90187-9](https://doi.org/10.1016/0890-4332(91)90187-9)
- Best, R., Rivera, W., 2015. A review of thermal cooling systems. *Appl. Therm. Eng.* 75, 1162–1175. <https://doi.org/10.1016/j.applthermaleng.2014.08.018>
- Best, R., Rivera, W., Hernandez, J., Oskam, A., 1993. Thermodynamic design data for absorption heat pump systems operating on ammonia-sodium thiocyanate-I. Cooling. *Heat Recover. Syst. CHP* 13, 1–9.
- Beutler, A., Hoffmann, L., Ziegler, F., Alefeld, G., Gommed, K., Grossman, G., Shavit, A., 1996. Experimental Investigation of Heat and Mass Transfer on Horizontal and Vertical Tubes, in: *Proceedings of the International Absorption Heat Pump Conference*, September 17-20. Montreal, Canada, pp. 409–419.
- Bigham, S., Yu, D., Chugh, D., Moghaddam, S., 2014. Moving beyond the limits of mass transport in liquid absorbent microfilms through the implementation of surface-induced vortices. *Energy* 65, 621–630. <https://doi.org/10.1016/j.energy.2013.11.068>
- Blytas, G.C., Daniels, F., 1962. Concentrated Solutions of NaSCN in Liquid Ammonia. Solubility, Density, Vapor Pressure, Viscosity, Thermal Conductance, Heat of Solution and Heat Capacity. *J. Am. Chem. Soc.* 84. <https://doi.org/10.1021/ja00866a001>
- Bogart, M.J.P., 1982. Pitfalls in ammonia absorption refrigeration. *Int. J. Refrig.* 5, 203–208. [https://doi.org/10.1016/0140-7007\(82\)90020-2](https://doi.org/10.1016/0140-7007(82)90020-2)
- Bogart, M.J.P., 1981. Ammonia Absorption Refrigeration in Industrial Processes. Gulf Publishing Company, Houston (US).
- Bong, T.Y., Ng, K.C., Tay, A.O., 1987. Performance study of a solar-powered air-conditioning system. *Sol. Energy* 39, 173–182. [https://doi.org/10.1016/S0038-092X\(87\)80025-7](https://doi.org/10.1016/S0038-092X(87)80025-7)
- Borde, I., Jelinek, M., 1987. Development of absorption refrigeration units for cold storage of agricultural products. *Int. J. Refrig.* 10, 53–56.
- Borde, I., Jelinek, M., Daltrophe, N., 1997. Working fluids for an absorption system based on R124 (2-chloro-1,1,1,2-tetrafluoroethane) and organic absorbents. *Int. J. Refrig.* 20, 256–266. [https://doi.org/10.1016/S0140-7007\(97\)00090-X](https://doi.org/10.1016/S0140-7007(97)00090-X)
- Borde, I., Jelinek, M., Daltrophe, N.C., 1995. Absorption system based on the refrigerant R134a. *Int. J. Refrig.* 18, 387–394. [https://doi.org/10.1016/0140-7007\(95\)98161-D](https://doi.org/10.1016/0140-7007(95)98161-D)
- Boudard, E., Bruzzo, V., 2004. Exchange Device and Heat Transfer Especially for Automotive Vehicle. French Patent 2,871,221.
- Boudéhenn, F., Demasles, H., Wytenbach, J., Jobard, X., Chèze, D., Papillon, P., 2012. Development of a 5 kW cooling capacity ammonia-water absorption chiller for solar cooling applications. *Energy Procedia* 30, 35–43. <https://doi.org/10.1016/j.egypro.2012.11.006>
- Bredow, D., Jain, P., Wohlfeil, A., Ziegler, F., 2008. Heat and mass transfer characteristics of a horizontal tube absorber in a semi-commercial absorption chiller. *Int. J. Refrig.* 31, 1273–1281. <https://doi.org/10.1016/j.ijrefrig.2008.01.016>
- Brendel, T., Zetsche, M., Müller-Steinhagen, H., 2010. Development of a small scale ammonia/water absorption chiller, in: 9th IIR Gustav Lorentzen Conference. Sydney, Australia.
- Brotzu, A., Felli, F., Natali, S., Pilone, D., 2015. Pipeline Corrosion Failure in an Absorption Chiller. *Procedia Eng.* 109, 43–54. <https://doi.org/10.1016/j.proeng.2015.06.205>
- Bubalo, M.C., Radošević, K., Redovniković, I.R., Slivac, I., Srček, V.G., 2017. Toxicity mechanisms of ionic liquids. *Arh Hig Rada Toksikol* 68, 171–179. <https://doi.org/10.1515/aiht-2017-68-2979>
- Bulgan, A.T., 1995. Optimization of the thermodynamic model of aqua-ammonia absorption refrigeration systems. *Energy Convers. Manag.* 36, 135–143. [https://doi.org/10.1016/0196-8904\(94\)00028-X](https://doi.org/10.1016/0196-8904(94)00028-X)
- Burdukov, A.P., Dorokhov, A.R., Paniev, G.A., 1989. Combined heat and mass transfer in absorption on droplets. *Sov. J. Appl. Phys.* 3, 39–45.
- Butz, D., Stephan, K., 1989. Dynamic behaviour of an absorption heat pump. *Int. J. Refrig.* 12, 204–212.
- Cai, D., He, G., Tian, Q., Tang, W., 2014a. Thermodynamic analysis of a novel air-cooled non-adiabatic absorption refrigeration cycle driven by low grade energy. *Energy Convers. Manag.* 86, 537–547. <https://doi.org/10.1016/j.enconman.2014.06.008>
- Cai, D., He, G., Tian, Q., Tang, W., 2014b. Exergy analysis of a novel air-cooled non-adiabatic absorption refrigeration cycle with NH₃-NaSCN and NH₃-LiNO₃ refrigerant solutions. *Energy Convers. Manag.* 88, 66–78. <https://doi.org/10.1016/j.enconman.2014.08.025>

- Cai, D., Jiang, J., He, G., Li, K., Niu, L., Xiao, R., 2016. Experimental evaluation on thermal performance of an air-cooled absorption refrigeration cycle with $\text{NH}_3\text{-LiNO}_3$ and $\text{NH}_3\text{-NaSCN}$ refrigerant solutions. *Energy Convers. Manag.* 120, 32–43. <https://doi.org/10.1016/j.enconman.2016.04.089>
- Cai, W., Sen, M., Paolucci, S., 2007. Dynamic modeling of an absorption refrigeration system using ionic liquids, in: ASME International Mechanical Engineering Congress and Exposition, Proceedings (IMECE). <https://doi.org/10.1115/IMECE200741335>
- Calm, J.M., 2008. The next generation of refrigerants - Historical review, considerations, and outlook. *Int. J. Refrig.* 31, 1123–1133. <https://doi.org/10.1016/j.ijrefrig.2008.01.013>
- Cardenas, R., Narayanan, V., 2011. Heat and mass transfer characteristics of a constrained thin-film ammonia-water bubble absorber. *Int. J. Refrig.* 34, 113–128. <https://doi.org/10.1016/j.ijrefrig.2010.08.010>
- Castro, J., Oliet, C., Rodríguez, I., Oliva, A., 2009. Comparison of the performance of falling film and bubble absorbers for air-cooled absorption systems. *Int. J. Therm. Sci.* 48, 1355–1366. <https://doi.org/10.1016/j.ijthermalsci.2008.11.021>
- Castro, J., Oliva, A., Pérez-Segarra, C.D., Cadafalch, J., 2007. Evaluation of a Small Capacity, Hot Water Driven, Air-Cooled $\text{H}_2\text{O-LiBr}$ Absorption Machine. *HVAC&R Res.* 13, 59–75. <https://doi.org/10.1080/10789669.2007.10390944>
- Castro, J., Oliva, A., Pérez-Segarra, C.D., Oliet, C., 2008. Modelling of the heat exchangers of a small capacity, hot water driven, air-cooled $\text{H}_2\text{O-LiBr}$ absorption cooling machine. *Int. J. Refrig.* 31, 75–86. <https://doi.org/10.1016/j.ijrefrig.2007.05.019>
- Cera-Manjarres, A., Salavera, D., Coronas, A., 2018. Vapour pressure measurements of ammonia/ionic liquids mixtures as suitable alternative working fluids for absorption refrigeration technology. *Fluid Phase Equilib.* <https://doi.org/10.1016/j.fluid.2018.01.006>
- Cerezo, J., Best, R., Bourouis, M., Coronas, A., 2010. Comparison of numerical and experimental performance criteria of an ammonia-water bubble absorber using plate heat exchangers. *Int. J. Heat Mass Transf.* 53, 3379–3386. <https://doi.org/10.1016/j.ijheatmasstransfer.2010.02.031>
- Cerezo, J., Best, R., Chan, J.J., Romero, R.J., Hernandez, J.I., Lara, F., 2018a. A theoretical-experimental comparison of an improved ammonia-water bubble absorber by means of a helical static mixer. *Energies* 11, 1–14. <https://doi.org/10.3390/en11010056>
- Cerezo, J., Bourouis, M., Vallès, M., Coronas, A., Best, R., 2009. Experimental study of an ammonia-water bubble absorber using a plate heat exchanger for absorption refrigeration machines. *Appl. Therm. Eng.* 29, 1005–1011.
- Cerezo, J., Romero, R., Ibarra, J., Rodríguez, A., Montero, G., Acuña, A., 2018b. Dynamic Simulation of an Absorption Cooling System with Different Working Mixtures. *Energies* 11, 259. <https://doi.org/10.3390/en11020259>
- Chan-González, J.D.J., Castillo-Téllez, M., Castillo-Téllez, B., Andrade-Durán, J.E., Best-y-Brown, R., 2017. Experimental study of a bubble mode absorption with inner gas distributor in a PHE-type absorber with $\text{NH}_3\text{-H}_2\text{O}$. *DYNA Energía y Sostenibilidad* 6, 1–21. <https://doi.org/http://dx.doi.org/10.6036/ES8192>
- Chan, J.J., Best, R., Cerezo, J., Barrera, M.A., Lezama, F.R., 2018. Experimental study of a bubble mode absorption with an inner vapor distributor in a plate heat exchanger-type absorber with $\text{NH}_3\text{-LiNO}_3$. *Energies* 11. <https://doi.org/10.3390/en11082137>
- Chen, J., Chang, H., Chen, S.R., 2006. Simulation study of a hybrid absorber-heat exchanger using hollow fiber membrane module for the ammonia-water absorption cycle. *Int. J. Refrig.* 29, 1043–1052. <https://doi.org/10.1016/j.ijrefrig.2006.02.002>
- Chen, J.F., Dai, Y.J., Wang, R.Z., 2017. Experimental and analytical study on an air-cooled single effect $\text{LiBr-H}_2\text{O}$ absorption chiller driven by evacuated glass tube solar collector for cooling application in residential buildings. *Sol. Energy* 151, 110–118. <https://doi.org/10.1016/j.solener.2017.05.029>
- Chen, W., Bai, Y., 2016. Thermal performance of an absorption-refrigeration system with $[\text{emim}]\text{Cu}_2\text{Cl}_5/\text{NH}_3$ as working fluid. *Energy* 112, 332–341. <https://doi.org/10.1016/j.energy.2016.06.093>
- Chen, W., Liang, S., Guo, Y., Cheng, K., Gui, X., Tang, D., 2012. Thermodynamic performances of $[\text{mmim}]\text{DMP}/\text{methanol}$ absorption refrigeration. *J. Therm. Sci.* 21, 557–563. <https://doi.org/10.1007/s11630-012-0581-y>
- Chen, W., Liang, S., Guo, Y., Tang, D., 2014. Thermodynamic analysis of an absorption system using $[\text{bmim}]\text{Zn}_2\text{Cl}_5/\text{NH}_3$ as the working pair. *Energy Convers. Manag.* 85, 13–19. <https://doi.org/10.1016/j.enconman.2014.05.024>
- Christensen, R.N., Garimella, S., Kang, Y.T., Garrabrant, M.A., 1998. Perforated fin heat and mass transfer device. US5704417A.
- Clerx, M., Trezek, G.J., 1987. Performance of an aqua-ammonia absorption solar refrigerator at sub-freezing evaporator conditions. *Sol. Energy* 39, 379–389. [https://doi.org/10.1016/S0038-092X\(87\)80056-7](https://doi.org/10.1016/S0038-092X(87)80056-7)
- Crepinsek, Z., Goricaneč, D., Kropce, J., 2009. Comparison of the performances of absorption refrigeration cycles. *WSEAS Trans. Heat Mass Transf.* 4, 65–76.
- Cvjetko Bubalo, M., Radošević, K., Radojčić Redovniković, I., Halambek, J., Gaurina Srček, V., 2014. A brief overview of the potential environmental hazards of ionic liquids. *Ecotoxicol. Environ. Saf.* 99, 1–12. <https://doi.org/10.1016/j.ecoenv.2013.10.019>
- Dardouch, J., Charia, M., Bernatchou, A., 2018. Study of an Absorption Refrigeration Machine Improved with Distillation Column. *J. Mater. Environ. Sci.* 9, 772–783.
- Davis, R.O.E., Olmstead, L.B., Lundstrum, F., 1921. Vapor Pressure of Lithium Nitrate: Ammonia System. *J. Am. Chem. Soc.* 43, 1575–80. <https://doi.org/10.1021/ja01440a019>
- De Francisco, A., Illanes, R., Torres, J.L., Castillo, M., De Blas, M., Prieto, E., García, A., 2002. Development and testing of a prototype of low-power water-ammonia absorption equipment for solar energy applications. *Renew. Energy* 25, 537–544. [https://doi.org/10.1016/S0960-1481\(01\)00093-3](https://doi.org/10.1016/S0960-1481(01)00093-3)
- de Vega, M., Almendros-Ibañez, J.A., Ruiz, G., 2006. Performance of a LiBr-water absorption chiller operating with plate heat exchangers. *Energy Convers. Manag.* 47, 3393–3407. <https://doi.org/10.1016/j.enconman.2006.01.005>
- de Vega, M., Venegas, M., García-Hernando, N., 2018. Modeling and performance analysis of an absorption chiller with a microchannel membrane-based absorber using $\text{LiBr-H}_2\text{O}$, $\text{LiCl-H}_2\text{O}$, and $\text{LiNO}_3\text{-NH}_3$. *Int. J. Energy Res.* 1–15. <https://doi.org/10.1002/er.4098>
- Delahanty, J.C., Garimella, S., Garrabrant, M.A., 2015. Design of compact microscale geometries for ammonia–water desorption. *Sci. Technol. Built Environ.* 21, 365–374. <https://doi.org/10.1080/23744731.2015.1015906>
- Demesa, N., Huicochea, A., Hernandez, J.A., Siqueiros, J., 2017. Heat transfer coefficients for evaporator with nested helical coils. *Int. J. Therm. Sci.* 121, 390–397. <https://doi.org/10.1016/j.ijthermalsci.2017.08.002>

- Deng, S.M., Ma, W.B., 1999. Experimental studies on the characteristics of an absorber using LiBr/H₂O solution as working fluid. *Int. J. Refrig.* 22, 293–301. [https://doi.org/10.1016/S0140-7007\(98\)00067-X](https://doi.org/10.1016/S0140-7007(98)00067-X)
- Determan, M., Garimella, S., 2010. A Microscale Monolithic Absorption Heat Pump, in: *International Refrigeration and Air Conditioning Conference*. pp. 1–7.
- Determan, M.D., Garimella, S., 2012. Design, fabrication, and experimental demonstration of a microscale monolithic modular absorption heat pump. *Appl. Therm. Eng.* 47, 119–125. <https://doi.org/10.1016/j.applthermaleng.2011.10.043>
- Determan, M.D., Garimella, S., 2011. Ammonia-water desorption heat and mass transfer in microchannel devices. *Int. J. Refrig.* 34, 1197–1208. <https://doi.org/10.1016/j.ijrefrig.2011.02.004>
- Determan, M.D., Garimella, S., 2005. Ammonia-water desorption heat and mass transfer in microchannel devices, in: *International Sorption Heat Pump Conference*. Denver, CO.
- Determan, M.D., Garimella, S., Lee, S., 2004. Experimental demonstration of a microchannel desorber for ammonia-water heat pumps, in: *Seventeenth National Heat and Mass Transfer Conference and Sixth ISHMT/ASME Heat and Mass Transfer Conference*. Kalpakkam, India, pp. 453–458.
- Dixit, R., 2018. Innovative Technologies Improve Absorption Chiller Performance [WWW Document]. *Eng. Syst. Mag.* URL <https://www.esmagazine.com/articles/98886-innovative-technologies-improve-absorption-chiller-performance> (accessed 10.8.18).
- Djordjevic, E., Kabelac, S., 2008. Flow boiling of R134a and ammonia in a plate heat exchanger. *Int. J. Heat Mass Transf.* 51, 6235–6242. <https://doi.org/10.1016/j.ijheatmasstransfer.2008.01.042>
- Domínguez-Inzunza, L.A., Hernández-Magallanes, J.A., Soto, P., Jiménez, C., Gutiérrez-Urueta, G., Rivera, W., 2016. Experimental assessment of an absorption cooling system utilizing a falling film absorber and generator. *Appl. Therm. Eng.* 103, 1105–1111. <https://doi.org/10.1016/j.applthermaleng.2016.05.014>
- Drost, M.K., Friedrich, M., 1997. Miniature heat pumps for portable and distributed space conditioning applications. *Energy Convers. Eng. Conf.* 1997. IECEC-97., Proc. 32nd Intersoc. 1271-1274 vol.2 ST-Miniature heat pumps for por. <https://doi.org/10.1109/IECEC.1997.661951>
- EAW, 2018a. Wegracal Maral 1 - Technische Beschreibung für Absorptionskälteanlage.
- EAW, 2018b. Wegracal Maral 2 - Technische Beschreibung für Absorptionskälteanlage.
- EAW, 2010a. Wegracal SE 15 - Technische Beschreibung für Absorptionskälteanlage.
- EAW, 2010b. Wegracal SE 30 - Technische Beschreibung für Absorptionskälteanlage.
- EAW, 2010c. Wegracal SE 50 - Technische Beschreibung für Absorptionskälteanlage.
- Eisa, M.A.R., Devotta, S., Holland, F.A., 1986. Thermodynamic design data for absorption heat pump systems operating on water-lithium bromide: Part I-Cooling. *Appl. Energy* 24, 287–301. [https://doi.org/10.1016/0306-2619\(86\)90068-1](https://doi.org/10.1016/0306-2619(86)90068-1)
- Electrolux Ltd, 1930. Improvements in or relating to absorption refrigerating apparatus. GB436736 (A).
- Elmaaty, T.M.A., Kabeel, A.E., Mahgoub, M., 2017. Corrugated plate heat exchanger review. *Renew. Sustain. Energy Rev.* 70, 852–860. <https://doi.org/10.1016/j.rser.2016.11.266>
- Elperin, T., Fominykh, A., Orenbakh, Z., 2007. Coupled heat and mass transfer during nonisothermal absorption by falling droplet with internal circulation. *Int. J. Refrig.* 30, 274–281. <https://doi.org/10.1016/j.ijrefrig.2006.07.006>
- Evola, G., Le Pierrès, N., Boudehenn, F., Papillon, P., 2013. Proposal and validation of a model for the dynamic simulation of a solar-assisted single-stage LiBr/water absorption chiller. *Int. J. Refrig.* 36, 1015–1028. <https://doi.org/10.1016/j.ijrefrig.2012.10.013>
- Farnós, J., Papakokinos, G., Castro, J., Morales, S., Oliva, A., 2017. Dynamic modelling of an air-cooled LiBr-H₂O absorption chiller based on heat and mass transfer empirical correlations, in: *12th IEA Heat Pump Conference*. Rotterdam.
- Farshi, L.G., Infante Ferreira, C.A., Mahmoudi, S.M.S., Rosen, M.A., 2014. First and second law analysis of ammonia/salt absorption refrigeration systems. *Int. J. Refrig.* 40, 111–121. <https://doi.org/10.1016/j.ijrefrig.2013.11.006>
- Fernández-seara, J., Pardiñas, Á.A., Diz, R., 2016a. Experimental heat transfer coefficients of pool boiling and spray evaporation of ammonia on a horizontal plain tube. *Int. J. Refrig.* 67, 259–270. <https://doi.org/10.1016/j.ijrefrig.2016.02.019>
- Fernández-seara, J., Pardiñas, Á.A., Diz, R., 2016b. Heat transfer enhancement of ammonia pool boiling with an integral-fin tube. *Int. J. Refrig.* 69, 175–185. <https://doi.org/10.1016/j.ijrefrig.2016.05.012>
- Fernández-Seara, J., Sieres, J., 2006. The importance of the ammonia purification process in ammonia-water absorption systems. *Energy Convers. Manag.* 47, 1975–1987. <https://doi.org/10.1016/j.enconman.2005.09.002>
- Fernández-Seara, J., Uhía, F.J., 2012. Heat transfer and friction characteristics of spirally corrugated tubes for outer ammonia condensation. *Int. J. Refrig.* 35, 2022–2032. <https://doi.org/10.1016/j.ijrefrig.2012.05.021>
- Fernández-Seara, J., Uhía, F.J., Diz, R., 2009. Experimental analysis of ammonia condensation on smooth and integral-fin titanium tubes. *Int. J. Refrig.* 32, 1140–1148. <https://doi.org/10.1016/j.ijrefrig.2009.01.026>
- Flores Flores, V.H., Cerezo Román, J., Montero Alpíres, G., 2014. Performance Analysis of Different Working Fluids for an Absorption Refrigeration Cycle. *Am. J. Environmental Eng.* 4, 1–10. <https://doi.org/10.5923/s.ajee.201401.01>
- Flórides, G.A., Kalogirou, S.A., Tassou, S.A., Wrobel, L.C., 2003. Design and construction of a LiBr-water absorption machine. *Energy Convers. Manag.* 44, 2483–2508. [https://doi.org/10.1016/S0196-8904\(03\)00006-2](https://doi.org/10.1016/S0196-8904(03)00006-2)
- Furukawa, M., Sasaki, N., Kaneko, T., Nohetani, T., 1993. Enhanced heat transfer tubes for absorber of absorption chiller/heater. *Trans. Japan Soc. Refrig. Air Cond. Eng.* 10, 219–226.
- García-Hernando, N., Almendros-Ibáñez, J.A., Ruiz, G., De Vega, M., 2011. On the pressure drop in Plate Heat Exchangers used as desorbers in absorption chillers. *Energy Convers. Manag.* 52, 1520–1525. <https://doi.org/10.1016/j.enconman.2010.10.020>
- García-Hernando, N., de Vega, M., Venegas, M., 2019a. Experimental characterisation of a novel adiabatic membrane-based micro-absorber using H₂O-LiBr. *Int. J. Heat Mass Transf.* 129, 1136–1143. <https://doi.org/10.1016/j.ijheatmasstransfer.2018.10.046>
- García-Hernando, N., Venegas, M., de Vega, M., 2019b. Experimental performance comparison of three flat sheet membranes operating in an adiabatic microchannel absorber. *Appl. Therm. Eng.* 152, 835–843. <https://doi.org/10.1016/j.applthermaleng.2019.02.129>

- Garimella, S., 1999. Miniaturized heat and mass transfer technology for absorption heat pumps, in: Proceedings of the International Sorption Heat Pump Conference. Munich, Germany, Germany, pp. 661–670.
- Garimella, S., Determan, M.D., Meacham, J.M., Lee, S., Ernst, T.C., 2011. Microchannel component technology for system-wide application in ammonia/water absorption heat pumps. *Int. J. Refrig.* 34, 1184–1196. <https://doi.org/10.1016/j.ijrefrig.2011.03.005>
- Garimella, S., Keinath, C.M., Delahanty, J.C., Hoysall, D.C., Staedter, M.A., Goyal, A., Garrabrant, M.A., 2016. Development and demonstration of a compact ammonia-water absorption heat pump prototype with microscale features for space-conditioning applications. *Appl. Therm. Eng.* 102, 557–564. <https://doi.org/10.1016/j.applthermaleng.2016.03.169>
- Garrabrant, M.A., Christensen, R.N., 1997. Modeling and experimental verification of a Perforated Plate-Fin Absorber for aqua-ammonia absorption systems, in: Proceedings of the 1997 ASME International Mechanical Engineering Congress and Exposition. ASME, Fairfield, NJ, USA, Dallas, TX, USA, pp. 337–347.
- Giannetti, N., Rocchetti, A., Yamaguchi, S., Saito, K., 2018. Heat and mass transfer coefficients of falling-film absorption on a partially wetted horizontal tube. *Int. J. Therm. Sci.* 126, 56–66. <https://doi.org/10.1016/j.ijthermalsci.2017.12.020>
- Giraud, F., 2015. Vaporization of water at subatmospheric pressure: fundamentals of boiling phenomena and path towards the design of compact evaporators for sorption chillers. INSA Lyon.
- Giraud, F., Toublanc, C., Rullière, R., Bonjour, J., Clause, M., 2016. Experimental study of water vaporization occurring inside a channel of a smooth plate-type heat exchanger at subatmospheric pressure. *Appl. Therm. Eng.* 106, 180–191. <https://doi.org/10.1016/j.applthermaleng.2016.05.151>
- Goel, N., Goswami, D.Y., 2007. Experimental Verification of a New Heat and Mass Transfer Enhancement Concept in a Microchannel Falling Film Absorber. *J. Heat Transfer* 129, 154–161. <https://doi.org/10.1115/1.2402182>
- Goel, N., Goswami, D.Y., 2005a. A Compact Falling Film Absorber. *J. Heat Transfer* 127, 957. <https://doi.org/10.1115/1.1929781>
- Goel, N., Goswami, D.Y., 2005b. Analysis of a counter-current vapor flow absorber. *Int. J. Heat Mass Transf.* 48, 1283–1292. <https://doi.org/10.1016/j.ijheatmasstransfer.2004.10.009>
- Gogoi, T.K., Inwar, D., 2016. Exergy analysis of a H₂O-LiCl absorption refrigeration system with operating temperatures estimates through inverse analysis. *Energy Convers. Manag.* 110, 436–447. <https://doi.org/10.1016/j.enconman.2015.12.037>
- Gonda, A., Lancereau, P., Bandelier, P., Luo, L., Fan, Y., Benezech, S., 2014. Water falling film evaporation on a corrugated plate. *Int. J. Therm. Sci.* 81, 29–37. <https://doi.org/10.1016/j.ijthermalsci.2014.02.010>
- González-Gil, A., 2011. Novel single – double-effect LiBr / H₂O absorption prototype with a highly efficient direct air-cooled adiabatic absorber. PhD Universidad Carlos III de Madrid.
- González-Gil, A., Izquierdo, M., Marcos, J.D., Palacios, E., 2012. New flat-fan sheets adiabatic absorber for direct air-cooled LiBr/H₂O absorption machines: Simulation, parametric study and experimental results. *Appl. Energy* 98, 162–173. <https://doi.org/10.1016/j.apenergy.2012.03.019>
- González-Gil, A., Izquierdo, M., Marcos, J.D., Palacios, E., 2011. Experimental evaluation of a direct air-cooled lithium bromide-water absorption prototype for solar air conditioning. *Appl. Therm. Eng.* 31, 3358–3368. <https://doi.org/10.1016/j.applthermaleng.2011.06.019>
- Goyal, A., Staedter, M.A., Hoysall, D.C., Ponkala, M.J., Garimella, S., 2017. Experimental evaluation of a small-capacity, waste-heat driven ammonia-water absorption chiller. *Int. J. Refrig.* 79, 89–100. <https://doi.org/10.1016/j.ijrefrig.2017.04.006>
- Goyal, A., Staedter, M.A., Hoysall, D.C., Ponkala, M.J., Garimella, S., 2016. Experimental evaluation of a small-capacity, waste-heat driven ammonia-water absorption chiller, in: International Refrigeration and Air Conditioning Conference.
- Grover, G.S., Eisa, M.A.R., Holland, F.A., 1988. Thermodynamic design data for absorption heat pump systems operating on water-lithium chloride-Part One. *Cooling. Heat Recover. Syst. CHP* 8, 33–41.
- Gutiérrez-Urueta, G., 2009. Thermo-Fluid Dynamic Evaluation of Components in Adiabatic Absorption Systems. PhD Universidad Carlos III de Madrid.
- Gutiérrez-Urueta, G., Rodríguez, P., Venegas, M., Ziegler, F., Rodríguez-Hidalgo, M.C., 2011. Experimental performances of a LiBr-water absorption facility equipped with adiabatic absorber. *Int. J. Refrig.* 34, 1749–1759. <https://doi.org/10.1016/j.ijrefrig.2011.07.014>
- Gutiérrez-Urueta, G., Rodríguez, P., Ziegler, F., Lecuona, A., Rodríguez-Hidalgo, M.C., 2012. Extension of the characteristic equation to absorption chillers with adiabatic absorbers. *Int. J. Refrig.* 35, 709–718. <https://doi.org/10.1016/j.ijrefrig.2011.10.010>
- Hammad, M., Abuzahra, B., 1995. Optimization Study of a Solar refrigeration System Works by Li-Br – H₂O Absorption Cycle. *J. Appl. Energy* 52, 519–533.
- Hammad, M., Habali, S., 2000. Design and performance study of a solar energy powered vaccine cabinet. *Appl. Therm. Eng.* 20, 1785–1798. [https://doi.org/10.1016/S1359-4311\(99\)00099-X](https://doi.org/10.1016/S1359-4311(99)00099-X)
- Hammad, M., Zurigat, Y., 1998. Performance of a second generation solar cooling unit. *Sol. Energy* 62, 79–84. [https://doi.org/10.1016/S0038-092X\(97\)00105-9](https://doi.org/10.1016/S0038-092X(97)00105-9)
- Hammad, M.A., Audi, M.S., 1992. Performance of a solar LiBr-water absorption refrigeration system. *Renew. Energy* 2, 275–282. [https://doi.org/10.1016/0960-1481\(92\)90039-6](https://doi.org/10.1016/0960-1481(92)90039-6)
- Hartley, D.E., Murgatroyd, W., 1964. Criteria for the break-up of thin liquid layers flowing isothermally over solid surfaces. *Int. J. Heat Mass Transf.* 7, 1003–1015.
- Hassan, H.Z., Mohamad, A.A., 2012. A review on solar cold production through absorption technology. *Renew. Sustain. Energy Rev.* 16, 5331–5348. <https://doi.org/10.1016/j.rser.2012.04.049>
- Haywood, A., Sherbeck, J., Phelan, P., Varsamopoulos, G., Gupta, S.K.S., 2012. Thermodynamic feasibility of harvesting data center waste heat to drive an absorption chiller. *Energy Convers. Manag.* 58, 26–34. <https://doi.org/10.1016/j.enconman.2011.12.017>
- Heard, C.L., Ayala, R., 2003. Carbon and stainless steel in solutions of lithium nitrate in ammonia at moderate temperatures. *Mater. Corros.* 54, 609–611. <https://doi.org/10.1002/maco.200390133>
- Heard, C.L., Ayala, R., Best, R., 1996. An experimental comparison of an absorption refrigerator using ammonia/water and ammonia/lithium nitrate, in: Proceedings of International Sorption Heat Pump Conference. Montreal, Canada.

- Helbing, U., Würfel, R., Fratzscher, W., 2000. Comparative investigations of non-adiabatic absorption in film flow and bubble flow. *Chem. Eng. Technol.* 23, 1081–1085. [https://doi.org/10.1002/1521-4125\(200012\)23:12<1081::AID-CEAT1081>3.0.CO;2-8](https://doi.org/10.1002/1521-4125(200012)23:12<1081::AID-CEAT1081>3.0.CO;2-8)
- Herbine, G.S., Perez-Blanco, H., 1995. Model of an ammonia-water bubble absorber, in: *ASHRAE Trans.* pp. 1324–1332.
- Hernández-Magallanes, J.A., Domínguez-Inzunza, L.A., Gutiérrez-Urueta, G., Soto, P., Jiménez, C., Rivera, W., 2014. Experimental assessment of an absorption cooling system operating with the ammonia/lithium nitrate mixture. *Energy* 78, 685–692. <https://doi.org/10.1016/j.energy.2014.10.058>
- Herold, K., Rademacher, R., Klein, S., 2016. *Absorption Chillers and Heat Pumps*, 2nd ed. CRC Press, Taylor & Francis Group, Boca Raton, FL.
- Herrera, J. V., García-Valladares, O., Gómez, V.H., Best, R., 2010. Numerical simulation and experimental results of horizontal tube falling film generator working in a $\text{NH}_3\text{-LiNO}_3$ absorption refrigeration system. *Appl. Therm. Eng.* 30, 1751–1763. <https://doi.org/10.1016/j.applthermaleng.2010.04.006>
- Hesselgreaves, J.E., 1990. The Impact of Compact Heat Exchangers on Refrigeration Technology and CFC Replacement. *Int. Refrig. Air Cond. Conf.* 492–500.
- Hesselgreaves, J.E., Law, R., Reay, D., 2016. *Compact Heat Exchangers: Selection, Design and Operation*, Butterworth. ed. Elsevier Ltd.
- Hidalgo, M.C.R., Aumente, P.R., Millán, M.I., Neumann, A.L., Mangual, R.S., 2008. Energy and carbon emission savings in Spanish housing air-conditioning using solar driven absorption system. *Appl. Therm. Eng.* 28, 1734–1744. <https://doi.org/10.1016/j.applthermaleng.2007.11.013>
- Hoffmann, L., Greiter, I., Wagner, A., Weiss, V., Alefeld, G., 1996. Experimental investigation of heat transfer in a horizontal tube falling film absorber with aqueous solutions of LiBr with and without surfactants. *Int. J. Refrig.* 19, 331–341. [https://doi.org/10.1016/S0140-7007\(96\)00026-6](https://doi.org/10.1016/S0140-7007(96)00026-6)
- Hong, S.J., Hihara, E., Dang, C., 2018. Analysis of adiabatic heat and mass transfer of microporous hydrophobic hollow fiber membrane-based generator in vapor absorption refrigeration system. *J. Memb. Sci.* <https://doi.org/10.1016/j.memsci.2018.07.048>
- Hong, S.J., Hihara, E., Dang, C., 2016. Novel absorption refrigeration system with a hollow fiber membrane-based generator. *Int. J. Refrig.* 67, 418–432. <https://doi.org/10.1016/j.ijrefrig.2016.04.012>
- Horuz, I., 1998a. A comparison between ammonia-water and water lithium bromide solutions in vapor absorption refrigeration systems. *Int. Commun. Heat Mass Transf.* 25, 711–721.
- Horuz, I., 1998b. An alternative road transport refrigeration. *Turkish J. Eng. Environ. Sci.* 22, 211–222.
- Horuz, I., Callander, T.M.S., 2004. Experimental investigation of a vapor absorption refrigeration system. *Int. J. Refrig.* 27, 10–16. [https://doi.org/10.1016/S0140-7007\(03\)00119-1](https://doi.org/10.1016/S0140-7007(03)00119-1)
- Hoysall, D.C., Keniar, K., Garimella, S., 2017. Visualization of Two-Phase Flow in Serpentine Heat Exchanger Passages With Microscale Pin Fins. *J. Heat Transfer* 140, 011802. <https://doi.org/10.1115/1.4037342>
- Hoysall, D.C., Keniar, K., Garimella, S., 2015. Visualization of Two-Phase Flow Through Microchannel Heat Exchangers, in: *ASME 2015 13th International Conference on Nanochannels, Microchannels, and Minichannels.* <https://doi.org/10.1115/ICNMM2015-48821>
- Hu, J.S., Chao, C.Y.H., 2008. Study of a micro absorption heat pump system. *Int. J. Refrig.* 31, 1198–1206. <https://doi.org/10.1016/j.ijrefrig.2008.02.004>
- Hu, T., Xie, X., Jiang, Y., 2017. Design and experimental study of a plate-type falling film generator for a LiBr/H₂O absorption heat pump. *Int. J. Refrig.* 74, 302–310. <https://doi.org/10.1016/j.ijrefrig.2016.09.024>
- Ibarra-Bahena, J., Dehesa-Carrasco, U., Romero, R.J., Rivas-Herrera, B., Rivera, W., 2017. Experimental assessment of a hydrophobic membrane-based desorber/condenser with H₂O/LiBr mixture for absorption systems. *Exp. Therm. Fluid Sci.* <https://doi.org/10.1016/j.expthermflusci.2017.05.024>
- Ibarra-bahena, J., Romero, R.J., 2014. Performance of different experimental absorber designs in absorption Li heat pump cycle technologies: A review. *Energies* 7, 751–766. <https://doi.org/10.3390/en7020751>
- IEA, 2018. *The Future of Cooling*. Paris, France.
- Infante Ferreira, C.A., 1995. Operating characteristics of $\text{NH}_3\text{-LiNO}_3$ and $\text{NH}_3\text{-NaSCN}$ absorption refrigeration machines, in: *Nineteenth International Congress of Refrigeration*. pp. 321–328.
- Infante Ferreira, C.A., 1985. Vertical tubular absorbers for ammonia-salt absorption refrigeration. PhD Technische Hogeschool Delft.
- Infante Ferreira, C.A., 1984. Thermodynamic and physical property data equations for ammonia-lithium nitrate and ammonia-sodium thiocyanate solutions. *Sol. Energy* 32, 231–236. [https://doi.org/10.1016/S0038-092X\(84\)80040-7](https://doi.org/10.1016/S0038-092X(84)80040-7)
- Islam, M.R., 2008. Absorption process of a falling film on a tubular absorber: An experimental and numerical study. *Appl. Therm. Eng.* 28, 1386–1394. <https://doi.org/10.1016/j.applthermaleng.2007.10.004>
- Islam, M.R., Wijesundera, N.E., Ho, J.C., 2003. Performance study of a falling-film absorber with a film-inverting configuration. *Int. J. Refrig.* 26, 909–917. [https://doi.org/10.1016/S0140-7007\(03\)00078-1](https://doi.org/10.1016/S0140-7007(03)00078-1)
- Izquierdo, M., Lizarte, R., Marcos, J.D., Gutiérrez, G., 2008. Air conditioning using an air-cooled single effect lithium bromide absorption chiller: Results of a trial conducted in Madrid in August 2005. *Appl. Therm. Eng.* 28, 1074–1081. <https://doi.org/10.1016/j.applthermaleng.2007.06.009>
- Izquierdo, M., Martín, E., Palacios, E., 2011. Absorber and absorber-evaporator assembly for absorption machines and lithium bromide-water absorption machines that integrate said absorber and absorber-evaporator assembly. EP1641.448.
- Izquierdo, M., Venegas, M., Rodríguez, P., Lecuona, A., 2004. Crystallization as a limit to develop solar air-cooled LiBr-H₂O absorption systems using low-grade heat. *Sol. Energy Mater. Sol. Cells* 81, 205–216. <https://doi.org/10.1016/j.solmat.2003.11.002>
- Jelinek, M., Levy, A., Borde, I., 2007. Density of organic binary mixtures from equilibrium measurements. *Int. J. Refrig.* 30, 471–481. <https://doi.org/10.1016/j.ijrefrig.2006.08.012>
- Jenks, J., Narayanan, V., 2008. Effect of Channel Geometry Variations on the Performance of a Constrained Microscale-Film Ammonia-Water Bubble Absorber. *J. Heat Transfer* 130, 112402. <https://doi.org/10.1115/1.2970065>

- Jeong, S., Garimella, S., 2002. Falling-film and droplet mode heat and mass transfer in a horizontal tube LiBr/water absorber. *Int. J. Heat Mass Transf.* 45, 1445–1458. [https://doi.org/10.1016/S0017-9310\(01\)00262-9](https://doi.org/10.1016/S0017-9310(01)00262-9)
- Jiang, J., He, G., Liu, Yilin, Liu, Yue, Cai, D., 2017a. Flow boiling heat transfer characteristics and pressure drop of ammonia-lithium nitrate solution in a smooth horizontal tube. *Int. J. Heat Mass Transf.* 108, 220–231. <https://doi.org/10.1016/j.ijheatmasstransfer.2016.12.004>
- Jiang, J., Liu, Yue, He, G., Liu, Yilin, Cai, D., Liang, X., 2017b. Experimental investigations and an updated correlation of flow boiling heat transfer coefficients for ammonia/lithium nitrate mixture in horizontal tubes. *Int. J. Heat Mass Transf.* 112, 224–235. <https://doi.org/10.1016/j.ijheatmasstransfer.2017.04.135>
- Jiangsu Huineng New Energy Technology Co., 2019. Small Type Hot Water Absorption Chiller Parameters [WWW Document]. URL http://www.tynkt.com/en/param_XX.asp
- Jiménez-García, J.C., Rivera, W., 2018. Parametric analysis of the performance of an experimental ammonia/lithium nitrate absorption cooling system. *Int. J. Energy Res.* 42, 4402–4416. <https://doi.org/10.1002/er.4185>
- Johnston, A.M., O’Sullivan, C.H., 1981. A Single-Stage Ammonia/Water Absorption Cycle With Integrated Heat Exchange Components. *J. Sol. Energy Eng.* 103. <https://doi.org/10.1115/1.3266205>
- Kalogirou, S., Florides, G., Tassou, S., Wrobel, L., 2001. Design and Construction of a Lithium Bromide Water Absorption Refrigerator, in: CLIMA 2000 World Congress. Napoli, pp. 15–18.
- Kang, Y., Hashiwaki, T., Christensen, R., 1998. Ammonia–water bubble absorber with a plate heat exchanger, in: ASHRAE Trans. pp. 956–966.
- Kang, Y.T., Akisawa, A., Kashiwagi, T., 2000. Analytical investigation of two different absorption modes: falling film and bubble types. *Int. J. Refrig.* 23, 430–443.
- Kang, Y.T., Akisawa, A., Kashiwagi, T., 1999. Experimental correlation of combined heat and mass transfer for NH₃-H₂O falling film absorption. *Int. J. Refrig.* 22, 250–262. [https://doi.org/10.1016/S0140-7007\(98\)00076-0](https://doi.org/10.1016/S0140-7007(98)00076-0)
- Kang, Y.T., Nagano, T., Kashiwagi, T., 2002a. Mass transfer correlation of NH₃-H₂O bubble absorption. *Int. J. Refrig.* 25, 878–886.
- Kang, Y.T., Nagano, T., Kashiwagi, T., 2002b. Visualization of bubble behavior and bubble diameter correlation for NH₃-H₂O bubble absorption. *Int. J. Refrig.* 25, 127–135.
- Karakas, A., Egrican, N., Uygur, S., 1990. Second-Law Analysis of Solar Absorption-Cooling Cycles using Lithium Bromide / Water and Ammonia / Water as Working Fluids Auxiliary source. *Appl. Energy* 37, 169–187. [https://doi.org/10.1016/0306-2619\(90\)90031-8](https://doi.org/10.1016/0306-2619(90)90031-8)
- Karamangil, M.I., Coskun, S., Kaynakli, O., Yamankaradeniz, N., 2010. A simulation study of performance evaluation of single-stage absorption refrigeration system using conventional working fluids and alternatives. *Renew. Sustain. Energy Rev.* 14, 1969–1978. <https://doi.org/10.1016/j.rser.2010.04.008>
- Kareem, Z.S., Mohd Jaafar, M.N., Lazim, T.M., Abdullah, S., Abdulwahid, A.F., 2015. Heat transfer enhancement in two-start spirally corrugated tube. *Alexandria Eng. J.* 54, 415–422. <https://doi.org/10.1016/j.aej.2015.04.001>
- Karno, A., Ajib, S., 2008. Thermodynamic analysis of an absorption refrigeration machine with new working fluid for solar applications. *Heat Mass Transf. und Stoffuebertragung* 45, 71–81. <https://doi.org/10.1007/s00231-008-0408-2>
- Kaushik, S.C., Bhardwaj, S.C., 1982. Theoretical analysis of ammonia-water absorption cycles for refrigeration and space conditioning systems. *Int. J. Energy Res.* 6, 205–225. <https://doi.org/10.1002/er.4440060302>
- Kaushik, S.C., Kumar, R., 1985. Thermodynamic study of a two-stage vapour absorption refrigeration system using NH₃ refrigerant with liquid/solid absorbents. *Energy Convers. Manag.* 25, 427–431.
- Kays, W.M., London, A.L., 1984. Compact heat exchanger. New York: McGraw-Hill.
- Keinath, C.M., Hoysall, D., Delahanty, J.C., Determan, M.D., Garimella, S., 2015. Experimental assessment of a compact branched tray generator for ammonia–water desorption. *Sci. Technol. Built Environ.* 21, 348–356. <https://doi.org/10.1080/23744731.2014.1000797>
- Khamooshi, M., Parham, K., Atikol, U., 2013. Overview of ionic liquids used as working fluids in absorption cycles. *Adv. Mech. Eng.* 2013. <https://doi.org/10.1155/2013/620592>
- Kilic, M., Kaynakli, O., 2007. Second law-based thermodynamic analysis of water-lithium bromide absorption refrigeration system. *Energy* 32, 1505–1512. <https://doi.org/10.1016/j.energy.2006.09.003>
- Killion, J.D., Garimella, S., 2003. Gravity-driven flow of liquid films and droplets in horizontal tube banks. *Int. J. Refrig.* 26, 516–526. [https://doi.org/10.1016/S0140-7007\(03\)00009-4](https://doi.org/10.1016/S0140-7007(03)00009-4)
- Kim, B.J., Kang, I.S., 1995. Absorption of water vapor into wavy-laminar falling film of aqueous lithium-bromide. *KSME J.* 9, 115–122. <https://doi.org/10.1007/BF02954359>
- Kim, D.S., Ferreira, C.A.I., 2008. Flow patterns and heat and mass transfer coefficients of low Reynolds number falling film flows on vertical plates : Effects of a wire screen and an additive. *Int. J. Refrig.* 32, 138–149. <https://doi.org/10.1016/j.ijrefrig.2008.08.005>
- Kim, D.S., Infante Ferreira, C.A., 2009. Air-cooled LiBr-water absorption chillers for solar air conditioning in extremely hot weathers. *Energy Convers. Manag.* 50, 1018–1025. <https://doi.org/10.1016/j.enconman.2008.12.021>
- Kim, J.K., Park, C.W., Kang, Y.T., 2003. The effect of micro-scale surface treatment on heat and mass transfer performance for a falling film H₂O/LiBr absorber. *Int. J. Refrig.* 26, 575–585. [https://doi.org/10.1016/S0140-7007\(02\)00147-0](https://doi.org/10.1016/S0140-7007(02)00147-0)
- Kim, K.J., Berman, N.S., Wood, B.D., 1996. The interfacial turbulence in falling film absorption: Effects of additives. *Int. J. Refrig.* 19, 322–330. [https://doi.org/10.1016/S0140-7007\(96\)00025-4](https://doi.org/10.1016/S0140-7007(96)00025-4)
- Kim, N., 2015. An Experimental Study on the Effect of Low Fin Tube Geometry on Pool Boiling of a LiBr Solution. *Trans. Korean Soc. Mech. Eng.* 39, 591–598.
- Kim, S., 2014. An Absorption Refrigeration System Using Ionic Liquid and Hydrofluorocarbon Working Fluids. Georgia Institute of Technology.
- Kim, S., Kim, Y.J., Joshi, Y.K., Fedorov, A.G., Kohl, P.A., 2012. Absorption Heat Pump/Refrigeration System Utilizing Ionic Liquid and Hydrofluorocarbon Refrigerants. *J. Electron. Packag.* 134, 031009. <https://doi.org/10.1115/1.4007111>

- Kim, S., Kohl, P.A., 2014. Analysis of [hmim][PF₆] and [hmim][Tf₂N] ionic liquids as absorbents for an absorption refrigeration system. *Int. J. Refrig.* 48, 105–113. <https://doi.org/10.1016/j.ijrefrig.2014.09.003>
- Kim, S., Kohl, P.A., 2013. Theoretical and experimental investigation of an absorption refrigeration system using R134a/[bmim][PF₆] working fluid. *Ind. Eng. Chem. Res.* 52, 13459–13465. <https://doi.org/10.1021/ie400985c>
- Kim, S., Patel, N., Kohl, P.A., 2013. Performance Simulation of Ionic Liquid and Hydrofluorocarbon Working Fluids for an Absorption Refrigeration System. *Ind. Eng. Chem. Res.* 52, 6329–6335.
- Kim, Y.J., Gonzalez, M., 2014. Exergy analysis of an ionic-liquid absorption refrigeration system utilizing waste-heat from datacenters. *Int. J. Refrig.* 48, 26–37. <https://doi.org/10.1016/j.ijrefrig.2014.08.008>
- Kim, Y.J., Joshi, Y.K., Fedorov, A.G., 2008. An absorption based miniature heat pump system for electronics cooling. *Int. J. Refrig.* 31, 23–33. <https://doi.org/10.1016/j.ijrefrig.2007.07.003>
- Kim, Y.J., Kim, S., Joshi, Y.K., Fedorov, A.G., Kohl, P.A., 2012. Thermodynamic analysis of an absorption refrigeration system with ionic-liquid/refrigerant mixture as a working fluid. *Energy* 44, 1005–1016. <https://doi.org/10.1016/j.energy.2012.04.048>
- Kim, Y.J., Kim, S., Joshi, Y.K., Fedorov, A.G., Kohl, P.A., 2011. Waste-heat driven miniature absorption refrigeration system using ionic-liquid as a working fluid, in: 5th International Conference on Energy Sustainability. Washington, DC.
- Kiyota, M., Morioka, I., Matsuyama, T., 2003. Steam absorption into aqueous lithium bromide solution films falling inside vertical pipes. *Heat Transf. - Asian Res.* 32, 740–752. <https://doi.org/10.1002/htj.10128>
- Kiyota, M., Morioka, I., Ousaka, A., Fujikawa, K., 1996. Steam Absorption into Films of Aqueous Solution of LiBr Flowing over Multiple Horizontal Pipes. *Heat Transf. - Japanese Res.* 25, 476–485.
- Koehler, J., Tegethoff, W.J., Westphalen, D., Sonnekalb, M., 1997. Absorption refrigeration system for mobile applications utilizing exhaust gases. *Heat Mass Transf.* 32, 333–340. <https://doi.org/10.1007/s002310050130>
- Kohlenbach, P., 2006. Solar cooling with absorption chillers: Control strategies and transient chiller performance. PhD TU Berlin. <https://doi.org/10.14279/depositonce-1364>
- Kohlenbach, P., Ziegler, F., 2008a. A dynamic simulation model for transient absorption chiller performance. Part I: The model. *Int. J. Refrig.* 31, 217–225. <https://doi.org/10.1016/j.ijrefrig.2007.06.009>
- Kohlenbach, P., Ziegler, F., 2008b. A dynamic simulation model for transient absorption chiller performance. Part II: Numerical results and experimental verification. *Int. J. Refrig.* 31, 226–233. <https://doi.org/10.1016/j.ijrefrig.2007.06.010>
- Kotenko, O., Moser, H., Rieberer, R., 2011. Thermodynamic analysis of ammonia/ionic liquid absorption heat pumping processes, in: International Sorption Heat Pump Conference. Padova, Italy, Italy.
- Kouremenos, D.A., Antonopoulos, K.A., Rogdakis, E., 1987. PERFORMANCE OF SOLAR NH₃/H₂O ABSORPTION CYCLES IN THE ATHENS AREA. *Sol. Energy* 39, 187–195.
- Kühn, A., 2013. Thermally driven heat pumps for heating and cooling. Deutsche Nationalbibliothek, Berlin.
- Kühn, A., Meyer, T., Ziegler, F., 2008. Operational results of a 10 kW absorption chiller in heat pump mode, in: 9th International IEA Heat Pump Conference. Zürich, Switzerland.
- Kühn, A., Özgür-Popanda, C., Ziegler, F., 2011. A 10 kW indirectly fired absorption heat pump: concepts for a reversible operation, in: 10th International Heat Pump Conference. Tokyo, Japan.
- Kühn, A., Petersen, S., Ziegler, F., Kohlenbach, P., Harm, M., Schweigler, C., 2005. Operational results of a 10 kW absorption chiller for low-grade driving heat, in: International Sorption Heat Pump Conference. Denver, USA, USA.
- Kwon, K., Jeong, S., 2004. Effect of vapor flow on the falling-film heat and mass transfer of the ammonia/water absorber. *Int. J. Refrig.* 27, 955–964. <https://doi.org/10.1016/j.ijrefrig.2004.06.009>
- Kyung, I.-S., Herold, K.E., 2002. Performance of Horizontal Smooth Tube Absorber With and Without 2-Ethyl-Hexanol. *J. Heat Transfer* 124, 177. <https://doi.org/10.1115/1.1418366>
- Labus, J., Bruno, J.C., Coronas, A., 2013. Performance analysis of small capacity absorption chillers by using different modeling methods. *Appl. Therm. Eng.* 58, 305–313. <https://doi.org/10.1016/j.applthermaleng.2013.04.032>
- Labus, J.M., Bruno, J.C., Coronas, A., 2013. Review on absorption technology with emphasis on small capacity absorption machines. *Therm. Sci.* 17, 739–762. <https://doi.org/10.2298/TSCI120319016L>
- Lazzarin, R.M., Gasparella, A., Longo, G.A., 1996. Ammonia-water absorption machines for refrigeration: theoretical and real performances. *Int. J. Refrig.* 19, 239–246. [https://doi.org/10.1016/0140-7007\(96\)00016-3](https://doi.org/10.1016/0140-7007(96)00016-3)
- Le Lostec, B., Galanis, N., Millette, J., 2013. Simulation of an ammonia-water absorption chiller. *Renew. Energy* 60, 269–283. <https://doi.org/10.1016/j.renene.2013.05.027>
- Le Lostec, B., Galanis, N., Millette, J., 2012. Experimental study of an ammonia-water absorption chiller. *Int. J. Refrig.* 35, 2275–2286. <https://doi.org/10.1016/j.ijrefrig.2012.05.012>
- Le Lostec, B., Millette, J., Galanis, N., 2010. Finite time thermodynamics study and exergetic analysis of ammonia-water absorption systems. *Int. J. Therm. Sci.* 49, 1264–1276. <https://doi.org/10.1016/j.ijthermalsci.2010.02.005>
- Lecuona, A., Ventas, R., Vereda, C., López, R., 2015. Absorption solar cooling systems using optimal driving temperatures. *Appl. Therm. Eng.* 79, 140–148. <https://doi.org/10.1016/j.applthermaleng.2014.10.097>
- Lee, J.C., Lee, K.B., Chun, B.H., Lee, C.H., Ha, J.J., Kim, S.H., 2003. A study on numerical simulations and experiments for mass transfer in bubble mode absorber of ammonia and water. *Int. J. Refrig.* 26, 551–558. [https://doi.org/10.1016/S0140-7007\(03\)00002-1](https://doi.org/10.1016/S0140-7007(03)00002-1)
- Lee, K.B., Chun, B.H., Lee, J.C., Hyun, J.C., Kim, S.H., 2002a. Comparison of heat and mass transfer in falling film and bubble absorbers of ammonia-water. *Exp. Heat Transf.* 15, 191–205. <https://doi.org/10.1080/08916150290082621>
- Lee, K.B., Chun, B.H., Lee, J.C., Lee, C.H., Kim, S.H., 2002b. Experimental analysis of bubble mode in a plate-type absorber. *Chem. Eng. Sci.* 57, 1923–1929. [https://doi.org/10.1016/S0009-2509\(02\)00089-1](https://doi.org/10.1016/S0009-2509(02)00089-1)
- Lee, S., Bohra, L.K., Garimella, S., Nagavarapu, A.K., 2012. Measurement of absorption rates in horizontal-tube falling-film ammonia-water absorbers. *Int. J. Refrig.* 35, 613–632. <https://doi.org/10.1016/j.ijrefrig.2011.08.011>

- Levy, A., Jelinek, M., Borde, I., 2001. Single stage absorption system based on refrigerants R125 and R134a with DMETEG. *J. Mech. Eng.* 47, 497–500.
- Li, M., Xu, C., Hassanién, R.H.E., Xu, Y., Zhuang, B., 2016. Experimental investigation on the performance of a solar powered lithium bromide–water absorption cooling system. *Int. J. Refrig.* 71, 46–59. <https://doi.org/10.1016/j.ijrefrig.2016.07.023>
- Liang, S., Chen, W., Cheng, K., Guo, Y., Gui, X., 2011. The Latent Application of Ionic Liquids in Absorption Refrigeration, in: *Applications of Ionic Liquids in Science and Technology*. pp. 467–494. <https://doi.org/10.5772/1769>
- Liang, S., Chen, W., Guo, Y., Tang, D., 2013. Ionic Liquids Facilitate the Development of Absorption Refrigeration, in: *Ionic Liquids - Current State of the Art*. InTech, pp. 75–100. <https://doi.org/10.5772/58515>
- Liang, S.Q., Zhao, J., Wang, L., Huai, X.L., 2010. Absorption refrigeration cycle utilizing a new working pair of ionic liquid type. *J. Eng. Thermophys.* 31, 1627–1630.
- Lizarte, R., Izquierdo, M., Marcos, J.D., Palacios, E., 2012. An innovative solar-driven directly air-cooled LiBr-H₂O absorption chiller prototype for residential use. *Energy Build.* 47, 1–11. <https://doi.org/10.1016/j.enbuild.2011.11.011>
- Llamas-Guillén, S.U., Cuevas, R., Best, R., Gómez, V.H., 2014. Experimental results of a direct air-cooled ammonia-lithium nitrate absorption refrigeration system. *Appl. Therm. Eng.* 67, 362–369. <https://doi.org/10.1016/j.applthermaleng.2014.03.050>
- Llamas, S.U., Herrera, J.V., Cuevas, R., Gómez, V.H., García-Valladares, O., Cerezo, J., Best, R., 2007. Development of a small capacity ammonia-lithium nitrate absorption refrigeration system, in: *2nd International Conference Solar Air-Conditioning*. Regensburg, Germany, pp. 470–475.
- Mahvi, A.J., Garimella, S., 2017. Visualization of flow distribution in rectangular and triangular header geometries. *Int. J. Refrig.* 76, 170–183. <https://doi.org/10.1016/j.ijrefrig.2017.02.002>
- Mansoori, G.A., Patel, V., 1979. Thermodynamic basis for the choice of working fluids for solar absorption cooling systems. *Sol. Energy* 22, 483–491. [https://doi.org/10.1016/0038-092X\(79\)90020-3](https://doi.org/10.1016/0038-092X(79)90020-3)
- Marc, O., Lucas, F., Sinama, F., Monceyron, E., 2010. Experimental investigation of a solar cooling absorption system operating without any backup system under tropical climate. *Energy Build.* 42, 774–782. <https://doi.org/10.1016/j.enbuild.2009.12.006>
- Marc, O., Sinama, F., Praene, J.P., Lucas, F., Castaing-Lasvignottes, J., 2015. Dynamic modeling and experimental validation elements of a 30 kW LiBr/H₂O single effect absorption chiller for solar application. *Appl. Therm. Eng.* 90, 980–993. <https://doi.org/10.1016/j.applthermaleng.2015.07.067>
- Marcos, J.D., Izquierdo, M., Palacios, E., 2011. New method for COP optimization in water- and air-cooled single and double effect LiBr-water absorption machines. *Int. J. Refrig.* 34, 1348–1359. <https://doi.org/10.1016/j.ijrefrig.2011.03.017>
- Martín, Á., Bermejo, M.D., 2010. Thermodynamic analysis of absorption refrigeration cycles using ionic liquid + supercritical CO₂ pairs. *J. Supercrit. Fluids* 55, 852–859. <https://doi.org/10.1016/j.supflu.2010.10.012>
- Martínez, J.C., Martínez, P.J., Bujedo, L.A., 2016. Development and experimental validation of a simulation model to reproduce the performance of a 17.6 kW LiBr-water absorption chiller. *Renew. Energy* 86, 473–482. <https://doi.org/10.1016/j.renene.2015.08.049>
- Martínez, P.J., Martínez, J.C., Lucas, M., 2012. Design and test results of a low-capacity solar cooling system in Alicante (Spain). *Sol. Energy* 86, 2950–2960. <https://doi.org/10.1016/j.solener.2012.06.030>
- Matsuda, A., Choi, K.H., Hada, K., Kawamura, T., 1994. Effect of pressure and concentration on performance of a vertical falling-film type of absorber and generator using lithium bromide aqueous solutions. *Int. J. Refrig.* 17, 538–542. [https://doi.org/10.1016/0140-7007\(94\)90030-2](https://doi.org/10.1016/0140-7007(94)90030-2)
- Meacham, J.M., Garimella, S., 2004. Ammonia-water absorption heat and mass transfer in microchannel absorbers with visual confirmation, in: *ASHRAE Trans.* pp. 525–532.
- Meacham, J.M., Garimella, S., 2003. Modeling of local measured heat and mass transfer variations in a microchannel ammonia-water absorber, in: *ASHRAE Trans.* pp. 412–422.
- Meacham, J.M., Garimella, S., 2002. Experimental demonstration of a prototype microchannel absorber for space-conditioning systems, in: *International Sorption Heat Pump Conference*. Shanghai, China, China, pp. 270–276.
- Medrano, M., Bourouis, M., Coronas, A., 2002. Absorption of water vapour in the falling film of water-lithium bromide inside a vertical tube at air-cooling thermal conditions. *Int. J. Therm. Sci.* 41, 891–898. [https://doi.org/10.1016/S1290-0729\(02\)01383-2](https://doi.org/10.1016/S1290-0729(02)01383-2)
- Medrano, M., Bourouis, M., Coronas, A., 2001. Double-lift absorption refrigeration cycles driven by low-temperature heat sources using organic fluid mixtures as working pairs. *Appl. Energy* 68, 173–185. [https://doi.org/10.1016/S0306-2619\(00\)00048-9](https://doi.org/10.1016/S0306-2619(00)00048-9)
- Mendes, L.F., Collares-Pereira, M., Ziegler, F., 2007. A rich solution spray as a refining method in a small capacity, single effect, solar assisted absorption machine with the pair NH₃/H₂O: Experimental results. *Energy Convers. Manag.* 48, 2996–3000. <https://doi.org/10.1016/j.enconman.2007.06.037>
- Michel, B., Le Pierrès, N., Stutz, B., 2017. Performances of grooved plates falling film absorber. *Energy* 138, 103–117. <https://doi.org/10.1016/j.energy.2017.07.026>
- Miller, W. a, Perez-Blanco, H., 1994. Vertical-tube aqueous LiBr falling film absorption using advanced surfaces. *Int. Absorption Heat Pump Conf.* 185–202.
- Miller, W.A., Keyhani, M., 2001. The Correlation of Simultaneous Heat and Mass Transfer Experimental Data for Aqueous Lithium Bromide Vertical Falling Film Absorption. *J. Sol. Energy Eng.* 123, 30. <https://doi.org/10.1115/1.1349550>
- Mittermaier, M., Ziegler, F., 2015. Theoretical evaluation of absorption and desorption processes under typical conditions for chillers and heat transformers. *Int. J. Refrig.* 59, 91–101. <https://doi.org/10.1016/j.ijrefrig.2015.07.015>
- Monné, C., Alonso, S., Palacín, F., Serra, L., 2011. Monitoring and simulation of an existing solar powered absorption cooling system in Zaragoza (Spain). *Appl. Therm. Eng.* 31, 28–35. <https://doi.org/10.1016/j.applthermaleng.2010.08.002>
- Moreno, D., Ferro, V.R., de Riva, J., Santiago, R., Moya, C., Larriba, M., Palomar, J., 2018. Absorption refrigeration cycles based on ionic liquids: Refrigerant/absorbent selection by thermodynamic and process analysis. *Appl. Energy* 213, 179–194. <https://doi.org/10.1016/j.apenergy.2018.01.034>
- Morioka, I., Kiyota, M., Ousaka, A., Kobayashi, T., 1992. Analysis of steam absorption by a subcooled droplet of aqueous solution of LiBr. *JSME Int. J.* 35, 458–464. <https://doi.org/10.1248/cpb.37.3229>

- Mortazavi, M., Nasr Isfahani, R., Bigham, S., Moghaddam, S., 2015. Absorption characteristics of falling film LiBr (lithium bromide) solution over a finned structure. *Energy* 87, 270–278. <https://doi.org/10.1016/j.energy.2015.04.074>
- Mouchka, G., Apreotesi, M., Davis, K., Pence, D., 2007. Co-flowing of ammonia desorption in a fractal-like branching heat exchanger, in: *Proceedings of IPACK2007*. ASME, Vancouver, Canada.
- Muthu, V., Saravanan, R., Renganarayanan, S., 2008. Experimental studies on R134a-DMAC hot water based vapour absorption refrigeration systems. *Int. J. Therm. Sci.* 47, 175–181. <https://doi.org/10.1016/j.ijthermalsci.2007.02.004>
- Nagavarapu, A.K., Garimella, S., 2011a. Design of Microscale Heat and Mass Exchangers for Absorption Space Conditioning Applications. *J. Therm. Sci. Eng. Appl.* 3. <https://doi.org/10.1115/1.4003720>
- Nagavarapu, A.K., Garimella, S., 2011b. Design of Microscale Heat and Mass Exchangers for Absorption Space Conditioning Applications. *J. Therm. Sci. Eng. Appl.* 3, 021005. <https://doi.org/10.1115/1.4003720>
- Nakahara, N., Miyakawa, Y., Yamamoto, M., 1977. Experimental study on house cooling and heating with solar energy using flat plate collector. *Sol. Energy* 19, 657–662. [https://doi.org/10.1016/0038-092X\(77\)90026-3](https://doi.org/10.1016/0038-092X(77)90026-3)
- Nakoryakov, V.E., Grigor'eva, N.I., 1977. Combined heat and mass transfer during absorption in drops and films. *J. Eng. Phys.* 32, 243–247. <https://doi.org/10.1007/BF00865776>
- Narayanan, V., Kanury, A.M., Jenks, J., 2009. Heat Exchanger Analysis Modified to Account for a Heat Source, in: *ASME/JSME 2007 Thermal Engineering Heat Transfer Summer Conference Collocated with the ASME 2007 InterPACK Conference*. American Society of Mechanical Engineers Digital Collection, Vancouver, Canada, pp. 1063–1068.
- Nasr Isfahani, R., Bigham, S., Mortazavi, M., Wei, X., Moghaddam, S., 2015. Impact of micromixing on performance of a membrane-based absorber. *Energy* 90, 997–1004. <https://doi.org/10.1016/j.energy.2015.08.006>
- Nasr Isfahani, R., Fazeli, A., Bigham, S., Moghaddam, S., 2014. Physics of lithium bromide (LiBr) solution dewatering through vapor venting membranes. *Int. J. Multiph. Flow* 58, 27–38. <https://doi.org/10.1016/j.ijmultiphaseflow.2013.08.005>
- Nasr Isfahani, R., Moghaddam, S., 2013. Absorption characteristics of lithium bromide (LiBr) solution constrained by superhydrophobic nanofibrous structures. *Int. J. Heat Mass Transf.* 63, 82–90. <https://doi.org/10.1016/j.ijheatmasstransfer.2013.03.053>
- Nasr Isfahani, R., Sampath, K., Moghaddam, S., 2013. Nanofibrous membrane-based absorption refrigeration system. *Int. J. Refrig.* 36, 2297–2307. <https://doi.org/10.1016/j.ijrefrig.2013.07.019>
- Ng, K.C., Bong, T.Y., Chua, H.T., Bao, H.L., 1994. Theoretical and experimental analysis of an absorption chiller. *Int. J. Refrig.* 17, 351–358. [https://doi.org/10.1016/0140-7007\(94\)90066-3](https://doi.org/10.1016/0140-7007(94)90066-3)
- Obame Mve, H., 2014. Compréhension des écoulements et optimisation des transferts de chaleur et de masse au sein d'une structure capillaire. PhD Thesis INSA Lyon.
- Obame Mve, H., Rullière, R., Goulet, R., Haberschill, P., 2014. Numerical Analysis of Heat Transfer of a Flow Confined by Wire Screen in Lithium Bromide Absorption Process. *Defect Diffus. Forum* 348, 40–50. <https://doi.org/10.4028/www.scientific.net/DDF.348.40>
- Obame Mve, H., Rullière, R., Haberschill, P., 2015. Modeling and Parametric Study of the Heat Transfer Inside a Lithium Bromide Flow Confined by Wire Screen. *J. Energy Power Eng.* 9, 417–425. <https://doi.org/10.17265/1934-8975/2015.05.001>
- Ohuchi, T., Aizawa, M., Kawakami, R., Nishiguchi, A., Hatada, T., Kunugi, Y., 1994. A Study on a Hot-Water Driven Air-Cooled Absorption Refrigerating Machine. *Int. Refrig. Air Cond. Conf.* 275–280.
- Ornel, C., Amaris, C., Bourouis, M., Vallès, M., 2013. Heat and mass transfer in a bubble plate absorber with $\text{NH}_3/\text{LiNO}_3$ and $\text{NH}_3/(\text{LiNO}_3 + \text{H}_2\text{O})$ mixtures. *Int. J. Therm. Sci.* 63, 105–114. <https://doi.org/10.1016/j.ijthermalsci.2012.07.007>
- Osta-Omar, S.M., Micallef, C., 2017. Effect of the Vapour-Solution Interface Area on a Miniature Lithium-Bromide/Water Absorption Refrigeration System Equipped with an Adiabatic Absorber, in: *2nd International Conference on Advances on Clean Energy Research*. Berlin, Germany, pp. 243–247. <https://doi.org/10.1016/j.egypro.2017.07.009>
- Palacios, E., Izquierdo, M., Lizarte, R., Marcos, J.D., 2009a. Lithium bromide absorption machines: Pressure drop and mass transfer in solutions conical sheets. *Energy Convers. Manag.* 50, 1802–1809. <https://doi.org/10.1016/j.enconman.2009.03.023>
- Palacios, E., Izquierdo, M., Marcos, J.D., Lizarte, R., 2009b. Evaluation of mass absorption in LiBr flat-fan sheets. *Appl. Energy* 86, 2574–2582. <https://doi.org/10.1016/j.apenergy.2009.04.033>
- Paniev, G.A., 1983. Absorption heat and mass transfer on droplets in a polydispersed spray. *Heat Transf. Sov. Res.* 15, 62–72.
- Parham, K., Atikol, U., Yari, M., Agboola, O.P., 2013. Evaluation and optimization of single stage absorption chiller using $(\text{LiCl} + \text{H}_2\text{O})$ as the working pair. *Adv. Mech. Eng.* 2013. <https://doi.org/10.1155/2013/683157>
- Patel, J., Pandya, B., Mudgal, A., 2017. Exergy Based Analysis of $\text{LiCl-H}_2\text{O}$ Absorption Cooling System, in: *International Conference on Recent Advancement in Air Conditioning and Refrigeration*. Pp. 261–269. <https://doi.org/10.1016/j.egypro.2017.03.061>
- Patil, K.R., Chaudhari, S.K., Katti, S.S., 1991. Thermodynamic design data for absorption heat pump systems operating on water-lithium iodide-Part I. Cooling*. *Heat Recover. Syst. CHP* 11, 341–350.
- Pence, D., 2010. The simplicity of fractal-like flow networks for effective heat and mass transport. *Exp. Therm. Fluid Sci.* 34, 474–486. <https://doi.org/10.1016/j.expthermflusci.2009.02.004>
- Perez-Blanco, H., 1984. Absorption heat pump performance for different types of solutions. *Int. J. Refrig.* 7, 115–122.
- Pilatowsky, I., Rivera, W., Romero, R.J., 2001. Thermodynamic analysis of monomethylamine-water solutions in a single-stage solar absorption refrigeration cycle at low generator temperatures. *Sol. Energy Mater. Sol. Cells* 70, 287–300. [https://doi.org/10.1016/S0927-0248\(01\)00071-X](https://doi.org/10.1016/S0927-0248(01)00071-X)
- PINK, 2012. Absorption chiller PinkChiller PC19 (English).
- Pongtornkulpanich, A., Thepa, S., Amornkitbamrung, M., Butcher, C., 2008. Experience with fully operational solar-driven 10-ton $\text{LiBr}/\text{H}_2\text{O}$ single-effect absorption cooling system in Thailand. *Renew. Energy* 33, 943–949. <https://doi.org/10.1016/j.renene.2007.09.022>
- Pons, M., Anies, G., Boudehenn, F., Bourdoukan, P., Castaing-lasvignottes, J., Evola, G., Le Denn, A., Le Pierrès, N., Marc, O., Mazet, N., Stitou, D., Lucas, F., 2012. Performance comparison of six solar-powered air-conditioners operated in five places. *Energy* 46, 471–483. <https://doi.org/10.1016/j.energy.2012.08.002>

- Prabhanjan, D.G., Raghavan, G.S. V., Rennie, T.J., 2002. Comparison of heat transfer rates between a straight tube heat exchanger and a helically coiled heat exchanger. *Int. Commun. Heat Mass Transf.* 29, 185–191. [https://doi.org/10.1016/S0735-1933\(02\)00309-3](https://doi.org/10.1016/S0735-1933(02)00309-3)
- Præne, J.P., Marc, O., Lucas, F., Miranville, F., 2011. Simulation and experimental investigation of solar absorption cooling system in Reunion Island. *Appl. Energy* 88, 831–839. <https://doi.org/10.1016/j.apenergy.2010.09.016>
- Prasartkaew, B., 2014. Performance test of a small size LiBr-H₂O absorption chiller. *Energy Procedia* 56, 487–497. <https://doi.org/10.1016/j.egypro.2014.07.183>
- Prasartkaew, B., Kumar, S., 2013. Experimental study on the performance of a solar-biomass hybrid air-conditioning system. *Renew. Energy* 57, 86–93. <https://doi.org/10.1016/j.renene.2013.01.034>
- Prasartkaew, B., Kumar, S., 2010. A low carbon cooling system using renewable energy resources and technologies. *Energy Build.* 42, 1453–1462. <https://doi.org/10.1016/j.enbuild.2010.03.015>
- PURIX ApS, 2018. Product catalogue A25 EN ver01a.
- Radspieler, M., Schweigler, C., 2011. Experimental investigation of ionic liquid Emim EtSO₄ as solvent in a single-effect cycle with adiabatic absorption and desorption, in: *International Sorption Heat Pump Conference*. Padua, Italy, Italy, pp. 125–34.
- Riffat, S.B., Wu, S., Bol, B., 2004. Pervaporation membrane process for vapour absorption system. *Int. J. Refrig.* 27, 604–611. <https://doi.org/10.1016/j.ijrefrig.2004.03.005>
- Rivera, W., Best, R., 1999. Boiling heat transfer coefficients inside a vertical smooth tube for water/ammonia and ammonia/lithium nitrate mixtures. *Int. J. Heat Mass Transf.* 42, 905–921. [https://doi.org/10.1016/S0017-9310\(98\)00211-7](https://doi.org/10.1016/S0017-9310(98)00211-7)
- Robeson, L.M., 1999. Polymer membranes for gas separation. *Curr. Opin. Solid State Mater. Sci.* 4, 549–552. [https://doi.org/10.1016/S1359-0286\(00\)00014-0](https://doi.org/10.1016/S1359-0286(00)00014-0)
- ROBUR, 2017. Manuale di progettazione.
- Rogdakis, E.D., Antonopoulos, K.A., 1995. Thermodynamic cycle, correlations and nomograph for NH₃-NaSCN absorption refrigeration systems. *Heat Recover. Syst. CHP* 15, 591–599. [https://doi.org/10.1016/0890-4332\(95\)90069-1](https://doi.org/10.1016/0890-4332(95)90069-1)
- Rodríguez Carabias, J.A., 2014. Desarrollo de un banco de ensayos multifuncional y de los procedimientos para caracterizar equipos térmicos de refrigeración y bombas de calor de pequeña potencia. PhD Universitat Rovira i Virgili.
- Romero, R.J., Guillen, L., Pilatowsky, I., 2005. Monomethylamine-water vapour absorption refrigeration system. *Appl. Therm. Eng.* 25, 867–876. <https://doi.org/10.1016/j.applthermaleng.2004.08.007>
- Römich, C., Merkel, N., Schaber, K., Schubert, T., Koch, M., 2011. Comparison between lithiumbromide-water and ionic liquid-water as working solution for absorption refrigeration cycles., in: *International Congress of Refrigeration*. Prague, Czech Republic, p. 287.
- Roriz, L., Mortal, A., Mendes, L.F., 2004. Study of a plate heat exchanger desorber with a spray column for a small solar powered absorption machine, in: *3rd International Conference on Heat Powered Cycles*. Cyprus.
- Rossi, F., Filipponi, M., Presciutti, A., 2005. Ultrasonic vibrations for improving absorption chillers performances, in: *IASME TRANSACTIONS*.
- ROTARTICA, n.d. ROTARTICA SOLAR 045v - INSTALLATION AND MAINTENANCE MANUAL.
- Ruiz, E., Ferro, V.R., De Riva, J., Moreno, D., Palomar, J., 2014. Evaluation of ionic liquids as absorbents for ammonia absorption refrigeration cycles using COSMO-based process simulations. *Appl. Energy* 123, 281–291. <https://doi.org/10.1016/j.apenergy.2014.02.061>
- Ryan, W., Ruiz, F., Wurm, J., 1995. Model development and verification of spray absorption for gas driven cooling systems, in: *International Gas Research Conference*. pp. 126–136.
- Ryan, W.A., 1994. Water absorption in an adiabatic spray of aqueous lithium bromide solution, in: *International Absorption Heat Pump Conference*. pp. 155–162.
- Said, S.A.M., El-Shaarawi, M.A.I., Siddiqui, M.U., 2015. Analysis of a solar powered absorption system. *Energy Convers. Manag.* 97, 243–252. <https://doi.org/10.1016/j.enconman.2015.03.046>
- Said, S.A.M., Spindler, K., El-Shaarawi, M.A., Siddiqui, M.U., Schmid, F., Bierling, B., Khan, M.M.A., 2016. Design, construction and operation of a solar powered ammonia-water absorption refrigeration system in Saudi Arabia. *Int. J. Refrig.* 62, 222–231. <https://doi.org/10.1016/j.ijrefrig.2015.10.026>
- Sakura Corporation, 2010. Absorption Chiller Heat Pump 2010.
- Salgado, R., Burguete, A., Rodríguez, M.C., Rodríguez, P., 2008. Simulation of an absorption based solar cooling facility using a geothermal sink for heat rejection, in: *Proceedings of The First International Conference on Solar Heating, Cooling and Buildings, EUROSUN*. Lisbon, Portugal.
- Salim, M., 2001. Technical Potential for Thermally Driven Mobile A/C Systems. *SAE Tech. Pap. Ser.* 1–12. <https://doi.org/10.4271/2001-01-0297>
- Sánchez, J., Reséndiz, C., Rodríguez, M., Rivera, W., 2017. Análisis de un generador horizontal de un sistema de refrigeración solar por absorción. *Rev. Ing. Mecánica* 1, 1–9.
- Saravanan, R., Maiya, M.P., 1998. Thermodynamic comparison of water based working fluid combinations for a vapor absorption refrigeration system. *Appl. Therm. Eng.* 18, 553–568.
- Scammells, P.J., Scott, J.L., Singer, R.D., 2005. Ionic liquids: The neglected issues. *Aust. J. Chem.* 58, 155–169. <https://doi.org/10.1071/CH04272>
- Schaal, F., Weimer, T., Hasse, H., 2008. Membrane Contactors for Absorption Refrigeration, in: *International Sorption Heat Pump Conference*. Seoul, Korea.
- Schaal, F., Weimer, T., Stroh, N., Walitza, E., Mattes, H., Hasse, H., 2015. Membrane contactors for absorption refrigeration, in: *10th Aachen Membrane Colloquium*. Aachen, pp. 529–538.
- Seddon, K.R., 2003. Ionic liquids: A taste of the future. *Nat. Mater.* 2, 363–365. <https://doi.org/10.1038/nmat907>
- Seiler, M., Kühn, A., Ziegler, F., Wang, X., 2013. Sustainable cooling strategies using new chemical system solutions. *Ind. Eng. Chem. Res.* 52, 16519–16546.

- Sel, K., Demirci, S., Ozturk, O.F., Aktas, N., Sahiner, N., 2015. NH₃ gas sensing applications of metal organic frameworks. *Microelectron. Eng.* 136, 71–76. <https://doi.org/10.1016/j.mee.2015.04.035>
- Sen, M., Paolucci, S., 2006. Using carbon dioxide and ionic liquids for absorption refrigeration, in: 7th IIR Gustav Lorentzen Conference on Natural Working Fluids. Trondheim, Norway, pp. 160–163.
- Shandong Lucy New Energy Technology Co. LTD, 2014. Product Catalog.
- She, X., Yin, Y., Xu, M., Zhang, X., 2015. A novel low-grade heat-driven absorption refrigeration system with LiCl-H₂O and LiBr-H₂O working pairs. *Int. J. Refrig.* 58, 219–234. <https://doi.org/10.1016/j.ijrefrig.2015.06.016>
- Shelide, B., 2006. Study of ionic liquid applications in absorption refrigeration. University of Notre Dame: Notre Dame, IN.
- Shi, C., Chen, Q., Jen, T.C., Yang, W., 2010. Heat transfer performance of lithium bromide solution in falling film generator. *Int. J. Heat Mass Transf.* 53, 3372–3376. <https://doi.org/10.1016/j.ijheatmasstransfer.2010.02.051>
- Shiflett, M., Yokozeki, A., 2013. Absorption cycle utilizing ionic liquid and water as working fluids. US00850 6839B2. [https://doi.org/10.1016/j.\(73\)](https://doi.org/10.1016/j.(73))
- Shiflett, M., Yokozeki, A., 2006. Absorption cycle using ionic liquids as working fluid. WO 2006/08426A1.
- Shiflett, M.B., Yokozeki, A., 2005. Solubilities and Diffusivities of Carbon Dioxide in Ionic Liquids: [bmim][PF 6] and [bmim][BF 4]. *Ind. Eng. Chem. Res.* 44, 4453–4464. <https://doi.org/10.1021/ie058003d>
- Shiran, Y., Shitzer, A., Degani, D., 1982. Computerized Design and Economic Evaluation of an Aqua-Ammonia Solar Operated Absorption System. *Sol. Energy* 29, 43–54.
- Sieres, J., Fernández-Seara, J., 2006. Evaluation of the column components size on the vapour enrichment and system performance in small power NH₃-H₂O absorption refrigeration machines. *Int. J. Refrig.* 29, 579–588. <https://doi.org/10.1016/j.ijrefrig.2005.10.004>
- Sim, Y.-S., Kim, N.-H., 2015a. Pool boiling performance of lithium bromide solution on enhanced tubes. *J. Mech. Sci. Technol.* 29, 2555–2563. <https://doi.org/10.1007/s12206-015-0550-y>
- Sim, Y.-S., Kim, N.-H., 2015b. Pool Boiling Performance of Enhanced Tubes for the Generator of an Absorption Chiller. *J. Korea Acad. Coop. Soc.* 16, 1684–1691. <https://doi.org/10.5762/KAIS.2015.16.3.1684>
- SolarNext AG, 2008a. chillii@ PSC10 - Absorption Chiller - Technical Data.
- SolarNext AG, 2008b. chillii@ PSC12 - Absorption Chiller - Technical Data.
- SONNENKLIMA, 2009. SONNENKLIMA package solution description.
- Sözen, A., Altiparmak, D., Usta, H., 2002. Development and testing of a prototype of absorption heat pump system operated by solar energy. *Appl. Therm. Eng.* 22, 1847–1859. [https://doi.org/10.1016/S0960-1481\(01\)00093-3](https://doi.org/10.1016/S0960-1481(01)00093-3)
- Srikhirin, P., Aphornratana, S., Chungpaibulpatana, S., 2001. A review of absorption refrigeration technologies. *Renew. Sustainable Energy Rev.* 5, 343–372.
- Staedter, M.A., Garimella, S., 2018. Development of a micro-scale heat exchanger based, residential capacity ammonia-water absorption chiller. *Int. J. Refrig.* 89, 93–103. <https://doi.org/10.1016/j.ijrefrig.2018.02.016>
- Sterner, D., Sunden, B., 2006. Performance of plate heat exchangers for evaporation of ammonia. *Heat Transf. Eng.* 27, 45–55. <https://doi.org/10.1080/01457630600559611>
- Stutz, B., Altamirano, A., Stepec, M., Le Pierrès, N., 2016. Falling film evaporators (in French), in: *Congrès Société Française de Thermique*, May 31 - June 3. Toulouse, pp. 1–8.
- Sujatha, I., Venkatarathnam, G., 2018. Comparison of performance of a vapor absorption refrigeration system operating with some hydrofluorocarbons and hydrofluoroolefins as refrigerants along with ionic liquid [hmim][TF₂N] as the absorbent. *Int. J. Refrig.* 88, 370–382. <https://doi.org/10.1016/j.ijrefrig.2018.03.004>
- Summerer, F., Alefeld, F., Zeigler, F., Riesch, P., 1996. Hydroxide absorption heat pumps with spray absorber, in: *American Society of Heating, Refrigerating and Air-Conditioning Engineers, Inc.* Atlanta, GA, p. No. CONF-960254.
- Sun, D.-W., 1997. Thermodynamic design data and optimum design maps for absorption refrigeration systems. *Appl. Therm. Eng.* 17, 211–221. [https://doi.org/10.1016/S1359-4311\(96\)00041-5](https://doi.org/10.1016/S1359-4311(96)00041-5)
- Sun, D., 1998. Comparison of the performances of NH₃-H₂O, NH₃-LiNO₃ and NH₃-NaSCN absorption refrigeration systems. *Energy Convers. Manag.* 39, 357–368.
- Sun, J., Fu, L., Zhang, S., 2012. A review of working fluids of absorption cycles. *Renew. Sustain. Energy Rev.* 16, 1899–1906. <https://doi.org/10.1016/j.rser.2012.01.011>
- Swartman, R.K., 1975. COMPARISON OF AMMONIA-WATER AND AMMONIA-SODIUM THIOCYANATE AS THE REFRIGERANT-ABSORBENT IN A SOLAR REFRIGERATION SYSTEM. *Sol. Energy* 17, 123–127.
- Syed, A., Izquierdo, M., Rodríguez, P., Maidment, G., Missenden, J., Lecuona, A., Tozer, R., 2005. A novel experimental investigation of a solar cooling system in Madrid. *Int. J. Refrig.* 28, 859–871. <https://doi.org/10.1016/j.ijrefrig.2005.01.007>
- Táboas, F., 2006. Estudio del proceso de ebullición forzada de la mezcla amoniaco/agua en intercambiadores de placas para equipos de refrigeración por absorción. PhD Universitat Rovira i Virgili.
- Táboas, F., Bourouis, M., Valles, M., 2016. Boiling heat transfer and pressure drop of NH₃/LiNO₃ and NH₃/(LiNO₃+H₂O) in a plate heat exchanger. *Int. J. Therm. Sci.* 105, 182–194. <https://doi.org/10.1016/j.ijthermalsci.2016.02.003>
- Táboas, F., Bourouis, M., Vallès, M., 2014. Analysis of ammonia/water and ammonia/salt mixture absorption cycles for refrigeration purposes in fishing ships. *Appl. Therm. Eng.* 66, 603–611. <https://doi.org/10.1016/j.applthermaleng.2014.02.065>
- Táboas, F., Vallès, M., Bourouis, M., Coronas, A., 2012. Assessment of boiling heat transfer and pressure drop correlations of ammonia/water mixture in a plate heat exchanger. *Int. J. Refrig.* 35, 633–644. <https://doi.org/10.1016/j.ijrefrig.2011.10.003>
- Táboas, F., Vallès, M., Bourouis, M., Coronas, A., 2010. Flow boiling heat transfer of ammonia/water mixture in a plate heat exchanger. *Int. J. Refrig.* 33, 695–705. <https://doi.org/10.1016/j.ijrefrig.2009.12.005>
- Taha Al-Zubaydi, A.Y., 2011. Solar Air Conditioning and Refrigeration with Absorption Chillers Technology in Australia – An Overview on Researches and Applications. *J. Adv. Sci. Eng. Res.* 1, 23–41.
- THERMAX, 2010. LT Series Catalog.

- Thonon, B., 1995. Design method for plate evaporators and condensers, in: 1st Int. Conf. Process Intensification for the Chemical Industry. pp. 37–47.
- Thonon, M., Aiane, M., Bouyaud, M., Boudard, E., Stutz, B., 2018. Etude du comportement d'un évaporateur adiabatique à films tombants entre grilles, in: Congrès Société Française de Thermique. Pau, France.
- Thorud, J.D., Liburdy, J.A., Pence, D. V., 2006. Microchannel membrane separation applied to confined thin film desorption. *Exp. Therm. Fluid Sci.* 30, 713–723. <https://doi.org/10.1016/j.exptthermflusci.2006.03.001>
- Tranter Solarice, 2012a. XS30 Absorption Cooling System.
- Tranter Solarice, 2012b. XS50 Absorption Cooling System.
- Triché, D., Bonnot, S., Perier-Muzet, M., Boudéhenn, F., Demasles, H., Caney, N., 2017. Experimental and numerical study of a falling film absorber in an ammonia-water absorption chiller. *Int. J. Heat Mass Transf.* 111, 374–385. <https://doi.org/10.1016/j.ijheatmasstransfer.2017.04.008>
- Triché, D., Bonnot, S., Perier-Muzet, M., Boudéhenn, F., Demasles, H., Caney, N., 2016. Modeling and Experimental Study of an Ammonia-water Falling Film Absorber. *Energy Procedia* 91, 857–867. <https://doi.org/10.1016/j.egypro.2016.06.252>
- Tsai, B. Bin, Horacio, P.B., 1998. Limits of mass transfer enhancement in lithium bromide-water absorbers by active techniques. *Int. J. Heat Mass Transf.* 41, 2409–2416. [https://doi.org/10.1016/S0017-9310\(97\)00287-1](https://doi.org/10.1016/S0017-9310(97)00287-1)
- Tyagi, K.P., 1984. Ammonia-salts vapour absorption refrigeration systems. *J. Heat Recover. Syst.* 4, 427–431. [https://doi.org/10.1016/0198-7593\(84\)90079-1](https://doi.org/10.1016/0198-7593(84)90079-1)
- Ullah, K.R.R., Saidur, R., Ping, H.W.W., Akikur, R.K.K., Shuvo, N.H.H., 2013. A review of solar thermal refrigeration and cooling methods. *Renew. Sustain. Energy Rev.* 24, 499–513. <https://doi.org/10.1016/j.rser.2013.03.024>
- Uppal, A.H., Norton, B., Probert, S.D., 1986. A Low-Cost Solar-Energy Stimulated Absorption Refrigerator for Vaccine Storage. *Appl. Energy* 25, 167–174.
- Van Rooyen, E., 2011. Boiling on a Tube Bundle : Heat Transfer , Pressure Drop and Flow Patterns. PhD École Polytechnique Fédérale de Lausanne.
- Varma, H.K., Mehrotra, R.K., Agrawal, K.N., Singh, S., 1994. Heat transfer during pool boiling of LiBr-water solutions at subatmospheric pressures. *Int. Commun. Heat Mass Transf.* 21, 539–548. [https://doi.org/10.1016/0735-1933\(94\)90053-1](https://doi.org/10.1016/0735-1933(94)90053-1)
- Venegas, M., Arzoz, D., Rodríguez, P., Izquierdo, M., 2003. Heat and mass transfer in LiNO₃-NH₃ spray absorption system. *Int. Commun. Heat Mass Transf.* 30, 805–815. [https://doi.org/10.1016/S0735-1933\(03\)00128-3](https://doi.org/10.1016/S0735-1933(03)00128-3)
- Venegas, M., De Vega, M., García-Hernando, N., 2016a. Parametric study of operating and design variables on the performance of a membrane-based absorber. *Appl. Therm. Eng.* 98, 409–419. <https://doi.org/10.1016/j.applthermaleng.2015.12.074>
- Venegas, M., de Vega, M., García-Hernando, N., Ruiz-Rivas, U., 2017. Adiabatic vs non-adiabatic membrane-based rectangular micro-absorbers for H₂O-LiBr absorption chillers. *Energy* 134, 757–766. <https://doi.org/10.1016/j.energy.2017.06.068>
- Venegas, M., de Vega, M., García-Hernando, N., Ruiz-Rivas, U., 2016b. A simple model to predict the performance of a H₂O-LiBr absorber operating with a microporous membrane. *Energy* 96, 383–393. <https://doi.org/10.1016/j.energy.2015.12.059>
- Venegas, M., Izquierdo, M., Rodríguez, P., Lecuona, A., 2004. Heat and mass transfer during absorption of ammonia vapour by LiNO₃-NH₃ solution droplets. *Int. J. Heat Mass Transf.* 47, 2653–2667. <https://doi.org/10.1016/j.ijheatmasstransfer.2003.12.014>
- Venegas, M., Rodríguez, P., Lecuona, A., Izquierdo, M., 2005. Spray absorbers in absorption systems using lithium nitrate-ammonia solution. *Int. J. Refrig.* 28, 554–564. <https://doi.org/10.1016/j.ijrefrig.2004.10.005>
- Venegas, M., Zacarías, A., Vereda, C., Lecuona, A., Ventas, R., 2012. Subcooled and saturated boiling of ammonia-lithium nitrate solution in a plate-type generator for absorption machines. *Int. J. Heat Mass Transf.* 55, 4914–4922. <https://doi.org/10.1016/j.ijheatmasstransfer.2012.04.061>
- Ventas, R., Lecuona, A., Legrand, M., Rodríguez-Hidalgo, M.C., 2010. On the recirculation of ammonia-lithium nitrate in adiabatic absorbers for chillers. *Appl. Therm. Eng.* 30, 2770–2777. <https://doi.org/10.1016/j.applthermaleng.2010.08.001>
- Ventas, R., Vereda, C., Lecuona, A., Venegas, M., Rodríguez-Hidalgo, M.D.C., 2012. Effect of the NH₃-LiNO₃ concentration and pressure in a fog-jet spray adiabatic absorber. *Appl. Therm. Eng.* 37, 430–437. <https://doi.org/10.1016/j.applthermaleng.2011.11.067>
- Wang, J.Z., Zheng, D.X., 2008. Performance analysis of absorption cooling cycle utilizing TFE-[BmIm] Br as working fluid. *J. Eng. Thermophys.* 29, 1813–1816.
- Wang, K., Abdelaziz, O., Kisari, P., Vineyard, E.A., 2011. State-of-the-art review on crystallization control technologies for water/LiBr absorption heat pumps. *Int. J. Refrig.* 34, 1325–1337. <https://doi.org/10.1016/j.ijrefrig.2011.04.006>
- Wang, L., Sundén, B., Manglik, R.M., 2007. Plate Heat Exchangers. Design, Applications and Performance. Wit Press. <https://doi.org/10.1081/E-EAFE>
- Wang, Z., Gu, Z., Feng, S., Li, Y., 2009. Application of vacuum membrane distillation to lithium bromide absorption refrigeration system. *Int. J. Refrig.* 32, 1587–1596. <https://doi.org/10.1016/j.ijrefrig.2009.07.002>
- Warnakulasuriya, F.S.K., Worek, W.M., 2008a. Heat transfer and pressure drop properties of high viscous solutions in plate heat exchangers. *Int. J. Heat Mass Transf.* 51, 52–67. <https://doi.org/10.1016/j.ijheatmasstransfer.2007.04.054>
- Warnakulasuriya, F.S.K., Worek, W.M., 2008b. Drop formation of swirl-jet nozzles with high viscous solution in vacuum-new absorbent in spray absorption refrigeration. *Int. J. Heat Mass Transf.* 51, 3362–3368. <https://doi.org/10.1016/j.ijheatmasstransfer.2007.11.015>
- Warnakulasuriya, F.S.K., Worek, W.M., 2006. Adiabatic water absorption properties of an aqueous absorbent at very low pressures in a spray absorber. *Int. J. Heat Mass Transf.* 49, 1592–1602. <https://doi.org/10.1016/j.ijheatmasstransfer.2005.11.003>
- Wilbur, P.J., Manchini, T.R., 1976. A comparison of solar absorption air conditioning systems. *Sol. Energy* 18, 569–576. [https://doi.org/10.1016/0038-092X\(76\)90077-3](https://doi.org/10.1016/0038-092X(76)90077-3)
- Wu, W., Wang, B., Shi, W., Li, X., 2014. An overview of ammonia-based absorption chillers and heat pumps. *Renew. Sustain. Energy Rev.* 31, 681–707. <https://doi.org/10.1016/j.rser.2013.12.021>
- Wu, W., Zhang, X., Li, X., Shi, W., Wang, B., 2012. Comparisons of different working pairs and cycles on the performance of absorption heat pump for heating and domestic hot water in cold regions. *Appl. Therm. Eng.* 48, 349–358. <https://doi.org/10.1016/j.applthermaleng.2012.04.047>

- Yazaki Corporation, n.d. Installation and Service Manual: Blue Panel Flat Plate Solar Collector and Compact Type FC400S/ WFC600S.
- Yazaki Energy Systems Inc., n.d. Yazaki WFC-SC5 Series chiller installation instructions.
- Yazaki Energy Systems Inc., n.d. Yazaki WFC-SC10 Series chiller installation instructions.
- Yeung, M.R., Yuen, P.K., Dunn, A., Cornish, L.S., 1992. Performance of a solar-powered air conditioning system in Hong Kong. *Sol. Energy* 48, 309–319. [https://doi.org/10.1016/0038-092X\(92\)90059-J](https://doi.org/10.1016/0038-092X(92)90059-J)
- Yin, Y.L., Song, Z.P., Li, Y., Wang, R.Z., Zhai, X.Q., 2012. Experimental investigation of a mini-type solar absorption cooling system under different cooling modes. *Energy Build.* 47, 131–138. <https://doi.org/10.1016/j.enbuild.2011.11.036>
- Yokozeiki, A., Shiflett, M.B., 2007a. Vapor-liquid equilibria of ammonia + ionic liquid mixtures. *Appl. Energy* 84, 1258–1273. <https://doi.org/10.1016/j.apenergy.2007.02.005>
- Yokozeiki, A., Shiflett, M.B., 2007b. Ammonia solubilities in room-temperature ionic liquids. *Ind. Eng. Chem. Res.* 46, 1605–1610. <https://doi.org/10.1021/ie061260d>
- Yoon, J.-I., Phan, T.T., Moon, C.-G., Lee, H.-S., Jeong, S.-K., 2008. Heat and mass transfer characteristics of a horizontal tube falling film absorber with small diameter tubes. *Heat Mass Transf.* 44, 437–444. <https://doi.org/10.1007/s00231-007-0261-8>
- Yoon, J., Kwon, O.-K., Moon, C.-G., 1999a. Experimental study of heat and mass transfer on an absorber with several enhancement tubes. *Heat Transf. Res.* 28, 664–674. [https://doi.org/10.1002/\(SICI\)1523-1496\(1999\)28:8<664::AID-HTJ4>3.0.CO;2-P](https://doi.org/10.1002/(SICI)1523-1496(1999)28:8<664::AID-HTJ4>3.0.CO;2-P)
- Yoon, J., Kwon, O., Moon, C., 1999b. Experimental investigation of heat and mass transfer in absorber with enhanced tubes. *KSME Int. J.* 13, 640–646. <https://doi.org/10.1007/BF03184574>
- Yoon, J.I., Kim, E., Choi, K.H., Seol, W.S., 2002. Heat transfer enhancement with a surfactant on horizontal bundle tubes of an absorber. *Int. J. Heat Mass Transf.* 45, 735–741. [https://doi.org/10.1016/S0017-9310\(01\)00202-2](https://doi.org/10.1016/S0017-9310(01)00202-2)
- Yoon, J.I., Kwon, O.K., Bansal, P.K., Moon, C.G., Lee, H.S., 2006. Heat and mass transfer characteristics of a small helical absorber. *Appl. Therm. Eng.* 26, 186–192. <https://doi.org/10.1016/j.applthermaleng.2005.05.009>
- Yu, D., Chung, J., Moghaddam, S., 2012. Parametric study of water vapor absorption into a constrained thin film of lithium bromide solution. *Int. J. Heat Mass Transf.* 55, 5687–5695. <https://doi.org/10.1016/j.ijheatmasstransfer.2012.05.064>
- Zacariás, A., Venegas, M., Lecuona, A., Ventas, R., 2013. Experimental evaluation of ammonia adiabatic absorption into ammonia-lithium nitrate solution using a fog jet nozzle. *Appl. Therm. Eng.* 50, 781–790. <https://doi.org/10.1016/j.applthermaleng.2012.07.006>
- Zacariás, A., Venegas, M., Lecuona, A., Ventas, R., Carvajal, I., 2015. Experimental assessment of vapour adiabatic absorption into solution droplets using a full cone nozzle. *Exp. Therm. Fluid Sci.* 68, 228–238. <https://doi.org/10.1016/j.expthermflusci.2015.05.001>
- Zacariás, A., Venegas, M., Ventas, R., Lecuona, A., 2011. Experimental assessment of ammonia adiabatic absorption into ammonia-lithium nitrate solution using a flat fan nozzle. *Appl. Therm. Eng.* 31, 3569–3579. <https://doi.org/10.1016/j.applthermaleng.2011.07.019>
- Zacariás, A., Ventas, R., Venegas, M., Lecuona, A., 2010. Boiling heat transfer and pressure drop of ammonia-lithium nitrate solution in a plate generator. *Int. J. Heat Mass Transf.* 53, 4768–4779. <https://doi.org/10.1016/j.ijheatmasstransfer.2010.06.015>
- Zambrano, D., Bordons, C., Garcia-Gabin, W., Camacho, E.F., 2008. Model development and validation of a solar cooling plant. *Int. J. Refrig.* 31, 315–327. <https://doi.org/10.1016/j.ijrefrig.2007.05.007>
- Zamora, M., 2012. Industrial Optimization and Control Strategy of an Air-cooled Ammonia/lithium Nitrate Absorption Chiller (in Spanish). PhD Universitat Rovira i Virgili.
- Zamora, M., Bourouis, M., Coronas, A., Vallès, M., 2015. Part-load characteristics of a new ammonia/lithium nitrate absorption chiller. *Int. J. Refrig.* 56, 43–51. <https://doi.org/10.1016/j.ijrefrig.2014.11.005>
- Zamora, M., Bourouis, M., Coronas, A., Vallès, M., 2014. Pre-industrial development and experimental characterization of new air-cooled and water-cooled ammonia/lithium nitrate absorption chillers. *Int. J. Refrig.* 45, 189–197. <https://doi.org/10.1016/j.ijrefrig.2014.06.005>
- Zamora, M., Bourouis, M., Vallès, M., Coronas, A., 2011. A new ammonia/lithium nitrate absorption chiller for solar cooling applications, in: *Proceedings of the International Conference on Ammonia Refrigeration Technology*. Ohrid, Macedonia, p. e16.
- Zeng, X., Chyu, M.C., 1995. Heat Transfer and Fluid Flow Study of Ammonia Spray Evaporators, in: Texas Tech University, Lubbock, Texas, USA.
- Zetzsche, M., Koller, T., Brendel, T., Spindler, K., 2010. Entwicklung einer Ammoniak/Wasser Kälteanlage zur solaren Kühlung - abschließende Bewertung, in: *Jahrestagung Des Deutschen Kälte- Und Klimatechnischen Vereins AA.II.1.17*. Magdeburg, Deutschland.
- Zhai, X., Li, Y., Cheng, X., Wang, R., 2015. Experimental Investigation on a Solar-powered Absorption Radiant Cooling System. *Energy Procedia* 70, 552–559. <https://doi.org/10.1016/j.egypro.2015.02.160>
- Zhai, X.Q., Wang, R.Z., 2009. A review for absorption and adsorption solar cooling systems in China. *Renew. Sustain. Energy Rev.* 13, 1523–1531. <https://doi.org/10.1016/j.rser.2008.09.022>
- Zheng, D., Dong, L., Huang, W., Wu, X., Nie, N., 2014. A review of imidazolium ionic liquids research and development towards working pair of absorption cycle. *Renew. Sustain. Energy Rev.* 37, 47–68. <https://doi.org/10.1016/j.rser.2014.04.046>
- Zhu, L., Gu, J., 2010. Second law-based thermodynamic analysis of ammonia/sodium thiocyanate absorption system. *Renew. Energy* 35, 1940–1946. <https://doi.org/10.1016/j.renene.2010.01.022>
- Zhu, L., Gu, J., 2009. Thermodynamic analysis of a novel thermal driven refrigeration system. *Int. J. Mech. Mechatronics Eng.* 3, 351–355.
- Zhu, L., Wang, S., Gu, J., 2008. Performance investigation of a thermal-driven refrigeration system. *Int. J. energy Res.* 32, 939–949. <https://doi.org/10.1002/er.1408>
- Ziegler, F., Alefeld, G., 1987. Coefficient of performance of multistage absorption cycles. *Int. J. Refrig.* 10, 285–295.
- Zotter, G., Rieberer, R., 2015. Experimental analysis of a novel concept of a “thermally driven” solution pump operating a small-capacity ammonia/water absorption heat pumping system. *Int. J. Refrig.* 60, 190–205. <https://doi.org/10.1016/j.ijrefrig.2015.06.024>

Chapter II. Thermal and mass effectivenesses as a tool for the characterization of absorption chillers and models comparison

Based on:

Altamirano, A., Stutz, B., Le Pierrès, N., Coronas, A.
Experimental characterization by thermal and mass effectivenesses of plate heat exchangers in NH₃-LiNO₃ absorption chillers
Online Int. Sorption Heat Pump Conf., Berlin (Germany)
DOI: 10.14279/depositonce-10430.2

Altamirano, A., Le Pierrès, N., Stutz, B., Coronas, A.
Performance characterization methods for absorption chillers applied to an NH₃-LiNO₃ single-stage prototype
Appl. Therm. Eng. 185, 116435
Int. J. Refrig. 114 (2020) 118–147
DOI: 10.1016/j.applthermaleng.2020.116435

Chapter II is a result of a collaboration stay at the CREVER Research Group of the Rovira I Virgili University (Spain), as part of the InnoEnergy PhD Program of the EIT (European Institute of Innovation and Technology). It addresses the use of thermal and mass effectivenesses, in their most general definition (the case of non-adiabatic sorption exchangers), as performance evaluation parameters of the sorption elements of absorption chillers and their implementation in an entire machine simulation. Other characterization methods with different physical insight levels are also discussed. Section 2.2 presents the experimental characterization of plate heat exchangers used as the absorber and the desorber with the innovative NH₃-LiNO₃ working pair. Section 2.3 presents the characterization of a 10-kW NH₃-LiNO₃ absorption chiller by means of four different methods: the characteristic equation method, the adapted characteristic equation method, the Carnot function model, and the “effectiveness model,” based on thermal and mass effectivenesses.

“

*“O correr da vida embrulha tudo, a vida é assim:
esquenta e esfria, aperta e daí afrouxa, sossega e depois desinquieta.
O que ela quer da gente é coragem.”*

*“The flow of life envelopes everything. Life is like this:
it heats up and cools down, it squeezes and then loosens, it becomes calm and then restless.
What it wants from us is courage.”*

– Guimarães Rosa

2.1. Introduction

As mentioned in Section 1.3, the absorber and desorber of absorption chillers have been pointed out as the technological "bottlenecks" in absorption chillers (Goyal et al., 2017). The same section also allows to observe that heat/mass transfer coefficients or fluxes are commonly used as parameters to characterize them. However, the overall heat transfer coefficient using the classical definition of log-mean-temperature-difference is not valid as it does not take into account the heat of sorption (Narayanan et al., 2009). Furthermore, this coefficient usually neglects the sensible heat part involved in the sorption exchanger elements (Herold et al., 2016). In addition, even though heat and mass transfers are coupled, they are separate physical processes and either of them can control the overall transfer process (Herold et al., 2016).

Absorption chillers are more complex machines than vapor compression systems. Therefore, their modeling is of fundamental importance for the evaluation and characterization of their performance, especially when they are operated outside their nominal conditions. In this regard, most of the methods consider the sorption phenomena (i.e., the absorption and desorption) to be controlled by the heat transfer and the solution is considered to reach equilibrium conditions with the vapor phase at the outlet of the components (i.e., the absorber and generator), which is never the case in real operating conditions (Aiane et al., 2017b). Moreover, the overall heat transfer coefficient employed to group both the heat and mass transfer phenomena is considered constant for the entire range of operating conditions. Therefore, a more precise approach can be the implementation of a thermal and a mass effectiveness (ϵ_{th} and ϵ_m , respectively) which consider both the heat and mass transfer as independent.

The present section introduces the global definition of the thermal and mass effectiveness for sorption exchangers and their implementation in plate heat exchangers used as the absorber and the desorber of a $\text{NH}_3\text{-LiNO}_3$ absorption chiller pre-industrial prototype. In Section 2.2 after defining the thermal and mass effectivenesses, the characterization of plate heat exchangers used as an absorber and a desorber is presented. Section 2.3 presents the characterization of a 10-kW $\text{NH}_3\text{-LiNO}_3$ absorption chiller by means of four different methods (with different physical insight levels) that use the external heat transfer fluid temperatures to situate the machine operating conditions, either through a characteristic temperature difference (in the case of the CE-based models), or through the COP_{carnot} : the characteristic equation (CE) method, the adapted CE method, the Carnot function model (CFM), and the effectiveness model (EM), based on thermal and mass effectivenesses. The COP_{carnot} is used as a common parameter to express the machine operating conditions and, therefore, to represent the results from the different models and the effectivenesses of the components. The different studied methods as well as their advantages and disadvantages are discussed.

2.2. Characterization of the sorption exchangers

2.2.1. Thermal and mass effectivenesses definition

The studied exchangers (absorber and desorber) possess a counter-current configuration of the liquid phases (solution/heat transfer fluid) and, on the two-phase flow side, the $\text{NH}_3\text{-LiNO}_3$ solution and the ammonia vapor both flow upwards in a co-current configuration, as represented in Figure II.1 for the case of the absorber. Their performance is defined on the basis of thermal and mass effectivenesses (ϵ_{th} and ϵ_m , respectively). The thermal effectiveness (Eq. (I.3)) is defined as the ratio of the actual transferred heat to the maximum theoretical transferable heat. On the other hand, the mass effectiveness (Eq. (II.2)) is defined

as the ratio of the actual transferred mass (absorbed or desorbed) to the maximum theoretical exchangeable mass.

$$\varepsilon_{th} = \dot{Q}/\dot{Q}_{max} \quad (II.1)$$

$$\varepsilon_m = \dot{m}_{sorp}/\dot{m}_{sorp}^{max} \quad (II.2)$$

The proposed effectivenesses are dependent on fewer parameters compared with heat/mass transfer coefficients as they take into account the side of the exchanger that limits the transfers (solution or HTF side) and the state of the solution (subcooled or super-heated solution) at the inlet of the component to calculate the maximum transferable conditions. In the case of nonadiabatic sorption exchangers, these conditions also depend on the HTF temperature deviation from the solution equilibrium conditions. The more the HTF temperature deviates from the solution equilibrium temperature, the higher the absorption/desorption potential on the solution side. This gap is represented by the HTF equilibrium deviation temperature (Eq. (II.3)). If $\Delta T_{htf}^{eq} > 0$, the HTF has the potential to generate a desorption effect. Otherwise, the HTF induces an absorption process. On the other hand, the deviation of the solution from the equilibrium conditions is represented by the solution equilibrium deviation temperature (Eq. (II.4)). If $\Delta T_s^{eq} > 0$, the solution possesses a desorption potential, whereas if it is below 0, it possesses an absorption potential. In the following, only the case of the absorber will be discussed to explain the procedure followed in this work. A similar procedure is followed in the case of the generator.

$$\Delta T_{htf}^{eq,i/o} = t_{htf}^{i/o} - T_{eq}(P_v, x_{i/o}) \quad (II.3)$$

$$\Delta T_s^{eq,i/o} = T_s^{i/o} - T_{eq}(P_v, x_{i/o}) \quad (II.4)$$

The maximum absorbable mass depends on the solution flow rate and the potential of the HTF to cool it. This potential is represented by the equilibrium factor (Eq. (II.5)), defined as the ratio between the maximum heat that can be transferred to the HTF ($\dot{Q}_{htf,a}^{max}$) to the maximum heat that can be transferred by the solution ($\dot{Q}_{s,a}^{max}$). The maximum amount of heat that can be transferred to the HTF in an infinitely long exchanger is proportional to the maximum enthalpy difference in the HTF itself when achieving an outlet temperature (t_{htf}^o) equal to the maximum temperature that the solution side can achieve (T_s^{max} , Eq. (II.6)). When the inlet solution temperature is lower than the equilibrium solution temperature ($\Delta T_s^{eq,i} < 0$), it has a tendency to absorb vapor (increase its temperature). Consequently, the maximum solution temperature corresponds to an adiabatic absorption in an infinitely long exchanger ($T_s^{max} = T_{s,o}^{ad,\infty}$). Otherwise, it means that the solution enters the absorber in a super-heated state, in which case the solution would have a tendency to desorb vapor (decrease its temperature) and therefore, the maximum solution temperature would correspond to the inlet solution temperature itself ($T_{sol}^{max} = T_{sol}^i$). $T_{s,o}^{ad,\infty}$ is obtained through an iterative procedure in order to obtain the validity of Eqs. (II.8) to (II.11), with a $\dot{Q}_a^{max} = 0$ (the maximum absorbable mass for the case of an adiabatic absorption $\dot{m}_a^{ad,\infty}$ is obtained with the same iterative procedure). Finally, the maximum amount of heat that can be transferred by the solution ($\dot{Q}_{s,a}^{max}$) corresponds to an energy balance for an isothermal absorption in which the outlet solution temperature is equal to the inlet HTF temperature.

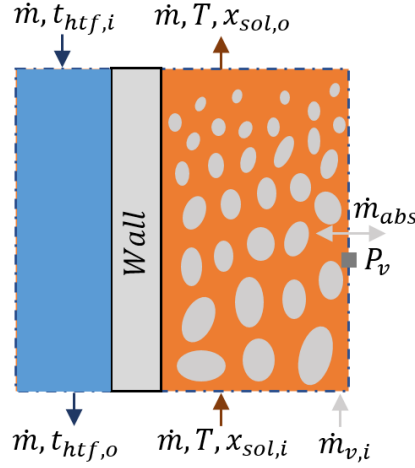


Figure II.1: Control volume of the bubble absorber.

$$R_{abs} = \frac{\dot{Q}_{htf,a}^{max}}{\dot{Q}_{s,a}^{max}} = \frac{\dot{m}_{htf}[H_{htf}^o(T_s^{max}) - H_{htf}^i]}{\dot{m}_s^i H_s^i - \dot{m}_s^{o,iso} H_s^{o,iso}(t_{htf}^i; x_s^{o,iso}) + \dot{m}_a^{iso} H_v} \quad (II.5)$$

$$T_s^{max} = \max[T_s^i, T_{s,o}^{ad,\infty}] \quad (II.6)$$

The maximum absorbable mass and transferable heat are obtained by solving the energy, mass, and species balances (Eqs. (II.8) to (II.10)) in the absorber using the maximum transferable heat depending on the limiting fluid (Eq. (II.7)). If $R > I$, then the solution is the limiting fluid and the maximum transferable heat corresponds to an isothermal absorption in an infinitely long absorber where the outlet solution temperature reaches the inlet HTF temperature (Eq. (II.12)), in which case $\dot{Q}_a^{max} = \dot{Q}_{s,a}^{max}$ and $\dot{m}_a^{max} = \dot{m}_a^{iso}$. On the other hand, if $R < I$, the HTF is the limiting fluid and the maximum transferable conditions are achieved when it transfers its entire potential ($\dot{Q}_a^{max} = \dot{Q}_{htf,a}^{max}$) and the solution reaches equilibrium conditions with the vapor phase (Eq. (II.11)).

$$\dot{Q}_a^{max} = \min[\dot{Q}_{htf,a}^{max}; \dot{Q}_{s,a}^{max}] \quad (II.7)$$

$$\dot{m}_{s,i} + \dot{m}_v - \dot{m}_{s,o} = 0 \quad (II.8)$$

$$\dot{m}_{s,i} x_{s,i} - \dot{m}_{s,o} x_{s,o} = 0 \quad (II.9)$$

$$\dot{m}_{s,i} H_{s,i} + \dot{m}_v H_v - \dot{m}_{s,o} H_{s,o} - \dot{Q}_a^{max} = 0 \quad (II.10)$$

$$T_s^o(h_s^o; P_a; x_s^o) = T_s^{eq}(P_a; x_s^o) \quad (II.11)$$

$$T_s^{o,iso} = t_{htf}^i = T_s^{eq}(P_a; x_s^o) \quad (II.12)$$

2.2.2. Exchanger's geometries and experimental conditions

PHE and $\text{NH}_3\text{-LiNO}_3$ were investigated as the exchanger technology and working fluid, respectively. The PHE technology has been recently investigated owing to its high compactness and low cost. On the other hand, the $\text{NH}_3\text{-LiNO}_3$ working pair possesses different advantages over the conventional working pairs ($\text{NH}_3\text{-H}_2\text{O}$ and $\text{H}_2\text{O-LiBr}$) such as its wide range of operating conditions without crystallization and no need of a rectifier. The exchangers' geometrical characteristics and operating conditions are presented in Table II.1 and Table II.2, respectively (Amaris Castilla, 2013; Zacarías Santiago, 2009). Two tests were conducted to study the absorption performance, the first one (test 1) was aimed to study the effect of the

solution flow rate and the HTF inlet temperature, while the second one (test 2) was aimed to study the effect of the HTF inlet temperature and the HTF flow rate (Amaris Castilla, 2013). In the experiments performed to characterize the desorber (Zacariás Santiago, 2009), the main interest was to study the heat transfer phenomenon and there was no strict control on the inlet solution temperature, concentration, and operating pressure. Instead, two parameters were changed: the outlet solution temperature, which was fixed at five different values (78, 82, 86, 80, and 95°C), and the solution mass flow rate, which was fixed at three levels (151.2, 208.8, and 298.8 kg h⁻¹). For more details about the experimental set-ups, see the referenced works (Amaris Castilla, 2013) and (Zacariás Santiago, 2009).

Table II.1: Geometrical characteristics of the studied absorber (Amaris Castilla, 2013) and desorber (Zacariás Santiago, 2009).

	Absorber	Desorber
Model	Alfa Laval NB51	Alfa Laval AN76
Number of plates	4	20
Absorber length (m)	0.53	0.576
Absorber width (m)	0.112	0.175
Heat transfer effective area (m ²)	0.1	1.8
Spacing between the plates (m)	0.002	0.0024
Plate thickness (m)	0.0004	0.0004
Corrugation angle with horizontal axis (degrees)	30	58.5

Table II.2: Experimental operating conditions of the tested absorber (Amaris Castilla, 2013) and desorber (Zacariás Santiago, 2009).

	Absorber	Desorber
Inlet solution temperature, $T_{sol,i}$ (°C)	45 (test 1 and test 2)	56 to 69.6
Inlet HTF temperature, $T_{htf,i}$ (°C)	35 and 40 (test 1 and test 2)	80.1 to 100.9
LiNO ₃ inlet solution mass fraction, $x_{sol,i}$ (kg kg ⁻¹)	0.55 (test 1 and test 2)	0.538 to 0.548
Operating pressure (kPa)	510 (test 1 and test 2)	977.7 to 1606
Inlet solution mass flowrate, $\dot{m}_{sol,i}$ (kg h ⁻¹)	10 to 50 (test 1 with $\dot{m}_{htf} = 265$ kg h ⁻¹)	(151.2, 208.8, 298.8)
HTF mass flowrate, \dot{m}_{htf} (kg h ⁻¹)	132 to 447 (test 2 with $\dot{m}_{sol,i} = 40$ kg h ⁻¹)	602.36 to 745.64
Outlet solution temperature, $T_{sol,o}$ (°C)	36.9 to 44.2	(78, 82, 86, 90, 95)

2.2.3. Results

Figure II.2a shows the impact of the solution flow rate and the HTF inlet temperature on the equilibrium factor (R), or Test 1. During this test, the solution side remains the limiting fluid ($R > I$). For Test 2 (Figure II.2b), while Re_{sol} remains at values around 35, R increases linearly with the Reynolds number on the heat transfer fluid side (Re_{htf}), varying from 0.9 to 3 with a Re_{htf} from 470 to 1600. The inlet HTF temperature does not seem to have a significant impact on R . This happens because the variation on $T_{htf,i}$ impacts in a

similar way the maximum transferable conditions on the HTF side ($\dot{Q}_{htf,abs}^{max}$) as on the solution side ($\dot{Q}_{sol,abs}^{max}$). Figure II.2c and Figure II.2c show the evolution of ε_m and ε_{th} of the studied absorber with Re_{sol} for both tests. The highest effectivenesses are reached at the lowest Re_{sol} due to the low solution velocity that generates two phenomena: a high hydrodynamic bubble disturbance and a high flow residence time in the channel. As Re_{sol} increases, these phenomena decrease and both ε_m and ε_{th} decrease to an asymptote that indicates an approach to a $R=1$ (the solution side is reaching the limit of the maximum potential of transferable heat by the HTF). Moreover, ε_{th} is systematically higher than ε_m . This happens because even though the mass transfer is coupled to the heat transfer, it is also impacted by the driving force of the absorption process (deviation from the equilibrium conditions). Figure II.2c and Figure II.2d show that the variation of Re_{htf} and $T_{htf,i}$ don't significantly impact ε_m and ε_{th} in the studied conditions.

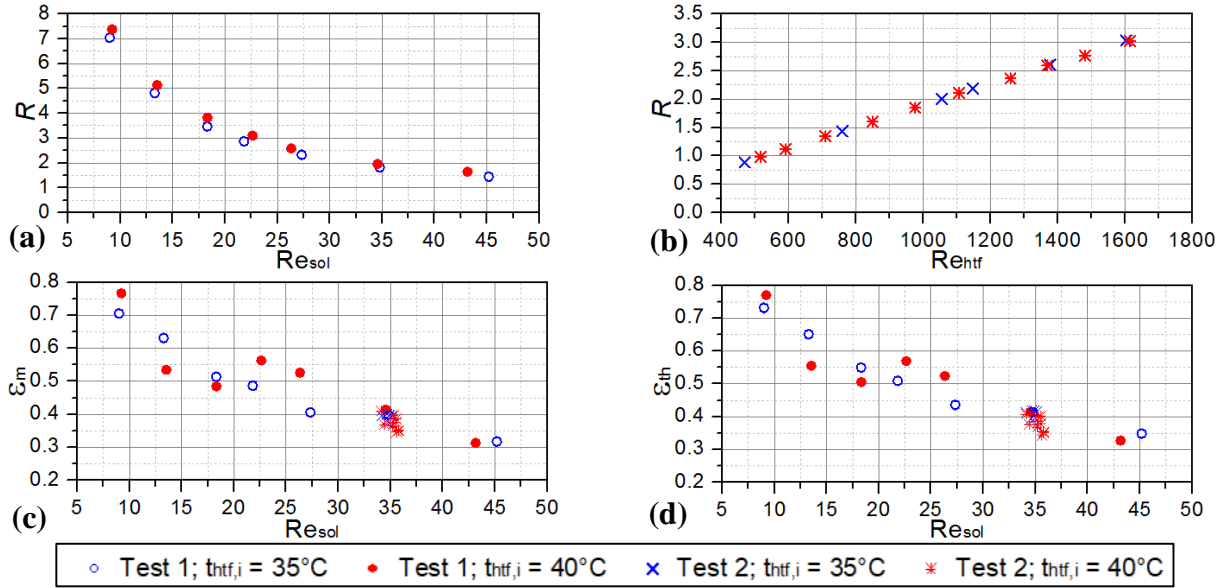


Figure II.2: Evolution of R with (a) Re_{sol} (Test 1) and (b) Re_{htf} (Test 2), and evolution of (c) ε_m and (d) ε_{th} vs Re_{sol} for both Test 1 and Test 2 in the absorber.

Figure II.3a shows the evolution of R with Re_{sol} for the desorber. The three Re_{sol} grouped zones represent the three solution mass flow rates (see Table II.2), and the variation in Re in each zone is due to the change in the inlet solution dynamic viscosity. The data is grouped in five outlet solution temperatures (Table II.2). The solution side was the limiting fluid in the whole range of tested conditions ($R > 1$), with high R values at low Re_{sol} , and as Re_{sol} increases, R decreases. Moreover, the thermophysical properties' evolution and inlet conditions seem to have a stronger positive impact on R at low Re_{sol} . Regarding the mass and thermal effectivenesses (Figure II.3b and Figure II.3c), the same tendency as for the absorber can be observed with higher effectivenesses for low Re_{sol} and a decrease approaching an asymptote as R comes close to 1. ε_m is again systematically lower than ε_{th} , however, in this case the gap is much higher due to the high subcooled state of the solution at the inlet of the desorber (subcooling of between 15 and 25°C), leading to poor mass transfer performances. Moreover, for each solution mass flow rate (151.2, 208.8, and 298.8 kg h⁻¹), there is an increase of both ε_{th} and ε_m with Re_{sol} induced by a decrease in the solution's dynamic viscosity. Indeed, a lower viscosity increases the hydrodynamic bubble disturbance, enhancing the mass transfer and increasing ε , which is in agreement with other works that have blamed the elevated viscosity of NH₃-LiNO₃ for its low experimental performance compared with other low viscosity solutions such as NH₃-H₂O (Altamirano et al., 2019a).

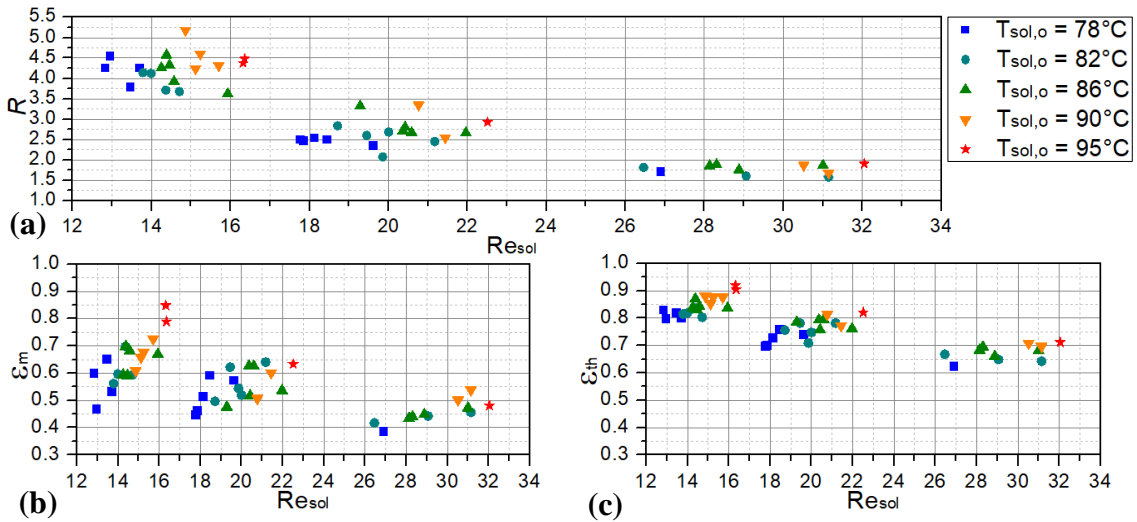


Figure II.3: Evolution of (a) R , (b) ε_m and (c) ε_{th} vs Re_{sol} for the different tested conditions in the desorber.

2.3. Characterization methods applied to a NH_3 - $LiNO_3$ single stage prototype

In Section 2.2, the behavior of the nonadiabatic sorption exchangers operating with the NH_3 - $LiNO_3$ working fluid was studied by the use of thermal and mass effectivenesses. As observed before, apart from the inlet solution equilibrium temperature deviations, other factors such as the mass flow rate and the thermophysical properties have a considerable influence on these exchangers' performance. Therefore, the study of their behavior for the different operating conditions of an absorption chiller (especially those far from its nominal design conditions) is of great interest. Moreover, as mentioned before, the simulation of absorption chillers is of fundamental importance owing to their technical complexity if compared with conventional vapor compression systems. For these reasons, the present section deals with the characterization of a 10-kW NH_3 - $LiNO_3$ absorption chiller prototype through modeling methods with different physical insight levels.

The different existing models for absorption chillers can be divided into three categories depending on their nature: white box (physical), when it contains complete insight into the physical process or system; gray box (semi-empirical), when there is some degree of physical insight and the model parameters can be physically interpreted; and black box (empirical), when no physical insight is necessary and the model describes a dataset of experimental results (J. Labus et al., 2013; Sjöberg et al., 1995). The characteristic equation (CE) method is a gray-box-type model commonly used for modeling of absorption chillers as it allows the thermal loads of the components to be calculated by means of simple linear functions (J. Labus et al., 2013). In this method as in most of the methods (physical or semi-empirical) present in the literature, the sorption phenomena (i.e., the absorption and desorption) are considered to be controlled by the heat transfer and the solution is considered to reach equilibrium conditions with the vapor phase at the outlet (i.e., the solution has used its entire absorption/desorption potential at a point at which, at the outlet, the temperature, pressure, and chemical local potential between the phases is equal and, therefore, there are no more transfers between them (Herold et al., 2016)) of the components (i.e., the absorber and generator), which is never the case in real operating conditions (Aiame et al., 2017b). Moreover, the overall heat transfer coefficient employed to regroup both the heat and mass transfer phenomena is considered constant during the entire range of operating conditions. Owing to these and other simplifying assumptions, the characteristic equation method possesses considerable deviations from the experimental results. An alternative to this is the use of empirical methods based on numerical fits of the experimental

results. In this regard, Kühn and Ziegler (Kühn and Ziegler, 2005) and Boudéhenn et al. (Boudéhenn et al., 2014) presented the “adapted characteristic equation (CE) method” and the “Carnot function model (CFM),” respectively. The former is based on the characteristic equation method and uses an arbitrary parameter to estimate the evaporator/generator heat rates as linear functions, whereas the latter represents the cooling capacity and the thermal COP as functions of the chiller COP_{carnot} . Despite the increase in the accuracy of these models compared with the CE method, the underlying physical mechanisms of the machine operation are hidden at all times (Buchin et al., 2016).

In sorption exchangers, even though heat and mass transfers are coupled, they are separate processes and either of them can control the overall transfer process (Herold et al., 2016). Therefore, a more precise approach can be the implementation of an effectiveness model (EM) that considers both the heat and mass transfer as independent. In this regard, a physical (thermodynamic) model of a small-capacity NH_3-LiNO_3 pre-industrial prototype (Zamora, 2012) has been developed based on thermal and mass effectivenesses that takes into account the non-equilibrium conditions of the solution with the vapor phase in the machine (i.e., conditions at which, at a given vapor pressure and solution concentration, the solution is at a subcooled ($T_{sol} < T_{sol}^{eq}$) or super-heated ($T_{sol} > T_{sol}^{eq}$) state), which facilitates a better consideration of the sensible heat effects on the sorption elements. To the best of our knowledge, no physical model has been presented before with similar characteristics for the characterization of absorption chillers.

The present section shows the characterization of the prototype by the CE method, the adapted CE method, the CFM, and the EM. All the studied models use the external heat transfer fluid temperatures to situate the machine operating conditions, either through a characteristic temperature difference (in the case of the CE-based models) or through the COP_{carnot} . The use of the external temperatures in the modelling of absorption chillers results very practical since these are variables that are easily obtained during the machine operation with barely no need of additional instrumentation. Furthermore, the manufacturers use these variables for the characterization of commercial chillers. The results from the CE-based models and the effectivenesses of the exchangers are for the first time represented in the COP_{carnot} domain, giving a different perspective on their interpretation. Additionally, models with different insight levels were selected to discuss on their advantages and disadvantages depending on the user requirements. The thermodynamic model, being the one with the most complete physical insight into the machine, was used to analyze the individual exchanger performances and the internal thermodynamic non-equilibrium conditions of the solution with the vapor phase under part-load conditions. A better understanding of the machine allowed us to identify opportunities for thermal and electric COP improvements.

2.3.1. System description

The machine was developed through a partnership between the CREVER group of the Rovira i Virgili University and the CIAT company (Zamora, 2012). It is a 10-kW water-cooled NH_3-LiNO_3 single-stage absorption chiller fully equipped with brazed plate heat exchangers (BPHE) in all its thermal components, inspired by a previously published patent (Bourouis et al., 2011). A simplified diagram of the machine is shown in Figure II.4. In this system, the diluted solution coming from the solution storage tank is pre-heated in the SHX, after which it enters the generator to absorb heat and desorb NH_3 vapor. The desorbed vapor is then condensed and the liquid refrigerant is stored in a refrigerant storage tank. Depending on the cooling requirements and low operating pressure (P_l), the refrigerant expansion valve (REV) allows for the flow of refrigerant through the evaporator, after which the vapor is sent to the plate absorber where the concentrated solution (coming from the generator and pre-cooled in the solution heat exchanger [SHX]) absorbs it while it is cooled down by an external fluid. The resulting solution is then sent to the solution storage tank, where the process starts again.

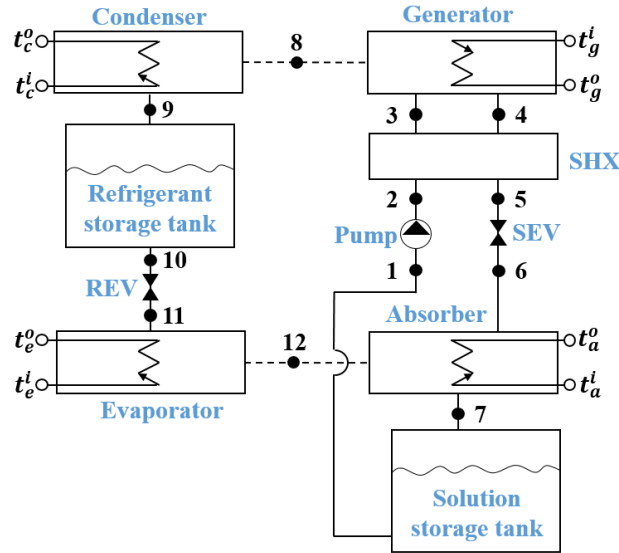


Figure II.4: Simplified diagram of the 10-kW $\text{NH}_3\text{-LiNO}_3$ water-cooled absorption chiller developed by Zamora (Zamora, 2012).

During experiments, the heat transfer fluid (HTF; water) of the heat sink flowed in parallel through the condenser and the absorber ($t_c^i = t_a^i = t_{ac}^i$). The nominal operating conditions of the chiller were defined at an inlet generator temperature (t_g^i) of 90°C , an intermediate cooling temperature (t_{ac}^i) of 37.5°C , and a chilled water temperature (t_e^o) of 15°C (Zamora, 2012). The machine was characterized under part-load operation with the conditions and accuracies shown in Table II.3. The cooling and generator heat rates were directly calculated using temperature measurements (inlet/outlet) from PT-100 probes and flow rate measurements from magnetic flowmeters. Regarding the heat sink, temperature measurements were performed at the inlet and outlet of the parallel source, and the HTF flow rate and exchanged heat were indirectly calculated using a global energy balance assuming no heat losses with the environment. Finally, considering the technical data of the solution pump and the pressure losses in the circuit, the solution mass flow rate was calculated to be approximately 0.12 kg s^{-1} (with an uncertainty of $\pm 4\%$). The experimental results of the characterization test campaign, obtained from (Zamora, 2012), are presented in Table II.4.

Table II.3: Operating conditions of the characterized $\text{NH}_3\text{-LiNO}_3$ absorption chiller prototype (Zamora, 2012).

Variable	Measurement values or ranges	Uncertainty
t_e^o ($^\circ\text{C}$)	8.4; 15.5	$\pm 0.1^\circ\text{C}$
t_{ac}^i ($^\circ\text{C}$)	30–40.2	$\pm 0.1^\circ\text{C}$
t_g^i ($^\circ\text{C}$)	85; 90; 95	$\pm 0.1^\circ\text{C}$
\dot{v}_e ($\text{m}^{-3} \text{ h}^{-1}$)	3	$\pm 0.5 \%$
\dot{v}_{ac} ($\text{m}^{-3} \text{ h}^{-1}$)	6	$\pm 4.7 \%$
\dot{v}_g ($\text{m}^{-3} \text{ h}^{-1}$)	3	$\pm 0.5 \%$
\dot{Q}_e (kW)	3.15–17.82	$\pm 0.5 \text{ kW}$
\dot{Q}_{ac} (kW)	11.62–46.08	$\pm 0.71 \text{ kW}$
\dot{Q}_g (kW)	8.47–28.26	$\pm 0.5 \text{ kW}$
COP_{th}	0.37–0.65	± 0.03

Table II.4: Experimental results of the characterization test campaign of the NH₃- LiNO₃ absorption chiller prototype (Zamora, 2012).

Test	t_{ac}^i (°C)	t_{ac}^o (°C)	t_e^i (°C)	t_e^o (°C)	t_g^i (°C)	t_g^o (°C)	\dot{V}_{ac} (m ⁻³ h ⁻¹)	\dot{V}_e (m ⁻³ h ⁻¹)	\dot{V}_g (m ⁻³ h ⁻¹)	\dot{Q}_e (kW)	\dot{Q}_g (kW)	COP
1	30	34.4	11.7	8.4	85	79.5	5.91	3.02	3	11.53	18.96	0.61
2	32	35.7	11.1	8.4	85	80.2	59.5	3	3	9.53	16.34	0.58
3	34	37	10.5	8.4	85	81	5.97	3.03	2.99	7.34	13.55	0.54
4	36	38.3	9.9	8.4	85	81.8	6.05	3.04	3.01	5.29	11.1	0.48
5	38	39.6	9.3	8.4	85	82.5	6.21	3.03	3.03	3.15	8.47	0.37
6	30	35	12	8.4	90	83.8	5.86	3	3	12.77	21.1	0.61
7	32	36.2	11.4	8.4	90	84.7	5.89	3.01	3	10.44	18.05	0.58
8	34	37.6	10.9	8.4	90	85.3	5.96	3.02	2.99	8.88	16.01	0.55
9	30	35.8	12.8	8.4	95	87.6	5.92	3	2.98	15.18	25.02	0.61
10	32	37	12.1	8.4	95	88.5	5.97	3.01	3	12.9	22.03	0.59
11	34	38.8	11.6	8.4	95	89.2	5.55	3.01	3	11.36	19.63	0.58
12	36	39.9	11	8.4	95.1	90.2	5.68	3.02	3	8.99	16.52	0.54
13	38	40.7	10.1	8.4	95	91.2	5.83	3.02	2.98	5.68	12.77	0.44
14	40	42.5	9.7	8.3	94.9	91.6	5.58	3.01	3	4.83	11.4	0.42
15	29.8	36	20.3	15.4	90	82.2	6.09	3.01	3	17.33	26.52	0.65
16	32.3	37.6	19.7	15.4	89.9	82.8	6.48	3.03	3.04	15.35	24.44	0.63
17	33.9	39.8	19.5	15.4	90	83.2	5.43	3.01	3	14.35	22.72	0.63
18	38.1	41.7	18.2	15.5	90	85.2	6.22	3.02	3.01	9.32	16.44	0.57
19	40.2	43	17.6	15.4	89.9	85.7	6.70	3.04	3	7.67	14.29	0.54
20	32	-	19.9	14.8	94.9	86.6	6.26	3.03	3.04	17.82	28.26	0.63
21	33.9	39.8	20.1	15.4	94.9	87.3	6.25	3.03	3	16.54	26.09	0.63
22	36	-	19.4	15.4	95	88.2	6.25	3.04	2.98	13.99	23.01	0.61
23	38.2	42.6	18.8	15.3	95	89	6.26	3.02	3.01	12.04	20.27	0.59
24	40.1	43.3	17.9	15.4	95	90.3	6.69	3.02	3.01	8.57	16.24	0.53

2.3.2. Characterization of the system

In this section, the different approaches to characterize the system within its range of operating conditions are presented. First, the original CE method is introduced, after which the adapted CE method and the CFM are presented. Finally, the EM based on thermal and mass effectivenesses is described. The CE-based methods use characteristic temperature differences (ΔT or $\Delta T'$) function of the external temperatures to represent the different operating conditions of the absorption chiller. However, these are not universal parameters as they are a result of the specific configuration of the machine studied (e.g., the machine capacity, the heat transfer coefficients, the working fluid properties, or the dataset used for the regression). In the present work, THE Carnot coefficient of performance (COP_{carnot}) of the chiller was used as a common tool to situate the results of models of different nature over the entire range of operating conditions of the absorption chiller. The COP_{carnot} (Eq. (I.3)) represents the maximum theoretical efficiency of the chiller as a reversible process with isothermal heat transfers at the three temperature levels (Altamirano et al., 2019a), allowing for the graphical comparison of different absorption chillers (regardless of their cooling capacity) (Boudéhenn et al., 2016) and modeling methods, which is the case of the present study.

2.3.2.1. Characteristic equation method

The CE method is a semi-empirical method that was originally developed for single-stage H₂O-LiBr absorption chillers (Hellmann et al., 1999; Ziegler, 1998). It has shown high flexibility as it has been adapted to other working pairs (Jakob, 2005; Ochoa and Coronas, 2016), direct-fired machines (Hellmann and Ziegler, 1999), and systems with adiabatic absorbers (Gutiérrez-Urueta et al., 2012). The most widespread method was presented by Hellmann et al. (Hellmann et al., 1999). Its main goal is to represent the cooling capacity and thermal COP of the chiller as functions of the temperatures of the external HTFs.

For this, the heat transfers in the main four components are represented as functions of the arithmetic mean temperatures of the internal (T) and external (t) fluids (Eqs. (II.13)-(II.16)). In these equations, z is the correction factor (due to the fact that logarithmic mean temperature differences are not taken into account).

$$\dot{Q}_e = UA_e \cdot z_e \cdot (t_e^{avg} - T_e^{sat}) \quad (II.13)$$

$$\dot{Q}_c = UA_c \cdot z_c \cdot (t_c^{avg} - T_c^{sat}) \quad (II.14)$$

$$\dot{Q}_a = UA_a \cdot z_a \cdot (t_a^{avg} - T_a^{avg}) \quad (II.15)$$

$$\dot{Q}_g = UA_g \cdot z_g \cdot (t_g^{avg} - T_g^{avg}) \quad (II.16)$$

Moreover, in the case of single-stage absorption chillers, the internal temperatures of the exchangers can be integrated into a single equation thanks to Dühring's rule expressing the saturation properties of the working fluid (Eq. (II.17)).

$$T_g^{avg} - T_a^{avg} = B \cdot (T_c^{sat} - T_e^{sat}) \quad (II.17)$$

On the basis of certain procedures described in (Hellmann et al., 1999), it is demonstrated that the evaporator and generator heat transfers can be expressed as functions of a total temperature difference $\Delta\Delta t$, defined by Eq. (II.18), which represents the difference between the "temperature thrust" ($t_g^{avg} - t_a^{avg}$) and the "temperature lift" ($t_c^{avg} - t_e^{avg}$) corrected with the Dühring coefficient (B). If a parallel flow is being used for the absorber and the condenser, their average external temperatures (t_a^{avg} and t_c^{avg}) can be replaced with the average external intermediate temperature (t_{ac}^{avg}).

$$\Delta\Delta t = t_g^{avg} - t_a^{avg} - B \cdot (t_c^{avg} - t_e^{avg}) \quad (II.18)$$

The thermal loads at the evaporator/generator and the COP are described by Eqs. (II.19)-(II.24), where A , C , and G are ratios of enthalpy differences of the internal components and \dot{Q}_{loss} represents the SHX loss or, as defined by Hellmann et al. (Hellmann et al., 1999), the heat required in the generator for heating and rejected in the absorber for cooling the solution streams to the appropriate internal equilibrium temperatures. Finally, $\Delta\Delta t_{min}$ expresses the minimum total temperature difference ($\Delta\Delta t$) required to overcome the SHX loss so that the chiller produces cold.

$$\dot{Q}_e^{ce} = q \cdot \Delta\Delta t - \alpha \cdot \dot{Q}_{loss} = q \cdot (\Delta\Delta t - \Delta\Delta t_{min}) \quad (II.19)$$

$$\dot{Q}_g^{ce} = G \cdot [q \cdot (\Delta\Delta t - \Delta\Delta t_{min})] + \frac{q}{\alpha} \cdot \Delta\Delta t_{min} \quad (II.20)$$

$$COP_{ce} = \frac{\dot{Q}_e}{\dot{Q}_g} = \frac{\Delta\Delta t - \Delta\Delta t_{min}}{G \cdot (\Delta\Delta t - \Delta\Delta t_{min}) + \frac{\Delta\Delta t_{min}}{\alpha}} \quad (II.21)$$

$$s = \frac{1}{\frac{G}{UA_g z_g} + \frac{A}{UA_a z_a} + B \cdot \left(\frac{C}{UA_c z_c} + \frac{1}{UA_e z_e} \right)} \quad (II.22)$$

$$\alpha = \frac{\frac{1}{UA_g z_g} + \frac{1}{UA_a z_a}}{\frac{G}{UA_g z_g} + \frac{A}{UA_a z_a} + B \cdot \left(\frac{C}{UA_c z_c} + \frac{1}{UA_e z_e} \right)} \quad (II.23)$$

$$\Delta\Delta t_{min} = \frac{\alpha}{q} \cdot \dot{Q}_{loss} = \left(\frac{1}{UA_g z_g} + \frac{1}{UA_e z_e} \right) \cdot \dot{Q}_{loss} \quad (II.24)$$

Depending on the available information, the parameters of the CE can be determined from the machine design data or with the use of experimental operational results, as explained by Puig-Arnavat et al. (Puig-Arnavat et al., 2010). The commonly expected deviation for this method on the cooling capacity is below 20% (Hellmann et al., 1998; Puig-Arnavat et al., 2010). This is due to the fact that some important parameters are considered as constants (e.g., the arithmetic temperature difference correction factor, the internal enthalpies, the mass flow rates, the heat transfer coefficients, or $\Delta\Delta t_{min}$) while they are not (Albers et al., 2008; Albers and Ziegler, 2009; Kühn and Ziegler, 2005). Several improved models of the characteristic equation with better accuracy have been proposed to take into account the variation of different boundary conditions such as the mass flow rates or the exchanger design (absorber and generator) (Buchin et al., 2016). However, to date, the solution equilibrium deviation at the outlet of the sorption exchangers cannot be accounted for (Albers, 2019).

2.3.2.2. Adapted characteristic equation method and Carnot function model

The empirical methods do not require physical insight into the machine and are adapted to fit the experimental results. Consequently, they possess lower deviations compared with the CE method. Kühn and Ziegler (Kühn and Ziegler, 2005) proposed the adapted CE method: an empirical method in which a multiple linear regression is performed to obtain an arbitrary characteristic temperature function ($\Delta\Delta t'$, Eq. (II.25)) that is linearly correlated to the cooling capacity (Eq. (II.26)). A second fit is then performed for the generator heat rate, a function of the $\Delta\Delta t'$, leading to Eq. (II.27). Kühn and Ziegler (Kühn and Ziegler, 2005) used the external arithmetic mean temperatures of the generator, heat sink, and evaporator for the regression. However, in the present work, we propose the use of the inlet generator temperature, inlet heat sink temperature, and outlet evaporator temperature for the regressions (Eqs. (II.25)- (II.27)) as these variables are commonly used to characterize the part-load behavior of the absorption chillers (experimental prototypes and commercial machines).

$$\Delta\Delta t' = t_g^i - a \cdot t_{ac}^i + e \cdot t_e^o \quad (II.25)$$

$$\dot{Q}_e^{ce'} = q' \cdot \Delta\Delta t' + r = q' \cdot t_g^i - s' \cdot a \cdot t_{ac}^i + s' \cdot e \cdot t_e^o + r \quad (II.26)$$

$$\dot{Q}_g^{ce'} = b \cdot \Delta\Delta t' + c \quad (II.27)$$

The CFM is another empirical method described by Boudéhenn et al. (Boudéhenn et al., 2014). This method has proven to estimate the experimental COP and cooling capacity (\dot{Q}_e) of different commercial machines operating with the same working pair (NH_3-H_2O) with a unique equation function of the machine's COP_{carnot} (shown in Eq. (II.28)) (Boudéhenn et al., 2016, 2014, 2012), in which ω_1 , ω_2 , τ_1 , τ_2 , and F_0 are fitted parameters to calculate either the machine's \dot{Q}_e or its thermal COP .

$$F_{cfm} = \omega_1 \cdot e^{(-COP_{carnot}/\tau_1)} + \omega_2 \cdot e^{(-COP_{carnot}/\tau_2)} + F_0 \quad (II.28)$$

Both of the presented empirical models usually have an accuracy higher than 10% in cooling capacity (Boudéhenn et al., 2016, 2014; Kühn and Ziegler, 2005; Puig-Arnavat et al., 2010), which is sufficient for being implemented as a control algorithm in absorption chillers. However, the underlying physical mechanisms of the machine operation are hidden (Buchin et al., 2016).

2.3.2.3. Effectiveness model

A thermodynamic model based on the mass and energy balances of each component was developed using the thermodynamic properties of NH_3-LiNO_3 (Salavera and Coronas, 2018) and pure ammonia (Rowley et al., 2010). The presented model is able to account for the non-equilibrium conditions of the solution with the vapor phase at the inlet and the outlet of the sorption components (i.e., the absorber and generator) as it employs a thermal effectiveness and a mass effectiveness in each one. Moreover, the thermal and mass effectivenesses serve for the identification of the limiting components in the chiller and can then be

used to optimize its thermal and electric performances. Finally, being a thermodynamic model, the different machine boundary conditions can be easily manipulated.

The state points (solid dots) in [Figure II.4](#) represent the calculated internal thermodynamic states of the $\text{NH}_3\text{-LiNO}_3$ solution (1–7), the NH_3 vapor (8 and 12), and the liquid NH_3 (9–11). Whereas the empty dots represent the external thermodynamic states of the driving source (t_g^i and t_g^o), the heat sink (t_{ac}^i and t_{ac}^o), and the chilled water source (t_e^i and t_e^o). The simplifying assumptions in the model are as follows:

- Heat losses are not taken into account.
- The expansion valves are isenthalpic and the pump is isentropic.
- The vapor at the output of the generator is considered to be in equilibrium with the solution concentration at point 3 and the high operating pressure [$T_8 = T_{eq}(P_h, x_3)$] (Herold et al., 2016).
- The refrigerant is at saturation state at the outlet of the condenser and the evaporator (points 9 and 12).

The sorption elements and heat exchangers are characterized thermal and a mass effectiveness as defined in [Section 2.2.1](#). The thermal effectiveness employed in the phase-change exchangers considers isobaric condensation and evaporation processes.

The simulation consisted of an iterative process in which the steady-state condition is reached when the condensed NH_3 vapor mass flow is equal to the evaporated vapor flow ($\dot{m}_8 = \dot{m}_{12}$). The mass and energy balances implemented for each component are described in Eqs. [\(II.29\)](#)-[\(II.31\)](#). Finally, the thermal coefficient of performance is used as defined by [Eq. \(I.2\)](#).

$$\sum \dot{m}_i = \sum \dot{m}_o \quad (\text{II.29})$$

$$\sum (\dot{m}_i x_i) = \sum (\dot{m}_o x_o) \quad (\text{II.30})$$

$$\sum ((\dot{m}_i h_i) - (\dot{m}_o h_o)) + \sum (\dot{Q}) + \sum (\dot{W}) = 0 \quad (\text{II.31})$$

2.3.3. Results and validation of the models

In the following sections, the implementation of the different approaches presented in [Section 2.3.2](#) to the 10-kW $\text{NH}_3\text{-LiNO}_3$ water-cooled absorption chiller is presented. As mentioned before, the COP_{carnot} was used as a variable to represent the results from the different models as well as the experimental results, in which case the CFM was used to show the trend of the latter.

2.3.3.1. Characteristic equation method

Ochoa and Coronas (Ochoa and Coronas, 2016) presented the CE ([Section 2.3.2.1](#)) of the studied absorption chiller and obtained the coefficients presented in [Table II.5](#). The values of the heat rates (in the generator and the evaporator) and thermal COP are compared with the experimental results ([Table II.4](#)) in [Figure II.5a](#). The deviations in the cooling capacity remain below 15%, with the exception of two cases. On the other hand, the generator heat rate correlation presents deviations of less than 10%, with the exception of one operating condition.

In the CE ([Figure II.5a](#)), the cooling and generator heat rates are linearly dependent on ΔT (Eqs. [\(II.19\)](#) and [\(II.20\)](#)). An increase in the generator (t_g^{avg}) or evaporator (t_e^{avg}) temperatures increases ΔT ([Eq. \(II.18\)](#)); hence \dot{Q}_e and \dot{Q}_g also increase, whereas an increase in the heat sink temperature (t_{ac}^{avg}) has the opposite effect. These average external temperatures at the three levels have almost the same influence

on $\Delta\Delta t$ (the “temperature lift” terms, t_c^{avg} and t_e^{avg} , being corrected by a Dühring coefficient (B) that is close to 1 (1.18 in this case); hence their variation has almost the same impact on \dot{Q}_e and \dot{Q}_g . This generates an important data dispersion that is especially noticeable on the experimental COP at low $\Delta\Delta t$ values due to a stronger influence of the intermediate (heat dissipation) temperature that is not taken into account in the $\Delta\Delta t$ term (Kühn and Ziegler, 2005; Puig-Arnavat et al., 2010). Another factor that influences the data dispersion is the simplifying assumption of fundamental parameters (e.g., the heat transfer regimes or internal/external irreversibilities) as constants, as discussed in Section 2.3.2.1, which leads to functions with constant slopes and intersects (Albers et al., 2008; Albers and Ziegler, 2009; Kühn and Ziegler, 2005). Finally, the assumption of the solution being at equilibrium with the vapor phase at the outlet of the sorption components is another hypothesis that is not valid in real operating conditions, and it might add imprecision to the estimated results.

The representation of the characteristic equation results with the COP_{carnot} domain is shown in Figure II.5b. The trend followed by the experimental results with the COP_{carnot} is shown by the CFM (Eq. (II.28), Table II.7, and dashed lines in Figure II.5b), with deviations that remain below 10% for most of the cases. In this representation of the absorption chiller, the assumption of a linear dependence between the generator and evaporator heat rates with the external temperatures is not used. Different from the $\Delta\Delta t$ term, in the COP_{carnot} the weight of each temperature is not linear. From Eq. (I.3) and the external temperature conditions studied in the present work (Table II.3), it is evident that the one with the highest impact is the heat sink temperature (t_{ac}^i , especially at low COP_{carnot}), followed by the chilled water temperature (t_e^o , especially at high COP_{carnot}) and the inlet hot water temperature (t_g^i , especially at low COP_{carnot}), respectively. This distribution of the HTF temperatures effect seems to better represent the machine’s operating regime as there is a noticeable lower experimental COP dispersion (a CFM average deviation of 1.96% compared with 4.1% for the CE method), especially for two cases (tests 13 and 14, green dots in Figure II.5) in which the experimental results were situated at a lower regime in the COP_{carnot} domain due to a dominance of t_{ac}^i over t_g^i . In this representation, the evaporator and generator loads rapidly increase at low COP_{carnot} regimes, with a slope that decreases approaching an asymptote at high regimes, stabilizing the COP. Furthermore, the trends followed by the CE method and the CFM diverge considerably.

Table II.5: Coefficients of the characteristic equation (Eqs. (II.18)-(II.20)) (Ochoa and Coronas, 2016).

Coefficient	Value
s (kW K ⁻¹)	0.52
α (-)	0.29
G (-)	1.27
$\Delta\Delta t_{min}$ (K)	2.75
B (-)	1.18

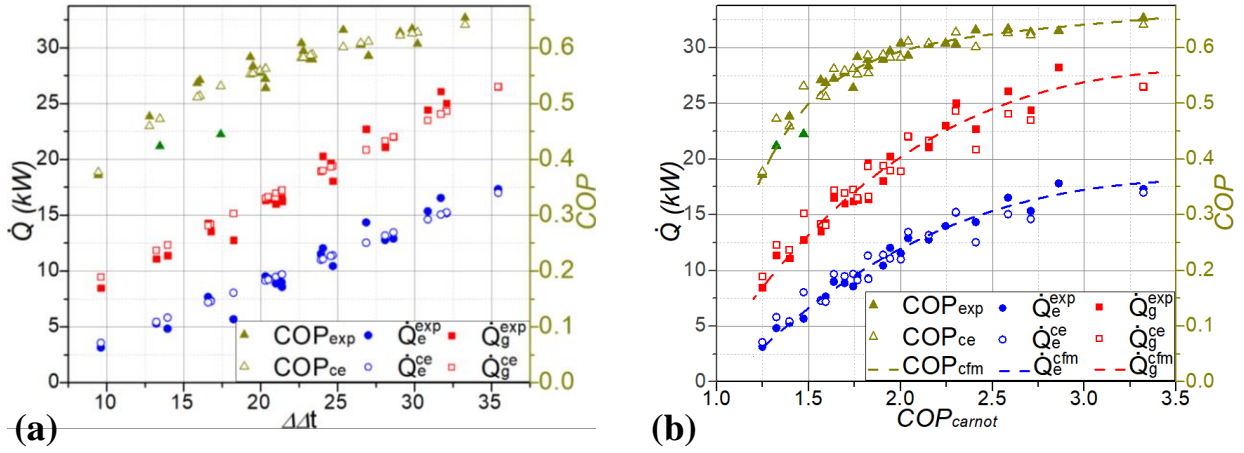


Figure II.5: Results of the characteristic equation method vs. experimental results represented in the (a) $\Delta\Delta t$ domain and in the (b) COP_{carnot} domain.

2.3.3.2. Adapted characteristic equation method and Carnot function model

The least squares method along with the generalized reduced gradient (GRG) nonlinear method of the Excel Solver were used to fit the parameters of the equations presented in section 2.3.2.2 to the data of Table II.4. The fitted parameters of the adapted CE method are presented in Table II.6, whereas those of the CFM are presented in

Table II.7. With the adapted CE method, the adapted characteristic temperature difference, $\Delta\Delta t'$ (Eq. (II.25)), is used to represent the functioning of the machine. This fitted parameter was proposed to better divide the effects of external temperatures (Kühn and Ziegler, 2005). Different from the COP_{carnot} , the external temperatures possess a constant influence on $\Delta\Delta t'$ (factors 1, a , and e for t_g^i , t_{ac}^i , and t_e^o in Eq. (II.25), respectively). However, in the present study, similar to the COP_{carnot} , the heat sink temperature (t_{ac}^i) possesses the highest influence ($a = 2.773$), followed by the chilled water temperature ($e = 1.88$) and the heat source temperature, respectively.

The adapted characteristic loads (generator and evaporator) and COP are compared with the experimental results in the COP_{carnot} domain in Figure II.6. The correlated results present considerably lower deviations compared with the conventional CE, showing deviations below 10% for most of the cases, with the exception of two conditions. However, in spite of the good model estimations, a physical understanding of the machine operation cannot be inferred. Therefore, it is not reliable to identify deviations from normal machine operating conditions, systematic deviations, or the limiting components in the system, for which models with a physical basis are required (Buchin et al., 2016).

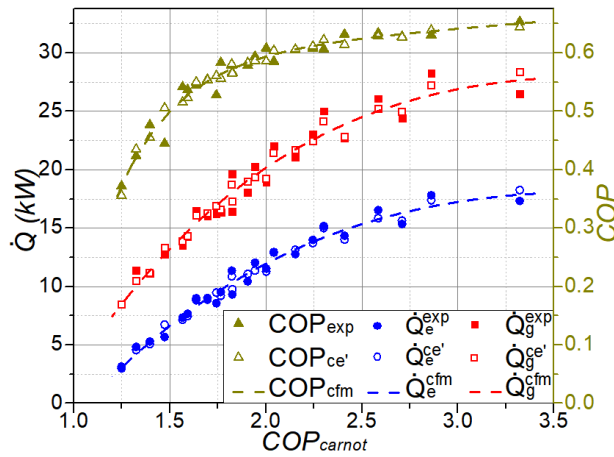
Both methods (the adapted CE method and the CFM), being regressions of the experimental dataset, are in good agreement; the CFM has less experimental COP dispersion (an average deviation of 1.96% versus 2.68% for the adapted CE method). The two empirical methods possess a deviation below 10% for most of the cases. Nevertheless, the CFM is based on a parameter (the COP_{carnot}) that has a thermodynamic basis and that does not depend on the specific machine's characteristics or experimental dataset; therefore, it can be employed for any machine or modeling method, which gives it an advantage over the adapted CE method. The COP_{carnot} thus seems to be a reliable parameter with which to represent the entire range of the machine operating conditions.

Table II.6: Coefficients of the adapted characteristic equation (Eqs. (II.25)-(II.27)).

Coefficient	Value
s'	0.373
a	2.773
e	1.88
r	4.716
b	0.489
c	10.691

Table II.7: Coefficients of the Carnot function model for the cooling capacity and COP (Eq. (II.28)).

	\dot{Q}_e^{cfm} (kW)	COP^{cfm}
ω_1	159.56	-0.44
ω_2	-172.09	-10.57
τ_1	4.59	13.14
τ_2	2.46	0.32
F_0	-14.93	0.99


 Figure II.6: Results of the adapted characteristic equation method vs. experimental results in the COP_{carnot} domain.

2.3.3.3. Effectiveness model

In the present section, the results from the modeling of the absorption chiller using its thermal and mass effectivenesses are presented. First, the different thermal and mass effectivenesses of the system components are obtained for the whole range of tested conditions, which allows for the identification of the limiting components. The present work proposes the use of the Carnot function model (Eq. (II.28)), which to date was used exclusively to estimate the absorption chiller cooling capacity and thermal COP, as a simple equation to represent the variable exchangers effectivenesses as a function of the COP_{carnot} . Second, the modeling results of the thermal loads and COP are presented and discussed.

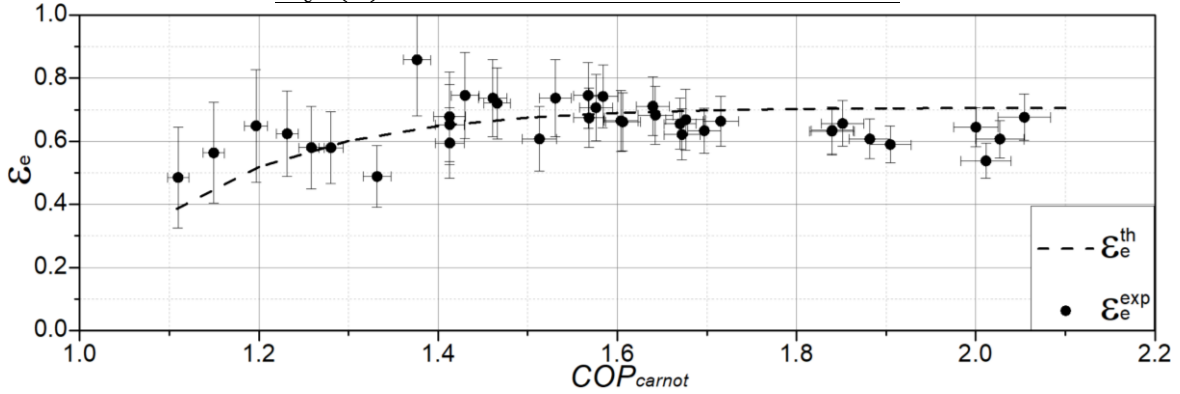
2.3.3.3.1. Thermal and mass effectivenesses of the components

In order to calculate the thermal effectiveness of the evaporator, the internal pressure data were used to obtain the internal saturation temperature conditions using the correlations of Rowley et al. (2010) and considering an isobaric evaporation process. These data, however, were available for a series of experiments in a shorter cooling capacity range (3.1–12 kW) than the total number of tests. The temperature measurement ranges and operating conditions and their uncertainties are presented in Table II.8. The experimental results and a correlation (see Table II.10) with a limit at an effectiveness of 0.7 were plotted against the COP_{carnot} (Figure II.7). The evaporator effectiveness decreases at very low cooling capacities due to the nature of the exchanger, which is a flooded evaporator whose refrigerant level is controlled by an electronic expansion valve (Zamora, 2012). The fact that the proposed correlation is out of the uncertainty range in some experimental conditions has no physical sense and is attributed to

other factors during experimentation. Indeed, as the evaporating load increases, the refrigerant level in the evaporator rises, increasing the heat exchange area. This, together with the confined pool boiling enhancement present for the studied conditions (capillary length of ammonia in the same range as the space between plates of 2 mm) (Rops et al., 2009), should increase the thermal effectiveness of the exchanger, achieving a maximum value of approximately 0.7.

Table II.8: Evaporator internal and external operating temperatures.

Variable	Measurement range	Uncertainty
t_e^i (°C)	8.9-18.4	$\pm 0.1^\circ\text{C}$
t_e^o (°C)	8; 15	$\pm 0.1^\circ\text{C}$
T_e^{sat} (°C)	6.32-14.2	$\pm 0.3^\circ\text{C}$


 Figure II.7: Evaporator thermal effectiveness against COP_{carnot} .

The operating conditions of the condenser are shown in Table II.9. In this case, as there is no direct temperature measurement at the outlet of the exchanger, t_c^o can be approximated by energy balances at the evaporator and condenser. Unfortunately, the effectiveness uncertainties of this calculation are too large and lead to condenser effectiveness greater than 1. Therefore, the theoretical effectiveness for the nominal operating conditions of the condenser was determined by means of the number of transfer units (NTU) (Bergman et al., 2011) calculated from the convection thermal resistance on the water side, the stainless steel wall conduction thermal resistance, and the conduction thermal resistance of the NH_3 refrigerant falling film in the conditions of the highest film thickness. These calculations led to a global heat transfer coefficient of at least $2683 \text{ W m}^{-2} \text{ K}^{-1}$, an NUT of at least 5.49, and a thermal condenser effectiveness of at least 0.989, showing that the condenser is not a limiting component in the system, which is in agreement with the over-dimensioning of 86% for its nominal conditions (Zamora, 2012). Therefore, a constant condenser effectiveness of 0.99 was used for the simulations.

Table II.9: Condenser internal and external temperature operating conditions.

Variable	Measurement range	Uncertainty
t_c^i (°C)	32.6-44	$\pm 0.1^\circ\text{C}$
t_c^o (°C)	Not measured	-
T_c^{sat} (°C)	36-46	$\pm 0.4^\circ\text{C}$

From the experimental characterization of PHE's used as sorption exchangers of absorption chillers presented in Section 2.2, the experimental effectivenesses in the nominal conditions of the machine (represented by solid dots in Figure II.8) are as follows: $\varepsilon_a^m = 0.479$, $\varepsilon_a^{th} = 0.492$, $\varepsilon_g^m = 0.629$, and $\varepsilon_g^{th} = 0.642$. In order to investigate the evolution of the effectivenesses for the range of COP_{carnot} studied, a program was run to identify the values of the corresponding thermal and mass effectivenesses that would lead to the experimental cooling capacity. Considering that both the absorber and generator are bubble plate heat exchangers, the evolution of the effectivenesses in both exchangers was considered to follow the same trend, i.e., the same correlation factor (f) is multiplied by the nominal absorber/generator effectivenesses at each COP_{carnot} condition. A correlation with the form of Eq. (II.28))

was then obtained from the scattered results to give the functions of the absorber and generator effectivenesses (see Figure II.8 and Table II.10). Figure II.8 shows the evolution of all the thermal and mass effectivenesses of the exchangers. An increase in the absorber and generator effectivenesses can be observed while increasing the COP_{carnot} . This can be explained by the fact that both operate in a bubble regime, and while increasing the cooling load, the bubble presence is progressively more common, generating instabilities in the solution flow and increasing the exchanger effectiveness. The effectivenesses will be discussed in more detail in Section 2.3.4. The generator/absorber thermal effectiveness and mass effectiveness calculated by the proposed correlation are in accordance with the experimental effectivenesses calculated under nominal conditions at a COP_{carnot} of 1.85 (solid dots in Figure II.8) (a deviation of less than 4%).

Finally, even though the solution heat exchanger was designed for a nominal thermal effectiveness of 0.9 (Zamora, 2012), no experimental data were available to support this value. Instead, a good agreement with the experimental results was found to occur at an SHX effectiveness of 0.65. Besides a possible experimental effectiveness lower than the nominal design value, other factors such as the non-idealities that were not taken into account (e.g., no heat losses to the environment or the variations in the solution mass flow rate) that lead to a lower machine performance might be reflected in this effectiveness. Therefore, this value was used as the SHX thermal effectiveness and kept as constant for the entire range of operating conditions since the available information does not allow us to estimate a variable behavior.

While the modeling methods usually consider a constant heat transfer coefficient (constant effectiveness) in the absorption chiller components for the entire range of operating conditions, it can be observed in Figure II.8 that there are some exchangers for which the effectivenesses decrease noticeably at low cooling loads. The absorber is clearly the most limiting component in the system, probably due to the high viscosities and low mass diffusivity values of the solution that operates at lower temperatures compared with the generator (Mittermaier and Ziegler, 2015). Indeed, some studies have reported lower than expected performances of the NH_3-LiNO_3 working fluid in sorption exchangers, which has been attributed to its elevated viscosity (Altamirano et al., 2020b). The evaporator also seems to be a limiting component due to a refrigerant level control that can be optimized by a variable chilled water flow rate, which would also have a positive impact on the total electric COP of the chiller. Moreover, its maximum effectiveness can be increased by increasing the length or the number of plates in the exchanger, at the cost of a depreciated system compactness. The same applies to the SHX and sorption exchangers, for which an increase in the number of plates or exchanger length would increase the solution residence time in the exchanger, improving its effectiveness.

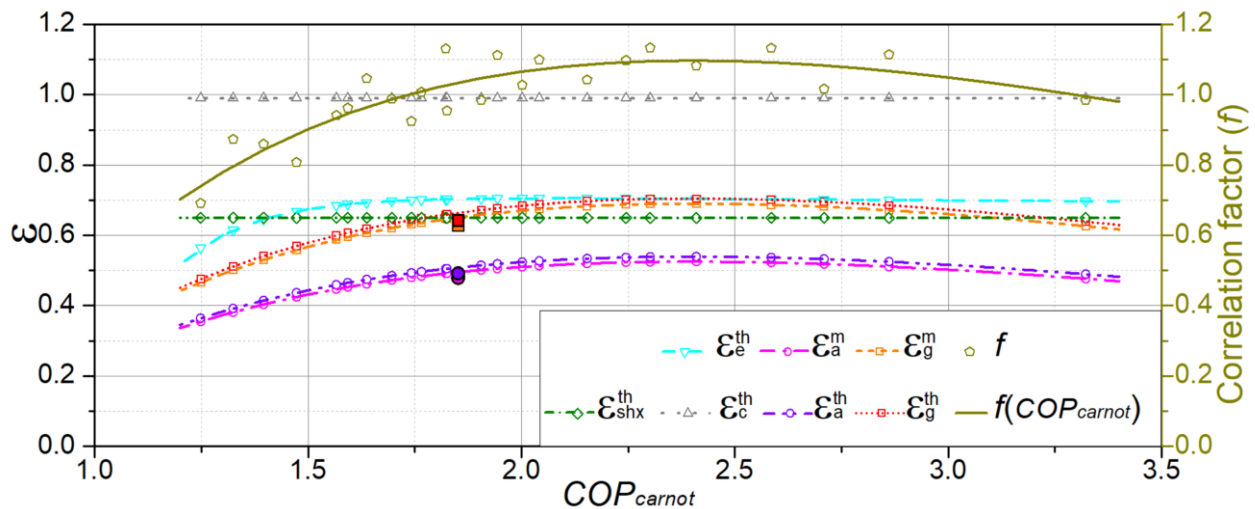


Figure II.8: Thermal and mass effectivenesses correlations of the exchanger components and correlation factor of the sorption exchangers (solid dots for the nominal experimental effectivenesses values).

Table II.10: Thermal and mass effectivenesses correlations of the system components for the range of $COP_{carnot} \in [1.2;3.4]$.

Component	Thermal effectiveness	Mass effectiveness
Evaporator	$\varepsilon_e^{th} = 0.5 \cdot e^{(-COP_{carnot}/61)}$ $- 155 \cdot e^{(-COP_{carnot}/0.18)} + 0.23$	-
Condenser	$\varepsilon_c^{th} = 0.99$	-
Solution heat exchanger	$\varepsilon_{shx}^{th} = 0.65$	-
Absorber*	$\varepsilon_a^{th} = 0.492 \cdot f(COP_{carnot})$	$\varepsilon_a^m = 0.479 \cdot f(COP_{carnot})$
Generator*	$\varepsilon_g^{th} = 0.642 \cdot f(COP_{carnot})$	$\varepsilon_g^m = 0.629 \cdot f(COP_{carnot})$

$$* f(COP_{carnot}) = 4.36 \cdot e^{(-COP_{carnot}/9.18)} - 4.16 \cdot e^{(-COP_{carnot}/0.98)} - 1.9$$

2.3.3.3.2. Effectiveness model validation

The correlations provided in Table II.10 and shown in Figure II.8 for the thermal and mass effectivenesses of the components were implemented in the EM and the results obtained are shown in Figure II.9. Most of the simulated results present deviations below 10% compared with the experimental results. The simulated cooling capacity follows the same trend as the experimental one, in close agreement with the CFM. On the other hand, the simulated generator heat rate, although in close agreement in most of the operating conditions, diverges somewhat at the lower COP_{carnot} values. This also has an impact on the simulated COP, which is higher than the experimental COP at low COP_{carnot} values. This divergence might be due to factors that were not taken into account as the variation of the SHX effectiveness in real operating conditions and heat losses to the environment. The model presented here, which is able to identify the internal non-equilibrium conditions of the solution with the vapor phase at any point, is used as a tool to better explain the behavior of the machine in the following.

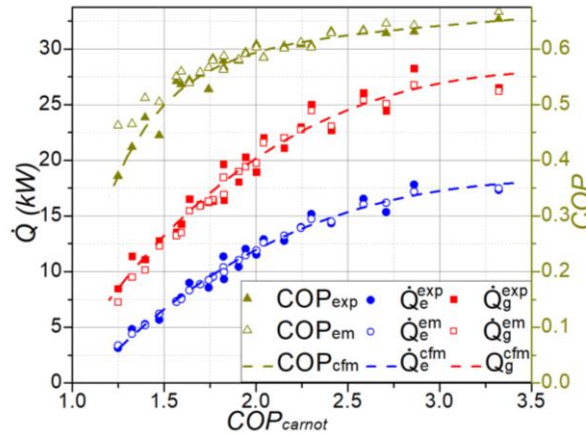


Figure II.9: Results of the effectiveness method vs. experimental results in the COP_{carnot} domain.

2.3.4. Discussion of the internal operating conditions through the effectiveness model

During the machine operation, the high pressure and low pressure are mainly controlled by the heat sink temperature and the chilled water temperature, respectively. Owing to the decrease in the heat sink

temperature for high COP_{carnot} values, the high pressure (P_h) is reduced as well, decreasing the solution saturation temperature conditions in the generator, thereby enhancing the desorption phenomenon for a given heat source temperature. On the other hand, higher chilled water temperatures lead to greater low pressures (P_l) at high COP_{carnot} values, increasing the solution saturation temperature conditions, which is favorable for the absorption phenomenon at a given heat sink temperature. The following sections discuss the internal operating conditions of the machine. This better understanding allows for the identification of opportunities to improve thermal and electric COPs.

2.3.4.1. Solution concentration conditions

Figure II.10 shows the internal solution concentrations (concentrated and diluted side) and the concentration difference (right axis). The concentrated side corresponds to the outlet concentration of the generator and the inlet concentration of the absorber and vice versa for the diluted side. These concentrations, result of all the heat and mass transfer phenomena in the machine, are of great importance since they have a direct impact on the solution thermophysical properties, which control the performance of the exchangers in the system. High absorber and generator temperatures lead to higher concentrations, whereas the evaporator and condenser temperatures have the opposite effect.

As COP_{carnot} increases, the refrigerant flow in the machine increases, proportionally increasing the concentration differences (Δx) between the inlet and outlet of the sorption components. In the entire range of operating conditions, the mass fraction on the concentrated side remained moderately stable with values between 0.5 and 0.536. As the cooling capacity increases, the diluted-side concentration decreases with values ranging from 0.512 to 0.435. The impact of the intermediate temperature is not the same on the generator as on the absorber. Whereas the outlet absorber mass fraction seems highly impacted by the intermediate temperature source that decreases with the $COP_{carnots}$, the outlet generator mass fraction does not follow the same trend. This is mostly due to the higher generator effectivenesses compared with those of the absorber (see Figure II.8) and the enhanced desorption potential due to a decrease in the high operating pressure (owing to the reduction of the intermediate temperature source with the COP_{carnot}).

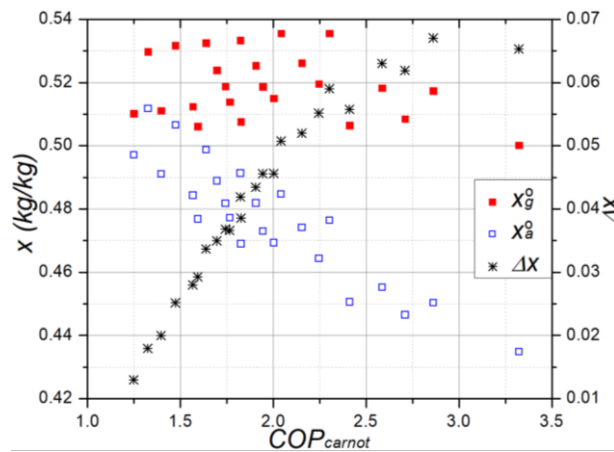


Figure II.10: Simulated machine internal solution concentrations and concentration differences at part-load operation.

2.3.4.2. Equilibrium factor

Figure II.11 shows the equilibrium factor (R , Eq. (II.5)) in the absorber and the generator for each operating condition. As mentioned before, this parameter represents the HTF potential to heat/cool down the solution. When $R > 1$, the maximum transferable heat and mass are limited by the solution flow conditions. As the cooling capacity increases, the equilibrium factors decrease. This happens because as the equilibrium conditions in the machine change, the heat transfer fluids deviate from them (Figure II.13a), increasing the absorption/desorption potential of the solution, and decreasing the equilibrium factor. One mark is outside the trend in the absorber ($COP_{carnot}=2.41$ in Figure II.11) due to an uncommon

low heat sink flow rate in test 7 (Table II.4), which decreases the HTF cooling potential and therefore the equilibrium factor.

While the solution side is the one limiting the sorption phenomena ($R > 1$), an increase in the HTF flow rate only leads to a decrease in the machine's electric COP (the absorber/generator effectivenesses are not substantially improved), as observed in (Altamirano et al., 2020c). Consequently, for an optimal electric COP, operation at equilibrium factors close to 1 is desirable. Figure II.11 shows the great potential of COP_{elect} improvement by a reduction in the HTF mass flow rates of up to 4–5 times at low COP_{carnot} values and approximately 2 times at high cooling regimes. Regarding the phase-change exchangers, the external condenser flow rate can also be reduced as it operates with an effectiveness close to 1, whereas the chilled water mass flow rate can be reduced at low cooling regimes to increase the thermal effectiveness of the evaporator, as mentioned in Section 2.3.3.3.1. A proper control of the external HTFs might subsequently lead to important improvements in the electric COP, which was a major concern during the machine development (Zamora et al., 2014).

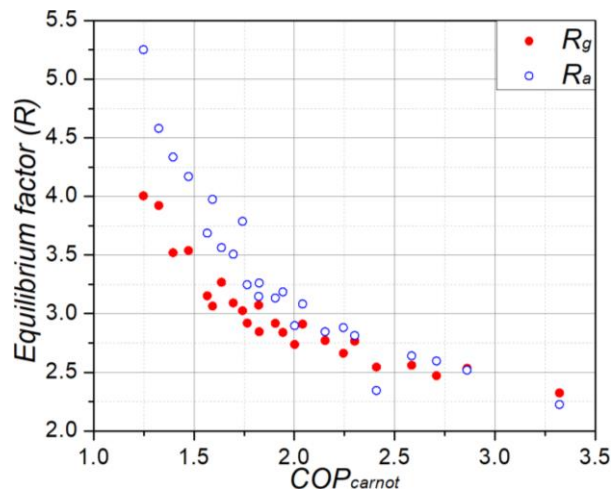


Figure II.11: Equilibrium factor for the sorption components (absorber and generator) in the different tested conditions.

2.3.4.3. Solution flow conditions

The analysis of the solution flow conditions in the sorption exchangers is of fundamental importance as it is the one that limits the transfers in the tested conditions ($R > 1$ from Figure II.11). Figure II.12 shows that the chilled water temperature is a dominant factor in the kinematic viscosity, volumetric flow rate, and therefore in the solution Reynolds number. Lower chilled water temperatures lead to higher viscosities due to the higher solution concentrations caused by a decreased absorption potential. Regarding the absorber, for each chilled water temperature, as the COP_{carnot} increases, the heat sink temperature decreases, lowering the solution absorber temperature, whereas the generator temperature increases, slightly increasing the solution concentration, and both phenomena increase the inlet viscosity of the solution in the absorber (Figure II.12a), this variation being less noticeable at high COP_{carnot} values due to a lower concentration variation in the concentrated solution side (Figure II.10). On the other hand, in the case of the generator, the viscosity for each evaporator temperature decreases with the COP_{carnot} mainly via the decrease in the concentration of the diluted solution side. From Figure II.12a, the difference in the operating solution viscosity range between the absorber and the generator is clear, which is one of the reasons why the absorber has lower performance compared with the generator (Figure II.8) (Mittermaier and Ziegler, 2015).

Figure II.12b shows the evolution of the inlet solution volumetric flow rate (\dot{V}) and the Reynolds number (Re) in the absorber and the generator. Besides the kinematic viscosity, the volumetric flow rate also has a direct impact on Re . Despite a constant solution mass flow rate, due to a decrease in the density at the

inlet of the generator, the volumetric flow rate increases with COP_{carnot} . On the other side, \dot{V}_a^i decreases with COP_{carnot} due to the decrease in the solution mass flow rate (higher refrigerant desorption at the generator). The variations in the solution kinematic viscosities and volumetric flow rates lead to an increase in Re at the generator and vice versa at the absorber.

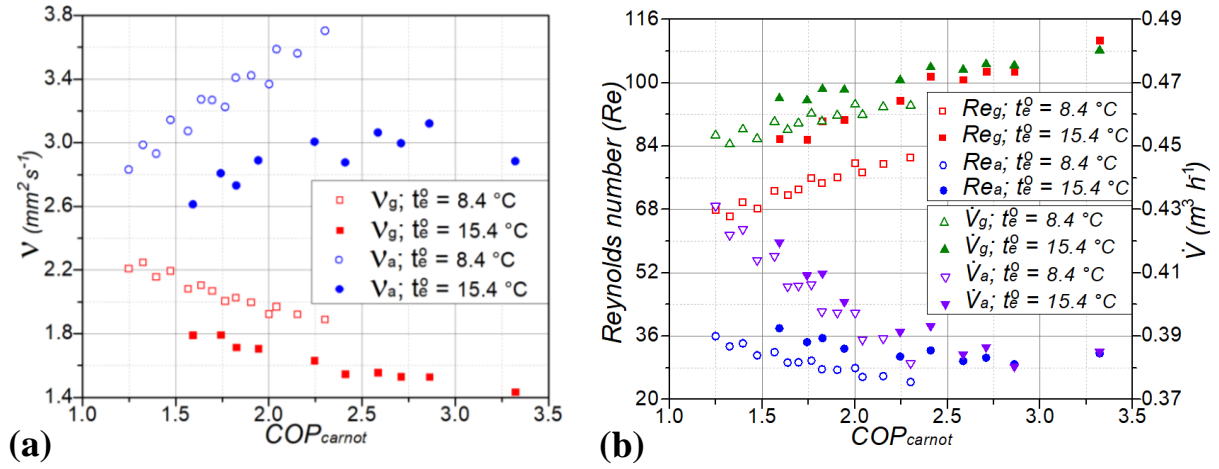


Figure II.12: Inlet solution conditions in the absorber and generator. (a) Dynamic viscosity and (b) Reynolds number.

2.3.4.4. Equilibrium deviation temperatures

Figure II.13 shows the HTF equilibrium deviation temperatures (Eq. (II.3)) at the inlet of the sorption components and the solution equilibrium deviation temperatures (Eq. (II.4)) at their inlet/outlet. According to Figure II.13a, as the COP_{carnot} increases, the HTF in the absorber and the generator increase their deviation from the solution equilibrium conditions, increasing the sorption potential on the solution side and therefore, increasing the machine's cooling capacity. From Figure II.13b, contrary to the standard assumption in the modeling of absorption chillers, it is clear that the solution is rarely in equilibrium conditions at the outlet of the sorption elements. The low evaporating pressures and high absorber temperatures at low COP_{carnot} increase the deviation from the equilibrium conditions of the solution at the inlet of the absorber. As the COP_{carnot} increases, the absorber temperature decreases and the operating pressure increases, which decreases the solution equilibrium deviation temperature until reaching a value of approximately $5^\circ C$. The $\Delta T_{sol}^{eq,0}$ reaches values of approximately $2.5^\circ C$ at the absorber at high COP_{carnot} . A similar behavior is observed at the generator inlet, for which the solution arrives highly subcooled at low cooling regimes. In these conditions, vapor is generated at the interface between the solution flow and the plate. The evaporation induces mass diffusion close to the interface and locally modifies the equilibrium temperature. The high concentration gradient induced in the solution flow (low mass diffusivity) seems to explain the average subcooling of the solution at the outlet of the component despite the clear vapor generation. This subcooled boiling phenomenon, also reported in (Venegas et al., 2012), is similar to the one observed in convective boiling of subcooled liquids (Carey, 1992). The decrease in the solution concentration at the generator inlet for high COP_{carnot} values (Figure II.10) brings the solution closer to the equilibrium conditions at the inlet of this component. This solution reaches a super-heated state at the outlet of the generator at high cooling regimes (high COP_{carnot}), showing the desorption potential that was unused owing to its limited thermal and mass effectivenesses.

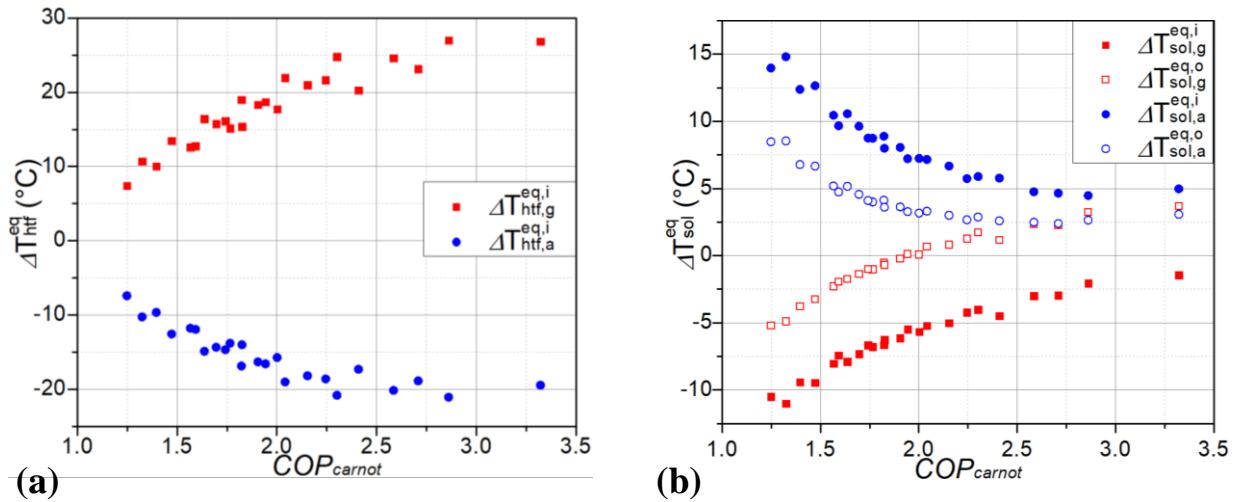


Figure II.13: Temperature deviation from the internal solution equilibrium conditions of the (a) heat transfer fluid and the (b) solution.

2.3.4.5. Thermal and mass effectivenesses of the sorption exchangers

Different factors exist that impact the absorber/generator thermal and mass effectivenesses. In an operation in which the solution limits the transfers ($R > 1$), the solution flow conditions and its deviations from equilibrium are of fundamental importance. Regarding the solution flow conditions (Figure II.12), both sorption exchangers present opposite effects. Indeed, a decreasing viscosity in the generator (Figure II.12a) increases the exchanger performance due to enhanced bubble hydrodynamic disturbance effects, whereas an increased volumetric flow rate (Figure II.12b) increases the solution velocity at the inlet of the exchanger, decreasing the solution residence time and therefore decreasing the exchanger performance. The same happens in the absorber but with opposite phenomena.

Considering that the viscosity effects are somewhat balanced by the change in the solution volumetric flow rates, the variation in the sorption effectivenesses might then be controlled by the solution equilibrium deviations. Indeed, a high subcooling of the solution at the inlet of the generator and a high super-heating at the inlet of the absorber (Figure II.13b) are in agreement with the low effectivenesses of the sorption exchangers at low COP_{carnot} values (Figure II.8). However, their approach to the equilibrium while increasing the COP_{carnot} is congruent with the increase in the effectivenesses. Another factor that might lead to an increase in the effectivenesses at higher COP_{carnot} values is the variation in the solution concentrations, especially at the inlet of the desorber (see Figure II.10). Lower solution concentrations lead to a lower viscosity and higher performances. Furthermore, the slight reduction in the absorber/generator effectivenesses at high COP_{carnot} (Figure II.8) might be the result of other factors (e.g., heat losses to the environment). A more detailed experimental study is required to determine the predominant parameter in the effectivenesses of the sorption exchangers and to more precisely characterize their evolution during the different operating regimes. It seems that the solution deviation from equilibrium conditions has a stronger impact on the mass effectiveness than on the thermal effectiveness (Altamirano et al., 2020c).

2.4. Conclusions

The present section introduced the general definition of the thermal and mass effectivenesses applied to the non-adiabatic sorption exchangers of absorption chillers (the mass effectiveness of adiabatic sorption exchangers is intrinsically included in this definition). First, the characterization of PHE as the absorber and desorber components of an $\text{NH}_3\text{-LiNO}_3$ absorption chiller based on their thermal and mass effectiveness was performed. The impact of the different conditions on the effectivenesses was observed. The studied absorber presented a mass effectiveness between 0.31 and 0.76 and a thermal effectiveness between 0.33 and 0.77. On the other hand, the studied desorber presented a mass effectiveness between 0.39 and 0.85 and a thermal effectiveness between 0.63 and 0.92. As the maximum transferable conditions (\dot{Q}_{sorp}^{max} and \dot{m}_{sorp}^{max}) in the studied exchangers were always dependent on the solution side ($R>I$), ε_{th} and ε_m were mostly impacted by the solution flow regime (Re_{sol}), leading to better performances at low Re_{sol} and lower dynamic viscosities (mainly due to a mass transfer enhancement by hydrodynamic bubble disturbances and an increased bubble residence time in the plate channels). The lowest Re_{htf} in order to maintain $R>I$ is desirable in the sorption exchangers to have a low pumping energy consumption. Finally, the solution's thermophysical properties and deviation from the equilibrium conditions have a stronger impact on the mass effectiveness than on the thermal effectiveness, especially at low solution flow regimes.

After the components' characterization, a characterization of a 10-kW water-cooled absorption chiller was performed by means of four different methods that use the external fluid temperatures to situate the machine operating conditions: the CE method (semi-empirical), the adapted CE method and the CFM (both empirical), and a thermodynamic model (physical), called the effectiveness model (EM), based on thermal and mass effectivenesses. The COP_{carnot} was used as a common parameter to represent the different operating conditions of the chiller and situate the different modeling results. When no information about the internal working fluid conditions is required and an extensive database of experimental results is available, the empirical models offer a simple tool to calculate the cooling power and thermal COP of the system. On the other hand, if the number of experimental results is limited but the machine components design data is available, the CE method is a viable option. Finally, if information about the thermal and mass effectivenesses of the internal components is available in the range of studied conditions, the proposed EM can be employed to identify the limiting components in the system and analyze at any time the internal non-equilibrium conditions of the solution with the vapor phase. Furthermore, in the present study, it allowed us to identify COP_{elect} improvement opportunities since the HTF flow rates in all the components can be reduced, especially at low cooling regimes.

The thermal and mass effectivenesses are parameters that, different from the heat/mass transfer coefficients/fluxes, depend on fewer parameters and consider the non-saturated conditions at the inlet and the outlet of the components. Therefore, they can be used to create more complete models to characterize the part-load behavior of absorption chillers (internal and external thermodynamic states) and identify optimization opportunities for each individual component, or be applied in dynamic models for the study of systems in constantly changing conditions (e.g., while using solar thermal energy or ambient temperature as heat sources). Furthermore, the mass effectiveness alone is a reliable parameter that can be used for the characterization of adiabatic sorption elements, that, as indicated in [Chapter I](#), are a promising technology for absorption chillers. This will be the subject of discussion in the following chapters.

References

- Aiane, M., Ramousse, J., Stutz, B., Bouyaud, M., Boudard, E., 2017. Dynamic Modeling Of An Automotive Air-Conditioning System By Absorption, in: International Sorption Heat Pump Conference, August 7-10. Tokyo, Japan.
- Albers, J., 2019. Extension of a calculation method for the regulation of absorption refrigeration systems (in German). PhD TU Berlin.
- Albers, J., Kühn, A., Petersen, S., Ziegler, F., 2008. Control of absorption chillers by insight: the characteristic equation. *Czas. Tech. Mech.* 105, 3–12.
- Albers, J., Ziegler, F., 2009. Influence of internal irreversibilities on the characteristic equation of absorption chillers, in: Heat Powered Cycles Conference, September 7-9. Berlin, Germany, pp. 69–70.
- Altamirano, A., Le Pierrès, N., Stutz, B., 2019. Review of small-capacity single-stage continuous absorption systems operating on binary working fluids for cooling: Theoretical, experimental and commercial cycles. *Int. J. Refrig.* 106, 350–373. <https://doi.org/10.1016/j.ijrefrig.2019.06.033>
- Altamirano, A., Stutz, B., Le Pierrès, N., 2020a. Review of small-capacity single-stage continuous absorption systems operating on binary working fluids for cooling: Compact exchanger technologies. *Int. J. Refrig.* 114, 118–147. <https://doi.org/10.1016/j.ijrefrig.2020.02.033>
- Altamirano, A., Stutz, B., Le Pierrès, N., Coronas, A., 2020b. Experimental characterization by thermal and mass effectivenesses of plate heat exchangers in $\text{NH}_3\text{-LiNO}_3$ absorption chillers, in: ISHPC 2021 – Online Pre-Conference. Berlin, Germany, pp. 56–60. <https://doi.org/10.14279/depositonce-10430.2>
- Amaris Castilla, C., 2013. Intensification of NH_3 Bubble Absorption Process using Advanced Surfaces and Carbon Nanotubes for $\text{NH}_3/\text{LiNO}_3$ Absorption Chillers. PhD Universitat Rovira i Virgili.
- Bergman, T.L., Lavine, A.S., Incropera, F.P., Dewitt, D.P., 2011. Fundamentals of Heat and Mass Transfer, 7th ed. John Wiley & Sons, Inc., Hoboken, US.
- Boudéhenn, F., Bonnot, S., Demasles, H., Lazrak, A., 2014. Comparison of different modeling methods for a single effect water-lithium bromide absorption chiller, in: International Conference on Solar Energy and Buildings, September 16-19. Aix-les-Bains, France.
- Boudéhenn, F., Bonnot, S., Demasles, H., Lefrançois, F., Perier-Muzet, M., Triché, D., 2016. Development and Performances Overview of Ammonia-water Absorption Chillers with Cooling Capacities from 5 to 100 kW. *Energy Procedia* 91, 707–716. <https://doi.org/10.1016/j.egypro.2016.06.234>
- Boudéhenn, F., Demasles, H., Wyttenbach, J., Jobard, X., Chèze, D., Papillon, P., 2012. Development of a 5 kW cooling capacity ammonia-water absorption chiller for solar cooling applications. *Energy Procedia* 30, 35–43. <https://doi.org/10.1016/j.egypro.2012.11.006>
- Bourouis, M., Coronas, A., Vallès, M., Zamora, M., 2011. Air/Water or Water/Water Absorption Water Cooler Using Ammonia and Lithium Nitrate. Patent No.: WO2011039397A1.
- Buchin, O., Albers, J., Ziegler, F., 2016. Review of regression models for absorption heat pumps, in: Heat Powered Cycles Conference, June 27-29. Nottingham, UK.
- Carey, V.P., 1992. Liquid-vapor phase-change phenomena, 1st ed. Taylor and Francis.
- Goyal, A., Staedter, M.A., Hoysall, D.C., Ponkala, M.J., Garimella, S., 2017. Experimental evaluation of a small-capacity, waste-heat driven ammonia-water absorption chiller. *Int. J. Refrig.* 79, 89–100. <https://doi.org/10.1016/j.ijrefrig.2017.04.006>

- Gutiérrez-Urueta, G., Rodríguez, P., Ziegler, F., Lecuona, A., Rodríguez-Hidalgo, M.C., 2012. Extension of the characteristic equation to absorption chillers with adiabatic absorbers. *Int. J. Refrig.* 35, 709–718. <https://doi.org/10.1016/j.ijrefrig.2011.10.010>
- Hellmann, H., Schweigler, C., Ziegler, F., 1998. A simple method for modeling the operating characteristics of absorption chillers, in: *Thermodynamics Heat and Mass Transfers of Refrigeration Machines and Heat Pumps Seminar EURO THERM 59*. France, pp. 219–226.
- Hellmann, H.M., Schweigler, C., Ziegler, F., 1999. The characteristic equations of absorption chillers, in: *International Sorption Heat Pump Conference*, March 24–26. Munich, Germany.
- Hellmann, H.M., Ziegler, F., 1999. Simple absorption heat pump modules for system simulation programs. *ASHRAE Trans.* 105, 780–787.
- Herold, K., Rademacher, R., Klein, S., 2016. *Absorbtion Chillers and Heat Pumps*, 2nd ed. CRC Press, Taylor & Francis Group, Boca Raton, FL.
- Jakob, U., 2005. *Investigations into solar powered diffusion-absorption cooling machines*. PhD Montfort University Leicester.
- Kühn, A., Ziegler, F., 2005. Operational results of a 10kW absorption chiller and adaptation of the characteristic equation., in: *First International Conference on Solar Air Conditioning*, October 6–7. Bad-Staffelstein, Germany.
- Labus, J., Bruno, J.C., Coronas, A., 2013. Performance analysis of small capacity absorption chillers by using different modeling methods. *Appl. Therm. Eng.* 58, 305–313. <https://doi.org/10.1016/j.applthermaleng.2013.04.032>
- Mittermaier, M., Ziegler, F., 2015. Theoretical evaluation of absorption and desorption processes under typical conditions for chillers and heat transformers. *Int. J. Refrig.* 59, 91–101. <https://doi.org/10.1016/j.ijrefrig.2015.07.015>
- Narayanan, V., Kanury, A.M., Jenks, J., 2009. Heat Exchanger Analysis Modified to Account for a Heat Source, in: *ASME/JSME 2007 Thermal Engineering Heat Transfer Summer Conference Collocated with the ASME 2007 InterPACK Conference*. American Society of Mechanical Engineers Digital Collection, Vancouver, Canada, pp. 1063–1068.
- Ochoa, A.A. V, Coronas, A., 2016. Aplicação do método da equação característica num chiller por absorção com $\text{NH}_3/\text{LiNO}_3$, in: *VI Congresso Ibero-Americano de Ciências e Técnicas Do Frio*, May 3–6. Coimbra, Portugal.
- Puig-Arnavat, M., López-Villada, J., Bruno, J.C., Coronas, A., 2010. Analysis and parameter identification for characteristic equations of single- and double-effect absorption chillers by means of multivariable regression. *Int. J. Refrig.* 33, 70–78. <https://doi.org/10.1016/j.ijrefrig.2009.08.005>
- Rops, C.M., Lindken, R., Velthuis, J.F.M., Westerweel, J., 2009. Enhanced heat transfer in confined pool boiling. *Int. J. Heat Fluid Flow* 30, 751–760. <https://doi.org/10.1016/j.ijheatfluidflow.2009.03.007>
- Rowley, R.L., Wilding, W.V., Oscarson, J.L., Giles, N.F., 2010. *DIPPR Data Compilation of Pure Chemical Properties*. Design Institute for Physical Properties, New York.
- Salavera, D., Coronas, A., 2018. Property Modeling of the Ammonia + Lithium Nitrate Mixture from New Experimental Data for Absorption Refrigeration Applications, in: *6th International Conference on Cryogenics and Refrigeration*, April 12–14. Shanghai, China.
- Sjöberg, J., Zhang, Q., Ljung, L., Benveniste, A., Delyon, B., Glorennec, P.Y., Hjalmarsson, H., Juditsky, A., 1995. Nonlinear black-box modeling in system identification: a unified overview. *Automatica* 31, 1691–1724. [https://doi.org/10.1016/0005-1098\(95\)00120-8](https://doi.org/10.1016/0005-1098(95)00120-8)
- Venegas, M., Zacarías, A., Vereda, C., Lecuona, A., Ventas, R., 2012. Subcooled and saturated boiling of ammonia-lithium nitrate solution in a plate-type generator for absorption machines. *Int. J. Heat*

Mass Transf. 55, 4914–4922. <https://doi.org/10.1016/j.ijheatmasstransfer.2012.04.061>

Zacarías Santiago, A., 2009. Heat and mass transfer in adiabatic absorbers with the use of the lithium nitrate-ammonia solution (in Spanish). PhD Universidad Carlos III de Madrid.

Zamora, M., 2012. Industrial Optimization and Control Strategy of an Air-cooled Ammonia/lithium Nitrate Absorption Chiller (in Spanish). PhD Universitat Rovira i Virgili.

Zamora, M., Bourouis, M., Coronas, A., Vallès, M., 2014. Pre-industrial development and experimental characterization of new air-cooled and water-cooled ammonia/lithium nitrate absorption chillers. Int. J. Refrig. 45, 189–197. <https://doi.org/10.1016/j.ijrefrig.2014.06.005>

Ziegler, F., 1998. Sorptionswärmepumpen (in German). Forschungsberichte des Dtsch. Kälte- und Klimatechnischen Vereins e.V., Nr. 57, DKV, Stuttgart.

Chapter III. Solar absorption air conditioner in the Mexican context

Based on:

Altamirano, A., Stutz, B., Le Pierrès, N.

Selection of High-Performance Working Fluid for a Solar-Geothermal Absorption Cooling System and Techno-Economic Study in the Northern Mexican Conditions

ISES EuroSun 2018 Conference – 12th International Conference on Solar Energy for Buildings and Industry, Sept. 10-13, Rapperswill (Switzerland)

DOI: 10.18086/eurosun2018.04.15

Altamirano, A., Le Pierrès, N., Stutz, B., Domain F.

H₂O-LiBr Single-Stage Solar Absorption Air Conditioner with an Innovative Bi-Adiabatic Configuration: Dynamic Model, Nominal Conditions and Typical Day Operation

ISES Solar World Congress 2019/IEA SHC International Conference on Solar Heating and Cooling for Buildings and Industry, Nov. 4-7, Santiago (Chili)

DOI: 10.18086/swc.2019.55.01

The present section deals with three of the main challenges to increase the competitiveness of absorption chillers against conventional vapor compression systems: the optimal working fluid, the most adapted heat sink source, and the machine architecture. Section 3.2 studies a small-capacity solar-geothermal absorption system in the Monterrey city (Mexico) climate conditions comparing the two more conventional working fluids (NH₃-H₂O and H₂O-LiBr) and an innovative working fluid (NH₃-LiNO₃). The dimensioning of the system's components and a quick economic viability study are performed. Once the most adapted working fluid was chosen, Section 3.3 deals with the proposal of a new machine architecture: a single-stage H₂O-LiBr solar absorption system with a bi-adiabatic configuration, which allows for a wide range of possibilities to enhance the mass transfer, leading to efficient and compact systems. Moreover, apart from the adiabatic sorption exchangers, only mass-produced standard components would be required. A dynamic model was created and used to define the system's operating conditions and to study the system's behavior when coupled to an evacuated tube collector and a simple model of a single-family house under a typical sunny day in the Monterrey climate conditions.

“

सफलता दो बार प्राप्त होती है। एक बार मन में और दूसरी बार वास्तविक दुनिया में।

“Success is achieved twice. Once in the mind and the second time in the real world.”

– Azim Premji

3.1. Introduction

In order to develop a new generation of solar absorption chillers designed to operate in sunny countries, such as Mexico, the simulation of the machine in the local real environment is necessary. This allows for a better understanding of the behavior of such a system in real conditions and helps define the minimum requirements in terms of cost and system performance. The present chapter introduces the simulation of an absorption machine in the Mexican climate under both steady-state and dynamic conditions.

As explained in previous chapters, there are a series of challenges to overcome to increase the competitiveness of absorption chillers against conventional vapor compression systems. One of the challenges for their proper operation is an adapted intermediate heat sink source. Indeed, these machines release more heat than vapor compression systems. Conventionally, cooling towers are employed for this purpose. However, they possess some disadvantages such as a high water consumption, high maintenance needs, electricity consumption, and there have been reported cases of legionella bacteria development (Bailo et al., 2010; Monné et al., 2011). For these reasons, some research groups are investigating alternative heat sink possibilities. Air-cooled systems have also been theoretically and experimentally investigated. Nevertheless, in this case, absorption chillers demand higher driving temperatures and, when operating with the H₂O-LiBr working pair, there is risk of solution crystallization. Moreover, the performance of air-cooled systems is highly influenced by the variable ambient temperature conditions (Chen et al., 2017). Geothermal heat exchangers (GHE) have recently been proposed as heat sinks for absorption systems. They possess some advantages compared to the conventional ones in terms of efficiency, operating costs, and maintenance (Noorollahi et al., 2018). Borehole heat exchangers are the most common GHE, while other options like pile GHE or horizontal loop GHE also exist, all of which present disadvantages in terms of cost or surface required (Moch et al., 2014). Helical geothermal heat exchangers (HGHE) have recently been proposed as they offer a good compromise between borehole heat exchangers and horizontal loops in terms of required surface and cost. However, there are very few studies that investigate their operation (Moch et al., 2015).

Another important challenge to overcome is the elevated price and size of absorption chillers. At the machine level, the main cost reduction potential is the decrease in the manufacturing costs and the increase in the demand to reach a mass-scale production (IEA, 2018a; Mugnier et al., 2017). The last option can be hardly assessed as the demand depends on different economic, demographic, governmental, and manufacturing aspects. As for the first option, the heat and mass exchangers have been pointed out as the limiting components in terms of size, performance, and cost; especially the absorber (Beutler et al., 1996; Kays and London, 1984). On this direction, adiabatic exchangers have gained attention in recent years as they could lead to compact, low-weight, and low-cost systems, through the separation of heat and mass transfers into two steps (Gutiérrez-Urueta et al., 2012; Venegas et al., 2003; Ventas et al., 2010). Usually, a conventional mass-manufactured plate heat exchanger is used for the heat transfer owing to its high compactness (Wang et al., 2007) and low cost. Whereas the mass transfer is performed in a different chamber where the solution can be distributed or dispersed in different forms to absorb or desorb refrigerant vapor. This allows for an immense number of possibilities to enhance the exchange area and generate flow instabilities, leading to high performance and compactness.

Section 3.2 presents a steady-state model of a small-capacity absorption system for hot climates (Figure III.1) coupled to a solar thermal panel and a geothermal heat sink source. The model is used to compare 3 different potential working fluids for the Monterrey city (in northern Mexico) climate conditions. Monterrey, the 3rd largest metropolitan area in Mexico, was chosen since it is a representative city of this region in which the need for AC and the irradiation levels are both very high. Two of the compared working fluids are the conventional NH₃-H₂O and H₂O-LiBr pairs, while the third working fluid is the recently studied NH₃-LiNO₃ working pair (see Section 1.2). A quick dimensioning of the main

components and a first techno-economic study is performed to evaluate the commercial feasibility of such a system in the Mexican context.

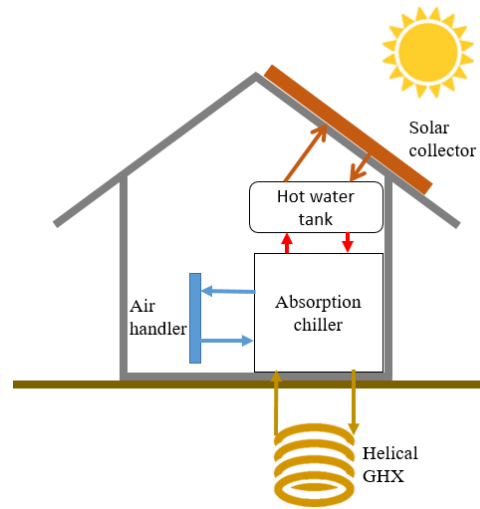


Figure III.1: Diagram of the proposed solar-geothermal absorption cooling system.

Once the working fluid chosen, Section 3.3 proposes the study of a new geometry of single-stage H₂O-LiBr absorption cooling system with a bi-adiabatic configuration. This new architecture would not only lead to high compactness, but also to avoid on-demand production by selecting only mass-produced standard heat exchangers. A dynamic model which employs the mass effectiveness (as defined in Chapter II) for the adiabatic sorption exchangers was developed. This model was used to identify the optimum operating conditions of the system and evaluate its operation for a typical summer day using real data from 2018 of the Monterrey (MEX) city. The typical day operation was performed by coupling the system with the model of an evacuated tube collector and a single-family house.

3.2. Selection of high-performance working fluid for a solar-geothermal absorption cooling system and techno-economic study in the northern Mexican conditions

3.2.1. Climatic conditions and ground temperature profiles

To determine the operating temperature profiles of the machine, data from the Mexican National Meteorological System (SMN, 2018) and the Integral System of Environmental Monitoring (SIMA, 2018) were used. This data is illustrated in Figure III.2.

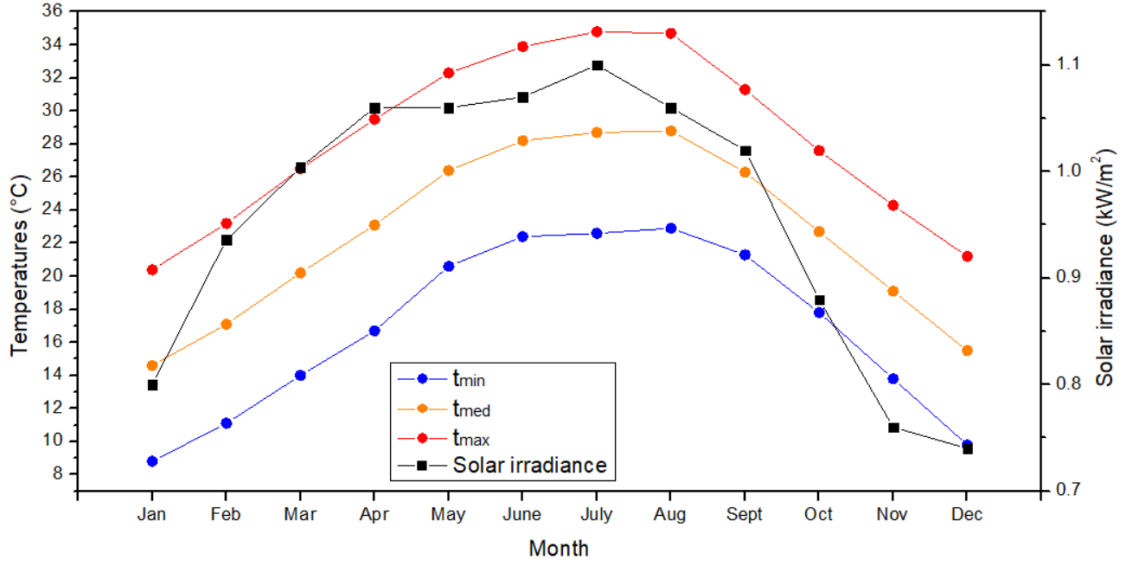


Figure III.2: Monterrey city maximum solar irradiance in 2017 (SIMA, 2018) and temperature profiles from 1981 to 2010 (SMN, 2018).

Considering the underground as a semi-infinite solid, spatially homogeneous, with thermal transfers only occurring by conduction, the underground undisturbed temperature profile can be obtained by Eq. (III.1) (Doughty et al., 1991). This equation allows to represent graphically the undisturbed underground temperature profiles in Monterrey for the different seasons, as observed in Figure III.3.

$$\tilde{t}(n, d) = t_{mean} - t_{amp} \exp\left(n \sqrt{\frac{\phi}{2a}}\right) \cos\left(\phi(d - d_c) + n \sqrt{\frac{\phi}{2a}}\right) \quad (III.1)$$

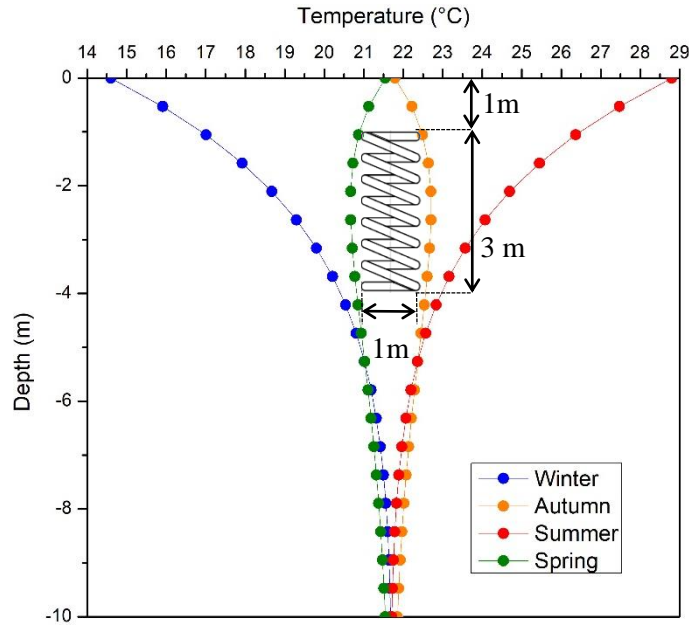


Figure III.3: Underground temperature profile of Monterrey city for different seasons.

Models available in the literature often do not take into account the effect of the distance between the HGHE coils and the local variations in temperature due to the heat transfer between the heat exchangers and the ground, which usually leads to unrealistic calculations (Agbossou et al., 2018). In the present study, these effects are taken into account to obtain more realistic results. HGHE usually have heights between 2 and 6 m, and diameters between 0.35 and 2 m. Their upper part generally being placed at 1 m

below the ground level (Figure III.3) (Moch et al., 2014). In the present study, HGHE coils of 1 m diameter and 3 m height inserted in a 4 m deep well were selected. Considering the hottest days during summer, the average undisturbed underground temperature is about 24°C (the temperature of the ground being between 26.3°C at 1 m depth and 22.7°C at 4 m depth). The increase of the underground temperature due to the heat released by the absorption system is estimated to be of around 9°C for the summer season using transient simulations (see Section 3.2.3.1). Considering a temperature difference of 2°C between the underground and the heat transfer fluid, and a difference of 5°C between the heat transfer fluid and the fluids in the absorption machine, a nominal equilibrium outlet intermediate temperature for the absorption system of around 40°C can be assumed (dots 1 and 8 in Figure III.4). While thanks to the irradiation levels during sunny days, equilibrium outlet generator temperatures in the range of 70-90°C (dot 4 in Figure III.4) can be achieved with flat solar collectors and a non-pressurized water tank for the hot source.

3.2.2. Thermodynamic comparison of the working fluids

3.2.2.1. Description of the system

Thanks to the state of the art of Section 1.2, the two most conventional working fluids in absorption systems (NH₃-H₂O and H₂O-LiBr) and one innovative working fluid (NH₃-LiNO₃) were selected. The simulated geometry is illustrated in Figure III.4. It consists of an evaporator, a condenser, an absorber, a generator, a solution pump, a solution heat exchanger (SHX) and two expansion valves. In the case of the NH₃-H₂O system, a rectifier is needed after the generator, however, in the case of the NH₃-LiNO₃ and H₂O-LiBr working pairs, the rectifier is eliminated of the diagram and points 11 and 12 disappear. The operating principle of this geometry was described in Section 1.1.

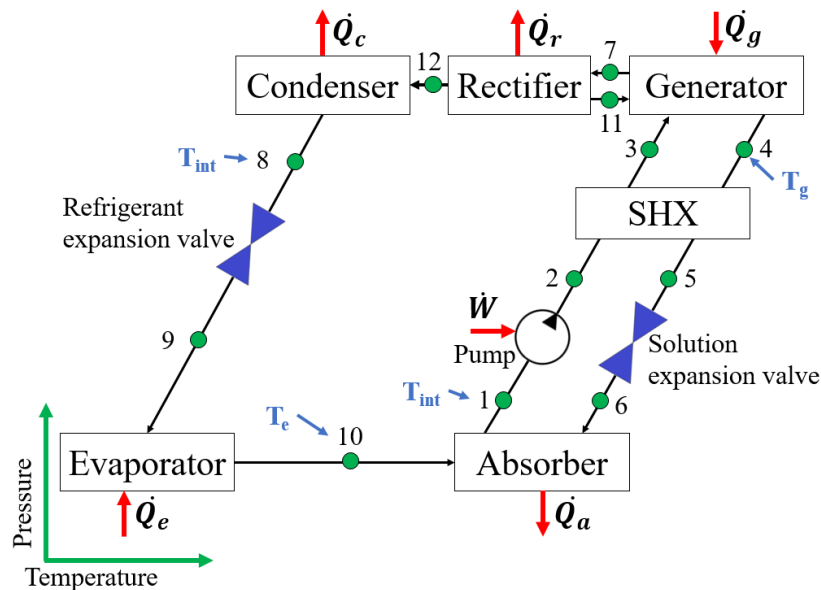


Figure III.4: Studied geometry of NH₃-H₂O single stage absorption cooling system (for the NH₃-LiNO₃ and H₂O-LiBr working fluids, the rectifier is eliminated and points 11 and 12 disappear).

3.2.2.2. Assumptions for the thermodynamic analysis

The assumptions that were taken into account to develop the simulations and analysis for the studied systems are as follows:

- The system operates under steady conditions.
- Pressure losses due to friction in the components and pipes are considered negligible.

- The refrigerant at the outlet of the condenser and evaporator (points 8 and 10 in Figure III.4) is under saturated conditions.
- The solution at the outlet of the generator and the absorber (points 1 and 4 in Figure III.4) is under equilibrium conditions.
- The vapor at the output of the generator is in equilibrium with the concentration of the solution at point 3 [$T_7 = T_{eq}(P_h, x_3)$].
- The heat losses to the surroundings are considered negligible.
- The cooling capacity remains constant at $\dot{Q}_e = 5$ kW.
- The evaporator outlet temperature remains constant at $T_{ev} = 10^\circ\text{C}$ (point 10 in Figure III.4).
- The SHX effectiveness is fixed at 0.8.
- For the $\text{NH}_3\text{-H}_2\text{O}$ working pair, an ideal rectifier (thermodynamically reversible) was considered ($T_{11}=T_7$ and $x_{11}=x_3$).

3.2.2.3. Thermodynamic analysis

Thermophysical properties of the studied working pairs are needed to calculate the performance of the proposed absorption refrigeration cycle. The thermophysical properties of pure ammonia were obtained from (Tillner-Roth et al., 1993). In the case of the $\text{NH}_3\text{-LiNO}_3$ solution, the equilibrium pressure and isobaric specific heat were obtained from (Hernández-Magallanes et al., 2017), and the specific enthalpy was obtained from (Farshi et al., 2014). The $\text{H}_2\text{O-LiBr}$ properties were obtained from (Pátek and Klomfar, 2006). Finally, the thermodynamic properties of the $\text{NH}_3\text{-H}_2\text{O}$ solution were obtained from (Ibrahim and Klein, 1993).

A mathematical model was developed based on the mass, species, and energy balances for each component in the absorption cycle, as defined in Eqs. (II.29)-(II.31). The implemented thermal COP is that of Eq. (I.2). Finally, the circulation rate is defined by Eq. (III.2).

$$\text{CR} = \frac{m_3}{m_9} \quad (\text{III.2})$$

An important parameter is the cut-off temperature of the cycle, which is the minimum generator temperature needed for the system to operate at given conditions. Two parametric studies were developed: the first one considering that the equilibrium temperature at the outlet of the absorber and condenser (T_1 and T_8), called intermediate temperature (T_{int}), is fixed at 40°C . The second case assumes two fixed generator outlet temperatures ($T_7 = T_g$): 75°C and 85°C .

3.2.2.4. Results and discussion

The comparison of COP vs T_{int} for the $\text{NH}_3\text{-H}_2\text{O}$, $\text{NH}_3\text{-LiNO}_3$, and $\text{H}_2\text{O-LiBr}$ working pairs can be observed in Figure III.5. As the intermediate temperature increases, the COP decreases. In the case of the outlet generator temperature of 75°C , the machine is able to operate at maximum intermediate temperatures T_{int} of 40°C , 41°C , and 40.5°C for the $\text{NH}_3\text{-H}_2\text{O}$, $\text{NH}_3\text{-LiNO}_3$, and $\text{H}_2\text{O-LiBr}$ working fluids, respectively. As the intermediate temperature gets close to its higher limit, the COP decreases drastically. Hence, it is recommended to limit the operating intermediate temperatures to keep acceptable COP values (of around 0.6) at T_{int} of 37°C , 39°C , and 40°C or less for the $\text{NH}_3\text{-H}_2\text{O}$, $\text{NH}_3\text{-LiNO}_3$, and $\text{H}_2\text{O-LiBr}$ cycles, respectively.

An increase in the generator temperature leads to higher allowable intermediate temperatures. When the generator temperature is increased to 85°C , the machine is able to operate at maximum intermediate temperatures T_{int} of 44°C , 46°C , and 45°C for the $\text{NH}_3\text{-H}_2\text{O}$, $\text{NH}_3\text{-LiNO}_3$, and $\text{H}_2\text{O-LiBr}$ working fluids, respectively. Moreover, in order to maintain a COP of at least 0.6, a T_{int} of 39°C , 42°C , and 44°C or less is required for the $\text{NH}_3\text{-H}_2\text{O}$, $\text{NH}_3\text{-LiNO}_3$, and $\text{H}_2\text{O-LiBr}$ cycles, respectively. For both generator temperatures, the $\text{H}_2\text{O-LiBr}$ working fluid is the working pair that can operate at highest intermediate temperatures with acceptable COP values. Moreover, as observed in Figure III.5 and Figure III.6, a

generator operating temperature higher than 75°C would be recommended, as lower generator temperatures limit the intermediate temperature to conditions that might not be achievable in real applications. In the optimum operating temperature conditions (summer conditions of Monterrey) of $T_{int} = 40^{\circ}\text{C}$ and $T_g = 85^{\circ}\text{C}$, the $\text{H}_2\text{O-LiBr}$ working fluid shows the highest COP.

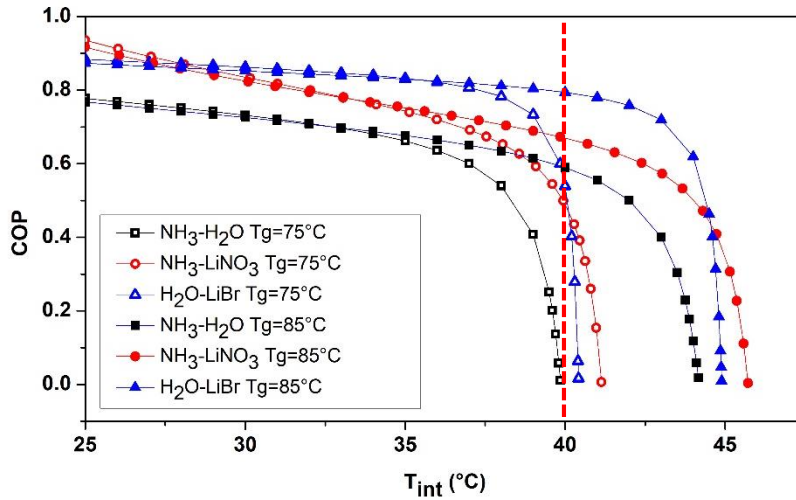


Figure III.5: Effect of T_{int} on COP at $T_e=10^{\circ}\text{C}$ and two different generator temperatures ($T_g=75^{\circ}\text{C}$ and $T_g=85^{\circ}\text{C}$).

Figure III.6 shows the effect of the intermediate temperature on the circulation ratio (CR) at two different outlet generator temperatures (75°C and 85°C). As the generator temperature increases, the circulation ratio also increases, and a higher circulation ratio requires more pumping capacity. Therefore, it is not recommended to operate the system at high intermediate temperatures. In the range of low intermediate temperatures, $\text{NH}_3\text{-LiNO}_3$ possesses the highest circulation ratios, and $\text{NH}_3\text{-H}_2\text{O}$ the lowest.

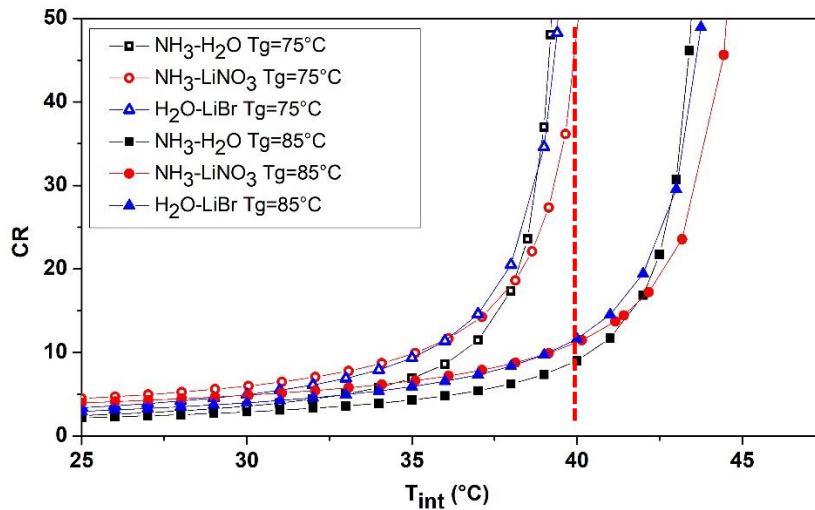


Figure III.6: Effect of T_{int} on Circulation Ratio at $T_e=10^{\circ}\text{C}$ and two different generator temperatures ($T_g=75^{\circ}\text{C}$ and $T_g=85^{\circ}\text{C}$).

Figure III.7 shows the COP variations comparison against generator temperatures, considering an intermediate temperature of 40°C . The hot water storage unit is able to provide heat transfer fluid in the range of $70\text{-}100^{\circ}\text{C}$. The compared systems have different cut-off temperatures. In the case of the $\text{NH}_3\text{-H}_2\text{O}$ system, its cut-off temperature is of 75°C , while for $\text{H}_2\text{O-LiBr}$ it is of 74°C . Finally, $\text{NH}_3\text{-LiNO}_3$ possesses the lowest cut-off temperature of 72°C . However, it does not necessarily mean that it is the most convenient working fluid in the studied case, as the COP values of the three fluids increase dramatically just above the cut-off temperature. The value of the generator temperatures for which the system starts to operate at acceptable performances (COP values higher than 0.6) is about 75.5°C for the

H₂O-LiBr pair, 78°C for NH₃-H₂O, and 87°C for NH₃-H₂O. Moreover, the H₂O-LiBr system reaches and maintains the highest COP values for the rest of the generating temperatures. This indicates that if a good control over the generating temperatures is maintained, the H₂O-LiBr working fluid would be the most convenient for the studied case in terms of performance.

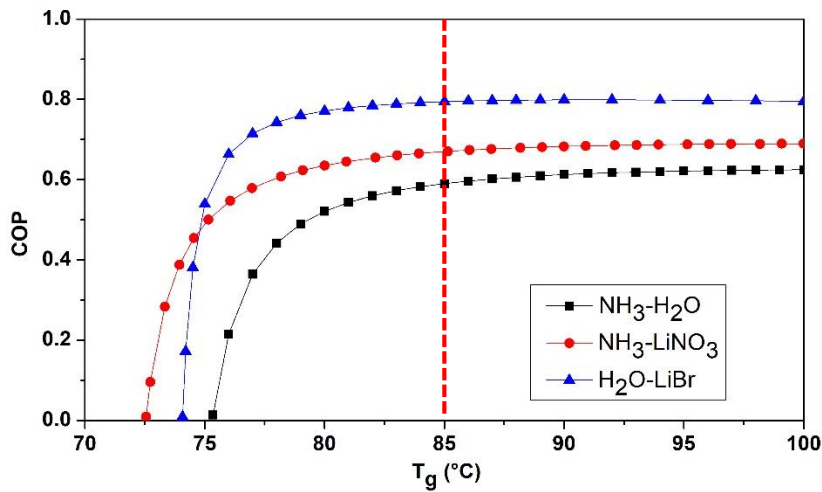


Figure III.7: Effect of T_g on COP at $T_e=10^\circ\text{C}$ and $T_{int}=40^\circ\text{C}$.

Figure III.8 illustrates the impact of the generator temperature on the circulation ratio at $T_{int}=40^\circ\text{C}$ and $T_e=10^\circ\text{C}$. In the lower limit conditions of the generator temperatures, the circulation ratio increases drastically. Hence, higher generator temperatures are recommended. At high generator temperatures, the NH₃-H₂O working pair has the lowest circulation ratios, and NH₃-LiNO₃ has the highest, but very close to the ones of H₂O-LiBr.

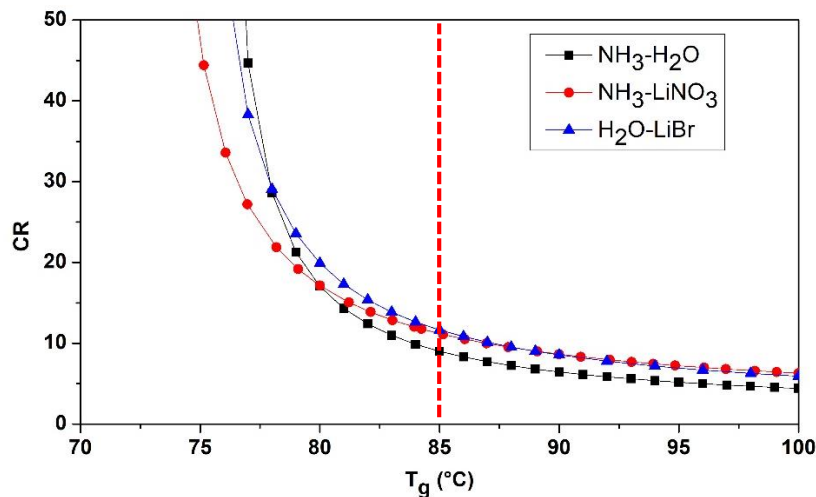


Figure III.8: Effect of T_g on COP at $T_e=10^\circ\text{C}$ and $T_{int}=40^\circ\text{C}$.

3.2.3. Integrated solar-geothermal system and economic feasibility study

3.2.3.1. Solar-geothermal absorption cooling system and dimensioning

Following the study of the cycle performances, the integration of the absorption cycle with the solar driving heat source and the geothermal heat sink source can be performed. The proposed configuration is the one illustrated in Figure III.1. The system consists of a solar thermal evacuated tubes collector system, a hot water storage tank, the absorption chiller, the air handling unit, and a HGHE. In order to make an

objective comparison of the proposed working fluids, an evaporator average power of 5 kW is fixed for the cooling system eight hours a day during the 6 hottest months in Monterrey (Apr-Sept), and an average solar irradiance of 1 kW m⁻² (which is acceptable according to Figure III.2) was taken into account for these conditions. The total power to be put into the ground would be approximately $\dot{Q}_{int} = \dot{Q}_a + \dot{Q}_c$, while the power of the evacuated tube collectors is approximately \dot{Q}_g if we consider that there is a good match between the solar irradiation availability and the cooling need. Therefore, the influence of the hot water storage tank over the system's thermal components would be negligible. These values depend on the performance of the different absorption working fluids. In order to evaluate the solar collector area (in m²) required for the system, Eqs. (III.3)-(III.5) were used.

$$A_{col} = \frac{\dot{Q}_g}{G^* \cdot \eta_{col}} \quad (III.3)$$

$$\eta_{col} = k(\theta) \cdot \eta_0 - a_1 \frac{t_{mean}^{col} - t_{amb}}{G^*} - a_2 \frac{(t_{mean}^{col} - t_{amb})^2}{G^*} \quad (III.4)$$

$$k(\theta) = 1 - 0.239 \left(\frac{1}{\cos\theta} - 1 \right) \quad (III.5)$$

In the calculations, a tilt angle of the collector of 25° and south orientation were considered, which is the recommended tilt angle for Monterrey's 25° 4' north latitude. While the collector's characteristics are the ones of the Thermomax – Mazdom vacuum tube solar collectors ($\eta_0 = 0.804$, $a_1 = 1.15 \frac{^{\circ}C \cdot m^2}{kW}$ and $a_2 = 0.0064 \frac{^{\circ}C \cdot m^2}{kW}$) (Vargas Bautista et al., 2011). In the case of the hot water storage tank, 60 liters were considered for every square meter of collector (Mateus and Oliveira, 2009). The work on the characterization and dimensioning of HGHE was presented in Moch's thesis (2013) and was followed by other papers on the subject (Agbossou et al., 2018; Moch et al., 2015, 2014). This study concerns geothermal heat pumps, and more precisely the impact of the heat transfers on the underground temperature near the HGHE and the temperature provided to the heat pump. The transient calculations were performed considering coils of standard size (1 m diameter and 3 m height) inserted in a 4 m deep well and assuming a quasi-constant heat flux along the day, whereas in the present study, the absorption heat pump operates only during eight hours a day, which somewhat underestimates the underground temperature even if the energy exchanges per day are the same for the two studies. Considering a heat exchange during the 6 hottest months of the year (Apr-Sept) with no phase change and a dry underground (worst case scenario for the thermal transfers), Moch's model leads to a capacity of 500 W for every helicoidal GHX and a separation of 4 meters between them to maintain a soil temperature perturbation under 9°C, that means a temperature of 33°C at the HGHE position (see Section 3.2.1). Knowing that every helicoidal GHX requires an area of 16 m² (4x4 m), the total surface area required for the HGHE is calculated by multiplying the number of coils by 16. The final values for the different systems requirements are shown in Table III.1.

Table III.1: Requirements and dimensioning for the studied conditions and the three studied working fluids.

	NH ₃ -H ₂ O	NH ₃ -LiNO ₃	H ₂ O-LiBr
COP	0.59	0.67	0.794
\dot{Q}_{int} (kW)	13	12.68	11.39
Number of HGHE coils	26	26	23
Surface required for the GHX (m²)	416	416	368
\dot{Q}_g (kW)	8.5	7.46	6.35
Solar collector area (m²)	15	13	11
Size of the hot water storage tank (m³)	1	1	1

3.2.3.2. Economic assessment

In spite of their low operating costs, the historical problem with solar absorption air conditioning has been the elevated initial investment. Therefore, an analysis of the initial investment costs and economic benefits of the system becomes fundamental. Three economic parameters were selected to evaluate the economic performance of the selected system: The Net Present Value (NPV), the payback period (PB), and the Return On Investment (ROI). In order to be a profitable system, the NPV should be positive, the PB should be at least half of the product lifetime, and the ROI should be higher than one. The parameters used for the economic study are shown in [Table III.2](#).

Table III.2: Economic data for the initial investment of the solar-geothermal absorption cooling system.

Concept	Data
Lifetime of absorption systems (years)	20 (Tsoutsos et al., 2003)
Inflation rate for the year 2017 (%)	6.77 (“Banco de México,” 2018)
Price of electricity (USD/kWh)	0.1484 (“CFE,” 2018)
Average energy inflation in Mexico from 2006 to 2017 (%)	2.62 (“CFE,” 2018)

The Mexican pesos – USD exchange rate considered was 1 MXN = 0.053 USD. The system’s cost of installation (not including the GHX) was considered to be 30% of the cost of the chiller and the hot storage tank was priced at 2600 USD m⁻³ (Viñas et al., 2016). The solar collectors were priced at 200 USD m⁻² and the absorption chiller at 572 USD kW⁻¹ (Vargas Bautista et al., 2011). The electricity consumption by the pumps and auxiliary elements was neglected considering the orders of magnitude of the other economic parameters. Finally, regarding the geothermal installation, a cost of 1,500 USD for every 100 m² of 4 m depth GHE was calculated (Acuña et al., 2017). Taking the presented economic parameters and the chillers operating conditions presented in [Section 3.2.3.1](#), the annual economic benefits were calculated by considering the energy savings and the operational costs. With the new energy reform in Mexico, new programs are being implemented to promote the use of renewable energies in the country. This is why for the economic evaluation; two scenarios were considered. In the first one, the user would cover the entire investment costs of the system, and in the second scenario, the government would subsidize 40% of it. The considered costs for the initial investment are presented in [Table III.3](#).

From the results in [Table III.3](#), the scenario 1 would not be economically viable, as the NPV results negative and the payback period is almost the same as the system’s lifetime. As observed by the ROI, at the end of the product lifetime, there is almost no economic gain. On the other hand, the second scenario seems economically viable, as the systems pay themselves after around 10 or 11 years of operation and their NPV is positive.

In order to make use of the system in other than hot months in Mexico, its use for domestic hot water production should be considered. Finally, the application of a solar-geothermal system like the one presented here in Mexico could only be viable in the current market conditions if new green subsidies are offered to the families, otherwise, the implementation is possible, but seems like not economically viable.

Table III.3: Considered costs for the initial investment of the solar-geothermal absorption cooling system and economic analysis considering two scenarios.

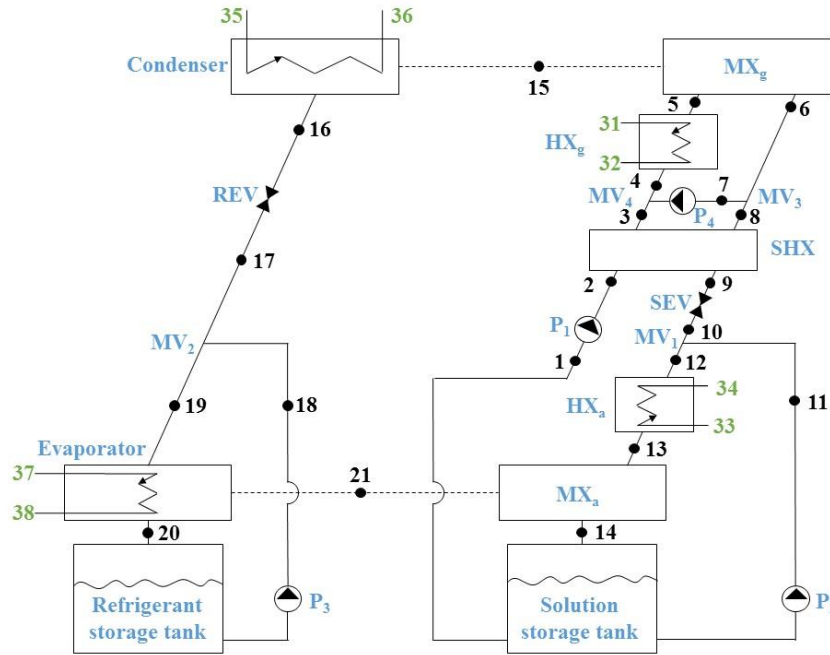
		NH ₃ -H ₂ O	NH ₃ -LiNO ₃	H ₂ O-LiBr
Initial investment	<i>Absorption chiller</i>	\$2,860.00	\$2,860.00	\$2,860.00
	<i>GHX construction and installation</i>	\$6,240.00	\$6,240.00	\$5,520.00
	<i>Solar evacuated tube collectors</i>	\$3,000.00	\$2,600.00	\$2,200.00
	<i>Hot storage tank</i>	\$2,600.00	\$2,600.00	\$2,600.00
	<i>System installation costs</i>	\$2,000.00	\$2,000.00	\$2,000.00
	<i>Required pumps</i>	\$604.00	\$604.00	\$604.00
	<i>Air handling unit</i>	\$1,500.00	\$1,500.00	\$1,500.00
	<i>Accessories</i>	\$1,200.00	\$1,200.00	\$1,200.00
	TOTALS	\$20,004.00	\$19,604.00	\$18,484.00
TOTALS WITH SUBVENTION 40%		\$12,002.40	\$11,762.40	\$11,090.40
SCENARIO 1	<i>NPV</i>	-\$2,985.57	-\$2,585.57	-\$1,465.57
	<i>PB</i>	18.08	17.72	16.71
	<i>ROI</i>	1.10	1.13	1.19
SCENARIO 2	<i>NPV</i>	\$5,016.03	\$5,256.03	\$5,928.03
	<i>PB</i>	10.86	10.64	10.03
	<i>ROI</i>	1.84	1.88	1.99

3.3. Solar absorption air conditioner with an innovative bi-adiabatic configuration: dynamic model, nominal conditions and typical day operation

3.3.1. System description

Section 3.2 allowed to identify that in the Mexican climate conditions, H₂O-LiBr seems to be the most convenient working fluid for residential air conditioning applications from the technical and the economic points of view. The present section introduces the design and proposal of an innovative machine architecture that would lead absorption chillers to be more compact and cost competitive compared with vapor compression systems. It studies a new configuration of H₂O-LiBr absorption heat pump whose main innovation can be found in the fully adiabatic sorption process (absorption and desorption, see Figure III.9). In this case, the heat transfer is performed in a conventional single-phase heat exchanger (HX_g for the generator, and HX_a for the absorber) and the mass transfer is performed in a separate adiabatic mass exchanger (MX_g and MX_a) that allows innovative distribution methods or surface geometries to enhance the mass transfer.

In the proposed configuration, the diluted solution at the HX_g is super-heated by the heat transfer fluid (HTF) and then sent to the adiabatic generator (MX_g), where the adiabatic desorption of refrigerant vapor happens. A refrigerant recirculation in the evaporator is generated by means of a pump (P_3). The vapor generated is then sent to the adiabatic absorber (MX_a) where it is absorbed by the concentrated solution (that has already been pre-cooled in the HX_a). The resulting solution goes to the solution storage tank. A solution heat exchanger (SHX) is placed between the absorber and the generator. Moreover, two recirculation pumps are added (P_2 and P_4) to increase the system's performance.

Figure III.9: H₂O-LiBr single effect bi-adiabatic absorption chiller.

3.3.2. Dynamic model

The study of the dynamic behavior of absorption chillers is of great importance owing to their high response time compared with conventional compression chillers of a similar capacity. This is in part due to the thermal inertia of their components and the liquid accumulation in them (Evola et al., 2013; Kohlenbach and Ziegler, 2008a; Ochoa et al., 2016). In the present case, the state points represented in Figure III.9 show the different internal thermodynamic conditions of the H₂O-LiBr solution (1-14), the water vapor (15 and 21), and the liquid water (16-20). Moreover, the green numbers represent the external thermodynamic states of the heat source (31 and 32), the cooling source (33-36), and the chilled source (37 and 38). The developed model is based on the mass and energy balances of each component. The thermodynamic properties of the H₂O-LiBr working pair were obtained from Yuan and Herold (2005). Finally, the simplifying assumptions taken into account in the model are as follows:

- There are no heat transfers with the ambient temperature.
- The refrigerant and solution in the storage tanks are fully mixed.
- The expansion valves are isenthalpic and the pumps are isentropic.
- The vapor at the output of the adiabatic generator is in equilibrium with the concentration of the solution at point 5 [$T_{15} = T_{eq}(P_h, x_5)$].
- The refrigerant is at saturation state at the output of the condenser and the evaporator.
- The characteristic time of the components is neglected with regards to the characteristic time of the storage tanks and the transport delay between them.
- The thermal inertia of the system's components is neglected.

Different dynamic simulations are present in the literature. In most of the cases, the performance of the heat and mass transfer exchangers is characterized by a thermal effectiveness or a heat transfer coefficient and the solution is considered in equilibrium with the outlet temperature and the operating pressure (Aiane et al., 2017a); however, this is never the case in real operating systems. For this reason, in the present model, the exchangers' performances are defined by their thermal or mass effectiveness (\mathcal{E}_{th} or \mathcal{E}_m , respectively). The thermal effectiveness of the heat exchangers (condenser, evaporator, SHX, HX_g, and

HX_a) is the same as the one of conventional single-phase and phase change exchangers defined as the ratio of the real transferred heat to the maximum theoretical transferable heat with the same input conditions (Eq. (II.1)). On the other hand, for the adiabatic exchangers (MX_a and MX_g), the mass effectiveness is defined as the ratio of the actual exchanged mass (absorbed or desorbed mass) to the maximum theoretical transferable mass of sorption under the same input conditions (Eq. (II.2)). The procedure used for calculating the mass effectiveness of a nonadiabatic absorber was described in Section 2.2.1. The case of the adiabatic absorber is simpler since the maximum transferable conditions are determined by an adiabatic absorption in an infinitely long exchanger, for which Eqs. (II.8)-(II.11) need to be solved. And a similar procedure is applied in the case of the generator.

A constant transport delay (l) of the solution and refrigerant was considered between every state point so that the properties at the output of each component were calculated with the outputs of the previous component at a time $-l$. Moreover, the equilibrium condition in the desorbed/condensed ($\dot{m}_{des} = \dot{m}_{cond}$) and evaporated/absorbed ($\dot{m}_{ev} = \dot{m}_{abs}$) vapor is always fulfilled. The mass, species, and energy balances of each component are described by Eqs. (II.29)-(II.31).

As mentioned before, absorption systems usually have a higher response time compared with conventional vapor compression systems; however, for small-capacity systems, the thermal inertia of the components and the liquid mass stored in them have a much lower impact. Therefore, in these conditions, the transport delay and the liquid mass content in the storage tanks are the elements that most impact the response time. The storage tanks' behavior is described by Eqs. (III.6)-(III.8).

$$\frac{d(M_{st})}{dt} = \sum \dot{m}_i - \sum \dot{m}_o \quad (III.6)$$

$$\frac{d(M_{st}x_{st})}{dt} = \sum (\dot{m}_i x_i) - \sum (\dot{m}_o x_o) \quad (III.7)$$

$$\frac{d(M_{st}H_{st})}{dt} = \sum (\dot{m}_i H_i) - \sum (\dot{m}_o H_o) \quad (III.8)$$

Here, a pumping ratio for the sorption elements (PR_{sorp}) defines \dot{m}_{p2} and \dot{m}_{p4} as functions of \dot{m}_{p1} , as shown in Eq. (III.9). Another important parameter is the thermal COP, which is defined by Eq. (1.2).

$$PR_{sorp} = \frac{\dot{m}_{p2}}{\dot{m}_{p1}} = \frac{\dot{m}_{p4}}{\dot{m}_{p1}} \quad (III.9)$$

Finally, a second law analysis was performed to identify the most exergy destructive components. The exergy, defined as the maximum work potential of a material or an energy stream compared to its surrounding environment, is defined by Eq. (III.10) (Kotas, 1985), in which H and s are the enthalpy and entropy of the fluid and H_{dead} and s_{dead} are the enthalpy and entropy of the same fluid at the ambient temperature and pressure. The exergy destruction (ED) by component is given by Eq. (III.11). Therefore, the total system exergy destruction is the sum of the exergy destruction in all its components.

$$\psi = (H - H_{dead}) - T_{dead}(s - s_{dead}) \quad (III.10)$$

$$\Delta\psi = \sum (\dot{m}_i \psi_i) - \sum (\dot{m}_o \psi_o) \quad (III.11)$$

3.3.2. Results and discussion

3.3.2.1. System's optimum operating conditions

The aim of the present section is to determine the optimum operating conditions of the proposed system with a nominal cooling capacity of 5 kW. The HTF in the different heat exchangers is assumed to be water. Therefore, considering a $\Delta T = 5^\circ\text{C}$ for the HTF in the evaporator, a $\dot{m}_{37} = 0.24 \text{ kg s}^{-1}$ was calculated. The same value was attributed to \dot{m}_{35} as the condenser would operate at similar capacities. \dot{m}_{p3} was calculated according to the need of a minimum flow rate required to have an acceptable performance on a helical falling film heat exchanger with a coil diameter of 30 cm. A minimum flow rate of 1 l min^{-1} was considered per meter of coil perimeter, which led to a $\dot{m}_{p3} = 0.016 \text{ kg s}^{-1}$. Finally, for the purposes of the study, constant HTF inlet temperatures at the evaporator and the condenser were defined at $T_5 = 15^\circ\text{C}$ and $t_{37} = 30^\circ\text{C}$, respectively. Regarding the heat exchangers, a constant thermal effectiveness of 0.8 was selected for the condenser, the evaporator, and the SHX. In the case of the HX_g and HX_a , as their capacities would vary depending on the operating conditions at steady-state, it is more practical at this stage to define a pinch of 3°C between the output of the solution and the inlet of the HTF ($Pinch_g = t_{31} - T_5 = 90 - 87^\circ\text{C}$ and $Pinch_a = T_{13} - t_{33} = 33 - 30^\circ\text{C}$).

A parametric study was performed to identify the optimum operating conditions of the system. This procedure was mainly based on two different parameters: the \dot{m}_{p1} and PR_{SORP} . For every \dot{m}_{p1} , the program would start at a very low PR_{SORP} and run until the stabilization condition is achieved ($\dot{m}_{ev} = \dot{m}_{cond}$), PR_{SORP} was iteratively increased until reaching the 5 kW set point capacity at the evaporator. Two scenarios were studied: one with $\mathcal{E}_m = 0.4$ for both adiabatic exchangers and another one with $\mathcal{E}_m = 0.6$. Results can be observed in Figure III.10. From this Figure, two acceptable $COP_{th,min}$ were considered (0.7 and 0.75). For a $COP_{th,min} = 0.7$, $\dot{m}_{p1} = 0.075 \text{ kg/s}$ and $PR_{SORP} = 10$ would be required with $\mathcal{E}_m = 0.4$, while $PR_{SORP} = 6.25$ is required with $\mathcal{E}_m = 0.6$. On the other hand, for $COP_{th,min} = 0.75$, \dot{m}_{p1} of around 0.05 kg/s is required with $PR_{SORP} = 17.3$ and $\mathcal{E}_m = 0.4$, and $PR_{SORP} = 11$ with $\mathcal{E}_m = 0.6$. It's worth mentioning that in none of those conditions there was a risk of crystallization.

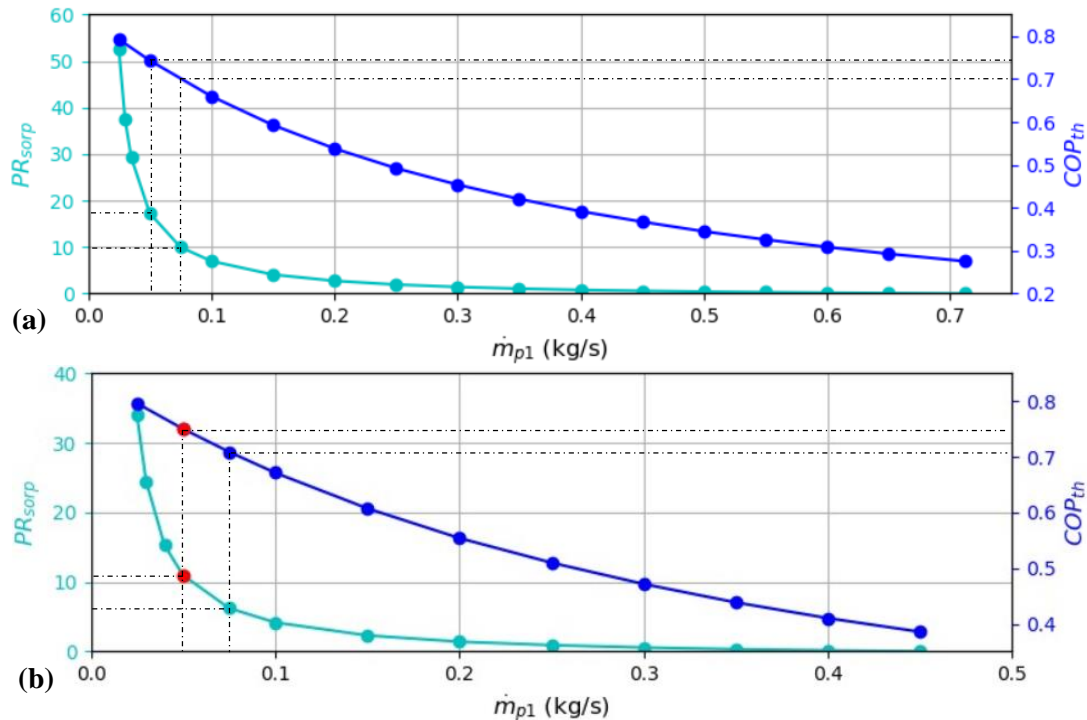


Figure III.10: Thermal COP and R vs \dot{m}_{p1} for a) $\mathcal{E}_m = 0.4$ and b) $\mathcal{E}_m = 0.6$ in the mass exchangers (● nominal conditions).

Taking into consideration the system stability and electric consumption limitation due to the pumps work, an PR_{sorp} close to 10 or less is preferable. Under these conditions, a $\mathcal{E}_m = 0.4$ would only be accepted by reducing the $COP_{th,min}$ to 0.7, while a $\mathcal{E}_m = 0.6$ would be preferable to obtain a thermal COP of 0.75; therefore, this last condition was selected as the nominal operating state of the machine ($COP_{th} = 0.75 // \dot{m}_{p1} = 0.05 \text{ kg/s} // \mathcal{E}_m = 0.6 // PR_{sorp} = 11$). Once this condition selected, a calculation of the HX_g and HX_a thermal effectiveness was performed (Eqs. (III.12)-(III.13)) with the rest of the parameters of the simulated results ($\dot{Q}_g = 6.67 \text{ kW} // \dot{Q}_a = 6.64 \text{ kW} // T_4/T_5/t_{31} = 81.47/87/90^\circ\text{C} // T_{12}/T_{13}/t_{33} = 38.37/33/30^\circ\text{C}$).

$$\varepsilon_{th,g} = \frac{T_5 - T_4}{t_{31} - T_4} = 0.65 \quad (\text{III.12})$$

$$\varepsilon_{th,a} = \frac{T_{12} - T_{13}}{T_{12} - t_{33}} = 0.64 \quad (\text{III.13})$$

These thermal effectiveness are acceptable considering that for the other heat exchangers a $\mathcal{E}_{th} = 0.8$ was taken into account. Finally, the required HTF flow rates are calculated (Eqs. (III.14)-(III.15)) for both heat exchangers assuming a $\Delta T = 5^\circ\text{C}$ for the HTF in both exchangers, a water C_p at 88.5°C for the HX_g , and a C_p at 28.5°C for the HX_a , which corresponds to 4202.81 and $4177.35 \text{ J kg}^{-1} \text{ K}^{-1}$, respectively.

$$\dot{m}_{htf,g} = \frac{\dot{Q}_g}{C_p * \Delta T} = \frac{6670}{4202.81 * 5} = 0.31725 \frac{\text{kg}}{\text{s}} \quad (\text{III.14})$$

$$\dot{m}_{htf,a} = \frac{\dot{Q}_a}{C_p * \Delta T} = \frac{6640}{4177.35 * 5} = 0.3065 \frac{\text{kg}}{\text{s}} \quad (\text{III.15})$$

Therefore, the nominal external parameters were defined as follows: $\dot{m}_{htf,g} = 0.32 \text{ kg s}^{-1}$; $t_{htf,g} = 90^\circ\text{C}$; $\dot{m}_{htf,a} = 0.31 \text{ kg/s}$; $t_{htf,a} = t_{htf,c} = 30^\circ\text{C}$; $\dot{m}_{htf,c} = \dot{m}_{htf,e} = 0.24 \text{ kg s}^{-1}$, $t_{htf,e} = 15^\circ\text{C}$, and the internal parameters were defined as: $\dot{m}_{p1} = 0.05 \text{ kg s}^{-1}$; $\dot{m}_{p2} = \dot{m}_{p4} = PR_{sorp} * \dot{m}_{p1} = 0.55 \text{ kg s}^{-1}$; $\dot{m}_{p3} = 0.015 \text{ kg s}^{-1}$. These parameters with the selected and calculated thermal effectiveness ($\mathcal{E}_{th,e}/\mathcal{E}_{th,c}/\mathcal{E}_{th,shx}=0.8$ and $\mathcal{E}_{th,g}=0.65/\mathcal{E}_{th,a}=0.64$) provide 5 kW of cooling with a thermal COP_{th} of 0.75. However, considering the implementation of PHE in all the thermal components and that this type of exchanger can easily achieve an effectiveness of 0.8, a nominal thermal effectiveness of 0.8 for all the components was selected. With this improved effectiveness in the HX_a and the HX_g , the chiller would provide a cooling power of 5.4 kW with a COP_{th} of 0.751.

3.3.2.2. Typical day operation

Once the nominal conditions defined, the system was studied under real simulated conditions coupled to an evacuated tube collector as the high-temperature source, a single-family house in the Monterrey (MEX) climate conditions as the low-temperature source, and a helical geothermal heat exchanger (GHX) as the intermediate-temperature source (Figure III.11a). The Monterrey's Integral System of Environmental Monitoring provided data of the global solar horizontal irradiance and the ambient temperature of the Monterrey city (SIMA, 2019). Data from the 23 July 2018 were used as it is a representative summer day in Monterrey (Figure III.11b). From this data, the selected evaluation period was from 6 A.M. to 8 P.M. as outside this period there is no irradiance.

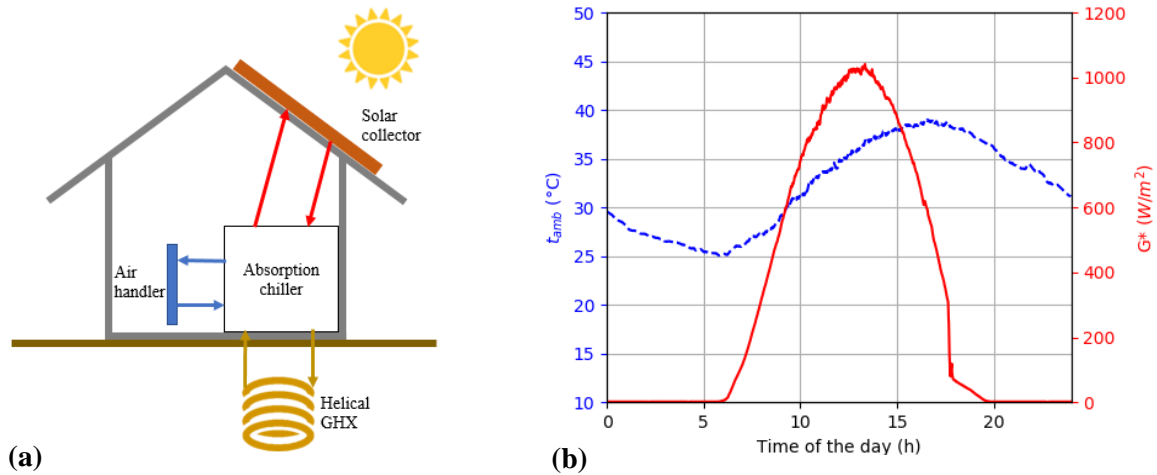


Figure III.11: (a) Diagram of the integrated solar-geothermal absorption cooling system (adapted from (Altamirano et al., 2018) and (b) Monterrey city climate conditions of the 23 July 2018 (SIMA, 2019).

The simulated collector corresponds to the Thermomax-Mazdom vacuum tube collector, as in Section 3.2.3.1 (Vargas Bautista et al., 2011). The collector was also considered to have a tilt angle of 25° , south orientation, and an area fixed at 10.5 m^2 .

Considering that the intermediate temperature source is composed by helical GHXs and assuming that the variation of the ground temperature is negligible in the simulated period of time (14 h), a parallel flow was considered for the absorber and the condenser with a constant HTF inlet temperature of 30°C , which, from Section 3.2, is reasonable for the Monterrey climate conditions. Finally, the house was simulated through a simple model based on an equivalent thermal resistance, capacitance, and solar gain factor ($1R1C + \text{solar gain}$, see Figure III.12c and Eq. (III.16) whose parameters ($R_{th} = 0.01282 \text{ K/W}$, $C_{th} = 5380 \text{ Wh/K}$, and $B_{solar} = 5$, respectively) were obtained after a characterization study based on experimental temperatures and irradiance measurements obtained from a single-family house with a wooden structure (see Figure III.12a and b), good insulation and good thermal inertia (Domain et al., 2015). The house is a two-floor house with 218 m^2 of wall surface, 60 m^2 of ground surface, 18 m^2 of windows' surface, and a total volume of around 240 m^3 . Only the irradiance on the south side of the house was taken into account as it contains the largest windows area (15 m^2) and the east and west side irradiances are mostly blocked by trees.

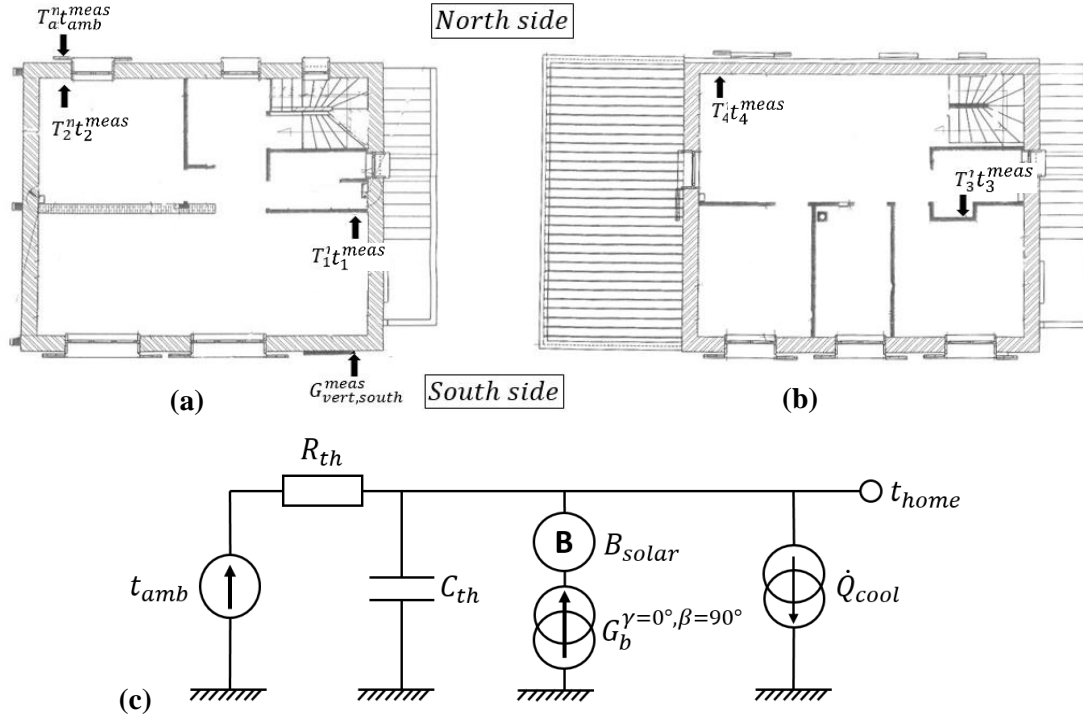


Figure III.12: Studied single-family house. (a) Ground floor and (b) first floor plans, and (c) 1R1C thermal model considering the cooling power and irradiance on the south face.

$$\frac{dt_{\text{home}}}{dt} = \frac{B_{\text{solar}} \cdot G_{\text{vert,south}}^* + [(t_{\text{amb}} - t_{\text{home}})/R_{\text{th}}] - \dot{Q}_{\text{cool}}}{C_{\text{th}}} \quad (\text{III.16})$$

The chiller was considered to operate at steady-state at the beginning of the simulation (6:00 A.M.) with the parameters defined in Section 3.3.2.1 except for the external inlet temperatures, which were defined as follows: an intermediate temperature ($t_{33} = t_{35}$) of 30°C coming from a geothermal source, an initial low-temperature (t_{37}) equal to the ambient temperature (25.2°C), and a driving temperature (t_{31}) equal to the cut-off temperature (temperature necessary for the system to generate a cooling effect) of those conditions (33.5°C). The initial home ambient temperature was that of the ambient temperature (25.2°C). Figure III.13 shows the evolution of the absorption system's external temperatures, the ambient temperature, and the home temperature with (t_{home1}) and without (t_{home2}) the effect of the chiller's cooling power. As there are no external thermal storage tanks to absorb the temperature variations of the hot and cold sources, their temperatures follow the sources' conditions achieving around 86°C at the hot transfer fluid and 6.2 kW of cooling capacity (Figure III.14). At the beginning there was not enough cooling power to compensate for the heat exchange with the ambient temperature and the solar gain; therefore, the home temperature slowly increased by up to 1°C until 9:00 A.M. After that, the house is effectively cooled by the absorption chiller achieving a temperature as low as 21.5°C until 17:30 hours, and maintaining a temperature lower than 22°C until the end of the day. Without the cooling power, the internal home temperature is highly affected by the ambient temperature and the solar gain, achieving a temperature of 30.6°C by the end of the day, which makes a temperature difference of almost 9°C compared with the cooled case. Using the absorption chiller, temperature conditions in the thermal comfort range according to the ANSI/ASHRAE Standard 55-2004 (ASHRAE, 2004) are always achieved, which is not the case for the non-cooled case. Finally, the system provided 46.5 kWh of cooling for 61.3 kWh at the generator and 108.5 kWh at the intermediate source, leading to a cumulative COP (integrated cooling capacity by the integrated heat input (Lazzarin, 1980)) of 0.765.

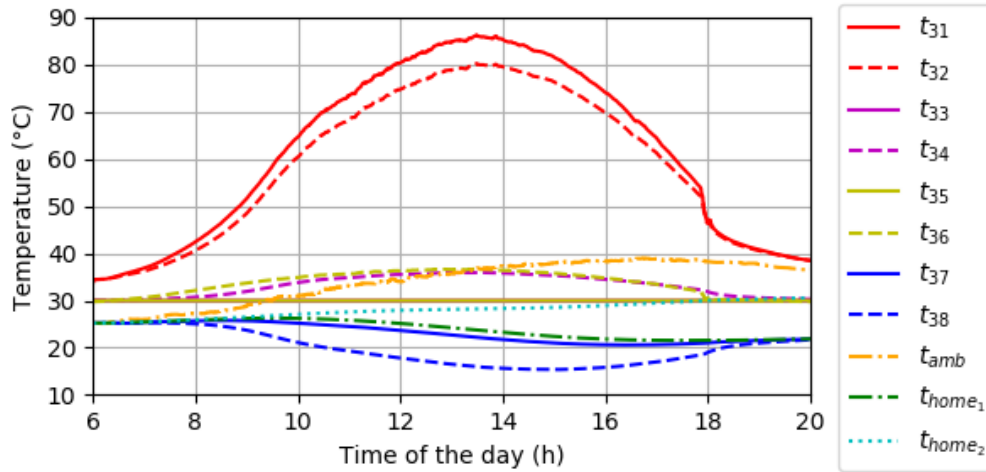


Figure III.13: Evolution of the absorption chiller's external temperatures, the ambient temperature, and home temperature with and without the cooling power.

The inlet-outlet temperature differences in Figure III.13 are proportional to the exchanged heat for each component in the system, which is better represented in Figure III.14. This figure shows that at full irradiation, the absorber and generator heat exchangers are the ones with the higher heat rates, followed by the condenser and the evaporator. At the end of the day, when the solar irradiation decreases, the heat exchanged at the generator and the condenser drops lower than that of the absorber and the evaporator, respectively, at around 15:30 hours. This is because, at the low-pressure stage, the thermal inertia in the solution and refrigerant storage tanks play an important role in the cooling generation. This is even more accentuated at around 18:00, when clouds arrive over the zone and there is a sudden drop in the solar irradiance (Figure III.11 b), drastically decreasing the generator temperature and increasing the exchanged heat difference between the two stages. The heat exchanged at the SHX is low at full operating conditions owing to the recirculation implemented in the absorber and the generator. However, as the solar irradiance decreases, this exchanged heat becomes predominant as the temperature difference between the intermediate and hot temperature sources is still considerable while the low cooling production regime (low absorption and desorption rates) leads to a low heat exchange in the rest of the exchangers.

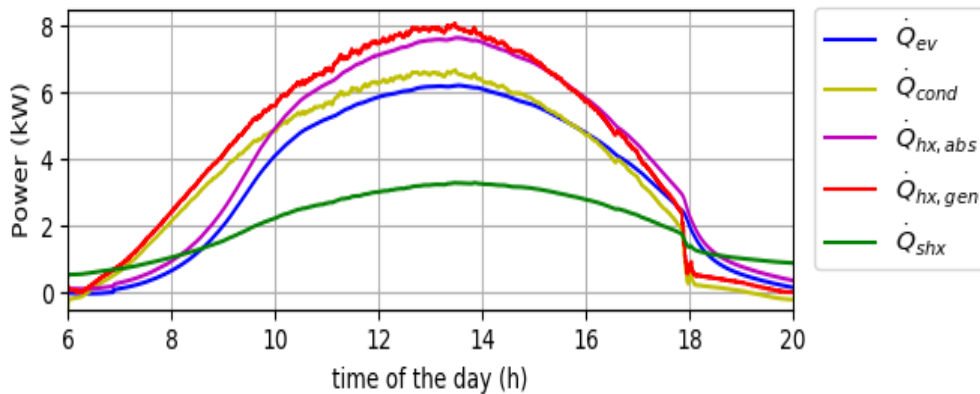


Figure III.14: Evolution of the heat exchanged in the different components of the absorption system for the studied period.

Figure III.15 shows the evolution of the content in the storage tanks and the concentrations at the inlet and outlet of the absorber and the generator. A short stabilization period is observed before 7:00, in which the irradiance is not sufficient to provide a temperature high enough to generate a desorption effect. Therefore, an absorption process happens, and the condenser evaporates for a short period. This can also be observed in Figure III.16, with a small period of negative condensed mass (\dot{m}_{15}). As the driving source temperature increases, the solution in the network increases in concentration to follow the new equilibrium conditions. This is better observed by the decrease in the content of the solution storage tank and the

increase in water content in the refrigerant storage tank between 7:00 and 14:00 hours (Figure III.15). As the generator temperature increases, the equilibrium concentration also increases and therefore, the difference in concentration between the absorber and the generator also increases, achieving a maximum concentration at the generator of 0.55, which does not imply a risk of crystallization.

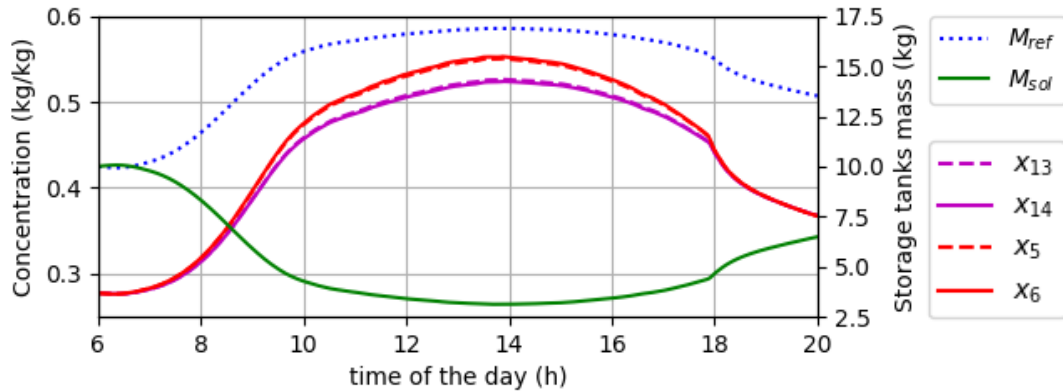


Figure III.15: Evolution of the (a) mass contained in the solution and refrigerant storage tanks and the (b) inlet-outlet solution concentrations at the absorber and desorber.

As mentioned before, the sudden drop in the solar irradiance of around 18:00 hours drastically affects the machine behavior decreasing the generator and condenser heat exchanges, and therefore affecting the condensed vapor, as observed in Figure III.16. After 19:00, the provided generator temperature is not sufficient anymore to desorb water vapor. However, the cooling generation continues thanks to the thermal inertia of the storage tanks, and this can be observed in the positive evaporated mass (\dot{m}_{21}).

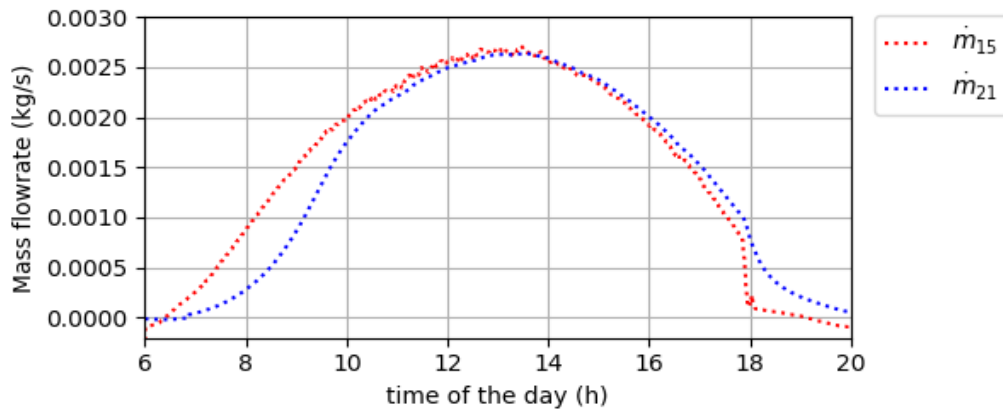


Figure III.16: Condensed (\dot{m}_{15}) and evaporated (\dot{m}_{21}) mass flow rates for the studied period.

Another figure of interest is the high and low pressures in the absorption system, which are shown in Figure III.17. An important influence of the generator (directly related to the solar irradiance) and evaporator temperatures can be observed, achieving a maximum high pressure of around 6.75 kPa and a minimum low pressure of around 1.59 kPa. The impact of the solar irradiance on the operating pressures can also be observed in the sudden pressure drop that happens when the available solar irradiance decreases at around 18:00 hours.

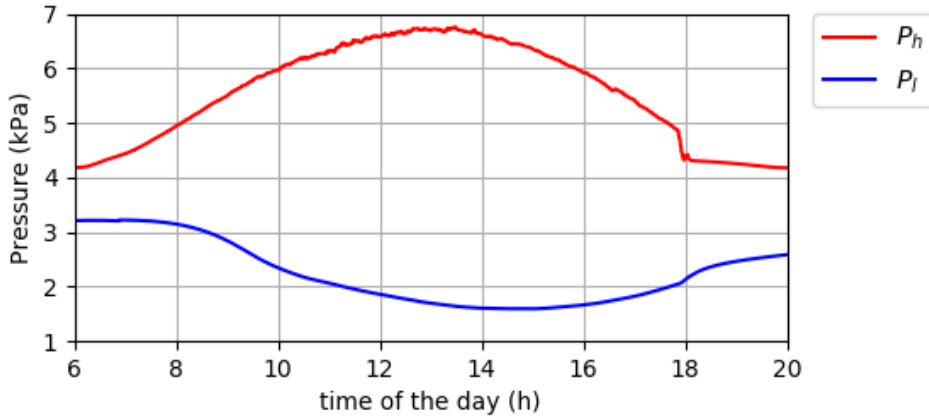


Figure III.17: Operating pressures in the system for the studied period.

Finally, Figure III.18 shows the exergy destruction in the main components and the total system's exergy destruction. At the beginning of the studied period, the components that destruct the most exergy are the condenser and the evaporator. This is because the enthalpy of vaporization/condensation plays an important role in these operating conditions compared with the single-phase exchangers and the enthalpy of mixing in the adiabatic sorption processes, especially for the condenser that, as described by the model, receives superheated vapor. However, as the generator temperature increases, the circulated refrigerant vapor increases and the concentration difference in the adiabatic absorber/generator becomes higher. In these conditions, the heat of mixing and the low mass effectiveness in the adiabatic absorber/desorber become the predominant factor for the exergy destruction, especially for the generator that operates at higher temperatures. At full operation, the adiabatic generator is the component that destructs the most exergy, followed by the adiabatic absorber, the condenser, the evaporator, the SHX, the HX_a , and the HX_g .

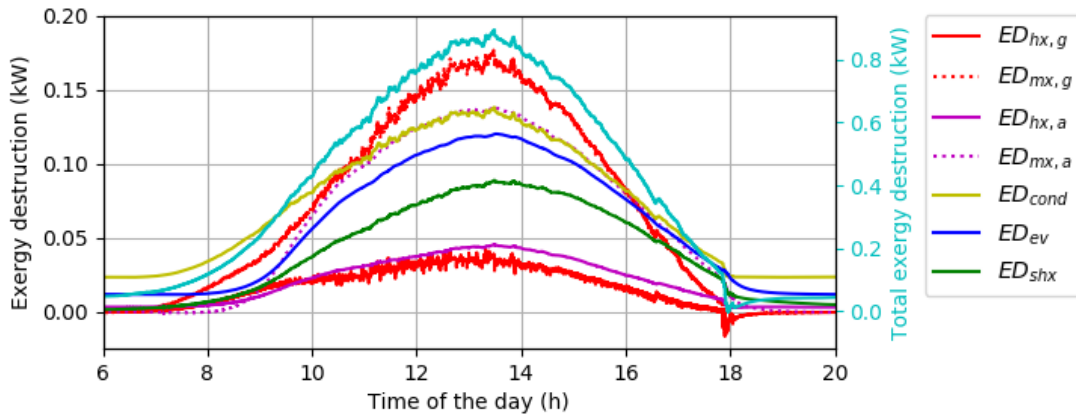


Figure III.18: Exergy destruction in the main components and total exergy destruction.

3.4. Conclusions

A small-capacity solar-geothermal absorption system for hot climates has been proposed and studied. The functioning of this system in the Monterrey city (Mexico) climate conditions has been analyzed. Three working fluids as possible candidates: the two conventional $\text{NH}_3\text{-H}_2\text{O}$ and $\text{H}_2\text{O-LiBr}$ working fluids and a third innovative working fluid ($\text{NH}_3\text{-LiNO}_3$). The system's components were dimensioned and a quick economic viability study was performed. In terms of thermodynamic performance, the $\text{H}_2\text{O-LiBr}$ resulted to be the most efficient working pair for the nominal conditions. However, from the economic point of view and under the hypothesis considered for the present study, the choice of the working fluid seems to have a relatively low impact on the initial investment cost of a small-capacity solar-geothermal absorption system. On the other hand, the proposed system would be technically feasible, but, unless economic incentives such as green subsidies are implemented, seems like not economically viable in the Mexican conditions. The geothermal system strongly impacts the already high initial investment cost of the solar absorption system. One option to increase the system's economic viability would be to take into account the use of the solar thermal collectors and the hot water storage tank as domestic hot water because, in arid regions like northern Mexico, the need for heating is also important during winter. In the context of the recently implemented Mexican energy reform, there is a big expectation and new implementation of programs to transit to a more sustainable energy market. New green subsidies could be an important factor to boost this transition and engage Mexicans with the challenge.

Once the $\text{H}_2\text{O-LiBr}$ working fluid chosen as the better option for a solar residential absorption air conditioning in the Mexican climate, a first and second law dynamic model of a bi-adiabatic small-capacity absorption chiller based on its components' thermal and mass effectivenesses was presented. The model was used to identify the system's nominal conditions and to study its behavior coupled to a solar thermal collector as the high temperature source, a helical geothermal heat exchanger as the intermediate temperature source, and a single-family house. This configuration can deliver cooling capacities to a single-family house that would lead to comfortable room temperatures and with a temperature difference as high as 9°C compared with a non-cooled home. In the present study, the system provided up to 6.2 kW of cooling and a cumulative COP of 0.77. Moreover, there was no risk of crystallization in the studied conditions. The dimensioning of the solution and refrigerant storage tanks are of great importance to reduce the response time of the system, but at the same time, a compromise must be found to give some thermal inertia to the system to smoothen the variations of the external conditions.

Finally, the exergetic study showed that the components that lead to the highest exergy destruction are the adiabatic desorber and absorber, respectively. This is due to the low mass effectiveness that were selected for these components and to the impact of the enthalpy of mixing. Indeed, in the nominal design conditions of this study, a mass effectiveness of 0.6 was selected; however, adiabatic absorbers and desorbers with a higher mass effectiveness than this would considerably improve the machine's performance and reduce its exergy destruction. For this reason, [Chapter IV](#) presents the design and experimental characterization of a new generation of adiabatic sorption exchangers for absorption chillers with elevated mass transfer performances.

References

- Acuña, A., Lara, F., Rosales, P., Suastegui, J., Velázquez, N., Ruelas, A., 2017. Impact of a vertical geothermal heat exchanger on the solar fraction of a solar cooling system. *Int. J. Refrig.* 76, 63–72. <https://doi.org/10.1016/j.ijrefrig.2017.02.007>
- Agbossou, A., Souyri, B., Stutz, B., 2018. Modelling of helical coil heat exchangers for heat pump applications: Analysis of operating modes and distance between heat exchangers. *Appl. Therm. Eng.* 129, 1068–1078. <https://doi.org/10.1016/j.applthermaleng.2017.10.089>
- Aiane, M., Ramousse, J., Bouyoud, M., Boudard, E., Stutz, B., 2017. Modélisation dynamique d'un système de climatisation par absorption, in: *Congrès Société Française de Thermique*, 30 May - 2 Juin. Marseille, France.
- Altamirano, A., Stutz, B., Le Pierrès, N., 2018. Selection of High-Performance Working Fluid for a Solar-Geothermal Absorption Cooling System and Techno-Economic Study in the Northern Mexican Conditions, in: *12th International Conference on Solar Energy for Buildings and Industry*, September 10-13. Rapperswil, Switzerland. <https://doi.org/10.18086/eurosun2018.04.15>
- ASHRAE, 2004. ANSI/ASHRAE Standard 55-2004: Thermal Environmental Conditions for Human Occupancy.
- Bailo, C.M., Garcés, S.A., Arizón, F.P., 2010. Analysis of a New Dissipation System for a Solar Cooling Installation. *J. Thermodyn.* 2010, 1–6. <https://doi.org/10.1155/2010/750675>
- Banco de México [WWW Document], 2018. Inflación. URL <http://www.anterior.banxico.org.mx/portal-inflacion/inflacion.html>
- Beutler, A., Hoffmann, L., Ziegler, F., Alefeld, G., Gommed, K., Grossman, G., Shavit, A., 1996. Experimental Investigation of Heat and Mass Transfer on Horizontal and Vertical Tubes, in: *Proceedings of the International Absorption Heat Pump Conference*, September 17-20. Montreal, Canada, pp. 409–419.
- CFE [WWW Document], 2018. Tarifas. URL https://app.cfe.mx/aplicaciones/ccfe/tarifas/tarifas/tarifas_casa.asp
- Chen, J.F., Dai, Y.J., Wang, R.Z., 2017. Experimental and analytical study on an air-cooled single effect LiBr-H₂O absorption chiller driven by evacuated glass tube solar collector for cooling application in residential buildings. *Sol. Energy* 151, 110–118. <https://doi.org/10.1016/j.solener.2017.05.029>
- Domain, F., Brabant, A., Souyri, B., Stutz, B., 2015. Estimation du comportement du bâti par analogie électrique RC - Application au délestage électrique, in: *JNES*. Perpignan, France.
- Doughty, C., Nir, A., Tsang, C.-F., 1991. *Seasonal Thermal Energy Storage in Unsaturated soil : Model Development and Field Validation Soils*.
- Evola, G., Le Pierrès, N., Boudehenn, F., Papillon, P., 2013. Proposal and validation of a model for the dynamic simulation of a solar-assisted single-stage LiBr/water absorption chiller. *Int. J. Refrig.* 36, 1015–1028. <https://doi.org/10.1016/j.ijrefrig.2012.10.013>
- Farshi, L.G., Infante Ferreira, C.A., Mahmoudi, S.M.S., Rosen, M.A., 2014. First and second law analysis of ammonia/salt absorption refrigeration systems. *Int. J. Refrig.* 40, 111–121. <https://doi.org/10.1016/j.ijrefrig.2013.11.006>
- Gutiérrez-Urueta, G., Rodríguez, P., Ziegler, F., Lecuona, A., Rodríguez-Hidalgo, M.C., 2012. Extension of the characteristic equation to absorption chillers with adiabatic absorbers. *Int. J. Refrig.* 35, 709–718. <https://doi.org/10.1016/j.ijrefrig.2011.10.010>
- Hernández-Magallanes, J.A., Rivera, W., Coronas, A., 2017. Comparison of single and double stage absorption and resorption heat transformers operating with the ammonia-lithium nitrate mixture. *Appl. Therm. Eng.* 125, 53–68. <https://doi.org/10.1016/j.applthermaleng.2017.06.130>
- Ibrahim, O.M., Klein, S.A., 1993. *Thermodynamic Properties of Ammonia—Water Mixtures*. ASHRAE Trans. 99, 1495–1502.
- IEA, 2018. *The Future of Cooling*. Paris, France.

- Kays, W.M., London, A.L., 1984. Compact heat exchanger. New York: McGraw-Hill.
- Kohlenbach, P., Ziegler, F., 2008. A dynamic simulation model for transient absorption chiller performance. Part I: The model. *Int. J. Refrig.* 31, 217–225. <https://doi.org/10.1016/j.ijrefrig.2007.06.009>
- Kotas, T., 1985. The exergy method of thermal plant analysis. Great Britain: Anchor Brendon Ltd.
- Lazzarin, R., 1980. Steady and transient behaviour of LiBr absorption chillers of low capacity. *Rev. Int. du Froid* 3, 213–218.
- Mateus, T., Oliveira, A.C., 2009. Energy and economic analysis of an integrated solar absorption cooling and heating system in different building types and climates. *Appl. Energy* 86, 949–957. <https://doi.org/10.1016/j.apenergy.2008.09.005>
- Moch, X., 2013. Étude théorique et expérimentale d'échangeurs géothermiques hélicoïdaux: Production de chaud et de froid par pompe à chaleur, et dimensionnement d'installations. Université de Grenoble.
- Moch, X., Palomares, M., Claudon, F., Souyri, B., Stutz, B., 2015. Geothermal helical heat exchangers: Coupling with a reversible heat pump in Western Europe. *Appl. Therm. Eng.* 81, 368–375. <https://doi.org/10.1016/j.applthermaleng.2015.01.072>
- Moch, X., Palomares, M., Claudon, F., Souyri, B., Stutz, B., 2014. Geothermal helical heat exchangers: Comparison and use of two-dimensional axisymmetric models. *Appl. Therm. Eng.* 73, 689–696. <https://doi.org/10.1016/j.applthermaleng.2014.06.051>
- Monné, C., Alonso, S., Palacín, F., Serra, L., 2011. Monitoring and simulation of an existing solar powered absorption cooling system in Zaragoza (Spain). *Appl. Therm. Eng.* 31, 28–35. <https://doi.org/10.1016/j.applthermaleng.2010.08.002>
- Mugnier, D., Neyer, D., White, S., 2017. *The Solar Cooling Design Guide: Case Studies of Successful Solar Air Conditioning Design*. Ernst & Sohn, Berlin, Germany.
- Noorollahi, Y., Saeidi, R., Mohammadi, M., Amiri, A., Hosseinzadeh, M., 2018. The effects of ground heat exchanger parameters changes on geothermal heat pump performance – A review. *Appl. Therm. Eng.* 129, 1645–1658. <https://doi.org/10.1016/j.applthermaleng.2017.10.111>
- Ochoa, A.A. V., Dutra, J.C.C., Henríquez, J.R.G., Santos, C.A.C., 2016. Dynamic study of a single effect absorption chiller using the pair LiBr/H₂O. *Energy Convers. Manag.* 108, 30–42. <https://doi.org/10.1016/j.enconman.2015.11.009>
- Pátek, J., Klomfar, J., 2006. A computationally effective formulation of the thermodynamic properties of LiBr-H₂O solutions from 273 to 500 K over full composition range. *Int. J. Refrig.* 29, 566–578. <https://doi.org/10.1016/j.ijrefrig.2005.10.007>
- SIMA, 2019. Monterrey climatic conditions of the 23 July 2018 (personal contact).
- SIMA, 2018. Reportes mensuales de calidad del aire.
- SMN, 2018. Información Climatológica por Estado.
- Tillner-Roth, R., Harms-Watzenberg, F., Baehr, H.D., 1993. Eine neue fundamentalgleichung für ammoniak. *Dkv-taungsbericht* 20, 167–181.
- Tsoutsos, T., Anagnostou, J., Pritchard, C., Karagiorgas, M., Agoris, D., 2003. Solar cooling technologies in Greece. An economic viability analysis. *Appl. Therm. Eng.* 23, 1427–1439. [https://doi.org/10.1016/S1359-4311\(03\)00089-9](https://doi.org/10.1016/S1359-4311(03)00089-9)
- Vargas Bautista, J.P., García Cuéllar, A.J., Rivera Solorio, C.I., 2011. Design and economic analysis of a solar air-conditioning system: case of study in Monterrey, Mexico, in: *EUROSUN 2011*.
- Venegas, M., Arzoz, D., Rodríguez, P., Izquierdo, M., 2003. Heat and mass transfer in LiNO₃-NH₃ spray absorption system. *Int. Commun. Heat Mass Transf.* 30, 805–815. [https://doi.org/10.1016/S0735-1933\(03\)00128-3](https://doi.org/10.1016/S0735-1933(03)00128-3)
- Ventas, R., Lecuona, A., Legrand, M., Rodríguez-Hidalgo, M.C., 2010. On the recirculation of ammonia-lithium nitrate in adiabatic absorbers for chillers. *Appl. Therm. Eng.* 30, 2770–2777. <https://doi.org/10.1016/j.applthermaleng.2010.08.001>
- Viñas, E., Best, R., Lugo, S., 2016. Simulation of solar air conditioning systems in coastal zones of

- Mexico. *Appl. Therm. Eng.* 97, 28–38. <https://doi.org/10.1016/j.applthermaleng.2015.09.104>
- Wang, L., Sundén, B., Manglik, R.M., 2007. *Plate Heat Exchangers. Design, Applications and Performance.* Wit Press. <https://doi.org/10.1081/E-EAFE>
- Yuan, Z., Herold, K.E., 2005. Thermodynamic properties of aqueous lithium bromide using a multiproperty free energy correlation. *HVAC R Res.* 11, 377–393. <https://doi.org/10.1080/10789669.2005.10391144>

This page intentionally left blank

Chapter IV. New-generation adiabatic falling film mass exchanger for absorption chillers

*Based on:
Altamirano, A., Stutz, B., Le Pierrès, N.
Adiabatic desorber for absorption chillers
Submitted to Heat Transfer Engineering*

After determining the minimum mass effectiveness requirements of the adiabatic sorption exchangers of an absorption chiller with a bi-adiabatic configuration, the present chapter provides the experimental characterization, by the mass effectiveness, of a new generation of 3D printed adiabatic falling film sorption exchanger for absorption chillers operating in desorption mode. The impact of four parameters were analyzed: the operating pressure, the solution mass flow rate, the solution concentration, and the solution equilibrium deviation temperature. In order to clearly identify the impact of the studied parameters and their interactions, a second-order design of experiments was implemented. Finally, in order to verify the compactness of the proposed exchanger, a comparison with other exchanger technologies is performed.

“

*“Considerate la vostra semenza:
fatti non foste a viver come bruti,
ma per seguir virtute e canoscenza.”*

*“Consider your origin:
you were not formed to live like brutes
but to follow virtue and knowledge.”*

– Dante Alighieri

4.1. Introduction

The different challenges to overcome to make of absorption chillers competitive with conventional vapor compression systems and different solution possibilities have been the subject of discussion in the precedent chapters. Until now, the study of the most adapted working pair, the possibility of a geothermal heat sink source, and the study of an innovative bi-adiabatic configuration have been addressed. The new machine architecture proposed in [Chapter III](#) is only useful if efficient, compact, and low cost adiabatic sorption exchangers are implemented. Indeed, the sorption exchangers in absorption chillers have been identified as one of the main “bottleneck” to increase their compactness.

The adiabatic sorption exchangers can be divided into three main categories: gravity-driven, nozzle driven, and membrane-based exchangers. Membrane-based and nozzle-driven exchangers have both proven to lead to high absorption performances. However, they require additional energy to overcome pressure drops in the component. Moreover, the durability of membrane-based sorption exchangers still needs to be studied (especially for salt-based solutions, which seem to have a tendency to block the membrane pores) and the nozzle-driven exchangers, which are limited in the solution flow rates, usually require a large chamber volume to achieve optimal solution distribution (Altamirano et al., 2020b). The gravity-driven adiabatic exchangers do not consume supplementary electricity as the solution flows freely in a chamber in which the vapor pressure remains constant, which leading to negligible pressure losses. These exchangers, which have shown promising mass exchange performances, have been mainly studied in three different configurations: falling droplets (Arzoz et al., 2005; Gutiérrez-Urueta et al., 2011), unstable jets (Arzoz et al., 2005), and falling film (Arzoz et al., 2005; Boudard and Bruzzo, 2004; Michel et al., 2017; Obame Mve et al., 2015). However, no special mass transfer enhancement method (e.g., a special distribution method or enhanced falling film surface) has been further investigated (Altamirano et al., 2020b). Indeed, the most limiting issues in these exchangers include the non-uniform distribution of the falling film over the exchange surface (Michel et al., 2017), the film interface temperature variation due to the sorption phenomenon, and the low mass diffusion coefficient of water in the solution (Islam et al., 2003).

Apart from performance and compactness concerns, the elevated manufacturing costs of absorption chillers due to their low demand and, therefore, the absence of serial production, is another fundamental concern (Mugnier et al., 2017). Additive manufacturing technology, which consists in the printing of successive layers of a given material formed on top of each other (Ngo et al., 2018), today allows for the construction of complex parts otherwise impossible to manufacture (Peng et al., 2018) and is a viable production alternative for end-products (Peng et al., 2018; Plocher and Panesar, 2019). Its implementation could potentially reduce the time and cost of small-volume components manufacturing (Peng et al., 2018), paving the way for new disruptive business models (Savolainen and Collan, 2020).

The present chapter shows the experimental characterization of a new patented generation of falling film sorption adiabatic exchanger (Altamirano Cundapí et al., 2020) produced by means of additive manufacturing, using the fused deposition modeling (FDM) method. The structure and solution distributor are designed to provide a uniform distribution of the solution over the exchange surface. Moreover, due to the design of the adiabatic sorption exchanger, the mass transfer phenomenon is enhanced by the renewal of the thermal and mass boundary layers due to flow instabilities that are generated as the solution film flows down. While the 3D-printing method serves as a tool to tackle the high cost and absence of mass production of absorption systems, the proposed exchanger geometry represents an alternative for solving some of the most performance-limiting issues in sorption exchangers. The adiabatic exchanger was tested in desorption mode, and its performance was experimentally characterized by mass effectiveness (Altamirano et al., 2020c, 2020a, 2019b; Michel et al., 2017). A second-order polynomial of the mass effectiveness was obtained through a design of experiments. The first part of this chapter presents the design of the adiabatic exchanger and the experimental set-up used for its characterization.

The design of experiments implemented for the characterization and the uncertainties of the investigated parameters are then described. Subsequently, the experimental results of the desorber characterization are presented, and the different parameters affecting the mass effectiveness are discussed. Finally, a comparison of the obtained results with other exchanger technologies is made.

4.2. Experimental set-up

4.2.1. Experimental facility

An experimental facility, observed in [Figure IV.1](#), was designed to test any adiabatic sorption exchanger geometry (in desorption or absorption mode) for a nominal cooling capacity of 2 kW. [Figure IV.2](#) presents the part of the facility required to characterize an adiabatic desorber (left section of [Figure IV.1a](#) and b). The generator-condenser chamber contains the adiabatic generator and the condenser (helical coil). Furthermore, there are two independent external circuits: the hot water circuit (red line) and the condenser cooling circuit (orange line). The hot water circuit, which is used to pre-heat the diluted solution in a plate heat exchanger before reaching the adiabatic generator, mainly consists of a 4.5-kW electric heater (operation temperature range between 5 and 110°C), a circulation pump, and a magnetic flowmeter. The condenser cooling circuit, which is used to release the refrigerant latent heat from the non-adiabatic condenser inside the chamber, consists of an air-cooled thermostatic bath with an internal circulation pump (operating temperatures: -20 to 40°C; nominal cooling capacity of 3 kW) and a magnetic flowmeter.

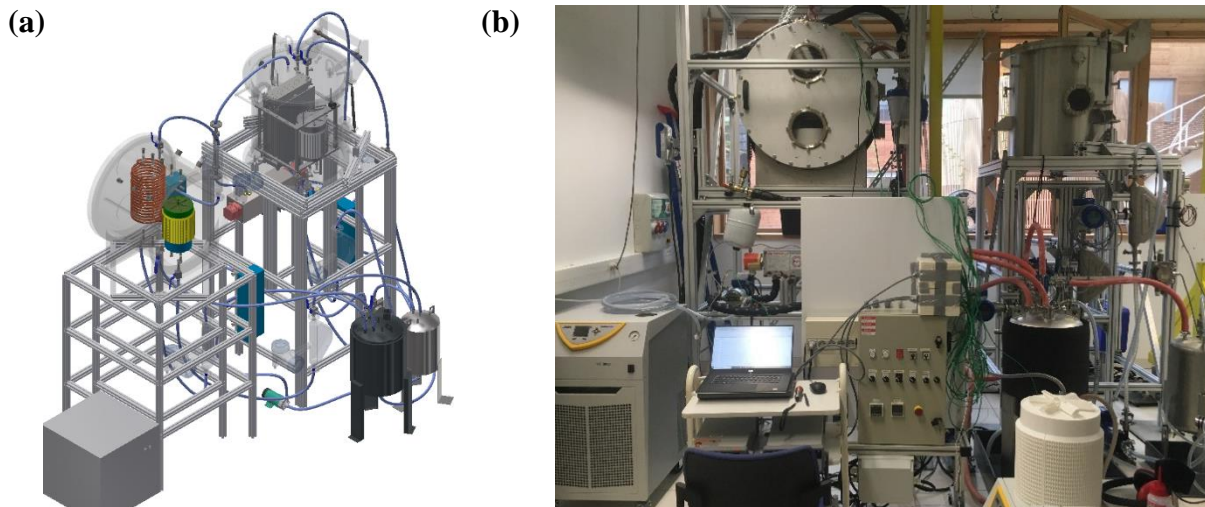


Figure IV.1: Experimental test facility for the characterization of adiabatic absorbers and desorber for small capacity absorption chillers: (a) 3D design and (b) experimental facility .

The internal circuits include: a concentrated solution circuit (dark green line) for the solution coming from the desorber; a diluted solution circuit (light green line) for the solution going to the desorber; and a circuit for the water coming from the condenser (gray line). The solution and refrigerant at the outlet of the desorber and condenser, respectively, are collected below the components by means of simple collectors (the solution collector is shown in [Figure IV.3](#)). A solution heat exchanger is placed between the two solution circuits to recover internal heat. Furthermore, Coriolis flowmeters are placed in all the internal circuits to obtain the mass flow rates and concentrations of the refrigerant and solutions at the inlet and outlet of the components inside the chambers. Two storage tanks (one for the solution and one for the refrigerant) are used to absorb the solution concentration fluctuations in the system. Moreover, a capacitive pressure sensor is placed in the chamber to constantly measure the vapor pressure. Finally, K-

type calibrated thermocouples measure the temperature of the fluids at the inlet and outlet of the heat and mass exchangers.

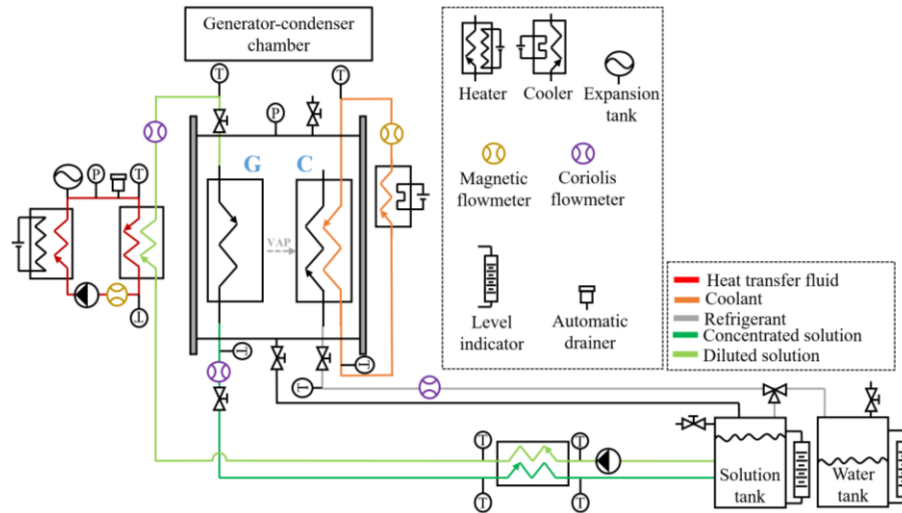


Figure IV.2: Schematic diagram of the experimental test facility for the characterization of adiabatic generators.

The chamber is operated in such a way that the desired solution inlet conditions and vapor pressure are achieved. At steady-state, the condensed refrigerant is directly sent to the solution container (and not to the refrigerant container) to maintain a stable concentration of diluted solution in the system. If a higher solution concentration is required, either to change the experimental steady-state condition or to represent a variable condition, then the condensed water is sent to the refrigerant container until reaching the desired concentration in the system. On the other hand, if a lower solution concentration is required, the required mass of water is directly added to the solution container through a valve connected to an external circuit.

4.2.2. Adiabatic sorption exchanger

A new patented geometry of adiabatic exchangers (Altamirano Cundapí et al., 2020) designed for a single-stage absorption chiller with a nominal cooling capacity of 2 kW, shown in Figure IV.3, is proposed. This exchanger was dimensioned with the aid of the experimental results of the adiabatic falling film plate absorber measuring 220 mm in length presented by Michel et al. (2017). Considering that the entry width of the equivalent plate is equal to the total equivalent width of the horizontal bars and the most unfavorable scenario in which the flash evaporation is neglected, and that only an adiabatic desorption at the film interface is taken into account, the number of horizontal bars was adapted to obtain a mass effectiveness of approximately 0.64 at nominal conditions (considering the minimum performance requirements of Chapter III). There are four main components in the proposed assembly: the solution distributor in which vapor is generated by flash evaporation, the sorption exchanger in which vapor is generated by desorption at the interface of falling films, the droplet separator, and the solution collector. The highly super-heated solution enters the distributor, where flash evaporation occurs, allowing the solution to approach its equilibrium state. The still overheated solution then flows along the 3D structure where it continues to desorb by diffusion. The low kinetics of desorption by diffusion requires the use of thin films associated with fluid mixing, which is obtained through the 3D cylindrical structure. The adiabatic exchanger itself (central part) consists of a 3D printed cylindrical structure composed of horizontal bars, vertical supports, and a central cylindrical support (Figure IV.3b and c). The horizontal bars and vertical supports are square-shaped with sides measuring 2mm (detailed view of Figure IV.3b). The 40 horizontal bars are symmetrically distributed on the horizontal plan (Figure IV.3c) and repeated 19 times along the vertical axis (Figure IV.3b). Furthermore, the vertical supports alternate between each step (detailed view of

Figure IV.3b) to generate hydrodynamic solution flow disturbances, allowing for the renewal of the thermal and mass boundary layers and enhancing the mass transfer phenomenon. The fixed number of symmetrically distributed horizontal axes allows for a linear variation of the vapor hydraulic diameter along the flow direction. In the case of the desorber, this makes it possible to limit the effects of pressure losses related to the increase in the vapor flow rate with the increase in the radius.

The exchanger structure has an external diameter of 200 mm and a height of 220 mm (Figure IV.3b and c). Whereas the internal cylindrical support has an external diameter of 25 mm and an internal diameter of 20 mm (Figure IV.3c), making an effective volume of $6.9 \cdot 10^{-3} \text{ m}^3$ for 2 kW of nominal cooling capacity. An effective exchange area can also be calculated if each horizontal bar (Figure IV.3c) is considered as the solution entrance width of a plate surface that continues all the way along the vertical axis; therefore, 40 plate-equivalent areas are present and the effective area of the exchanger would be equal to 0.77 m^2 ($40 \cdot (0.1 - 0.0125) \cdot 0.22$). The distance between the vertical axes for good printing quality is 5 mm (detailed view of Figure IV.3b). On the other hand, the vertical distance between the horizontal axes is 10 mm (detailed view of Figure IV.3b). This vertical separation can be reduced for a denser structure at the cost of increased 3D-printing time.

A 3D-printed droplet separator (Figure IV.3) is located on the external diameter of the mass exchanger structure. This separator makes it possible to trap the solution droplets that could be carried away by the refrigerant vapor flow toward the condenser to prevent the mixing of solution with the liquid refrigerant.

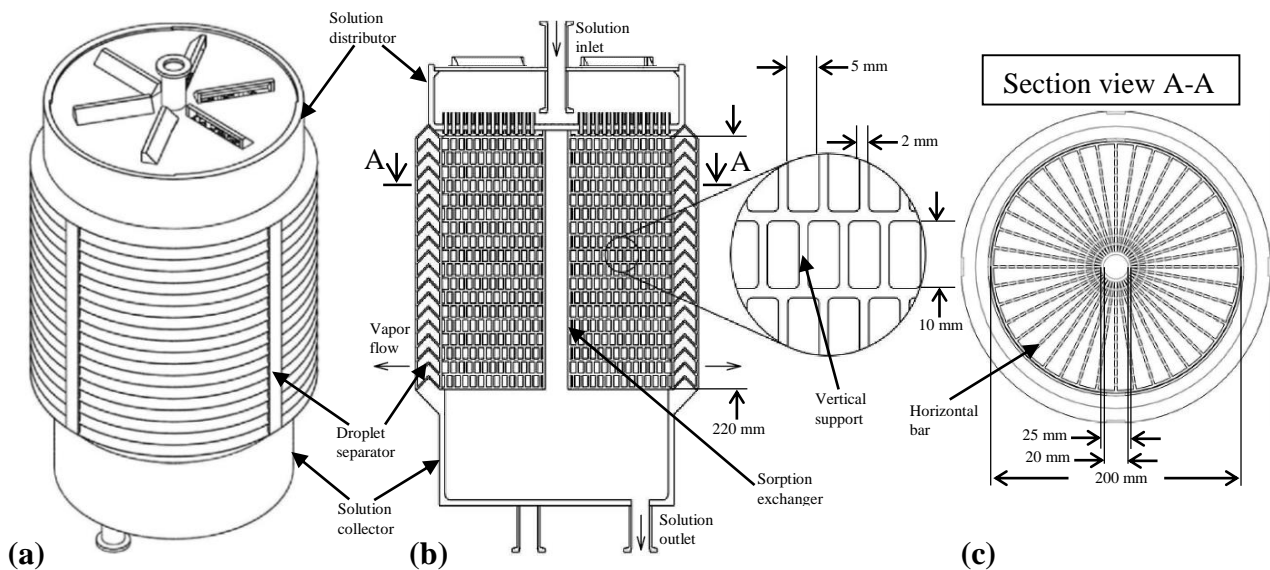


Figure IV.3: 3D design of the adiabatic sorption exchanger. (a) Isometric view, (b) section side view, and (c) section view A-A.

Finally, the distributor (Figure IV.3a and b) was especially designed to generate a uniformly distributed flow over the adiabatic exchanger. The tubes situated on the lower face of the solution distributor (Figure IV.3b) slightly exceed the lower surface to assure a solution flow in the tube direction and avoid a redistribution on the bottom surface. Moreover, splits at the distributor cover (Figure IV.3a and b) allow the refrigerant vapor desorbed in the distributor to be evacuated.

4.3. Data reduction and operating conditions

The test bench allows for the control and measurement of different parameters in the system. The parameters that were controlled during experiments include the operating pressure, the inlet solution concentration, the inlet solution temperature, and the inlet solution mass flow rate. An Agilent 34972A LXI data acquisition unit controlled with a Labview interface was used to collect the data from the different sensors. The acquisition frequency is 0.1 Hz. The steady-state is assumed to be reached when the operating conditions (pressure, temperature, and inlet solution concentration) are reached and kept stable for 10 min. At each steady-state experimental set point, 10 min of data recording is performed. The present section describes the different parameters that are used to assess the exchangers' performances and the design of experiments employed for this purpose.

4.3.1. Temperature equilibrium deviations

In an adiabatic desorber, the deviation of the solution from the equilibrium conditions at the inlet of the component is of fundamental importance. The higher the deviation, also called the driving force, the higher the desorption potential and the better the performance of the adiabatic exchanger (Michel et al., 2017). Depending on component performance, the solution might or might not reach equilibrium conditions at the outlet. The deviation of the solution from its equilibrium conditions at the inlet or outlet of the adiabatic desorber can be defined in terms of a temperature difference, as shown in Eq. (IV.1). In order to have a desorber operating mode, $\Delta T_{s,i}^{eq}$ must be positive (super-heated state). Otherwise, if $\Delta T_{s,i}^{eq} < 0$, the solution is then in a sub-cooled state and has the potential to absorb refrigerant vapor.

$$\Delta T_{s,i}^{eq} = T_{s,i} - T_{eq}(P_v, x_i) \quad (IV.1)$$

4.3.2. Desorbed mass and mass effectiveness

Different parameters can be used to evaluate the mass transfer in adiabatic sorption elements. Some of them, like the sorption mass flux (i.e., the sorption mass flow rate divided by the exchange area) or the overall mass transfer coefficient (the definition of which might vary depending on the author, as explained by (Venegas et al., 2005)), use a mass exchange area that might be barely and/or inaccurately calculated (e.g., in nozzle-driven adiabatic exchangers) (Altamirano et al., 2020b). In the present work, a mass effectiveness term, which is an analogy to the thermal effectiveness in heat exchangers, is implemented to assess the exchanger mass transfer performances. This mass effectiveness (Eq. (IV.2)), which can also be implemented in the absorption mode, is defined as the ratio of the experimental absorbed/desorbed mass to the maximum theoretical absorbable/desorbable mass. The maximum desorbable mass is obtained by an iterative process for which Eqs. (IV.3)–(IV.6) are satisfied (having $\dot{m}_{d,ad} = \dot{m}_{d,ad}^{max}$).

$$\varepsilon_m^d = \frac{\dot{m}_d}{\dot{m}_d^{\max}} \quad (IV.2)$$

$$\dot{m}_{s,i} - \dot{m}_{d,ad} - \dot{m}_{s,o} = 0 \quad (IV.3)$$

$$\dot{m}_{s,i}x_{s,i} - \dot{m}_{s,o}x_{s,o} = 0 \quad (IV.4)$$

$$\dot{m}_{s,i}H_{s,i} - \dot{m}_{d,ad}H_v - \dot{m}_{s,o}H_{s,o} = 0 \quad (IV.5)$$

$$T_{s,o}^{\text{ad}} = T_{s,o}(H_{s,o}; P_d; x_{s,o}) = T_{s,\text{eq}}(P_d; x_{s,o}) \quad (IV.6)$$

The desorbed mass is calculated by means of an enthalpy balance on the LiBr solution, as detailed in (Flores, 2014). In this method, the outlet enthalpy is obtained by means of a first-order Taylor expansion (Eq. (IV.7)). After some manipulation of Eqs. (IV.3)–(IV.5) and (IV.7), the desorbed mass can be expressed as in Eq. (IV.8).

$$H_{\text{sol},o} = H_s^{x_i, T_{s,o}} + \left. \frac{dH}{dx} \right|_{x_i, T_{s,o}} (x_o - x_i) \quad (IV.7)$$

$$\dot{m}_d = \frac{\dot{m}_{s,i} (H_{s,i} - H_s^{x_i, T_{s,o}})}{x_i \cdot \left. \frac{dH}{dx} \right|_{x_i, T_{s,o}} - H_s^{x_i, T_{s,o}} + H_v} \quad (IV.8)$$

4.3.3. Design of experiments and uncertainties

Four parameters were selected to characterize the performance of the adiabatic desorber: the operating pressure, the inlet solution concentration, the inlet solution equilibrium deviation temperature, and the mass flow rate. The operating conditions were defined after the modelling results from Chapter III and considering the limitations of the experimental equipment. Indeed, in the nominal operating conditions (Section 3.3.2.1) for the proposed machine architecture and for 2 kW of cooling capacity, the inlet solution's desorber state would be as follows: $P_d = 6.31 \text{ kPa}$; $\Delta T_{s,i}^{\text{eq}} = 10.37^\circ\text{C}$; $\dot{m}_{s,i} = 0.24 \text{ kg s}^{-1}$; $x_{s,i} = 0.579$. The operating conditions, together with the other directly or indirectly measured values, are presented in Table IV.1. The uncertainties of the measured and calculated values were obtained through the method described by Moffat (1982).

Table IV.1: Operating conditions and uncertainties.

Parameter	Type	Range	Uncertainty
Operating pressure (P_d , kPa)	Capacitive sensor	3.5–6	$\pm 0.25\%$
Inlet solution concentration ($x_{s,i}$, kg kg ⁻¹)	Calculated from $T_{s,i}$ and $\rho_{s,i}$	0.5–0.6	$\leq \pm 0.0006$
Inlet solution equilibrium deviation temperature ($\Delta T_{s,i}^{\text{eq}}$, °C)	Calculated from $T_{s,i}$, P_d , and $x_{s,i}$	2–10	$\leq \pm 0.28^\circ\text{C}$
Inlet solution mass flow rate ($\dot{m}_{s,i}$, kg s ⁻¹)	Coriolis flowmeter	0.139–0.278	$\pm 0.1\%$
Temperature measurements	Type K thermocouple	-	$\pm 0.15^\circ\text{C}$

In order to optimize the number of tested conditions for obtaining detailed information on the behavior of desorber effectiveness, a design of experiments was performed. Specifically, a Doehlert method of second order was employed due to its advantages in terms of high precision, optimized number of tests with a uniform repartition on the experimental domain, and easy adaptation of the number of studied parameters (Caldas et al., 2013). This method allows for the numerical representation of a phenomenon (in this case, the mass effectiveness) as a function of a set of selected parameters. In the case of four parameters, the second-order equation for the effectiveness corresponds to that of Eq. (IV.9). In this equation, the coded

variables (the variable defined in a range between -1 and 1 , where -1 corresponds to the lowest value of the parameter and $+1$ corresponds to the highest value of the parameter) are conveniently used to objectively evaluate the impact of the different parameters in the experimental domain regardless of their units and dimensions. In this regard, the center of the experimental domain is defined as the point at which all the parameters are in the middle of their range (coded variable of zero). When analyzing four variables, a minimum of 21 tests are required to obtain the polynomial of Eq. (IV.9). The targeted experimental conditions of these tests are presented in Table IV.2, in which the coded variables are represented in parentheses.

$$\begin{aligned} \varepsilon_m(P_{des}, \Delta T_{s,i}^{eq}, \dot{m}_{s,i}, x_{s,i}) &= \beta_0 + \beta_1 P_{des}^{cv} + \beta_2 \Delta T_{s,i}^{eq,cv} + \beta_3 \dot{m}_{s,i}^{cv} + \beta_4 x_{s,i}^{cv} + \beta_{12} P_{des}^{cv} \Delta T_{s,i}^{eq,cv} \\ &+ \beta_{13} P_{des}^{cv} \dot{m}_{s,i}^{cv} + \beta_{14} P_{des}^{cv} x_{s,i}^{cv} + \beta_{23} \Delta T_{s,i}^{eq,cv} \dot{m}_{s,i}^{cv} + \beta_{24} \Delta T_{s,i}^{eq,cv} x_{s,i}^{cv} \\ &+ \beta_{34} \dot{m}_{s,i}^{cv} x_{s,i}^{cv} + \beta_{11} P_{des}^{cv^2} + \beta_{22} \Delta T_{s,i}^{eq,cv^2} + \beta_{33} \dot{m}_{s,i}^{cv^2} + \beta_{44} x_{s,i}^{cv^2} \end{aligned} \quad (IV.9)$$

Table IV.2: Four-variables Doehlert design for desorber characterization. The coded variable values are represented in parentheses.

Test	P_d (kPa)	$\Delta T_{s,i}^{eq}$ (°C)	$\dot{m}_{s,i}$ (kg s ⁻¹)	$x_{s,i}$ (kg kg ⁻¹)
1	4.75 (0)	6 (0)	0.208 (0)	0.55 (0)
2	6 (1)	6 (0)	0.208 (0)	0.55 (0)
3	5.375 (0.5)	9.464 (0.866)	0.208 (0)	0.55 (0)
4	4.125 (-0.5)	9.464 (0.866)	0.208 (0)	0.55 (0)
5	3.5 (-1)	6 (0)	0.208 (0)	0.55 (0)
6	4.125 (-0.5)	2.536 (-0.866)	0.208 (0)	0.55 (0)
7	5.375 (0.5)	2.536 (-0.866)	0.208 (0)	0.55 (0)
8	5.375 (0.5)	7.156 (0.289)	0.265 (0.816)	0.55 (0)
9	4.125 (-0.5)	7.156 (0.289)	0.265 (0.816)	0.55 (0)
10	4.75 (0)	3.692 (-0.577)	0.265 (0.816)	0.55 (0)
11	5.375 (0.5)	4.844 (-0.289)	0.152 (-0.816)	0.55 (0)
12	4.125 (-0.5)	4.844 (-0.289)	0.152 (-0.816)	0.55 (0)
13	4.75 (0)	8.308 (0.577)	0.152 (-0.816)	0.55 (0)
14	5.375 (0.5)	7.156 (0.289)	0.223 (0.204)	0.59 (0.791)
15	4.125 (-0.5)	7.156 (0.289)	0.223 (0.204)	0.59 (0.791)
16	4.75 (0)	3.692 (-0.577)	0.223 (0.204)	0.59 (0.791)
17	4.75 (0)	6 (0)	0.166 (-0.612)	0.59 (0.791)
18	5.375 (0.5)	4.844 (-0.289)	0.194 (-0.204)	0.51 (-0.791)
19	4.125 (-0.5)	4.844 (-0.289)	0.194 (-0.204)	0.51 (-0.791)
20	4.75 (0)	8.308 (0.577)	0.194 (-0.204)	0.51 (-0.791)
21	4.75 (0)	6 (0)	0.251 (0.612)	0.51 (-0.791)
Level -	3.5 (-1)	2 (-1)	0.139 (-1)	0.5 (-1)
Level +	6 (+1)	10 (+1)	0.278 (+1)	0.6 (+1)

4.4. Results and discussion

4.4.1. Mass effectiveness regression

In total, 34 tests were performed: the 21 tests required to obtain the coefficients of the second-degree polynomial (Eq. (IV.9)), a series of tests to verify the experimental repeatability performed at different times between two other randomly chosen tests (tests 22–26 are repetitions of test 1, and tests 27 and 28 are a repetition of tests 11 and 17, respectively). Furthermore, in order to validate the model under operating conditions other than those in Table IV.2, two test validation series were performed in the center of the experimental domain ($P = 4.75$ kPa, $x_{s,i} = 0.55$), varying the solution flow rate at a $\Delta T_{s,i}^{eq}$ of 2°C (TV1, tests 29–31) and 6°C (TV2, tests 32–34). Results are presented in Table IV.3. The equivalent cooling capacity (\dot{Q}_{cool} , if the desorber was integrated in an absorption chiller) was calculated using the desorbed mass and water enthalpy of vaporization of 2264.76 kJ kg⁻¹. For the 34 tested experimental conditions, the desorber led to an equivalent cooling capacity in the range of 0.39–3.41 kW, with a mass effectiveness between 88 and 100% (uncertainty $\leq \pm 13.2\%$). Indeed, one observes from the experimental results that, while the desorber was conceived to operate at a nominal cooling capacity of 2 kW, it can deliver higher cooling loads if required and still with good performances (see test 3 in Table IV.3, for example).

The data from tests 1–28 were used to fit the coefficients of Eq. (IV.9) using the least-squares method along with the generalized reduced gradient (GRG) nonlinear method. The fitted coefficients are presented in Table IV.4. From Eq. (IV.9), β_0 is a representation of the average effectiveness in the center of the experimental domain, which in this case was 95.7%. Single and identical double subscripts correspond, respectively, to the linear and quadratic influence of the relevant parameter (1, 2, 3, and 4 for P_d^{cv} , $\Delta T_{s,i}^{eq,cv}$, $\dot{m}_{s,i}^{cv}$, and $x_{s,i}^{cv}$, respectively) on effectiveness. When there are two different subscripts, the coefficient describes the interaction between the two factors concerned (i.e., the failure of one factor to produce the same effect on effectiveness at different levels of the other factor (Montgomery, 2012)). The resulting function has a maximum deviation of 1.5% with respect to the experimental results. The experimental error on the coefficients in Table IV.4 was $\pm 0.9\%$. If the coefficients are equal to or lower than this error, the factor is considered as non-influential on effectiveness. Moreover, the experimental error due to random variations on the non-controlled parameters was calculated for the center of the experimental domain (tests 1 and 22–26) and was $\pm 1.14\%$.

From Table IV.4, one can observe that the inlet solution concentration ($x_{s,i}^{cv}$) presents the highest positive linear influence (β_4) on mass effectiveness, and this influence is accentuated by its positive quadratic coefficient, β_{44} . On the other hand, the inlet solution mass flow rate ($\dot{m}_{s,i}^{cv}$) has the highest negative influence on the effectiveness with its negative linear (β_3) and quadratic coefficients (β_{33}). Furthermore, the inlet equilibrium deviation temperature ($\Delta T_{s,i}^{eq,cv}$) has a positive linear influence (β_2) that is limited by a negative quadratic coefficient (β_{22}). Moreover, $\Delta T_{s,i}^{eq,cv}$ is also the parameter that showed the highest dependence with other factors, especially with $\dot{m}_{s,i}^{cv}$ (β_{23}) and $x_{s,i}^{cv}$ (β_{24}). Finally, pressure is the parameter with the lowest impact on the effectiveness, averaging a slight positive influence (from β_1 and β_{11}). A detailed analysis of the phenomena that might impact these influences is presented in Section 4.4.2 with the support of graphical representations of the obtained regression.

In the whole experimental domain, the regression indicates that the tested desorber can provide an equivalent cooling capacity of between 0.32 and 4.74 kW with a mass effectiveness in the range of 69.5–100%. Knowing that during an entire machine simulation (Altamirano et al., 2019b), a minimum adiabatic desorption effectiveness of 0.6 was required at the nominal conditions for the system to operate with a good coefficient of performance, these results confirm the potential of the proposed adiabatic sorption

technology. Indeed, for the nominal operating conditions described in Section 3.3.2.1, the second degree model indicates that the desorber will operate at a mass effectiveness close to one.

Table IV.3: Experimental results of the four-variables Doehlert design for desorber characterization.

Test	P_d (kPa)	$\Delta T_{s,i}^{eq}$ (°C)	$\dot{m}_{s,i}$ (kg s ⁻¹)	$x_{s,i}$ (kg kg ⁻¹)	ε_m (%)	\dot{Q}_{cool} (kW)
1	4.79	6	0.2077	0.5496	94.76	1.95
2	6	6.32	0.2074	0.5479	97.10	2.12
3	5.37	9.96	0.2085	0.5449	98.41	3.41
4	4.23	9.52	0.2075	0.5453	97.39	3.20
5	3.53	6.19	0.2080	0.5492	94.53	2
6	4.13	2.63	0.2092	0.5493	88.10	0.80
7	5.38	2.54	0.2083	0.5498	89.45	0.783
8	5.41	7.59	0.2637	0.5430	94.74	3.180
9	4.15	6.78	0.2635	0.5494	91.78	2.70
10	4.75	3.78	0.2635	0.5496	86.97	1.43
11	5.37	4.89	0.1525	0.5507	97.51	1.20
12	4.13	4.81	0.1522	0.5496	96.39	1.16
13	4.76	8.30	0.1511	0.5508	97.85	2.02
14	5.39	8.06	0.2225	0.58384	100.71	2.79
15	4.11	7.25	0.2218	0.5877	98.49	2.41
16	4.75	3.59	0.2225	0.5901	100.44	1.22
17	4.76	5.70	0.1659	0.5908	104.54	1.50
18	5.38	4.52	0.1943	0.5149	90.24	1.41
19	4.13	4.28	0.1952	0.5141	88.64	1.31
20	4.76	8.18	0.1937	0.5108	93.14	2.64
21	4.75	6	0.2504	0.5125	88.55	2.37
22	4.75	5.88	0.2086	0.5502	97.09	1.96
23	4.75	5.75	0.2083	0.5520	95.32	1.87
24	4.75	6.14	0.2075	0.54949	97.34	2.05
25	4.74	6.08	0.2078	0.5499	95.06	1.98
26	4.75	6.01	0.2089	0.5496	95.08	1.97
27	5.35	4.84	0.1511	0.5506	99.67	1.20
28	4.77	5.77	0.1665	0.59	105.77	1.55
29	4.76	1.66	0.1390	0.5504	102.11	0.39
30	4.76	1.90	0.1804	0.5501	98.98	0.56
31	4.76	2.09	0.2222	0.5499	94.08	0.72
32	4.75	6.07	0.1385	0.55	102.63	1.42
33	4.76	5.96	0.1808	0.5501	97.14	1.73
34	4.75	6.07	0.2214	0.5497	94.57	2.10

Table IV.4: Fitted coefficients of the mass effectiveness function (Eq. (IV.9)) with the experimental results of tests 1–28 (Table IV.3).

Coefficient	Value
β_0	95.73
β_1	1.64
β_2	4.35
β_3	-4.06
β_4	7.03
β_{12}	0.01
β_{13}	0.18
β_{14}	1.43
β_{23}	3.88
β_{24}	-5.01
β_{34}	-1.54
β_{11}	-0.10
β_{22}	-2.85
β_{33}	-1.28
β_{44}	1.12

As mentioned earlier, tests 29–34 were performed to validate the model for experimental conditions outside those in Table IV.2. Two $\Delta T_{s,i}^{eq}$ were tested (at around 2 and 6 °C for TV1 and TV2, respectively). The experimental versus the model effectiveness is plotted in Figure IV.4. As observed, the model predicted the experimental effectiveness with an error of less than 10%, thereby validating the model.

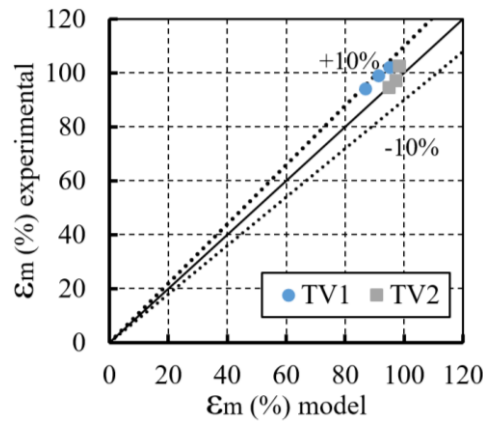


Figure IV.4: Comparison of experimental and second-order model effectiveness.

4.4.2. Model interpretation

The evolution of the effectiveness predicted by the second-order model as a function of the operating conditions is presented in Figure IV.5 for three levels of pressure (3.5, 4.75, and 6 kPa) and concentration (0.5, 0.55, and 0.6 kg kg⁻¹). The mass effectiveness is presented as a function of the inlet solution mass flow rate ($\dot{m}_{s,i}$) with iso- $\Delta T_{s,i}^{eq}$ lines at five different levels (2, 4, 6, 8, and 10°C). From these figures, it is clear that the operating conditions with the highest solution concentrations led to the highest effectiveness. This might seem contradictory at first since an increase in the solution concentration leads to a negative

impact on the thermophysical properties of the solution with regard to the heat and mass transfers in the solution. However, as $\Delta T_{s,i}^{eq}$ is a factor of study, it needs to be maintained constant as the other parameters change. Under this constraint, higher solution concentrations lead to higher solution equilibrium temperatures, and higher inlet solution temperatures are therefore required to maintain the same $\Delta T_{s,i}^{eq}$. In other words, higher inlet solution concentrations lead to higher inlet solution temperatures, which has a direct impact on the thermophysical properties of the solution for better heat and mass transfers. Therefore, the impact on the thermophysical properties due to the solution temperature variations seems dominant compared with the effects generated by the solution concentration variations themselves. This is the same reason why the pressure presents a slightly positive influence on the mass effectiveness, especially at high solution concentrations: for a $\Delta T_{s,i}^{eq} = 2\text{ }^\circ\text{C}$, $\dot{m}_{s,i} = 0.28\frac{\text{kg}}{\text{s}}$, and $x_{s,i} = 0.6$, for example, the mass effectiveness passes from 87.2% to 93.7% with a variation in pressure from 3.5 to 6 kPa (corresponding inlet solution temperatures of 72.5 and 83.6°C, respectively). However, the influence of the pressure is much lower compared with that of the solution concentration. This might be mainly due to the fact that the solution equilibrium temperature is more sensitive to concentration variations than to pressure variations, which has a direct impact on the inlet solution temperature (and thermophysical properties), as mentioned earlier.

The iso- $\Delta T_{s,i}^{eq}$ curves in Figure IV.5 show a clear positive influence of $\Delta T_{s,i}^{eq}$ on the mass effectiveness, which is probably due to the increase in the desorption potential by the generated deviation from the equilibrium conditions. It is worth mentioning that for each sub-graph of Figure IV.5, the iso- $\Delta T_{s,i}^{eq}$ lines are equivalent to iso- $T_{s,i}$ lines (due to the fixed pressure and concentration in each graph). Therefore, the thermophysical properties of the inlet solution are constant for each line.

During experiments, the increase in $\Delta T_{s,i}^{eq}$ led to an increased agitation of the solution in the distributor under the effect of a more intense generation of bubbles. The rate of bubble production increases with the increase in solution overheating and agitation (mainly due to bubble generation). The desorption kinetics depends on the specific exchange surface (interfacial air per unit volume). Thus, the higher the bubble density, the higher the agitation of the solution in the distributor and the higher the release of refrigerant by the superheated solution. Therefore, one expects to observe an increasing mass effectiveness of the distributor part (ϵ_m^{dist} , defined by Eq. (IV.10)) as the super-heating of the solution into the distributor increases.

$$\epsilon_m^{dist} = \frac{\dot{m}_{d,ad}^{dist}}{\dot{m}_{d,ad}^{max}} \quad (IV.10)$$

On the other hand, on the falling film part, the desorption kinetics and consequently the mass effectiveness of the falling film part (ϵ_m^{ff} , defined by Eq. (IV.11)) decreases with the increase in film thickness and thus the increase in solution flow rate.

$$\epsilon_m^{ff} = \frac{\dot{m}_{d,ad}^{ff}}{\dot{m}_{d,ad}^{max} - \dot{m}_{d,ad}^{dist}} \quad (IV.11)$$

The efficiency of the desorber depends then on the mass effectiveness of the distributor and the falling film parts, as shown by Eq. (IV.12). Indeed, these two joint effects can explain the trends described in Figure IV.5.

$$\varepsilon_m^d = \frac{\dot{m}_{d,ad}^{dist} + \dot{m}_{d,ad}^{ff}}{\dot{m}_{d,ad}^{max}} = \varepsilon_m^{dist} + \varepsilon_m^{ff} - (\varepsilon_m^{dist} \cdot \varepsilon_m^{ff}) \quad (IV.12)$$

Finally, Figure IV.5c shows a lower effectiveness for $\Delta T_{s,i}^{eq} = 10^\circ\text{C}$ at low solution flow rates compared with the other equilibrium deviation temperatures by a difference of approximately 2%. This might be related to the experimental uncertainties, which are not directly accounted for in the regression.

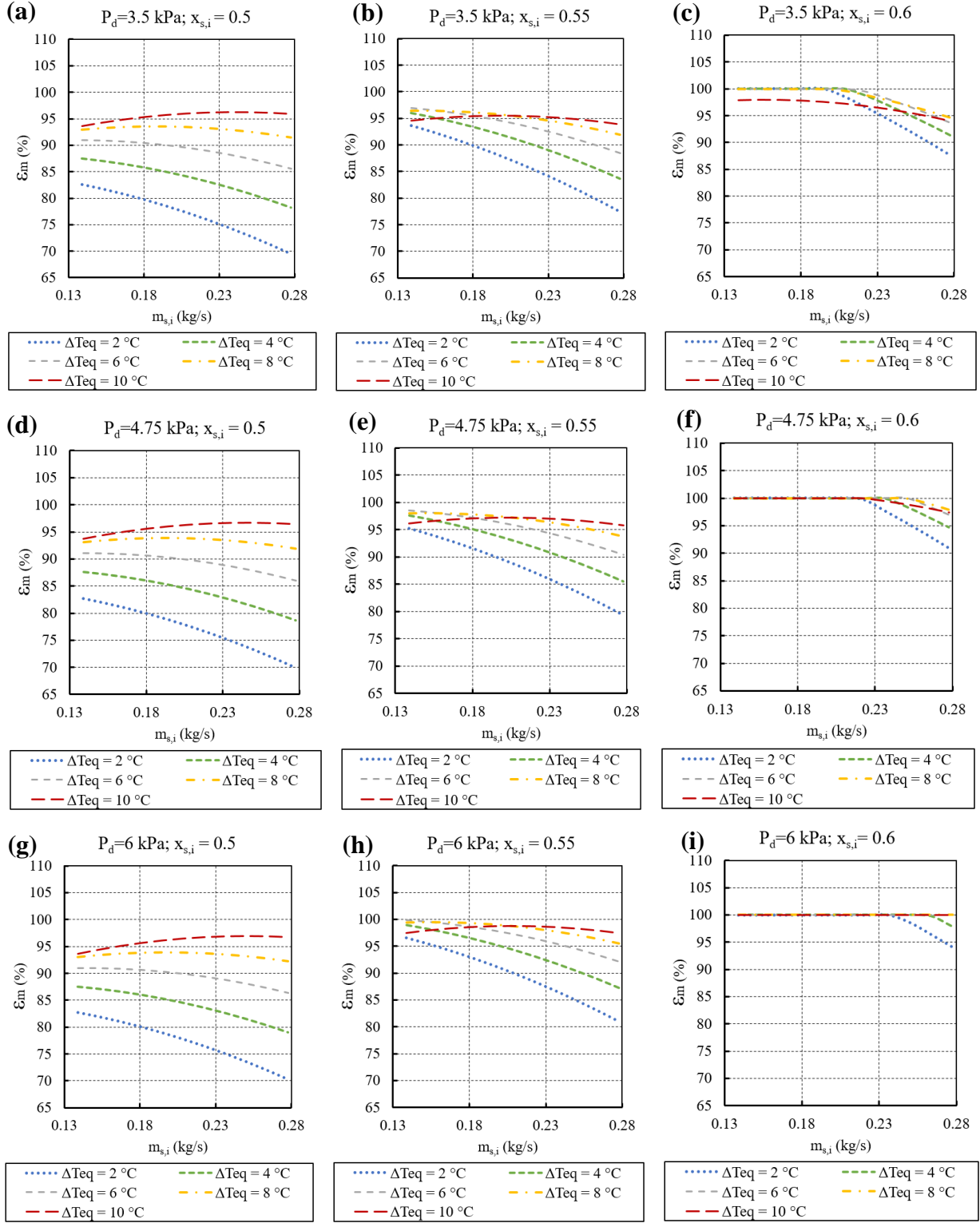


Figure IV.5: Experimental results of the desorber mass effectiveness as function of the inlet solution mass flow rate, for three different $x_{s,i}/P_d$ levels, and with iso- $\Delta T_{s,i}^{eq}$ lines.

Figure IV.6 presents the effectiveness as a function of the inlet solution mass flow rates for three fixed $\Delta T_{s,i}^{eq}$ and at the same pressure (4.75 kPa). The iso- $x_{s,i}$ lines are equivalent to iso- $T_{s,i}$ lines due to the fixed equilibrium deviation temperatures in each sub-graph. From these graphs, it is clear that, for the same solution equilibrium deviation temperature, the increase in solution concentrations has a positive influence on effectiveness. As discussed earlier, this might be related to the intrinsic increase in the solution temperature, which enhances the desorption phenomenon with the improvement of the solution thermophysical properties (decrease in viscosity and increase in diffusivity). Moreover, the impact of the concentration is stronger at low overheating levels of the solution for which the effectiveness of the desorber is mainly controlled by the falling film section. At high equilibrium deviation temperatures, the efficiency of the desorber is mainly controlled by the efficiency of the distributor part, limiting the effect of the solution mass fraction.

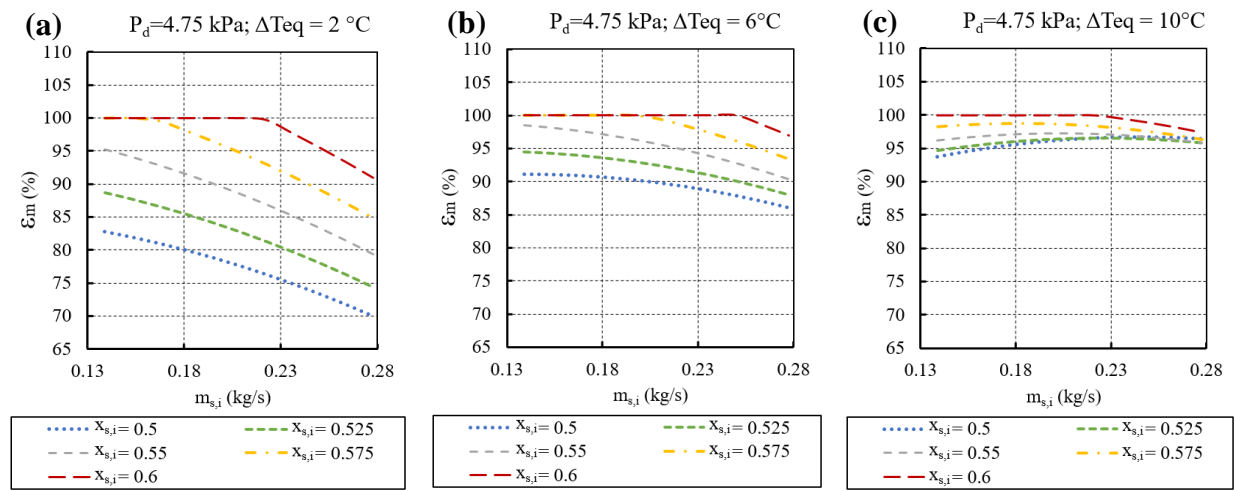


Figure IV.6: Mass effectiveness as function of the inlet solution mass flow rates a three different $\Delta T_{s,i}^{eq}$ and with iso- $x_{s,i}$ lines ($P=4.75$ kPa).

The definition of mass effectiveness presented here can be extended to applications in non-adiabatic sorption exchangers together with the use of a thermal effectiveness in parallel (Altamirano et al., 2020a, 2020c, 2019b; Michel et al., 2017). In these cases, most of the simulations in the literature consider that the sorption phenomenon is controlled by the heat transfer and use a thermal effectiveness or a global heat transfer coefficient to characterize the sorption elements in an absorption chiller (considering that the solution reaches equilibrium conditions at their outlet). However, it is clear that, due to the limited size of the exchanger, the solution rarely makes use of its entire sorption potential (Altamirano et al., 2020a). Moreover, the effectiveness of the exchangers is generally considered as constant during operations outside the nominal conditions. However, from Figure IV.5 and Figure IV.6, one can observe that the mass effectiveness changes considerably depending on the specific conditions studied. Hence, the implementation of characterization models for the thermal and mass effectiveness in a wide range of operating conditions offers a tool to more precisely describe the behavior of sorption exchangers. Furthermore, their implementation in an entire machine simulation would help to better describe the real (non-equilibrium) internal solution conditions, the cooling loads, and the thermal performances of the studied absorption chiller when operated at part-load conditions or when the driving sources are constantly changing (e.g., when using a solar thermal panel or the ambient temperature as driving sources).

4.5. Comparison with other technologies

In order to verify the compactness of the proposed exchanger, a comparison with other exchanger technologies is necessary. Unfortunately, according to the state-of-the-art review presented in [Chapter I](#), no adiabatic falling film desorber characterization has been presented before. However, there are a handful of studies based on hollow fiber membrane (HFM) and flat membrane (FM) modules as adiabatic desorbers (these technologies were discussed in more detail in Sections [1.3.2.3](#) and [1.3.3.3](#)). These studies, together with the results of this work, are presented in [Table IV.5](#). The information that was not directly provided was calculated when enough data were available. In the case of the exchanger volume, only the effective volume of the mass exchange occupied by the solution, the refrigerant vapor, and the mass exchange interface (membrane or adiabatic structure) were taken into account (the volume of insulating material or extra components was neglected). Moreover, for the cases in which the desorption/condensation was performed at atmospheric pressure (Ibarra-Bahena et al., 2020, 2017), since there was a small gap between the desorption and condensing surfaces (3 mm), the refrigerant vapor pressure was approximated to be that of the saturated condensate temperature, calculated with the condenser outlet heat transfer fluid temperature and a pinch of 5°C, that is, $P_v = P_{sat}^{water}(T_{htf}^{c,o} + 5)$.

4.5.1. Membrane desorbers effectiveness

The evolution of the mass effectiveness of the HFM and FM modules as function of a representative set of operating conditions is shown in [Figure IV.7](#). [Figure IV.7a](#) shows that in the case of the HFM₁ module, the increase in the solution mass flow rate, even if it increases the desorption mass flux, it leads to a decrease in the desorber mass effectiveness. This happens since the solution contained in the membrane increases in velocity, and its residence time in the exchanger decreases, decreasing the desorber effectiveness. In this case, the effect of the solution temperature can not be clearly observed since it is compensated by a change in pressure for both cases. Indeed, as observed in the previous sections, the increase in the solution temperature, apart from increasing the solution desorption potential, might lead to an improvement of the solution thermophysical properties for better mass exchange performances. However, the increase in pressure acts as a limiting component that reduces the desorption potential.

[Figure IV.7b](#) shows the performance, by the mass effectiveness, of the HFM₂ module. Clear trends can be observed for the concentrations of 0.55 and 0.57. However, for the other series, no special trend can be observed. This might be due to the uncertainties of the measurements or slight variations on the solution temperature that might not have been reported. However, from the curves of concentrations of 0.55 and 0.57, it can be observed that a lower concentration leads to higher performances (for the same solution temperature). This might be related to the variation on the thermophysical properties (such as the solution's viscosity) that this generates.

[Figure IV.7c](#) and [d](#) are the experimental results of desorption/condensation plate membrane modules tested at atmospheric pressures. From [Figure IV.7c](#) one can observe that indeed, as in the previous examples, an increase in the solution mass flow rate leads to a decrease in the desorber effectiveness. Moreover, from [Figure IV.7c](#) and [d](#), it is clear that the increase in the solution temperature has a positive impact on the performances. As previously mentioned, this might be related to the increase in the desorption potential of the solution, but also to the change in the thermophysical properties of the solution.

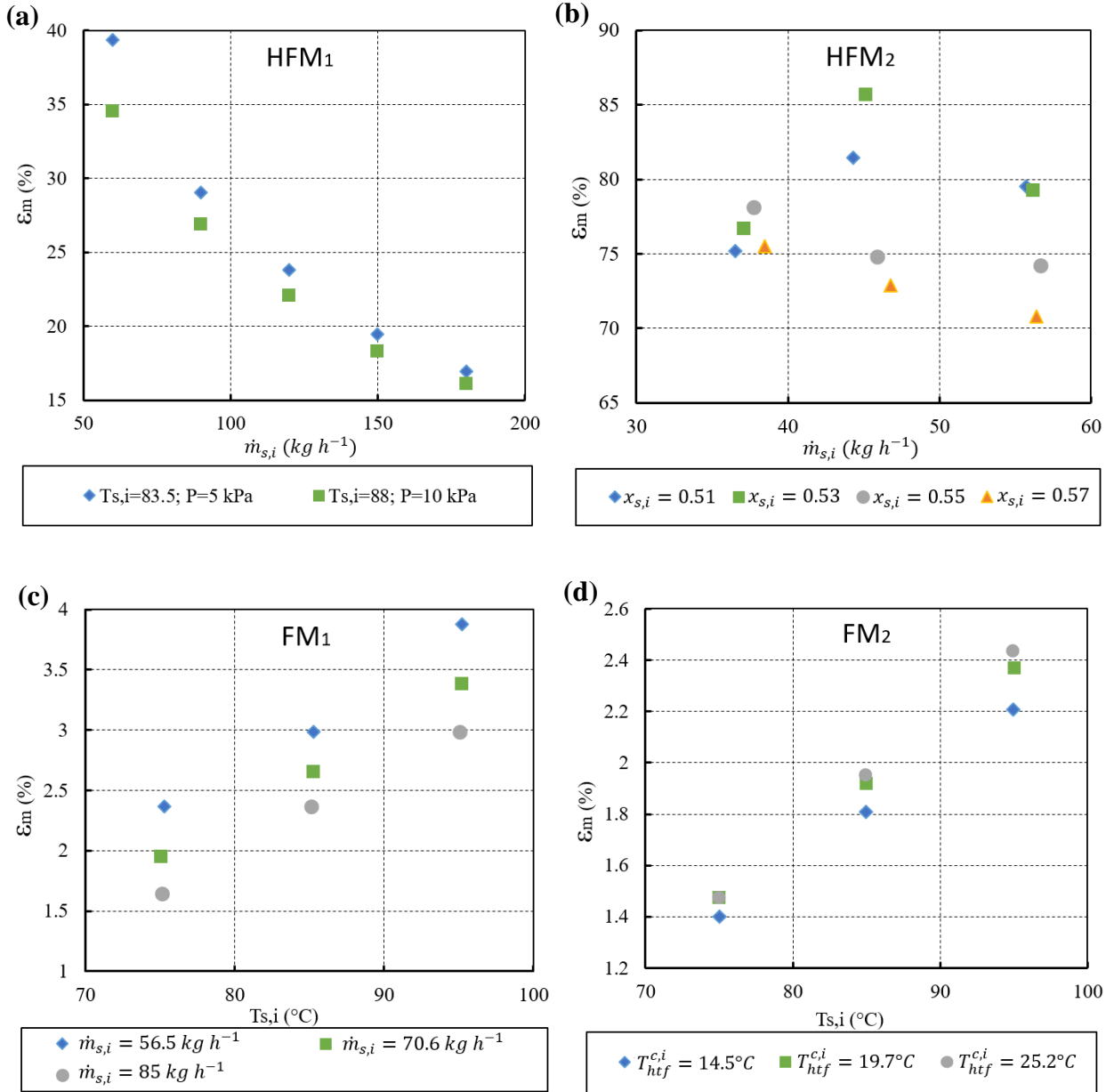


Figure IV.7: Mass effectivenesses of different investigated desorbers in representative operating conditions. (a) HFM₁ module by Wang et al. (2009) at $x_{s,i}=0.5$, (b) HFM₂ module by Hong et al. (2018) at $T_{s,i}= 80^\circ C$ and $P=4.7\ kPa$, (c) FM₁ module by Ibarra-Bahena et al. (2017) at $x_{s,i}=0.5$ and $2.56\ kPa < P_v < 3.1\ kPa$ and (d) FM₂ module by Ibarra-Bahena et al. (2020) at $\dot{m}_{s,i}=90\ kg\ h^{-1}$, $x_{s,i}=0.4978$, and $2.32\ kPa > P_v > 3.38\ kPa$.

4.5.2. Performance comparison

As mentioned in Section 1.3.1, different parameters exist in the literature to evaluate the performance and compactness of sorption exchangers. In this section, the parameters used for the comparison are the mass flux (Eq. (I.13)), the desorbed flow rate per unit volume of the exchanger, the desorption ratio (Eq. (IV.13)), and the mass effectiveness (Section 4.3.2).

$$Rd = \frac{\dot{m}_{des}}{\dot{m}_{s,i}} \quad (IV.13)$$

The mass flux is interesting when the effective exchange area can be clearly and easily defined, as is the case for the membrane and falling film desorbers presented in Table IV.5. Moreover, the volume occupied

by the exchanger is of fundamental importance for practical purposes. The desorption ratio was also used since it takes into account the amount of solution that is being circulated instead of the exchange area or the volume of the exchanger. Furthermore, it is a common parameter for evaluating adiabatic sorption exchangers. Finally, the adiabatic desorption mass effectiveness serves as a universal parameter to identify at what point the exchangers are really harvesting the total desorption potential. In all the cases, the maximum values were taken to compare the exchangers in their best conditions for each parameter. These maximum values are graphically represented in [Figure IV.8](#). From [Figure IV.8a](#), one can observe that the HFM exchangers seem to be the most compact in terms of volume. Indeed, these exchangers are known to contain a very high exchange area in a small volume (Wang et al., 2009). The falling film exchanger proposed in this work is not very far from the values of the HFM modules. Furthermore, its volume can be reduced if the density of the structure is increased. On the other hand, the FM modules are the ones that appear to be less compact (in terms of volume). Nevertheless, this may well be due to the fact that these modules were tested at atmospheric pressure conditions, in which air particles impede the natural flow of refrigerant vapor and generate elevated heat and mass transfer resistances.

[Figure IV.8b](#) shows the comparison of the maximum desorption mass flux for the different desorbers tested. From this figure one can see that the falling film desorber yielded the better performances. This might be related to the fact that the exchanger was designed to take the most advantage of the exchange area by means of hydrodynamic film disturbances generated along the flow. The FM modules followed in performance, while the hollow fiber membrane modules resulted in the lowest performances with respect to the effective exchange area. This suggests that the very high exchange area that these exchangers possess is not used as effectively as in the case of the other technologies. However, in terms of volume, this technology remains very compact. The elevated mass fluxes of the FM modules, if compared with those of the HFM modules ([Figure IV.8b](#)), is related to the high solution flow rates used in these modules per unit area. Indeed, the FM modules commonly use a metallic support to avoid deformation of the membrane at high solution flow regimes and temperatures, which gives it more versatility compared with the HFM modules. Therefore, if the increase in the pumping requirements generated by the higher pressure losses is not a problem, this is an advantage of the FM modules compared with the HFM modules.

[Figure IV.8c](#) shows that even if the FM modules desorb a high quantity of water vapor per unit area, the required circulated mass of solution is also high; therefore, the maximum desorption ratio in these modules is low. This, as mentioned earlier, is probably related to the fact that these modules were tested at atmospheric pressure. The maximum desorption ratio of the exchanger proposed here proved to be lower than those of the HFM modules. This could be improved by the increased density of the adiabatic exchanger. Finally, regarding the mass effectiveness, [Figure IV.8d](#) shows that the studied falling film desorber presented the highest effectiveness. Furthermore, one of the HFM modules also presented very good mass effectiveness.

Finally, [Table IV.6](#) shows the non-adiabatic desorbers that have been tested with the H₂O-LiBr working fluid. With the exception of one study, all of these are based on the FM technology. It is clear that the mass fluxes that can be obtained with these modules exceed those of the adiabatic desorbers since the same module heats the solution in parallel to the desorption phenomenon. However, when compared with the non-adiabatic falling film desorber, the proposed adiabatic falling film desorber has performances that are similar or even higher. While this may be partly due to the different conditions tested, the fact that it presents similar desorption performances to a non-adiabatic desorber is an indication of the potential of the proposed technology.

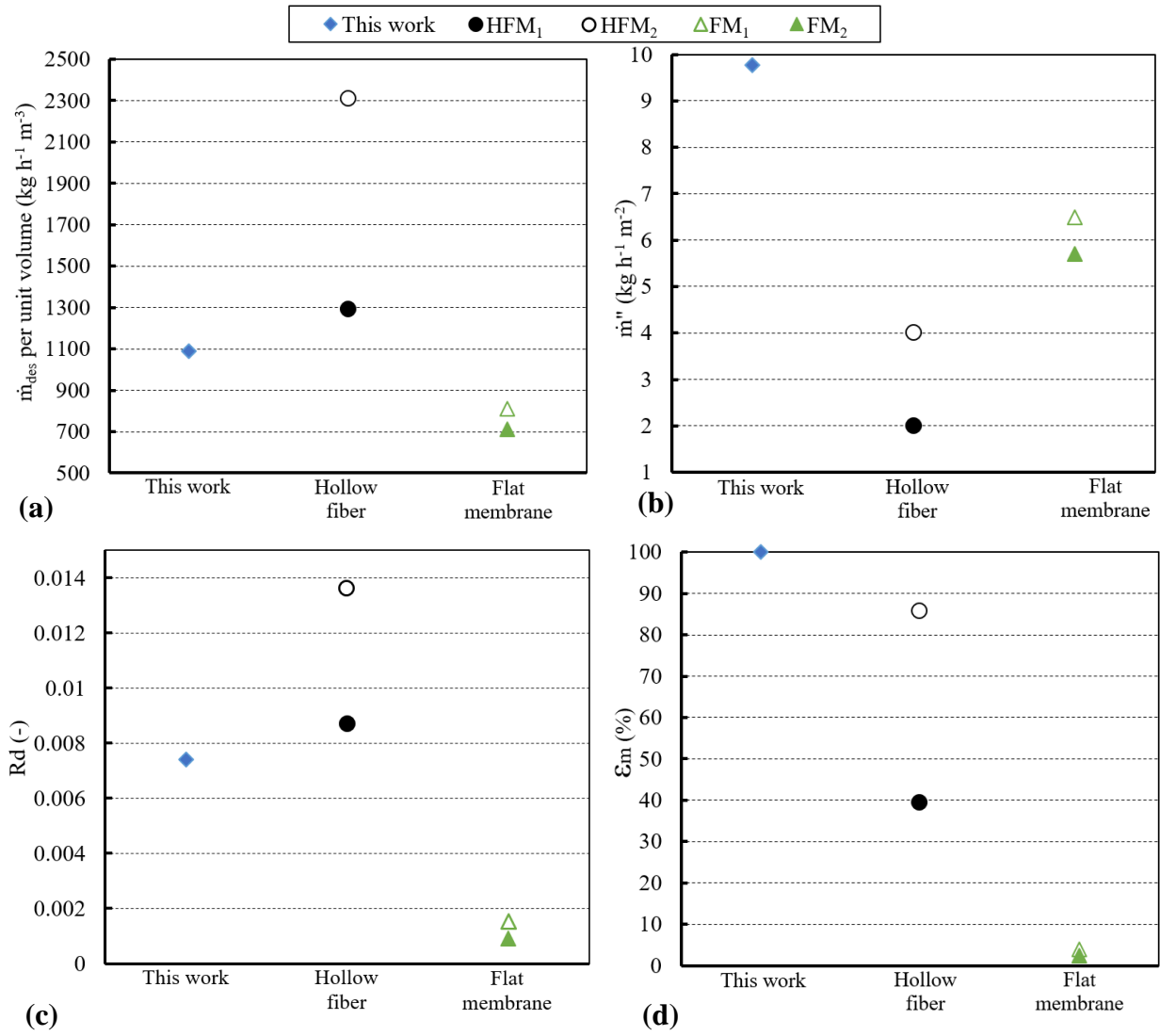


Figure IV.8: Maximum values of performance evaluation parameters for different adiabatic desorbers. (a) Desorbed flow rate per unit volume, (b) desorption mass flux, (c) desorption ratio, and (d) mass effectiveness.

Table IV.5: Adiabatic desorbers for absorption chillers: experimental results (~: approximated data).

Type	$\dot{m}_{s,i}$ (kg/h)	$x_{s,i}$ (kg kg ⁻¹)	$T_{s,i}$ (°C)	P_d (kPa)	V_{eff} (m ³)	A_{eff} (m ²)	\dot{m}_d^{max} (kg h ⁻¹)	\dot{m}_d^{max}/V_{eff} (kg h ⁻¹ m ⁻³)	\dot{m}_d^{max} (kg h ⁻¹ m ⁻²)	Rd^{max} (-)	ϵ_m^{max} (%)	Note	REF
Falling film	500–1000	0.5–0.6	52.38–91.62	3.5–6	0.007	0.77	7.5202	1088.07	9.77	0.0074	100		<i>This work</i>
HFM	~60–180	0.5	65–88	5–15	~0.000554	0.3581	0.7163	~1292.52	2	0.0087	39.37	PVDF pore size 0.16 μm	(Wang et al., 2009)
Flat membrane	56.2–88.2	0.5–0.587	72.4–95.9	$P_v \sim 2.56\text{--}3.1$	0.000115	0.0144	0.0936	812.5	6.5	0.0015	3.88	PTFE pore size 0.45 μm	(Ibarra-Bahena et al., 2017)
HFM	~36–57	0.51–0.58	65–83	3.5–5.5	~0.000337	0.1943	0.7772	~2307.9184	4	0.0136	85.68	PP pore size 0.158 μm	(Hong et al., 2018)
Flat membrane	90	0.4978	75.2–95.2	$P_v \sim 2.32\text{--}3.38$	0.000115	0.0144	0.08208	712.5	5.7	0.0009	2.44	PTFE pore size 0.22 μm	(Ibarra-Bahena et al., 2020)

Table IV.6: Non-adiabatic desorbers for absorption chillers: experimental results (~: approximated data).

Type	$\dot{m}_{s,i}$ (kg/h)	$x_{s,i}$ (kg kg ⁻¹)	$T_{s,i}$ (°C)	P_d (kPa)	\dot{m}_{htf}^i (kg/h)	T_{htf}^i (°C)	V_{eff} (m ³)	A_{eff} (m ²)	\dot{m}_d^{max} (kg h ⁻¹)	\dot{m}_d^{max}/V_{eff} (kg h ⁻¹ m ⁻³)	\dot{m}_d^{max} (kg h ⁻¹ m ⁻²)	\dot{Q}_d^{max} (kW)	\dot{Q}_d^{max}/V_{eff} (kw m ⁻³)	\dot{Q}_d^{max} (kW m ⁻²)	Rd^{max} (-)	REF
Plate falling film	93.6–100.8	0.51–0.54	52.9–71.8	3.55–6.72	648–972	58.2–83.8	~0.00288	0.24	1.91	662.5	7.95	2.01	465.28	4.1875	0.0204	(Hu et al., 2017)
Plate membrane	0.75–3.25	0.5	50–70	6–18	NA	$T_w = 50\text{--}125$	~0.000055	0.0051	0.18	~3294.16	36	-	-	-	0.2192	(Nasr Isfahani et al., 2013)
Plate membrane	0.75–3.25	0.48	70	6–18	NA	$T_w = 50\text{--}125$	~0.000055	0.0051	0.18	~3294.16	36	0.23	4148.63	45.34	0.2192	(Nasr Isfahani et al., 2014)
Plate membrane	2.5	0.48–0.51	60	6–10	NA	$T_w = 50\text{--}125$	~0.000055	0.0051	0.17	~3129.45	34.2	-	-	-	0.0584	(Bigham et al., 2014a)
Plate membrane	0.5–1.7	0.458	28	-	-	62–66	0.000105	0.0087	0.13	1257.59	15.12	-	-	-	0.0054	(Venegas et al., 2020)

4.5.3. Pressure drop comparison

The pressure drop generated by the membrane sorption exchangers has been the subject of discussion since IT can substantially increase the pumping energy consumption. The pressure drop is defined by Eq. (IV.14), in which f_D is the Darcy friction factor, ρ is the fluid density, v is the fluid velocity, and D_{hyd} is the hydraulic diameter of the pipe. For circular pipes (the case of the fibers in the HFM modules), D_{hyd} corresponds to the internal fiber diameter. In any other type of pipe, the hydraulic diameter is defined as in Eq. (IV.15), in which A is the cross-sectional area of the solution flow, and p is the wetted perimeter of the cross-section. Finally, in the laminar flow regime, the Darcy friction factor (f_D , Eq. (IV.16)) is inversely proportional to the Reynolds number (IV.17). In circular pipes, $C_D = 64$; otherwise, it depends on the specific pipe geometry.

In order to compare the pumping power consumption, the required hydraulic power was calculated by means of Eq. (IV.18). The pressure drop induced by the piping and the components located before the adiabatic desorber was not taken into account. Finally, only the pressure difference between the two pressure levels (i.e. the desorber and the absorber pressures), ΔP_{d-a} , is considered for the base case of the falling film (FF) desorber since the exchanger does not induce a pressure drop by itself.

$$\Delta P_{drop} = f_D \cdot \frac{\rho}{2} \cdot \frac{v^2}{D_{hyd}} \quad (IV.14)$$

$$D_{hyd} = \frac{4 \cdot A}{p} \quad (IV.15)$$

$$f_D = \frac{C_D}{Re} \quad (IV.16)$$

$$Re = \frac{\rho \cdot v \cdot D_{hyd}}{\mu} \quad (IV.17)$$

$$\dot{W}_p = (\Delta P_{d-a} + \Delta P_{drop}) \cdot \frac{\dot{m}_{s,i}}{\rho} \quad (IV.18)$$

A comparison was made of the nominal machine operating conditions of Section 3.3.2.1, in which $P_h = 6.31 \text{ kPa}$; $P_l = 1.1 \text{ kPa}$; $T_{s,i} = 88.51^\circ\text{C}$; $x_{s,i} = 0.579$; and with $0.027 \text{ kg s}^{-1} < \dot{m}_{s,i} < 0.55 \text{ kg s}^{-1}$. Apart from the falling film exchanger presented in Section 4.2.2, two HFM modules, and three FM modules were used for the comparison (characteristics in Table IV.7). The same volume as the falling film exchanger was considered for all the exchanger technologies (diameter of 0.2 m and length of 0.22 m). In the case of the HFM modules, two different cross-sectional densities (ratio of the area occupied by the fibers to the total cross-sectional area) were taken into account (10 and 30%, which lead to 13717 and 41152 fibers, respectively). Furthermore, the internal and external fiber diameters employed are those of Hong et al. (2018) (390 and 540 μm , respectively).

In the case of the FMs, the disposition of the plates was considered to be the same as those equivalent plates of the falling film desorber, which gives an equivalent entry length of 3.5 m ($40 \cdot (0.1 - 0.0125)$). In FM modules, the solution is usually constrained in microchannels. The number of channels in this study (Table IV.7) was calculated based on the work of Nasr Isfahani et al. (2015) (channels of 1 mm of width with 0.2 mm of spacing between them). Indeed, Nasr Isfahani et al. (2015) highlighted the importance of the depth of the microchannel on the solution pressure drop. Therefore, the same three depths were compared in this work: 100 μm , 160 μm , and 500 μm . According to each geometry, the theoretical C_D of these channels (in Table IV.7) corresponds to 84.7, 80, and 62.2, respectively (Cengel and Cimbala, 2017). Finally, the effect of the exchanger length was also addressed by comparing two different lengths (220 and 440 mm).

Table IV.7: Geometrical characteristics of the desorbers used for the comparison of the pressure drop.

	HFM – 10%	HFM – 30%	FM – 100- μm channel	FM – 160- μm channel	FM – 500- μm channel
Module diameter (m)	0.2	0.2	0.2	0.2	0.2
Module length (m)	0.22; 0.44	0.22; 0.44	0.22; 0.44	0.22; 0.44	0.22; 0.44
Number of fibers or channels	13717	41152	2916	2916	2916
D_{hyd} (μm)	390	390	181.82	275.86	666.67
C_D	64	64	84.7	80	62.2

Figure IV.9 shows the results of the pressure drop and required hydraulic power of the different desorbers. Since the differences between them are significant, a logarithmic scale was used for the vertical axis. From Figure IV.9a, one can see that among the membrane modules, the FM – 500- μm module was the one with the lowest pressure drops. Furthermore, the channel depth has a strong impact on the pressure drop, as reported by (Nasr Isfahani et al., 2015). Indeed, at the nominal solution flow rate design conditions ($\dot{m}_{s,i} = 0.24 \text{ kg s}^{-1}$), the pressure drop goes from 1.5 kPa (FM – 500 μm) to 77.5 (FM – 160 μm) and 302.4 kPa (FM – 100 μm) (Figure IV.9a), demanding 1.28, 15.84, and 58.9 times the hydraulic power than that required to take the solution from low pressure to high pressure (represented by the falling film exchanger in Figure IV.9c). Apart from the increase in pumping requirements, the increase in the solution pressure also changes the solution saturation temperature, making it more difficult to desorb water vapor. Therefore, in order to maintain a pressure drop lower than 10 kPa, only the FM–500 μm and HFM–30% modules are acceptable.

If the desorber length is increased to 440 mm, the pressure drop at nominal conditions would be of 3, 155, 604, 5.9, and 17.6 kPa for the FM–500 μm , FM–160 μm , FM–100 μm , HFM–30%, and HFM–10% modules, respectively (Figure IV.9b). On the other hand, the hydraulic power requirements are from 1.6 to 116 times that of the falling film exchanger (Figure IV.9d). From these results, it is clear that the design of a membrane desorber to optimize its hydraulic diameter in order to reduce the pressure drops as much as possible is of fundamental importance. Due to the higher pumping requirements and in order to keep a solution pressure drop lower than 10 kPa, from the membrane desorbers, only the 500- μm -deep microchannel FM desorber is suitable. Under these conditions (considering both desorber lengths), this exchanger would require approximately 30–60% more hydraulic power than that required to take the solution from the low- to the high-pressure level. Although this may not appear to be a significant problem at first, the manufacturing of such a desorber would be time-consuming and costly. Moreover, the performance characteristics of such a geometry are still unknown. On the other hand, the falling film desorber proposed here, apart from its proven good performances, is easy to produce and inexpensive owing to its manufacture using 3D-printing.

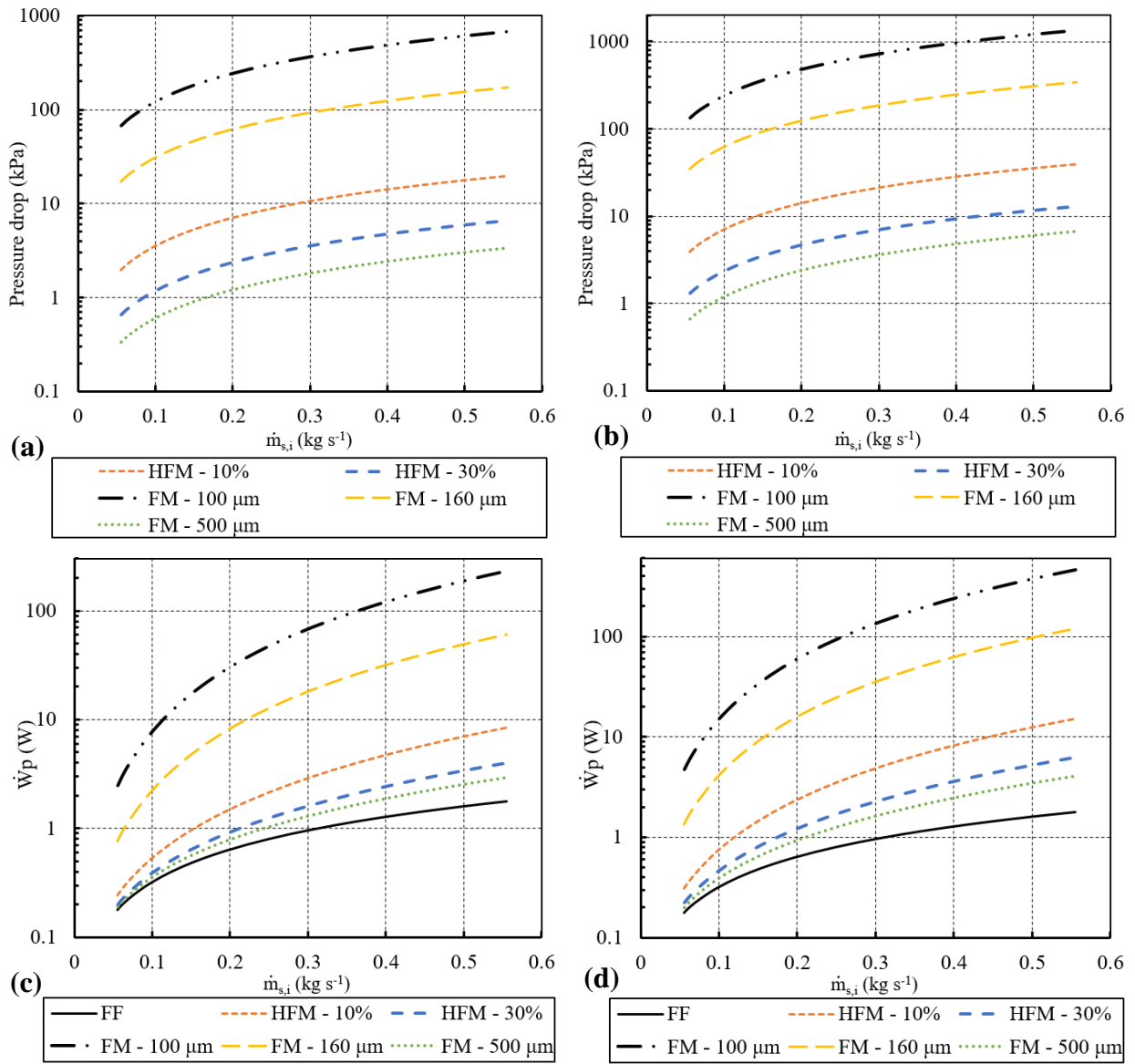


Figure IV.9: Pressure drop of different desorbers with (a) 220 and (b) 440 mm length; and hydraulic power requirements for the different desorbers with (c) 220 and (d) 440 mm length.

4.6. Conclusions

A new-generation adiabatic falling film sorption exchanger was experimentally characterized studying the influence of five parameters: the operating pressure, the inlet solution equilibrium deviation temperature, the inlet solution mass flow rate, and the inlet solution concentration. The experimental results led to a mass effectiveness of between 88 and 100%. Moreover, the second-order polynomial regression that resulted from the design of experiments indicates that the desorber can provide an equivalent cooling capacity of between 0.32 and 4.74 kW with an effectiveness in the range of 69.5–100% for the whole experimental domain studied ($3.5 \text{ kPa} \leq P_{des} \leq 6 \text{ kPa}$; $2 \text{ }^\circ\text{C} \leq \Delta T_{s,i}^{eq} \leq 10 \text{ }^\circ\text{C}$; $0.139 \text{ kg/s} \leq \dot{m}_{s,i} \leq 0.278 \text{ kg/s}$; $0.5 \leq x_{s,i} \leq 0.6$). In the nominal operating conditions defined in Section 3.3.2.1, the same model indicates that the desorber would operate at a mass effectiveness close to one. Therefore, on the basis of these results, the construction of an absorption chiller based on this technology seems very promising. Furthermore, the compactness of the designed desorber can be further increased by reducing its volume at the cost of a slightly lower mass effectiveness.

Desorption takes place in two stages in the desorber: firstly in the distributor part, where spontaneous boiling develops and intensifies with the overheating of the solution at the inlet. Then, in the falling film section, where diffusion phenomena take place. The increase in the solution mass flow rate leads to a decrease in performance due to the increase in solution film thickness, which increases the thermal resistance between the liquid solution and the vapor–liquid interface in the falling film section. The increase in the solution super-heating at the inlet leads to an increase in performance due to the intensification of the boiling phenomenon in the distributor.

The increase in the solution concentration led to a higher effectiveness by the increase in equilibrium temperature, which improves the thermophysical properties of the solution for a better desorption phenomenon. The same occurs with the increase in the operating pressure, but at a much smaller scale, since it has a lower impact on the equilibrium temperature of the solution. This suggests that the impact on the thermophysical properties due to the solution temperature variations is dominant compared with the effects generated by the solution concentration variations themselves. Finally, at high solution concentrations or equilibrium deviation temperatures, the impact of the solution thermophysical properties is reduced.

The proposed regression of the mass effectiveness, the concept of which can also be applied to the absorption functioning mode and non-adiabatic sorption exchangers (Altamirano et al., 2020a, 2020c, 2019b; Michel et al., 2017), offers a tool to more realistically characterize the sorption exchangers and, therefore, its implementation to simulate an entire machine would make it possible to better describe the chiller behavior and the non-equilibrium conditions of the solution in the machine, especially at part-load operation or when coupled to sources that are constantly changing (e.g., a solar thermal source or the ambient temperature).

After a comparison with other technologies tested in desorption operation, the proposed technology appears to be a promising alternative since it showed performances comparable to those of adiabatic membrane desorbers while having the advantages of a negligible solution pressure drop, as well as easy and low-cost manufacture. Furthermore, it even presented similar mass transfer performances to a non-adiabatic desorber. Finally, the characterization of the presented adiabatic mass exchanger in the absorber functioning mode remains to be studied. Moreover, in order to extend the use of the presented characterization to other similar geometries, the use of dimensionless numbers is required. For this, a more detailed analysis of the impact of the studied parameters on the different thermophysical properties of the solution might be required to better understand the physical phenomena controlling adiabatic desorber performance.

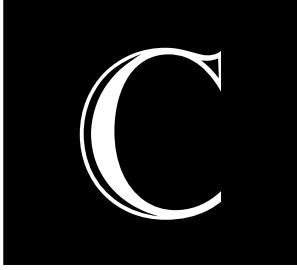
References

- Altamirano, A., Le Pierrès, N., Stutz, B., Coronas, A., 2020a. Performance characterization methods for absorption chillers applied to an $\text{NH}_3\text{-LiNO}_3$ single-stage prototype. *Appl. Therm. Eng.*
- Altamirano, A., Stutz, B., Le Pierrès, N., 2020b. Review of small-capacity single-stage continuous absorption systems operating on binary working fluids for cooling: Compact exchanger technologies. *Int. J. Refrig.* 114, 118–147. <https://doi.org/10.1016/j.ijrefrig.2020.02.033>
- Altamirano, A., Stutz, B., Le Pierrès, N., Coronas, A., 2020c. Experimental characterization by thermal and mass effectivenesses of plate heat exchangers in $\text{NH}_3\text{-LiNO}_3$ absorption chillers, in: *ISHPC 2021 – Online Pre-Conference*. Berlin, Germany, pp. 56–60. <https://doi.org/10.14279/depositonce-10430.2>
- Altamirano, A., Stutz, B., Le Pierrès, N., Domain, F., 2019. $\text{H}_2\text{O-LiBr}$ Single-Stage Solar Absorption Air Conditioner with an Innovative Bi-Adiabatic Configuration: Dynamic Model, Nominal Conditions and Typical Day Operation, in: *Solar World Congress*, Nov 4-7. <https://doi.org/10.18086/swc.2019.55.01>
- Altamirano Cundapí, A., Stutz, B., Le Pierrès, N., 2020. Sorption exchanger (in French). Patent FR N°20/09477.
- Arzoz, D., Rodriguez, P., Izquierdo, M., 2005. Experimental study on the adiabatic absorption of water vapor into $\text{LiBr-H}_2\text{O}$ solutions. *Appl. Therm. Eng.* 25, 797–811. <https://doi.org/10.1016/j.applthermaleng.2004.08.003>
- Bigham, S., Nasr Isfahani, R., Moghaddam, S., 2014. Direct molecular diffusion and micro-mixing for rapid dewatering of LiBr solution. *Appl. Therm. Eng.* 64, 371–375. <https://doi.org/10.1016/j.applthermaleng.2013.12.031>
- Boudard, E., Bruzzo, V., 2004. Exchange Device and Heat Transfer Especially for Automotive Vehicle. French Patent 2,871,221.
- Caldas, L.F.S., De Paula, C.E.R., Brum, D.M., Cassella, R.J., 2013. Application of a four-variables Doehlert design for the multivariate optimization of copper determination in petroleum-derived insulating oils by GFAAS employing the dilute-and-shot approach. *Fuel* 105, 503–511. <https://doi.org/10.1016/j.fuel.2012.10.026>
- Cengel, Y., Cimbala, J., 2017. *Fluid Mechanics Fundamentals and Applications*, 4th ed. McGraw-Hill Higher Education, New York (US).
- Flores, C., 2014. Étude des transferts de masse et de chaleur au sein d'un absorbeur eau/bromure de lithium. PhD Université de Grenoble.
- Gutiérrez-Urueta, G., Rodríguez, P., Venegas, M., Ziegler, F., Rodríguez-Hidalgo, M.C., 2011. Experimental performances of a LiBr-water absorption facility equipped with adiabatic absorber. *Int. J. Refrig.* 34, 1749–1759. <https://doi.org/10.1016/j.ijrefrig.2011.07.014>
- Hong, S.J., Hihara, E., Dang, C., 2018. Analysis of adiabatic heat and mass transfer of microporous hydrophobic hollow fiber membrane-based generator in vapor absorption refrigeration system. *J. Memb. Sci.* <https://doi.org/10.1016/j.memsci.2018.07.048>
- Hu, T., Xie, X., Jiang, Y., 2017. Design and experimental study of a plate-type falling film generator for a $\text{LiBr/H}_2\text{O}$ absorption heat pump. *Int. J. Refrig.* 74, 302–310. <https://doi.org/10.1016/j.ijrefrig.2016.09.024>
- Ibarra-Bahena, J., Dehesa-Carrasco, U., Romero, R.J., Rivas-Herrera, B., Rivera, W., 2017. Experimental assessment of a hydrophobic membrane-based desorber/condenser with $\text{H}_2\text{O/LiBr}$ mixture for absorption systems. *Exp. Therm. Fluid Sci.* <https://doi.org/10.1016/j.expthermflusci.2017.05.024>

- Ibarra-Bahena, J., Venegas-Reyes, E., Galindo-Luna, Y.R., Rivera, W., Romero, R.J., Rodríguez-Martínez, A., Dehesa-Carrasco, U., 2020. Feasibility Analysis of a Membrane Desorber Powered by Thermal Solar Energy for Absorption Cooling Systems. *Appl. Sci.* 10, 1110. <https://doi.org/10.3390/app10031110>
- Islam, M.R., Wijeyesundera, N.E., Ho, J.C., 2003. Performance study of a falling-film absorber with a film-inverting configuration. *Int. J. Refrig.* 26, 909–917. [https://doi.org/10.1016/S0140-7007\(03\)00078-1](https://doi.org/10.1016/S0140-7007(03)00078-1)
- Michel, B., Le Pierrès, N., Stutz, B., 2017. Performances of grooved plates falling film absorber. *Energy* 138, 103–117. <https://doi.org/10.1016/j.energy.2017.07.026>
- Moffat, R.J., 1982. Contributions to the theory of single-sample uncertainty analysis. *ASME. J. Fluids Eng.* 104, 250–258. <https://doi.org/10.1115/1.3241818>
- Montgomery, D.C., 2012. *Design and Analysis of Experiments*, 8th ed. John Wiley & Sons, Inc., Hoboken, US.
- Mugnier, D., Neyer, D., White, S., 2017. *The Solar Cooling Design Guide: Case Studies of Successful Solar Air Conditioning Design*. Ernst & Sohn, Berlin, Germany.
- Nasr Isfahani, R., Bigham, S., Mortazavi, M., Wei, X., Moghaddam, S., 2015. Impact of micromixing on performance of a membrane-based absorber. *Energy* 90, 997–1004. <https://doi.org/10.1016/j.energy.2015.08.006>
- Nasr Isfahani, R., Fazeli, A., Bigham, S., Moghaddam, S., 2014. Physics of lithium bromide (LiBr) solution dewatering through vapor venting membranes. *Int. J. Multiph. Flow* 58, 27–38. <https://doi.org/10.1016/j.ijmultiphaseflow.2013.08.005>
- Nasr Isfahani, R., Sampath, K., Moghaddam, S., 2013. Nanofibrous membrane-based absorption refrigeration system. *Int. J. Refrig.* 36, 2297–2307. <https://doi.org/10.1016/j.ijrefrig.2013.07.019>
- Ngo, T.D., Kashani, A., Imbalzano, G., Nguyen, K.T.Q., Hui, D., 2018. Additive manufacturing (3D printing): A review of materials, methods, applications and challenges. *Compos. Part B Eng.* 143, 172–196. <https://doi.org/10.1016/j.compositesb.2018.02.012>
- Obame Mve, H., Rullière, R., Haberschill, P., 2015. Modeling and Parametric Study of the Heat Transfer Inside a Lithium Bromide Flow Confined by Wire Screen. *J. Energy Power Eng.* 9, 417–425. <https://doi.org/10.17265/1934-8975/2015.05.001>
- Peng, T., Kellens, K., Tang, R., Chen, C., Chen, G., 2018. Sustainability of additive manufacturing: An overview on its energy demand and environmental impact. *Addit. Manuf.* 21, 694–704. <https://doi.org/10.1016/j.addma.2018.04.022>
- Plocher, J., Panesar, A., 2019. Review on design and structural optimisation in additive manufacturing: Towards next-generation lightweight structures. *Mater. Des.* 183, 108–164. <https://doi.org/10.1016/j.matdes.2019.108164>
- Savolainen, J., Collan, M., 2020. How Additive Manufacturing Technology Changes Business Models? – Review of Literature. *Addit. Manuf.* 32, 101070. <https://doi.org/10.1016/j.addma.2020.101070>
- Venegas, M., García-Hernando, N., de Vega, M., 2020. Experimental evaluation of a membrane-based microchannel desorber operating at low desorption temperatures. *Appl. Therm. Eng.* 167, 114781. <https://doi.org/10.1016/j.applthermaleng.2019.114781>
- Venegas, M., Rodríguez, P., Lecuona, A., Izquierdo, M., 2005. Spray absorbers in absorption systems using lithium nitrate-ammonia solution. *Int. J. Refrig.* 28, 554–564. <https://doi.org/10.1016/j.ijrefrig.2004.10.005>

Wang, Z., Gu, Z., Feng, S., Li, Y., 2009. Application of vacuum membrane distillation to lithium bromide absorption refrigeration system. *Int. J. Refrig.* 32, 1587–1596.
<https://doi.org/10.1016/j.ijrefrig.2009.07.002>

This page intentionally left blank



Conclusions and future work

“

不闻不若闻之，闻之不若见之，
见之不若知之，知之不若行之；
学至于行之而止矣。

*“Not hearing is not as good as hearing,
hearing is not as good as seeing,
seeing is not as good as knowing,
knowing is not as good as acting;
true learning continues until it is put into action.”*

– Xun Kuang

Conclusions

The increasing energy demand, in large part due to the increase of the cooling needs in the building sector, requires innovative solutions to better equilibrate the energy flows. Countries with high solar irradiation, such as Mexico, possess an enormous potential of solar energy harvesting to provide with cleaner solutions to fulfill the energy demands of their growing populations. Absorption chillers represent a clean alternative to satisfy the cooling demand and diversify the energy sources. The low market demand of these systems nowadays represents a big challenge to overcome their disadvantages of elevated cost and low compactness. However, new manufacturing methods provide with alternative solutions to reduce the fabrication costs of their components and bypass the need for a mass-scale production.

The present work's main objective was to develop a new generation of compact and low-cost absorption chillers. With this purpose, different aspects were investigated that would lead to a machine with the desired characteristics. For this, a deep state of the art regarding the different investigated working fluids and exchanger technologies for small-capacity absorption chillers was performed. From the working fluids perspective, it is clear that the unquestionable leader for the positive cooling applications remains to be the H₂O-LiBr working pair due to its advantages of reliability and high performances. Ionic liquids have presented an exploding interest in recent years to replace LiBr as absorbent for H₂O owing to their good properties; however, a lot of work remains to be done to study their behavior in the long term. Regarding the negative cooling applications, NH₃-H₂O is the only commercially available working pair. However, NH₃-LiNO₃ seems to be a promising alternative for commercial systems. Indeed, an adapted sorption exchanger geometry might help overcome the limited heat and mass transfer performances due to elevated viscosity if compared to the conventional NH₃-H₂O working pair. Finally, regarding the refrigerants, HFCs are not an option in the long term since they will be banned under the Kigali Amendment to the Montreal Protocol. CO₂ has also been proposed in recent years as refrigerant for absorption cooling systems and may be an option in the future; however, new absorbents for this refrigerant have to be studied for better performance, and special attention must be paid to its high operating pressures, which raise new challenges in terms of design.

Due to the complexity of the system compared with conventional vapor compression systems, the simulation of absorption chillers is of fundamental importance. In this regard, [Chapter I](#) allowed to observe that there is no standard parameter for the performance evaluation of the sorption elements in absorption chillers. For this reason, the general definition of the thermal and mass effectivenesses for non-adiabatic sorption exchangers was presented in [Chapter II](#) (the mass effectiveness of adiabatic sorption exchangers is intrinsically included in this definition). The characterization of plate heat exchangers operating in absorption and desorption mode with the NH₃-LiNO₃ working pair was also presented. In these exchangers, ε_{th} and ε_m were mostly impacted by the solution flow regime (Re_{sol}), leading to better performances at low Re_{sol} and lower dynamic viscosities (mainly due to a mass transfer enhancement by hydrodynamic bubble disturbances and an increased bubble residence time in the plate channels). Moreover, elevated heat transfer fluid flow rates, which increase the electricity consumption, wouldn't lead to higher effectivenesses. After the components' characterization, a characterization of a 10-kW water-cooled absorption chiller was performed by means of four different methods: the characteristic equation (CE) method (semi-empirical), the adapted CE method and the Carnot function model (CFM, both empirical), and a thermodynamic model (physical), called the effectiveness model (EM), based on thermal and mass effectivenesses. The COP_{carnot} was used as a common parameter to represent the different operating conditions (experimental and modelling results) of the chiller. Apart from the intrinsic characteristics of each method, the EM allows for a better understanding of the individual performance of the exchangers in the system and of the non-equilibrium conditions of the working fluid. Moreover, the EM allows for the identification of the limiting components in the system and COP_{elect} improvement opportunities.

Chapter III proposed the investigation of a small-capacity solar-geothermal absorption system in the Monterrey (Mexico) climate conditions. A first study used a steady-state model to compare the $\text{NH}_3\text{-H}_2\text{O}$, $\text{H}_2\text{O-LiBr}$, and $\text{NH}_3\text{-LiNO}_3$ working fluids. The system's components were dimensioned and a quick economic viability study was performed. From this study, the $\text{H}_2\text{O-LiBr}$ resulted to be the most adapted working pair. On the other hand, the proposed system does not seem economically viable in the Mexican conditions since the geothermal heat sink source strongly increases the already high initial investment cost of the solar absorption system. In this regard, new green subsidies could help boost the transition to renewable energies in Mexico.

With the $\text{H}_2\text{O-LiBr}$ working fluid chosen, a first and second law dynamic model of an innovative bi-adiabatic small-capacity absorption chiller based on its components' thermal and mass effectivenesses was developed. Simulations allowed to identify the system's nominal conditions and to study its behavior coupled to a solar thermal collector as the high temperature source, a helical geothermal heat exchanger as the intermediate temperature source, and a single-family house. This configuration can deliver comfortable room temperatures with an internal temperature 9°C cooler at the end of the day compared with a non-cooled home. Furthermore, the exergetic study showed that the components that lead to the highest exergy destruction are the adiabatic desorber and absorber, respectively, mainly due to the low mass effectiveness that were selected for these components. For this reason, a mass effectiveness of the adiabatic components of at least 0.6 is required for the system to be efficient.

Finally, in Chapter IV, a new generation falling film adiabatic sorption exchanger was presented and experimentally characterized in desorption mode. The experimental results led to a mass effectiveness between 88 and 100%. During experiments, the desorption took place in two stages: first in the distributor where spontaneous boiling develops and intensifies with the super-heating of the solution. Then, in the falling film section, where diffusion phenomena take place. The increase in the solution mass flow rate leads to a decrease in the performance due to the increase in the solution film thickness, which increases the thermal resistance between the liquid solution and the vapor-liquid interface in the falling film section. The increase in the solution super-heating at the inlet leads to an increase in the performance due to the intensification of the boiling phenomenon in the distributor. The increase in the solution concentration led to a higher effectiveness by the increase in the equilibrium temperature, which improves the solution thermophysical properties for a better desorption phenomenon. The same occurs with the increase in the operating pressure, but at a much smaller scale, since it has a lower impact on the solution equilibrium temperature. At high solution concentrations or equilibrium deviation temperatures, the impact of the solution thermophysical properties is reduced. The second-order polynomial indicates that in the nominal operating conditions defined in Section 3.3.2.1, the desorber would operate at a mass effectiveness close to one. Finally, the proposed falling film technology showed similar performances to adiabatic membrane desorbers while having the advantages of a negligible solution pressure drop and an easy and low-cost fabrication. Furthermore, it even presented similar mass transfer performances than a non-adiabatic desorber

Future work

The results obtained in the present work are very promising. Therefore, the construction and experimental characterization of a real-scale prototype based on the proposed technology seems worthwhile. The next steps to achieve this goal are the following:

Characterization of the desorber through dimensionless numbers

Even though the desorber was characterized by different solution mass flow rates, pressure, temperature, and concentration parameters, its characterization through dimensionless numbers would be preferable to better extend the use of the characterization to other similar geometries. This would also facilitate the implementation of the exchanger characterization into overall machine models operating in a wide range of conditions. In order to achieve this, a parametric analysis to study the variation of the different solution thermophysical properties for the different range of studied conditions might be required to understand the physical phenomena controlling the adiabatic desorber performance.

Characterization of the exchanger in the absorption mode

After fully understanding the behavior of the adiabatic desorber, the mass exchanger will be tested in absorber operation mode. With the obtained results, an interpretation of what happens in the case of the absorption phenomenon for the proposed geometry will be obtained. As in the case of the desorber, the characterization through dimensionless numbers and the study of the behavior of the solution's thermophysical properties will be performed. Once the performance characterization of both components are obtained, the design of an entire machine is feasible.

Design modifications

Some aspects of the design of the presented exchanger can still be improved. A re-design study can be implemented to observe the main limiting points in terms of manufacturing costs and time of production. Indeed, the 3D printing process can be slow depending on the complexity of the component being printed. Therefore, limiting the number of 3D printed parts might not only help in the production time reduction but also to decrease the manufacturing costs of a final product.

Real-scale prototype design and characterization

Finally, the design and construction of a real-scale prototype will be performed. Final design choices as the refrigerant phase-change exchangers geometry will be made. It seems that helical coils heat exchangers around the adiabatic structure of [Figure IV.3](#) would lead to an increased compactness of the entire system. The resulting prototype would then be composed of only low-cost mass-manufactured or 3D printed components, which might lead to a system that is compact and at the same time efficient.

A startup project, named CONFOTHER, has been approved and financed by the French SATT (Technology Transfer Accelerator Office) Linksium to continue with the development of the presented technology. The main objective of the following year is the construction and testing of a real-scale prototype and the search for industrial and commercial partners in order to bring a commercially attractive product to the market.

This page intentionally left blank



Abstract

This thesis deals with the development of a new generation of compact and low-cost absorption chillers, allowing to meet the growing demand for air conditioning in buildings without a noticeable impact on the electricity consumption by using solar thermal energy. For solar cooling applications in hot climate regions, the case of houses in the Mexican climate is particularly addressed. The proposed machine is a single-stage H₂O-LiBr chiller with an innovative bi-adiabatic configuration in combination with industrially produced plate heat exchangers. The specifications of the components have been determined on the basis of a dynamic model of the machine using the mass and thermal effectivenesses of the components. The theoretical results and the first experimental results validate the potential of the machine and the construction of a full-scale prototype is intended.

Keywords: absorption chiller, solar air conditioning, working fluid, exchanger technology, falling film, adiabatic exchanger.

French abstract

Cette thèse porte sur le développement d'une nouvelle génération de refroidisseurs à absorption compacts et peu coûteux, pour répondre à la demande croissante de climatisation des bâtiments sans impact sensible sur la consommation électrique en valorisant l'énergie solaire thermique. Pour des applications de refroidissement solaire dans des climats chauds, le cas des habitations dans le climat mexicain est abordé. La machine proposée est un refroidisseur H₂O-LiBr à simple étage mettant en œuvre une configuration bi-adiabatique innovante couplée à des échangeurs à plaques produits industriellement. Les caractéristiques des composants ont été déterminées sur la base d'une modélisation dynamique de la machine mettant en œuvre les efficacités massiques et thermiques de composants. Les résultats théoriques et les premiers résultats expérimentaux valident le potentiel de la machine et la construction d'un prototype à l'échelle réelle est envisagée.

Mots-clés : rafraichisseur à absorption, climatisation solaire, fluide de travail, technologie d'échangeur, film ruisselant, échangeur adiabatique.